Studies on Some Aspects of Multi-objective Optimization: A Case Study of Electrical Discharge Machining Process

A THESIS SUBMITTED IN FULFILLMENT OF
THE REQUIREMENT FOR THE AWARD OF THE DEGREE

OF

Doctor of Philosophy

IN

MECHANICAL ENGINEERING

by

Chinmaya Prasad Mohanty

(Roll No. 511ME123)

Department of Mechanical Engineering

National Institute of Technology, Rourkela 769008

ROURKELA - 769008, INDIA

June–2015

CERTIFICATE

This to certify that the thesis entitled "**Studies on Some Aspects of Multi-objective Optimization: A Case Study of Electrical Discharge Machining Process**" being submitted by **Chinmaya Prasad Mohanty** for the award of the degree of Doctor of Philosophy (Mechanical Engineering) of NIT Rourkela, is a record of bonafide research work carried out by him under our supervision and guidance. Mr. Chinmaya Prasad Mohanty has worked for more than three years on the above problem at the Department of Mechanical Engineering, National Institute of Technology, Rourkela and this has reached the standard fulfilling the requirements and the regulation relating to the degree. The contents of this thesis, in full or part, have not been submitted to any other university or institution for the award of any degree or diploma.

Dr. Siba Sankar Mahapatra
Professor
Department of Mechanical Engineering
National Institute of Technology,
Rourkela

Place: Rourkela
Date:

ACKNOWLEDGEMENT

This thesis is a result of research that has been carried out at National Institute of Technology, Rourkela. During this period, I came across a great number of people whose contributions in various ways helped my field of research and they deserve special thanks. It is a pleasure to convey my gratitude to all of them.

In the first place, I would like to express my deep sense of gratitude and indebtedness to my supervisor **Prof. Siba Sankar Mahapatra,** Head of Mechanical Engineering Department for his advice and guidance from early stage of this research and providing me extraordinary experiences throughout the work. Above all, he provided me unflinching encouragement and support in various ways which exceptionally inspired and enriched my growth as a student, a researcher and a scientist.I am proud to acknowledge that I had opportunity to work with an exceptionally experienced scientist like him.

I am grateful to **Prof. Sunil Kumar Sarangi,** Director and **Prof. Ranjit Kumar Sahoo**, former Head of Mechanical Engineering Department, National Institute of Technology, Rourkela, for their kind support and concern regarding my academic requirements.

I express my thankfulness to the faculty and staff members of the Mechanical Engineering Department for their continuous encouragement and suggestions. Among them, **Sri Prasanta Kumar Pal** deserves special thanks for his kind cooperation in non-academic matters during the research work.

I am indebted to **Dr. Saurav Dutta**, **Dr. Manas Ranjan Singh**, **Mr. Jambewar Sahu**, **Mr. Swayam Bikash Mishra, Mr. Prases Kumar Mohanty, Mr. Suman Chatterjee, Mr. Chitrasen Samantra, Mr. Kumar Abhisekh, Mr. Chhabi Ram Matawale, Miss. Sanjita Jaipuria,**and **Mrs.Bijaya Bijeta Nayak**for their support and co-operation which is difficult to express in words. The time spent with them will remain in my memory for years to come. Among them, I express my special gratitude to **Dr. Manas Ranjan Singh** for his valuable adviceand assistance during the research work.

I am grateful to **Ministry of Human Resource Development (MHRD), Government of India**, for the financial support provided during my tenure of staying at National Institute of Technology, Rourkela.

My parents and **relatives** deserve special mention for their inseparable support and prayers. They are the persons who show me the joy of intellectual pursuit ever since I was a child. I thank them for sincerely bringing up me with care and love.

The completion of this work came at the expense of my long days of absence from home. Words fail me to express my appreciation to my wife **Aparna** for her understanding, patience and active cooperation throughout the course of my doctoral dissertation. I thank them for being supportive and caring.Last, but not the least, I thank the one above all of us, the omnipresent God, for giving me the strength during the course of this research work.

Chinmaya Prasad Mohanty

Abstract

Electrical Discharge Machining (EDM) finds extensive application in manufacturing of dies, molds and critical parts used in the automobile and other industries. The present study investigates the effects of different electrodes, deep cryogenic treatment of tools subjected to different soaking duration and a hybrid approach of powder mixed EDM of cryogenically treated electrodes on machinability of Inconel 718 super alloy. Inconel 718 has been used as the work material owing to its extensive application in aerospace industries. A Box–Behnken design of response surface methodology (RSM) has been adopted to estimate the effect of machining parameters on the performance measures. The machining efficiency of the process is evaluated in terms of material removal rate (MRR), electrode wear ratio (EWR), surface roughness, radial overcut and white layer thickness which are function of process variables viz. open circuit voltage, discharge current, pulse-on-time, duty factor and flushing pressure. In this work, a novel multi-objective particle swarm optimization algorithm (MOPSO) has been proposed to get the Pareto-optimal solution. Mutation operator, predominantly used in genetic algorithm, has been introduced in the MOPSO algorithm to avoid premature convergence and to improve the solution quality. To avoid subjectiveness and impreciseness in the decision making, the Pareto-optimal solutions obtained through MOPSO have been ranked by the composite scores obtained through maximum deviation theory (MDT). Finally, a thermal model based on finite element method has been proposed to predict the MRR and tool wear rate (TWR) when work piece is machined with variety of electrode materials. A coupled thermo-structural model has been also proposed to estimate the residual stresses. The numerical models were validated through experimentations. Parametric study is carried out on the proposed model to understand the influence of important process parameters on the performance measures. The study offers useful insight into controlling the machining parameters to improve the machining efficiency of the EDMed components.

Keywords: Electrical discharge machining (EDM); Deep cryogenic treatment (DCT); Powder-mixed EDM (PMEDM); Finite element analysis (FEA);Multi-objective particle swarm optimization (MOPSO);Maximum deviation theory (MDT)

CONTENTS

Chapter No	Title	Page No
	Acknowledgement	I
	Abstract	III
	Contents	iv
	List of Tables	vi
	List of Figures	vii
1	**Back ground and Motivation**	
	1.1 Introduction	1
	1.2 Principle of EDM	2
	1.3 Classification of Electrical Discharge Machining process	2
	1.4 Important process parameters of the process	4
	1.5 Important performance measures of the process	5
	1.6 Need for research	7
	1.7 Research objective	9
	1.8 Organization of Thesis	10
2	**Critical literature review**	
	2.1 Introduction	13
	2.2 Discussions	24
	2.3 Conclusions	25
3	**Assessment of influence of different tool materials on performance of the EDM process**	
	3.1 Introduction	26
	3.2 Particle Swarm Optimization	27
	3.2.1 Proposed MOPSO algorithm	28
	3.3 Solution ranking	32
	3.4 Materials	34
	3.5 Experimental strategy	38
	3.5.1 Calculation of performance measures	40
	3.6 Results and discussions	43
	3.7 Conclusions	70
4	**Study on the effect of soaking duration in deep cryogenic treatment of the tool**	
	4.1 Introduction	72
	4.2 Proposed MOPSO	73
	4.3 Solution ranking	73
	4.4 Experimental strategy and materials	74
	4.4.1 Deep Cryogenic treatment	76
	4.4.2 Microstructural analysis and X-ray diffraction analysis	78
	4.4.3 Calculation of performance measures	80
	4.5 Result and discussions	83
	4.6 Conclusions	112
5	**Performance analysis of the EDM process through the powder mixed dielectric and cryogenically treated electrodes**	
	5.1 Introduction	114
	5.2 Powder-mixed EDM	115
	5.2.1 Experimental set up	116
	5.3 Experimental strategy and materials	118
	5.3.1 Scanning Electron Microscope analysis and X-ray diffraction analysis	119
	5.3.2 Calculation of performance measures	123
	5.4 Results and discussions	125

5.5 Performance estimation of Pareto frontiers obtained through MOPSO and NSGA II 151
5.6 Conclusions 159
6 Performance assessment of EDM process through thermo-structural model
6.1 Introduction 161
6.2 Proposed Integrated process model for EDM 161
6.3 Simulation of the EDM process 162
6.3.1 Thermal modeling of the process 162
6.3.2 Assumptions in the analysis 162
6.3.3 Governing equation required for the analysis 163
6.3.4 Desired boundary conditions 163
6.3.5 Heat input required for analysis 164
6.3.6 Spark radius calculation 164
6.3.7 Discharge energy 164
6.3.8 Total discharge energy distribution 165
6.3.9 Solution methodology of thermal analysis in ANSYS software 165
6.3.10 Solution methodology for coupled thermal-structural analysis 165
6.4 Model validation through experimentation 166
6.4.1 Experimental validation of residual stress 175
6.5 Parametric study on the proposed model 177
6.5.1 Effect of discharge current on MRR, TWR and residual stress 178
6.5.2 Effect of pulse-on-time on MRR, TWR and residual stress 180
6.5.3 Effect of duty factor on MRR, TWR and residual stress 183
6.6 Conclusions 183

7 Executive summery and conclusions
7.1 Introduction 185
7.2 Summery of findings 185
7.3 Contributions of the research work 189
7.4 Limitations of the study 190
7.5 Future scope 190

Bibliography 192
List of publications 203

LIST OF TABLES

TABLE NO	CAPTION	PAGE NO
2.1	Summary of the publications referred	13
3.1	Chemical composition of the Inconel 718 sample used in the present study	36
3.2	Thermal property of Inconel 718	36
3.3	Specifications of the CNC die sinker EDM machine ECOWIN MIC-432 C	38
3.4	Process parameters and their levels	39
3.5	Box-behnken experimental design along with obtained performance measures	42
3.6	ANOVA for MRR	44
3.7	ANOVA for EWR	45
3.8	ANOVA for surface roughness	46
3.9	ANOVA for radial overcut	47
3.10	ANOVA for white layer thickness	48
3.11	Pareto optimal solution for MRR and EWR with corresponding variable setting	67
3.12	Best ranked solution for multiple objectives	69
4.1	Specification of the CNC die sinker EDM machine Electronica Elektra S50 CNC	75
4.2	Process parameters and their levels	75
4.3	Mechanical property of brass tool before and after cryogenic treatment	77
4.4	Box-behnken experimental design along with obtained performance measures	81
4.5	ANOVA for MRR	84
4.6	ANOVA for EWR	85
4.7	ANOVA for surface roughness	86
4.8	ANOVA for radial overcut	87
4.9	ANOVA for white layer thickness	88
4.10	Pareto optimal solution for MRR and EWR with corresponding variable setting	109
4.11	Best ranked solution for multiple objectives	111
5.1	Specification of the CNC die sinker EDM machine ELECTRONICA-ELECTRAPLUS PS 50ZNC	116
5.2	Properties of the tool and work piece before and after cryogenic treatment	122
5.3	Process parameters and their levels	122
5.4	Box-behnken experimental design along with obtained performance measures	124
5.5	ANOVA for MRR	126
5.6	ANOVA for EWR	127
5.7	ANOVA for surface roughness	128
5.8	ANOVA for radial overcut	129
5.9	ANOVA for white layer thickness	130
5.10	Performance metrics of Pareto frontiers	155
5.11	Pareto optimal solution for MRR and EWR with corresponding variable setting	157
5.12	Best ranked solution for multiple objectives	158
6.1	Temperature dependent material properties of Inconel 718	167
6.2	Comparison of the predicted results of the numerical analysis with experimental results from chapter 3	167
6.3	Residual stress value obtained through experimental investigation in comparison with numerical results along with machining conditions	177

LIST OF FIGURES

TABLE NO	CAPTION	PAGE NO
1.1	Die sinking EDM	3
2.1	Literature appraisal in terms of percentage	24
3.1	Crowding distance	30
3.2	X-ray diffraction plot of the Inconel 718 work material	37
3.3	CNC die sinking EDM machine (ECOWIN PS 50ZNC) on experimental set up	39
3.4	Wok material Inconel 718 after machining with three electrodes	40
3.5	SEM Micrograph showing micro cracks and pores on the machined surface atA=80V B=3A C=100µs D=85% E=0.4bar F=copper electrode	50
3.6	SEM Micrograph showing micro cracks and pores on the machined surface at A=80V B=7A C=100µs D=85% E=0.4bar F=copper electrode	50
3.7(a)	SEM Micrograph showing white layer on the cross section of machined surface at A=80V B=5A C=100µs D=80% E=0.3bar F=Brass tool	51
(b)	SEM Micrograph showing white layer on the cross section of machined surface at A=80V B=5A C=200µs D=85% E=0.3bar F=copper tool	52
(c)	SEM Micrograph showing white layer on the cross section of machined surface at A=80V B=5A C=300µs D=90% E=0.3bar F=Graphite tool	52
3.8	Surface plot of MRR with Discharge current and open circuit voltage	53
3.9	Surface plot of MRR with discharge current and tool material	54
3.10	Surface plot of MRR with pulse-on-time and tool material	55
3.11	Surface plot of MRR with duty factor and tool material	55
3.12	Surface plot of EWR with discharge current and tool material	56
3.13	Surface plot of EWR with pulse-on-time and open circuit voltage	57
3.14	Surface plot of surface roughness with tool material and discharge current	58
3.15	Surface plot of surface roughness with tool material and pulse-on-time	59
3.16	Surface plot of radial overcut with tool material and discharge current	60
3.17	Surface plot of radial overcut with tool material and pulse-on-time	60
3.18	Surface plot of white layer thickness with discharge current and tool material	61
3.19	Surface plot of white layer thickness with pulse-on-time and tool material	62
3.20	Pareto front objectives for MRR and EWR	66
4.1	CNC EDM machine (Electronica Elektra S50 CNC)	74
4.2	Cryogenic freezer PLANER Kryo 560-16	77
4.3	Graphical representations of deep cryogenic treatment and two stage tempering process for both the cycle	77
4.4	Microstructures of three electrode samples used in the study	
(a)	Untreated brass	78
(b)	Cryogenic-treated brass with soaking duration 24-hrs	79
(c)	Cryogenic-treated brass with soaking duration 36-hrs	79
4.5	Work materials after machining with three brass electrodes	81
4.6	SEM images of tool tip	
(a)	Untreated Brass	90
(b)	Cryogenic-treated electrode with soaking duration of 24-hrs	90
(c)	Cryogenic-treated electrode with soaking duration of 36-hrs	91
4.7	SEM images of the machined surface of the work piece	
(a)	SEM micrograph at A=80V, B=5A, C=300µs, D=80%, E=0.3bar, F=0-hrs	92
(b)	SEM micrograph at A=80V, B=5A, C=300µs, D=80%, E=0.3bar, F=36-hrs	92
4.8	SEM micrograph showing white layer at on the cross section of the machined surface	
(a)	Micrograph at A=70V B=3A C=200µs D=80% E=0.3bar F=24 hrs	93
(b)	Micrograph at A=70V B=7A C=200µs D=80% E=0.3bar F=24 hrs	94
4.9	SEM micrograph showing white layer on the cross section of the machined surface	
(a)	Micrograph at A=80V B=5A C=100µs D=80% E=0.3bar F=0 hrs	95
(b)	Micrograph at A=80V B=5A C=100µs D=80% E=0.3bar F=36 hrs	95

4.10	Surface plot of MRR with open circuit voltage and discharge current	96
4.11	Surface plot of MRR with pulse-on time and discharge current	97
4.12	Surface plot of EWR with discharge current and soaking duration	98
4.13	Surface plot of EWR with Duty factor and pulse-on-time	99
4.14	Surface plot of surface roughness with discharge current and soaking duration	100
4.15	Surface plot of surface roughness with pulse-on-time and soaking duration	100
4.16	Surface plot of radial overcut with discharge current and soaking duration	101
4.17	Surface plot of radial overcut with duty factor and pulse-on-time	102
4.18	Surface plot of white layer thickness with soaking duration and discharge current	103
4.19	Surface plot of white layer thickness with pulse-on-time and soaking duration	104
4.20	Pareto front objectives for MRR and EWR	108
5.1	PMEDM experimental set up	
(a)	PMEDM experimental set up (Front view)	117
(b)	PMEDM experimental set up (Top view)	118
5.2	Microstructure of brass electrodes samples used in the present study	
(a)	Untreated brass	120
(b)	Cryogenic treated brass	120
5.3	Microstructure of work piece Inconel 718 samples used in the present study	
(a)	Untreated Inconel 718	121
(b)	Cryogenic treated Inconel 718	121
5.4	Three combinations of work-tool pair after machining	123
5.5	SEM images of the machined surface of the work piece	
(a)	SEM micrograph at A=80V, B=7A, C=200µs, D=85%, E=0gm/liter, F= NW-TT	132
(b)	SEM micrograph at A=80V, B=7A, C=200µs, D=85%, E=4gm/liter, F= NW-TT	132
5.6	SEM images of the machined surface of the work piece	
(a)	SEM micrograph at A=80V, B=5A, C=300µs, D=80%, E=2gm/liter, F= NW-TT	133
(b)	SEM micrograph at A=80V, B=5A, C=300µs, D=80%, E=2gm/liter, F= TW-TT	133
5.7	SEM micrograph showing white layer on the cross section of the machined surface	
(a)	SEM micrograph at A=80V, B=7A, C=200µs, D=85%, E=0gm/liter, F= NW-TT	134
(b)	SEM micrograph at A=80V, B=7A, C=200µs, D=85%, E=4gm/liter, F= NW-TT	134
5.8	SEM micrograph showing white layer on the cross section of the machined surface	
(a)	SEM micrograph at A=80V, B=5A, C=300µs, D=80%, E=2gm/liter, F= NW-TT	135
(b)	SEM micrograph at A=80V, B=5A, C=300µs, D=80%, E=2gm/liter, F= TW-TT	135
5.9	Surface plot of MRR with discharge current and open circuit voltage	136
5.10	Surface plot of MRR with discharge current pulse-on-time	137
5.11	Surface plot of MRR with powder concentration and work-tool pair	138
5.12	Surface plot of EWR with open circuit voltage and discharge current	139
5.13	Surface plot of EWR with powder concentration and work-tool pair	140
5.14	Surface plot of EWR with discharge current and pulse-on-time	141
5.15	Surface plot of EWR with discharge current and pulse-on-time	141
5.16	Surface plot of surface roughness with discharge current with powder	142

	concentration	
5.17	Surface plot of surface roughness with discharge current and work-tool pair	143
5.18	Surface plot of radial overcut with discharge current and pule-on-time	144
5.19	Surface plot of radial overcut with powder concentration and work-tool pair	145
5.20	Surface plot of white layer thickness with discharge current and pulse-on-time	146
5.21	Surface plot of white layer thickness with powder concentration and work-tool pair	147
5.22	Pareto front for objectives MRR and EWR	151
5.23	Pareto front for objectives MRR and Surface roughness	152
5.24	Pareto front for objectives MRR and Radial overcut	152
5.25	Pareto front for objectives MRR and white layer thickness	153
6.1	Proposed integrated process model for EDM	162
6.2	An axi-symmetric two dimensional model for the EDM process analysis	163
6.3	Wave form of current for a single discharge	165
6.4	Predicted crater of MRR 5.25 mm^3/min at open circuit voltage 80V, discharge current 5 A, pulse-on-time 300µs, duty factor 80% flushing pressure 0.3 bar machined with brass tool for 18^{th} reading	169
6.5	Predicted crater of MRR 38.1 mm^3/min at open circuit voltage 70V, discharge current 5 A, pulse-on-time 300µs, duty factor 90% flushing pressure 0.2 bar machined with copper tool for 27^{th} reading	169
6.6	Predicted crater of MRR 45 mm^3/min at open circuit voltage 80V, discharge current 5 A, pulse-on-time 100µs, duty factor 90% flushing pressure 0.3 bar machined with graphite tool for 23^{th} reading	169
6.7	Predicted TWR of 9 mm^3/min at open circuit voltage 80V, discharge current 7A, pulse-on-time 200µs, duty factor 85%, flushing pressure 0.2 bar, brass tool for 34^{th} reading	170
6.8	Predicted TWR of 6.1 mm^3/min at open circuit voltage 90V, discharge current 7A, pulse-on-time 200µs, duty factor 80%, flushing pressure 0.3 bar, copper tool for 4^{th} reading	170
6.9	Predicted TWR of 3.98 mm^3/min at open circuit voltage 80V, discharge current 7A, pulse-on-time 200µs, duty factor 85%, flushing pressure 0.2 bar, graphite tool for 38^{th} reading	170
6.10	Thermal stress directly after heat flux in radial direction at open circuit voltage 90V, discharge current 7A, pulse-on-time 200µs, duty factor 80%, flushing pressure 0.3 bar, copper tool for 4^{th} reading	171
6.11	Thermal stress directly after heat flux in circumferential direction at open circuit voltage 90V, discharge current 7A, pulse-on-time 200µs, duty factor 80%, flushing pressure 0.3 bar, copper tool for 4^{th} reading	171
6.12	Residual thermal stress in radial direction at open circuit voltage 90V, discharge current 7A, pulse-on-time 200µs, duty factor 80%, flushing pressure 0.3 bar, copper tool for 4^{th} reading	172
6.13	Residual thermal stress in circumferential direction at open circuit voltage 90V, discharge current 7A, pulse-on-time 200µs, duty factor 80%, flushing pressure 0.3 bar, copper tool for 4^{th} reading	172
6.14	Predicted residual thermal stress of 1660 M Pa in radial direction at open circuit voltage 80 V, discharge current 5 A, pulse-on-time 300µs, duty factor 80% flushing pressure 0.3 bar machined with brass tool for 18^{th} reading	173
6.15	Predicted residual thermal stress of 1800 M Pa in radial direction at open	173

	circuit voltage 70 V, discharge current 5 A, pulse-on-time 200µs, duty factor 90% flushing pressure 0.2 bar machined with copper tool for 27th reading	
6.16	Predicted residual thermal stress 1920 M Pa in radial direction at open circuit voltage 80V, discharge current 7 A, pulse-on-time 200µs, duty factor 85% flushing pressure 0.2 bar machined with graphite tool for 38th reading	174
6.17	X-ray Diffraction machine BRUKER D8 Discover	
(a)	X-ray Diffraction machine BRUKER D8 Discover	175
(b)	Work material Inconel 718 on Experimental set up	176
6.18	Strain Versus $Sin^2\psi$ plot	176
6.19	X-ray diffraction peak of Inconel 718 at different ψ angles	177
6.20	Variation of MRR with discharge current	178
6.21	Variation of TWR with discharge current	178
6.22	Variation of residual stress with discharge current	179
6.23	Variation of crater radius with discharge current	180
6.24	Variation of crater depth with discharge current	180
6.25	Variation of MRR with pulse-on-time	181
6.26	Variation of residual stress with pulse-on-time	181
6.27	Variation of TWR with pulse-on-time brass tool	182
6.28	Variation of crater radius with pulse-on-time	182
6.29	Variation of crater depth with pulse-on-time	183

CHAPTER 1

BACKGROUND AND MOTIVATION

1.1 Introduction

In 1770, English physicist, Joseph Priestley observed the erosive effect of electrical discharges which is used in today's Electrical Discharge Machining (EDM) process. Therefore, he may be considered as the pioneer of EDM process. But the process was not popular for a long period due to poor command over controlled machining. In 1943, two Russian scientists, B.R Lazarenko and N.I Lazarenko were working on prevention of erosion of tungsten electrical contacts due to sparking. Though they did not exactly succeed in the task but found that erosion can be more precisely controlled if the electrodes were immersed in a dielectric fluid. This led them to invent an EDM machine used for working on difficult-to- machine electrically conductive materials irrespective of its strength and shape. EDM is capable of machining geometrically complex components made of hard materials such as heat treated tool steels, composites, super alloys, ceramics, hastelloys, carbides, heat resistant steels etc. Now-a-days, EDM is being extensively used in die and mold making, aerospace and nuclear industries. The process is also used in fields such as medical and surgical instrument, manufacturing and automotive industries (Mohanty et al. 2013; Pradhan and Biswas 2010;Joshi and Pande 2009). In mid 1980s, EDM techniques became common after incorporation of computer numerical control (CNC) into the EDM machine. With due course of time and continuous process development, advanced EDM machines have become so proficient that they can work round the clock under supervision of an adaptive control system (Kumar et al. 2009). Later on, the growing benefits of EDM were closely looked by the manufacturing industries in the hunt for massive economic benefits and generating keen research interests.

In EDM, there is no mechanical contact between the tool and work material. However, small volume of material is repeatedly eroded from the work piece through a series of spark discharges. The ability of the process to machine difficult-to-machine materials and generate intricate part shapes within tighter tolerances makes the process distinctive among the non-conventional machining process. Toughened and high strength-to-weight ratio electrically conductive alloys and super alloys can be easily machined in EDM (Lee and Li 2001; Ho and Newman 2003).Now-a-days, EDM has become an established technology and frequently used in manufacturing industries to produce complex part shapes. However, its low machining efficiency, poor surface quality and dimensional accuracy of the machined surface are the major concerns for the tool engineers. Hence, the research and innovations woks are still in progress to improve the machining efficiency.

1.2 Principle of EDM Process

Electric discharge machining (EDM) works on the principle of conversion of electrical energy into thermal energy through a series of repetitive spark discharges occurring between the electrodes immersed in a dielectric fluid separated by a constricted spark gap. Owing to localized melting and evaporation, material is removed from the work surface and the molten material is flushed away from the spark gap by continuous flow of dielectric fluid. When the electrode moves towards the work material, the electric field within the spark gap increases and causes the breakdown of the dielectric fluid. The voltage falls and the current rises sharply shortly after the breakdown of the dielectric fluid. The dielectric fluid is ionized and a plasma channel is created between the electrodes. The plasma channel expands due to constant exchange of ions and electrons. This phenomenon leads to constant heating on the work material causing a local temperature rise in the order of $8,000^0$C to $12,000^0$C (Boothroyd and Winston1989). As a result, melting and evaporation takes place from both the electrodes and small molten metal pool is formed. The molten metal pool is removed by continuous flushing of dielectric fluid and a tiny crater cavity is produced on the work surface. The series of spark discharges successively removes material in form of debris and the molten material between the electrodes is removed through continuous dielectric flushing during machining. In this manner, numerous spark discharges takes place on the work surface and consequently, the replica of the tool material is transferred on to the work surface.

1.3 Classifications of Electric Discharge Machining

Depending up the requirement and application of the industries, EDM can be classified into different types such as (a) Die Sinking EDM (b) Wire EDM (c) Micro-EDM and (d) Electric Discharge Grinding (EDG)

(a) Die Sinking EDM:

In die sinking EDM, electrode and work material are submerged in an insulating dielectric fluid. The schematic diagram of a die sinker is shown in Figure 1.1.Pulse power is provided from a separate power supply unit in which both tool and work piece form a pair of conductive electrodes. Initially, resistance-capacitance type (R-C) circuit was used in these types of EDM machines but later on they are replaced by metal oxide semiconductor field effect transistor (MOS-FET) technology (Padhan 2010). A servo motor controller tool holder is used to maintain an inter-electrode gap between the tool and work piece during machining. The machining tank is provided with a pump, filter and

dielectric storage tank for suitable flushing action of the dielectric fluid from inter-electrode gap. The electrode material has the complementary shape of the finished product and accurately drops into work surface to produce complicate part shapes. The process finds extensive application in aerospace, automobile, die and mold making industries and many other industrial applications.

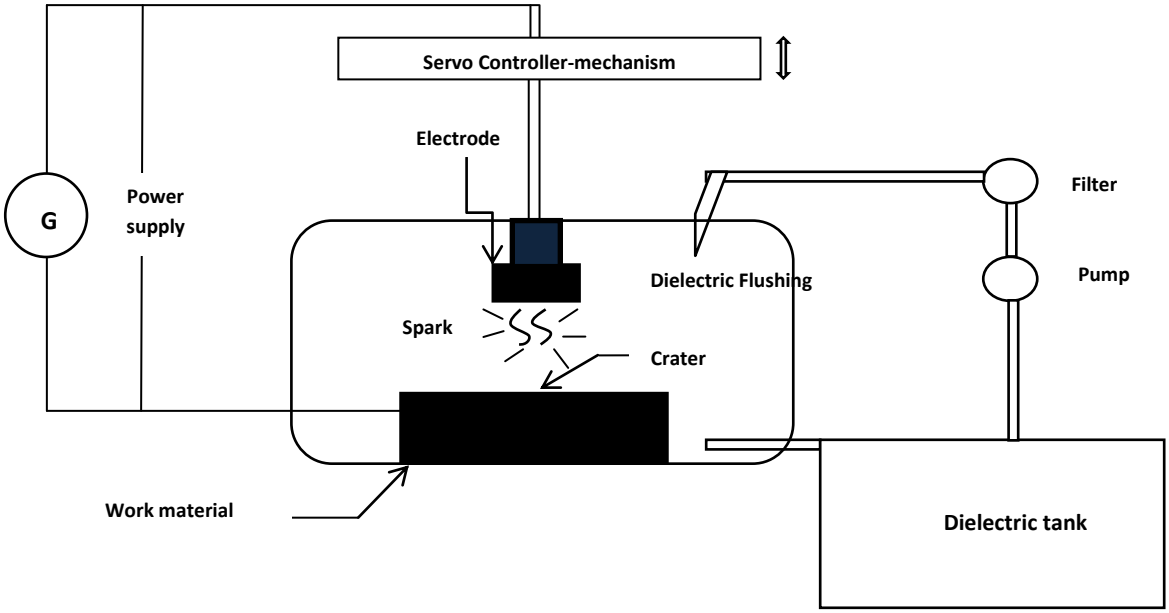

Figure 1.1 Die-sinking EDM

(b) Wire-EDM:

A thin continuous wire of diameter 0.02 to 0.40 mm is used as the electrode material which continuously wound round a number of pulleys. The wire is usually made of brass or copper. The work piece is cut by virtue of spark discharges occurring between the wire and the work piece. The wire continuously moves through the surface to be machined and new wire is being fed from the pulleys. The process is precise and accurate having machining accuracy up to ±0.0025mm. It is frequently used to produce intricate aerospace and automobile parts.

(c) Micro-EDM:

In Micro-EDM operation, micro-electrodes (usually of diameters range from 5 to 10 μm) are used to produce micro-holes on the work piece. In this operation, different techniques and devices can be used to help handling and manipulating small electrodes and parts. The process is quite capable of producing intricate three-dimensional shapes and manufacturing of tooling inserts for micro-injection molding (Rajurkar and Yu 2000). The process finds extensive application in the manufacturing of micro parts for

accelerometer, micro mold and dies, keyhole surgery, housings for micro-engines and also tooling inserts for fabrication of micro-filters, housings and packaging solutions for micro-optical and micro fluidics devices.

(d) Electric Discharge Grinding:

The stationary electrode used for machining in EDM is replaced with rotating electrode in EDG. The material removal in EDG process is quite similar as EDM. The process uses, an electrically conductive wheel as a tool electrode instead of stationary tool electrode employed in EDM. The process is quite suitable for machining electrically conductive hard materials and fabrication of micro electrodes.

1.4 Important Process parameters of the process

Some of the important process parameters significantly influencing performance measures in EDM are outlined as follows:

Discharge current: Discharge current is the most dominant process parameter as it directly governs the spark energy. The maximum amount of amperage that can be used is governed by the surface area of the cut for a work piece-tool combination. Higher value of discharge current results in higher material removal but in turn produces numerous adverse effects on the machined surface and increases the machining cost by rapid tool wear. It is measure in terms of Ampere.

Open circuit voltage: The Voltage which is applied between the electrodes is called as open circuit voltage. Prior to the flow of current, the open circuit voltage de-ionizes the dielectric medium which depends upon the electrode gap and the strength of the dielectric fluid. The open circuit voltage falls and stabilizes the inter-electrode gap when the current flow starts. It is an important parameter which significantly affects the spark energy and performance measures. It is measured in terms of Volt.

Pulse-on-time: The interval for which the total discharge energy is to be applied on the work surface is called as pulse-on-time. It is an important process parameter in EDM process as it decides the spark duration. It is measured in terms of micro seconds.

Pulse-off-time: Pulse-off-time is also called as pause time during which the spark energy supply is paused and after this duration next spark will occur. During pulse-off-time, flushing of debris takes place. The sum of pulse-on-time and pulse-off-time in a cycle is called pulse period or total spark time. It is also measured in terms of micro second.

Duty cycle or duty factor: The important process parameter which controls the number of sparks per unit time is duty factor. It is defined as the ratio of pulse-on-time to total spark

time. Higher values of duty factor imply increase in number of sparks per unit time. It is expressed in terms of percentage. Mathematically defined as,

$$\text{Duty Factor} = \frac{T_{on}}{T_{on} + T_{off}} \quad (1.1)$$

where T_{on} and T_{off} are the pulse-on-time and pulse-off-time respectively.

Polarity: The potential of the work material with respect to tool is called as polarity. Polarity may be of two types i.e. straight or positive polarity and reverse polarity or negative polarity. In positive polarity, the work material is positive whereas in reverse polarity work material is negative.

Inter electrode gap: The inter electrode gap is an important factor for spark stability and good dielectric flushing. The tool servo controller mechanism is used for maintaining working gap between the electrodes. Mostly electro mechanical (DC or stepper motors) and electro hydraulic systems are employed to respond to average gap voltage.

Dielectric fluid and flushing Pressure: The function of dielectric fluid is to flush away the debris from the machined surface and to cool the electrodes after spark discharges during machining. If the crater is deeper, flushing becomes difficult. Improper flushing may cause arcing problems and may deposit unwanted debris on the machined surface which can destroy the surface integrity of the work material. Therefore, proper flushing on the machined surface is vital. Most commonly used dielectric fluids are transformer oil, paraffin oil, kerosene and hydrocarbon compounds. It is measure in terms of bar or kgf /cm^2.

1.5 Important performance measures of the process

This section describes some of the important performance measures of the process. The most extensively considered regular performance measures are (i) Material removal rate (MRR), (ii) Electrode wear ratio (EWR), (iii)Surface roughness, (iv) Radial over cut and (v) White layer thickness

(i) Material removal rate (MRR): The average weight of material removed from work piece per unit time during machining is called as material removal rate. It is the most important performance measure as it directly determines the machining efficiency of the process. The material removal is directly related to spark energy. Higher the spark energy, higher the material removed from the machined surface but it turn has numerous adverse effect on the machined surface like decreasing the surface quality, dimensional accuracy and formation of recast layer on the machined surface. Hence, a stable machining process and optimal parametric setting is required to achieve higher MRR along with acceptable value of tool

wear and machined surface quality. It generally measured in terms of mm^3/min. Mathematically it can be expressed as

$$MRR = \frac{1000 \times \Delta W_w}{\rho_w \times T} \quad (1.2)$$

where ΔW_w is the work material weight loss during machining, ρ_w is the density of work material, T is the machining time and MRR is the material removal rate.

(ii)Electrode wear ratio (EWR):For precise and cost effective machining, it is essential to identify and estimate the changes those are taking place within tool material. The tool material life plays an important role in increasing productivity and subsequently, is an important economic aspect of the process. High wear rate of electrode material leads to interruption during machining which in turn increases machining time and declines productivity of the process by increasing the machining cost. Therefore, a good tool material should have high electrical conductivity to exhibit low tool wear rate. The average weight of the material eroded from tool per unit time during machining is called as tool wear rate (TWR). The process is quite similar to material removal rate as the tool and work material are considered as a set of electrodes in EDM. It is also measured in terms of mm^3/min.

Electrode wear ratio is defined as ratio of weight of material removed from tool material per unit time to weight of material removed from work piece per unit time. It is generally expressed in terms of percentage.

$$TWR = \frac{1000 \times \Delta W_t}{\rho_t \times T} \quad (1.3)$$

$$EWR = \frac{100 \times TWR}{MRR} \quad (1.4)$$

where ΔW_t is the tool weight loss during machining and ρ_t is the density of tool material.

(iii)Surface roughness: In EDM, the fatigue strength of the machined component is highly influenced by the machined surface quality. The surface quality of the machined surface is highly dependent on the energy per spark and dimension of craters. Higher the spark energy, larger is the formation of craters. As a result, the machined surface quality produced becomes poor. Generally, the surface quality of the machined surface is measured with a precision surface roughness tester. It is measured in terms of micrometer.

(iv) Radial overcut: Overcut or radial overcut is common in EDMed components. It refers to the deviation between the maximum diameter of crater cavity and diameter of the tool. For

precise and accurate machining, minimization of radial over cut is vital. It is measured in terms of mm.

(v)White layer thickness: There is an increase demand of fine surface finish and better surface integrity in manufacturing industries. The machined surface of EDM is comprised of three different layers viz. white layer or recast layer, heat affected zone (HAZ) and unaffected parent metal (Lee et al. 1988; Lee et al. 1990). The recast layer is formed due to improper flushing of molten metal pool by the dielectric and solidified on the machined surface after cooling. The layer is so heavily infiltrated with carbon that it is totally different from parent metal. The layer is composed of mainly retained austenite and martensite with some dissolved carbide. Formation of recast layer severely damages the surface integrity of the machined surface quality, increasing number of cracks and voids on the machined surface. Therefore, it is vital to find the optimum parametric setting which will minimize formation of recast layers on the machined surface to achieve better surface quality. It is measured in terms of micron.

1.6 Need for research

Alloys and super alloys find extensive applications in aerospace, automobile, chemical plant, power generation, oil and gas extraction, surgical instruments and other major industries due to their favorable characteristics such as high strength-to-weight ratio and corrosion resistance. Machining of such alloys by conventional machining processes using traditional tool materials becomes difficult due to their poor thermal diffusivity resulting in high temperature at tool tip and tendency to weld to the cutting tool. However, machining of such super alloys, composites and ceramics can be easily carried out by non-conventional machining process like electrical discharge machining (EDM). Meanwhile, EDM has been the backbone of manufacturing hub since more than six decades possessing the capability to machine hard and difficult-to-machine materials to required shape, size and dimensional accuracy.

The material removal, surface quality and dimensional accuracy of the machined surface on the work material are exactly related to the amount of spark energy used to erode material during machining. Increase in spark energy significantly improves the material removal but simultaneously creates numerous adverse effect such as increasing cracks, pores, heat affected zones (HAZ) and inducing residual stresses on the machined surface. Owing to the complex nature of the process involving the physics of series of spark discharges, it is difficult to observe the process experimentally and find suitable parametric

setting to improve machining efficiency. Thus, the low machining efficiency, poor surface finish and dimensional accuracy of the machined surface may limit its further applications. Therefore, innovations and research woks are still in progress to enhance the performance measures of the process. Extensive review of literature suggests that following literature gap must be addressed to provide quick solution for the tool engineers.

Past research work reports on working with work pieces made of tool steel, metal-matrix composites, conductive ceramics and titanium alloys. However, attempt has not been made to machine a relatively low conductive material like Inconel 718 which has a diversified application in aerospace engineering. Inconel 718, an aerospace material, has abundant usage in manufacturing of components for liquid fuled rockets, rings and casings, sheet metal parts for aircraft, land-based gas turbine engines, cryogenic tank fasteners and instrumentation parts. In spite of significant research done in the field of EDM, influence of use of variety of electrode tools on the machining efficiency of the process has not been adequately addressed. Deep cryogenic treatment of electrodes in EDM can enhance electrical, thermal and mechanical property of the electrodes due to micro-structural changes which results in improved machining characteristics (Kumar et al. 2012; Jafferson and Hariharan 2013; Kapoor et al. 2012; Gill and Singh 2010). Amongst the important parameters (cooling rate, soaking temperature, soaking duration and heating rate) involved in cryogenic treatment of materials, soaking duration happens to be most significant (Jaswin and Lal 2010; Collins and Dormer 1997). Therefore, studies on effect of soaking duration on the machining characteristics of EDM can immensely help the tool engineers to manufacture intricate parts with greater ease and accuracy within tight tolerances.It has been established that presence of electrically conductive suspended ceramic/metallic powder particles in the dielectric fluid causes to reduce the insulating strength of the dielectric fluid and increase the gap between the electrodes. As a result, the process becomes more stable; thereby improving material removal rate and surface finish (Padhee et al.2012; Wong et al.1998; Ming and He 1995; Chow et al. 2000). However, no attempt has been made to combine the benefit of both powder mixed EDM and deep cryogenic treatment of electrodes. Moreover, emphasis must be laid on finding best parametric combination in the machining process of EDM, cryo-treated EDM and combined powder mixed EDM and cryo-treated electrodes using different tool electrodes and relatively low conductive work piece like Inconel 718. Since the process is complex one and various process parameters and their interaction influence performance measures in a stochastic manner, predictive models need to be developed using statistical approach. Once the models are developed and statistically

validated, they can be used as objective functions in recently proposed nature inspired optimization algorithms to explore the optimization landscape in an effective manner to suggest best parametric combination. The objective must not be limited to optimization of a single performance measure; rather it should be extended to simultaneously optimize several performance measures. Further, numerical models need to be developed to analyse the EDM process and compared with experimental results.There exists a vast scope for application of nature inspired algorithms viz. Genetic algorithm (GA), particle swarm optimization (PSO), Cuckoo search etc. for optimization of the important performance measures of the process.

1.7 Research objective

The major performance measure of the EDM process are material removal rate (MRR), electrode wear rate (EWR), surface quality and dimensional accuracy of the machined surface. For cost effective machining, it is essential to identify and estimate the changes those are taking place within electrode materials. The electrode material life plays an important role in increasing productivity and subsequently, is an important economic aspect of the process. High wear rate of electrode material leads to interruption during machining which in turn increases machining time and declines productivity of the process by increasing the machining cost. Therefore, it is utmost important to have higher material removal and minimal tool wear to enhance productivity of the process and also better surface quality during machining. To understand the effect of important parameters on the performance measures, modeling of the process is vital.

The objectives of this dissertation rest on study of the effect of control parameters during machining of Inconel 718 super alloy in EDM process. The study will help the tool engineers to reduce the experimental cost and errors associated with the process and optimize the process by setting the requisite parameters. To this end, the following objectives are set for this research work.

1. To assess the influence of different tool materials on performance of the EDM process.
2. To study the effect of soaking duration in deep cryogenic treatment of electrodes in the EDM process.
3. To analyze the performance of the process through the hybrid approach of conductive ceramic powder mixed in dielectric and cryogenically treated electrodes.
4. To propose a thermo-structural model for improving prediction accuracy of performance measures.

5. To optimize the process parameters for best performance output using nature inspired algorithms.

To meet the above objectives, the thesis is organized into seven chapters including

1.8 Organization of Thesis

Chapter 1: Background and motivation

This chapter introduces the concept of EDM including working principles and basic applications. This chapter provides the justification, motivation and need for present research work.

Chapter 2: Critical literature review

The purpose of this chapter is to review related literature so as to provide background information on the issues to be considered in the thesis and emphasize the relevance of the present study. The chapter provides a summary of the base knowledge already available about EDM process. Finally, the chapter is concluded by summarizing a strong conclusion from the existing literatures and identifying the possible literature gap so as to relevance of the present study can be emphasized.

Chapter 3: Assessment of influence of different tool materials on performance of the EDM process

This chapter proposes an experimental investigation on machinability of Inconel 718 super alloy in EDM process in which the performance characteristics are measured in terms of material removal rate (MRR), electrode wear ratio (EWR), surface roughness, radial overcut and white layer thickness under the influence of process variables viz. open circuit voltage, discharge current, pulse-on-time, duty factor, flushing pressure and electrode material. The experiments are planned as per Box–Behnken design of response surface methodology (RSM) approach to obtain maximum information with limited number of experimental runs. Optimal parametric combination is found out using a proposed multi-objective particle swarm optimization (MOPSO) algorithm. However, MOPSO results in a large number of non-dominated solutions. Therefore, maximum deviation theory (MDT) proposed by Wang (1998) has been adopted for ranking the solution to ease the decision making process of choosing the best solution

Chapter 4: Study on the effect of soaking duration in deep cryogenic treatment of the tool

This chapter investigates the effect of deep cryo-treated (-196^0 C) brass electrodes subjected to different soaking durations on the machinability of Inconel 718 work material.

The machining performance of the process are evaluated in terms of material removal rate, electrode wear ratio, surface roughness, radial overcut and white layer thickness which are function of process variables viz. open circuit voltage, discharge current, pulse-on-time, duty factor, flushing pressure and cryogenic treatment soaking duration of electrodes. The experimental architecture is planned as per Box-Behnken design of response surface methodology. An evolutionary multi-objective particle swarm optimization algorithm has been proposed for simultaneous optimization of performance characteristics. Application of MOPSO results in a large number of non-dominated solutions. The best solution has been identified from a large number of non-dominated solutions using maximum deviation theory.

Chapter 5: Performance analysis of the EDM process through the powder mixed dielectric and cryogenically treated electrodes

This chapter compares the machining efficiency of different cryo-treated (-196^0 C) work-tool pair Inconel 718 super alloy and brass electrode in the presence of suspended fine graphite powder particles with an objective to enhance the machining efficiency and fulfill the requisite of minimum surface damage. The machining efficiency of the process has been evaluated in terms of material removal rate (MRR), electrode wear ratio (EWR), surface roughness, radial overcut and white layer thickness which are function of process parameters viz. open circuit voltage, discharge current, pulse-on-time, duty factor, concentration of fine graphite powder and cryogenically treated work-tool pair.Multi-objective particle swarm optimization technique is used with the goal of finding approximations of the optimal Pareto front and compared with non-dominated sorting genetic algorithm II (NSGA-II) in terms of four performance metrics. To avoid subjective-ness and impreciseness in the decision making, the Pareto-optimal solutions obtained through MOPSO have been ranked by the composite scores obtained through maximum deviation theory.

Chapter 6: Performance assessment of EDM process through thermo-structural model

This chapter proposes a thermal model based on finite element method to predict the MRR and TWR for three types of tool materials such as brass, copper and graphite using Inconel 718 as work piece material. A coupled thermo-structural model has been also proposed to estimate the residual stresses. The numerical models are experimentally validated. The data are collected from the models using a response surface methodology. Parametric analysis is carried out on the proposed model to investigate the effect of important process parameters on the performance measures. Finally, a non-dominated

sorting genetic algorithm (NSGA) has been proposed for obtaining optimal process parameters.

Chapter 7: Executive summery and conclusions

This chapter presents the summary of the results, recommendations and scope for future work in the direction of EDM process. It also discusses the specific contributions made in this research work and the limitations there in. This chapter concludes the work covered in the thesis with implications of the findings and general discussions on the area of research.

CHAPTER 2

LITERATURE REVIEW

2.1 Introduction

Currently manufacturing industries face the difficulties in reduction of process time and enhancement of performance through optimization of controllable process parameter using distinctive optimization strategy. This can be addressed through exhaustive experimentation or development of model obtained from experimental analysis. Although various studies have been reported till date for performance enhancement of EDM process, suitable selection of machining parameters for achieving improved machining efficiency is still a challenging job. In this direction, the current chapter provides details of the various research activities reported until now explaining the outcome of important process parameters on performance measurers on EDM. Literature review initiates with papers published after 1995 with maximum attention was paid to articles published between 2005 and 2015. Table 2.1 provides the name of the source and number of citations from each source. The majority of the citations are found in peer-reviewed journals.

Table 2.1 Summery of the publications referred

Source	Citation
Advanced Engineering Informatics	1
Applied Mathematical Modelling	1
Applied Soft Computing	1
Computer and Mathematics with Applications	1
Engineering Applications of Artificial Intelligence	1
European Journal of Operational Research	1
Evolutionary Multi-criterion Optimization	1
Genetic and Evolutionary Computation	1
IEEE Congress on Evolutionary Computation	1
IEEE Transactions on Evolutionary Computation	1
IEEE Transactions on Magnetics	1
IEEE Transactions on Power system	1
Information Sciences	1
Indian Journal of Engineering and Materials Sciences	1
International Journal of Advanced Manufacturing Technology	14
International Journal of Advanced Engineering Sciences and Technologies	1
International Journal of Advanced Technology and Engineering Research	1
International Journal of Mathematical, Physical and Engineering Sciences	1
International Journal of Mechanical and Aerospace Engineering	1
International Journal of Machine Tools and Manufacture	8
International Journal of Machining and Machinability of Materials	5
International Journal of Manufacturing Technology and Management	1
International Journal of Mechatronics and Manufacturing Systems	2
International Journal of Production Research	1
International Journal of Refractory Metals and Hard Materials	1
Journal of Intelligent Manufacturing	2
Journal of Manufacturing Processes	2
Journal of Materials Processing Technology	27
Journal of Mechanical Science and Technology	2
Journal of Safety Engineering	1
Japan Society of Mechanical Engineers International Journal Series C	1
Journal of Zhejiang University Science	1

Materials and Design	1
Mathematical and Computer Modeling	1
Materials and Manufacturing Processes	11
Measurement	1
Proceedings of IEEE International Conference on Neural Network	1
Proceedings of the 2003 IEEE Swarm Intelligence Symposium	1
Proceedings of the 2005 Conference on Genetic and Evolutionary Computation	2
Proceedings of the International Multi-Conference of Engineers and Computer Scientists	1
Proceedings of the Institution of Mechanical Engineers, Part B:Journal of Engineering Manufacture	3
Proceedings of the Institution of Mechanical Engineers, Part C: Journal of Mechanical Engineering Science	1
Proceedings of the 60th World Academy of Science, Engineering and Technology	1
Robotics and Computer Integrated Manufacturing	1
Sadhana	1
Surface and Coatings Technology	1
Engineering and Technology	1
Total	113

The literature review provides ample confidence to identify an appropriate gap or methodological weaknesses in the existing study area to solve the research problem. The research papers on EDM are principally classified into following five groups such as (1) Theoretical Model, (2) Numerical Model, (3) Statistical Model, (4) Soft Computing Model and (5) Technological Modification of EDM process.

(1) Theoretical model

Singh and Ghosh (1999) have proposed a theoretical thermo-electric model which provides estimation of the electrostatic force and the stress distribution inside the metal during a discharge. They have concluded that the major cause of material removal for short pulses is the electrostatic force and melting becomes the primary phenomenon for long pulses. The researchers have also concluded that the crater depth is proportional to square root of discharge current for short pulses. Marafona and Wykes (2000) have studied the effect of carbon which has migrated from the dielectric to tungsten-copper electrodes which leads to the development of a two-stage EDM machining process. Significant improvement on material removal rate at given tool wear ratio is observed when different EDM settings are used. Chen and Mahdivian (2000) have proposed a model to estimate the material removal rate and surface quality of the machined surface. Theoretical models have been proposed to compute the material removal rate and maximum peak-to-valley distance of the work material. Experimental investigation is carried out to investigate the variation of

performance measures with parameters such as discharge current, pulse duration time and interval time. Good agreement between theoretical and experimental result is observed. Yadav et al. (2000) have proposed a finite element based model to predict thermal stress fields in high speed steel (HSS) work material. The effect of various process parameters such as discharge current and duty factor on temperature distribution and thermal stress distribution have been extensively studied. It is observed that substantial compressive and tensile stresses develop in a thin layer around the spark location after one spark. It is also noticed that the thermal stresses go beyond the yield strength of the work piece in an extremely thin zone near the spark location. Marafona and Chousal (2006) have proposed a model based on Joule heating effect in the dielectric using the finite element analysis (FEA) to predict the material removal and tool wear along with the temperature distribution of the electrodes while machining iron with copper electrode. Hargrove and Ding (2007) have proposed a theoretical model to predict temperature distribution on the machined surface using finite element method in order to reduce the harmful result of the temperature on the surface which can satisfy a certain machining rate for wire electrical discharge machining (W-EDM) process. The predicted results of the model are in good agreement when compared with experimental results. Mahardika et al. (2008) have proposed a new approach to determine machining by EDM process for different work materials using the product of the thermal conductivity (λ), melting point (θ) and electrical resistivity (ρ) of the work piece. In the earlier theory, product of thermal conductivity (λ) and melting point (θ) were used. On comparison between the two approaches, it is observed that, the recent theory provides better result than the previous one.Salonitis et al. (2009) have proposed a thermal model based on finite element analysis to estimate the material removal rate and the average surface roughness. The model suggests that increase in open circuit voltage, discharge current and pulse duration increases the material removal but in turn produces poor surface quality. The model is validated through experimentation predicting results closer to the experimental analysis. Panda (2008) has proposed a theoretical model to estimate thermal stress on the machined surface to fill the drawbacks of the earlier published models. It is observed that the induced thermal stress surpasses the ultimate tensile stress of the material past crater.

(2) Numerical Model

In addition to some theoretical model, several numerical models have been proposed to gather information on process behavior to reduce the cost of experimentation and machining

time. In this direction, Das et al. (2003) have suggested an EDM simulation model using finite element method (FEM) for calculation of deformation, microstructure and residual stresses. Joshi and Pande (2009) have suggested a numeral model for EDM for prediction of performance characteristics such as material removal rate and tool wear rate using finite element method. The proposed model is also validated through experimentation by the same researchers (Joshi and Pande 2010). Izquierdo et al. (2009) have proposed a model which estimates the temperature fields within the work piece considering the effect of multiple discharges. The model can effectively predict material removal efficiency, diameter of the discharge channel and energy transferred in to the work piece. The proposed model is validated through experimentation indicating that material removal rate and surface roughness can be predicted with errors less than 6%. Schulze et al. (2004) have compared the cavity morphology obtained through a single discharge and a sequence of multiple discharges. Kansal et al. (2008) have proposed an axisymmetric two-dimensional model for powder mixed electric discharge machining (PMEDM) using finite element approach. The model uses the few essential features viz. material properties, shape and size of heat source, rate of distribution heat from electrodes, dielectric liquid, pulse duration and pulse-off- time to get the material removal mechanism. It is observed that the results predicted by the model are closer to experimental results. Vishwakarma et al. (2012) have proposed a numerical model based on finite element approach for predicting material removal rate (MRR) using an axisymmetric model for Al-SiC composite work piece. The model is validated through experimentation predicting results closer to experimental investigation. Salah et al. (2006) have suggested a numerical model which predicts the temperature distribution, material removal and total roughness in a work piece. It is observed that the numerical results provide better correlation with experimental investigations when temperature dependence of conductivity is considered. Chen and Allen (2007) have suggested a thermo-numerical model which simulates a single spark discharge for the micro-EDM process. The numerical model is authenticated by comparing with experimental work by means of scanning electron microscopy (SEM) and optical evaluation technique. A residual stress distribution on the molybdenum work piece with a tungsten tool is also presented by the same authors. Wei et al. (2011) have suggested for a FEM based model to predict material removal for Electro-Chemical Discharge Machining (ECDM) process taking in to account the occurrence of single spark. The results obtained through the model are validated by comparing with experimental data.

(3) Statistical Model

A large number of articles analyses the EDM process using statistical design of experiment (DOE) approach viz. Taguchi, responses surface methodology (RSM), grey relational analysis, principal component analysis. In this direction, Lee and Li (2001) have experimentally studied the influence of process variables such as electrode material, polarity, discharge current, open circuit voltage, pulse duration, pulse interval and flushing pressure on material removal rate, relative wear ratio and surface roughness of tungsten carbide. Lin et al. (2001) have adopted Taguchi Method to study material removal rate, surface roughness and improvement ratio of surface roughness through a combined process of electrical discharge machining (EDM) with ball burnish machining (BBM).The approach is quiet effective in reducing surface roughness and micro cracks on the machined surface. Huang and Liao (2003) have employed Taguchi experimental design along with grey relational analysis to find the optimal parametric setting for wire-EDM process. Puertas and Alvarez (2004) have used design of experiments to analyze the effect of discharge current, pulse-on-time and duty factor on material removal rate, electrode wear ratio and surface quality of the machined surface when cobalt-bonded tungsten carbide (WC-Co) is machined with copper electrode. Lin and Lin (2005) have used orthogonal array combined with grey-fuzzy logic for optimization of machining parameters viz. pulse on time, duty factor and discharge current for multiple responses such as electrode wear ratio, material removal rate and surface roughness. Keskin et al. (2006) have adopted DOE approach to plan the experiment and study the effect of power, spark time and pause time on surface roughness while machining a steel work piece with a copper tool. From analysis of variance (ANOVA), it is observed that discharge duration has significant effect on surface roughness. Chattopadhyay et al. (2009) have conducted experiments on a rotary EDM based on Taguchi's orthogonal array using EN8 steel and copper as work piece-tool pair and proposed empirical relations between responses and process variables viz. peak current, pulse-on-time and rotational speed of tool electrode. Habib (2009) has analyzed the effect of machining parameters viz. discharge current, pulse-on-time, open circuit voltage and the percentage volume fraction of silicon carbide present in work piece on material removal, surface quality, electrode wear ratio (EWR) and gap size through response surface methodology approach on the machinability of Al SiC work piece using copper electrode. Lin et al. (2009) have used Taguchi L_{18} orthogonal array to study the effect of polarity, discharge current, pulse-on-time high-voltage auxiliary current, no-load voltage and servo reference voltage on materials removal rate and surface quality in magnetic supported EDM.

Tomadi et al. (2009) have used full factorial design of experiment to study the influence of the parameters viz. current, voltage, pulse-on-time and pulse-off-time on MRR, EWR and surface roughness when tungsten carbide is eroded with a copper tungsten electrode. From analysis of variance, it is observed that pulse-on-time is the most influential parameter exhibiting significant effect on responses. Pradhan and Biswas (2009) have used response surface methodology (RSM) design to perform experiment and analyze the effect of parameters such as discharge current, pulse duration, pulse-off-time and voltage on performance measures when AISI D2 steel is machined with copper electrode. The study revealed that pulse-on-time and discharge current have significant effect on machined surface quality. Prabhu and Vinayagam (2010) have experimentally observed that improved surface quality and least micro-cracks on machined surface can be achieved if the tool is coated with a carbon nono-tube layer while machining AISI D2 steel work piece. Kuppan et al. (2011) have studied the effect of discharge current, pulse-on-time, duty factor and speed of electrode on performance measures viz. MRR and surface roughness using central composite design. It is observed that discharge current and pulse-on-time significantly influence the performance measures. Pellicer et al. (2011) have studied the effect of current, voltage, pulse-on-time and pulse-off-time on material removal rate, surface roughness and dimensional accuracy of the EDMed parts on AISI H13 steel using copper electrode. The study provides optimum parametric setting to improve the accuracy of the EDMed parts through statistical approach. Rao et al. (2011) have suggested an optimal parametric condition for surface roughness of Wire-EDM using Taguchi method. Beri et al. (2011) have found that improved machining characteristics can be achieved with the use of powder metallurgy mixed copper-tungsten (CuW) electrode in comparison with conventional copper tool material using Taguchi's L_{18} orthogonal array. Senthilkumar and Reddy (2012) have found that copper composite with 40% boron carbide reinforcement developed through powder metallurgy route exhibits better metal removal rate (MRR) and tool removal rate (TRR) compared to conventional copper tool material. Meena et al. (2012) have analyzed the effect of various flushing conditions on the accuracy of deep holes drilled by micro-electrical discharge machining. Prabhu and Vinayagam (2013) have proposed a grey relational analysis and fuzzy logic approach for simultaneous optimization of several performance characteristics of the process when dielectric fluid is mixed with carbon nano tube (CNT). Dewangan and Biswas (2013) have adopted Taguchi's experimental design combined grey relational analysis for optimization of multiple responses such as material removal rate and tool wear rate of electrical discharge machining process using AISI P20

tool steel as the work piece material and copper as electrode. Pradhan (2013a) has used response surface methodology in combination with grey relational analysis to optimize white layer thickness, surface roughness and surface crack density which are function of process variables viz. pulse current, pulse-on-time, duty factor and open circuit voltage. The same researcher has used a face-centered central composite design and grey relational analysis in combination with principal component analysis (PCA) to evaluate the effect of discharge current, pulse-on-time, duty cycle and open circuit voltage on material removal rate, tool wear rate and radial overcut (Pradhan 2013b). The study revealed that duty factor is the most important parameter followed by discharge current, open circuit voltage and pulse-on-time. In addition to these studies, several experimental investigations have been reported to analyze the machining efficiency of the process by machining metal matrix composites as the work materials (Dhar et al. 2007; Puhan et al. 2013; Murugesan et al. 2012; Singh et al. 2004; Mohan et al. 2002).

(4) Soft Computing Model

Recently, artificial intelligence (AI) and soft computational techniques are widely applied for process modeling and optimization of EDM process in order to overcome some of the drawbacks of conventional modeling methods. Lin et al. (2000) have used Taguchi experimental design along with fuzzy logic for optimization of material removal rate and electrode wear ratio which are function of process parameters viz. duty factor, voltage, current, pulse-on-time, dielectric liquid and polarity of work piece. Her and Weng (2002) have adopted Taguchi experimental design and genetic algorithm to find the optimal paramedic setting while machining semiconductor work piece, Barium Titanate ($BaTiO_3$). Wang et al. (2003) have used genetic algorithm with artificial neural network for optimization of machining parameters such as pulse-on-time, pulse-off-time, discharge current and open circuit voltage for responses material removal rate and surface roughness when nickel based alloy is machined with graphite electrode. Su et al. (2004) have used genetic algorithm based neural network model to find the optimal parametric setting for EDM process for rough and finishing machining condition when steel work piece is eroded with copper electrode. Kuriakose and Shunmugam (2005) have adopted for non-dominated sorting genetic algorithm (NSGA II) to optimize machining parameters in WEDM for multiple objectives such as surface quality and cutting speed. Tzeng and chen (2007) have used Taguchi method in combination with fuzzy logic to find the optimal parametric condition to enhance the process output. Mahapatra and Patnaik (2007) have used Taguchi

experimental design along with genetic algorithm to find optimal parametric setting for wire EDM process. Mandal et al. (2007) have used artificial neural networks based on back propagation algorithm to predict material removal rate and tool wear rate while machining C40 steel with copper electrode. Further, NSGA-II is used to find the Pareto-optimal solution set. Bharti et al. (2012) have adopted a similar approach while machining Inconel 718 with copper electrode. Ramakrishnan and Karunamoorthy (2008) have used back-propagation artificial neural network (BPANN) model to find the optimal parametric setting for material removal rate and surface roughness for wire-electrical discharge machining process when Inconel 718 work material is machined with brass wire electrode. Pradhan and Biswas (2010) have proposed neuro-fuzzy and neural network models for prediction of material removal rate, tool wear rate and radial overcut when AISI D2 steel is machining with copper electrode. Pradhan et al. (2009) have analyzed two distinct neural network model viz. back-propagation neural networks (BPN) and radial basis function neural network (RBFN) to predict surface quality of the machined surface of AISI D2 steel work piece. The study revealed that RBFN is faster than the BPNs but BPN provides more exact result than RBFN. Yang et al. (2009) have used simulated annealing with neural network to maximize the material removal rate and improving the surface quality. The effectiveness of the model is verified through numerous initial trail values. Material removal rate and surface roughness is optimized using neural network and NSGA II. The effect of pulse-on-time, discharge current, pulse-off-time on MRR and surface roughness is extensively studied. MahdaviNejad (2011) has used a similar approach after machining silicon carbide (SiC) work piece with a copper electrode. Mukherjee and Chakraborty (2012) have used biogeography-based (BB) algorithm with the goal of achieving ideal machining parameters to enhance the machining efficiency of process. Pradhan and Das (2011) have proposed an Elman network for the prediction of material removal rate in electrical discharge machining process. The proposed model is validated with a new set of experimental results which is not used in the training step and the model predicts mean percentage error less than 6 percent. Markopoulos et al. (2008) have used artificial neural network (ANN) based models for prediction of material removal rate and surface roughness. Panda and Bhoi (2005) have used back propagation neural network (BPNN) with Levenberg-Marquardt (LM) algorithm for the prediction of material removal rate. Similar methodologies have been adopted for modeling of EDM process for different work-tool material combination (Sen and Shah 2007; Gao et al. 2008; Rao et al. 2008). Joshi and Pande (2011) have proposed optimization of parameters by integrating artificial neural network with non-dominated sorting genetic algorithm (NSGA-II).

Somashekhar et al. (2010) have optimized process parameters for maximizing material removal rate in a micro-electrical discharge machining process using genetic algorithm embedded with artificial neural network. Panda and Yadava (2012) have proposed a model based on finite element method to predict material removal rate and average surface roughness for die-sinking electrical chemical spark machining for a single spark analysis. The model uses back propagation neural network (BPNN) to find optimal parametric machining condition. Prajapati et al. (2013) have studied the effect of wire feed, wire tension, pulse-on time, pulse-off-time and voltage on responses viz. MRR, surface roughness and Kerf. ANN is utilized for prediction responses of WEDM of AISI A2 steel. Golshan et al. (2012) have analyzed the effect of process parameters on material removal rate and surface roughness while machining metal matrix composite (Al/SiC) composite. The optimal process conditions are reported using non-dominated sorting genetic algorithm (NSGA-II).

(5) Technological Modification of basic EDM process

Several research approaches have been undertaken to improve the machining efficiency of process by machining in the presence of suspended powder particles. The presence of electrically conductive powders increases the spark gap between the electrodes and decreases the insulating strength of the dielectric fluid during machining (Padhee et al. 2012; Wong et al. 1998; Ming and He 1995; Chow et al. 2000). Therefore, the process becomes more stable and results in improved material removal and surface quality on the machined surface. In this direction, Kung et al. (2009) have investigated the effect of discharge current, pulse-on-time, grain size, and concentration of aluminum powder particle on the machinability evaluation of MRR and EWR using face-centered central composite design. The study proposes mathematical models for investigating the influence of parameters on performance measures. Pecas and Henriques (2008) have analyzed the effect of silicon powder concentration and the flushing flow rate on performance measures such as white layer thickness, surface roughness and crater dimension. The study shows significant improvement on crater diameter, surface quality and the white-layer thickness with the use of silicon powder particles suspended in the dielectric fluid. Many experimental studies have been reported on powder-mix EDM to find the optimal parametric setting using AISI D2 steel as work piece and copper as electrode material (Kansal et al. 2005; Kansal et al. 2006; Kansal et al. 2007). Patel et al. (2009) have studied the effect of discharge current, pulse-on-time and duty cycle on performance measures viz. surface quality and material removal rate on of ceramic composite Al_2O_3-SiCw-TiC work piece for rough and finishing

machining condition. The study reveals that high value of discharge energy can cause increase in material removal but produces poor surface integrity whereas small discharge energy produces gentle material removal and superior surface quality. Kumar et al. (2010) have studied the effect of concentration of silicon abrasive powder in dielectric fluid, peak current, pulse-on-time and duty factor on MRR and surface roughness. The research establishes an optimal parametric setting for multiple responses like MRR and surface roughness verified with confirmative test. Çogun et al. (2006) have used steel work piece and copper electrode with graphite and boric acid powders mixed with kerosene dielectric at different powder concentrations on various performance measures such as surface roughness, material removal rate, electrode wear rate, relative wear and microstructure of the work material. The experimental investigation reveals that powder concentration, type of powder mixed into the dielectric and the pulse time have significant influence on performance measures. Batish et al. (2012) have analyzed the effect of process parameters and mechanism of material deposition in powder-mix electrical discharge machine (PMEDM) on surface properties of EN31, H11 and high carbon high chromium (HCHCr) die steel. The study indicates that discharge current, powder concentration and interaction between work piece and electrode significantly influence the micro hardness of the machined surface for the three materials. Kansal et al. (2005) have investigated the effect of pulse-on-time, duty cycle, peak current and concentration of the silicon powder added into the dielectric fluid to maximize MRR and minimize surface roughness using response surface methodology approach. The optimal process conditions obtained through the approach are verified by conducting confirmative test. Padhee et al. (2012) have used non-dominated sorted genetic algorithm (NSGA-II) to optimize MRR and surface roughness for machining parameters such as concentration of silicon powder in the dielectric fluid, pulse-on-time, duty cycle and peak current. Chow et al. (2008) have studied the influence of addition of SiC powder with water as dielectric fluid water on material removal rate and electrode wear ratio when Ti-6Al-4V titanium alloy is machined with copper electrode. Yih-fong and Chen (2005) have studied the effect of addition of different powders viz. silicon carbide (SiC), chromium (Cr), aluminum (Al) and copper (Cu) powders on surface quality and recast layer when SKD-11 work material is machined with copper electrode. It is observed that smaller particle size produces fine surface quality but increases the recast layer on the machined surface. Klocke et al. (2004) have investigated the effect of silicon and aluminum powder added to the dielectric on recast layer when Inconel 718 work piece is eroded with tungsten tool. They conclude that the properties of the powder particles is an important factor for formation of recast layer, its

composition and quality of the machined surface. Zhao et al. (2002) have found significant improvement on machining efficiency and surface quality while machining steel work piece with copper electrode in the presence of fine aluminum powder. Bai and Koo (2006) have investigated the effect dielectric fluids viz. kerosene and distilled water on surface integrity of the machined surface using an Al-Mo composite electrode while machining Haynes 230 super alloy.

Many studies report that controlled cryogenic cooling of tool and work materials can enhance the machining efficiency of the process. In this direction, Jafferson and Hariharan (2013) have analyzed the machining performance of micro-EDM by cryogenically treated and untreated copper, brass and tungsten micro-electrodes. From the study, it is observed that significant reduction in tool wear rate can be achieved if the tools are cryogenically treated. Kapoor et al. (2012) have investigated the effect of deep cryogenic treated brass wire electrode using Taguchi experimental design. From the analysis of variance (ANOVA), it is observed that wire type, pulse width, time between two pulses and wire tension are important parameters for improving material removal rate. Gill and Singh (2010) have investigated the effect of deep cryogenic treatment of copper electrode on machinability of Ti 6246 alloy in electric discharge drilling. The study confirms that improved material removal rate (MRR), wear ratio (WR), tool wear rate (TWR) and precise drilled holes can be achieved with cryogenic treatment. Srivastava and Pandey (2011) have observed significant improvement on electrode wear ratio (EWR), surface roughness and retention of tool shape while machining M2 grade high speed steel work material with cryogenically cooled copper electrode. Abdulkareem et al. (2009) have used central composite design to study the effect of current intensity, pulse-on-time, pulse-off-time and gap voltage on electrode wear and surface roughness. The study reveals that twenty seven percent reduction in wear ratio can be obtained by the use of cryogenic cooled electrode. Srivastava, and Pandey (2012) have found that ultrasonic aided cryogenically cooled electrode can be suitably used in electrical discharge machining owing to improved wear resistance and retention of tool shape and surface integrity.

Recently, few experimental investigations have been reported in which researchers have attempted to combine both the modifications to achieve improved machining efficiency. Kumar et al. (2012a) have investigated the machinability of Inconel 718 work material with powder mixed in dielectric fluid using cryogenically treated copper electrode in electrical discharge machining. Kumar et al. (2014) have investigated the effect of pulse-on-time, discharge current, pulse-off-time and different cryo-treated work and tool materials onsurface roughness in the presence of suspended powder particles. Finally, artificial neural

network (ANN) has been used to predict and optimize the surface roughness.

2.2 Discussions

Literature on EDM is classified according to different models depending up on techniques and solution methodology used by the authors. Figure 2.1 shows a pie chart with distribution of literature in terms of percentage. It shows that twenty six percent (26%) of the studied literature employs some technological modification to basic EDM process whereas twenty five percent (25%) uses soft computational and artificial intelligence (AI) techniques for modeling the process. Thirty percent (30%) of the studied literature uses statistical approaches to improve the EDM performance. As for as numerical and theoretical models are concerned, the chart shows that inadequate studies have been reported till date limiting the number to ten (10%) and nine (9%) percent respectively. Most of the research approaches have been undertaken for technological modification of the EDM process to improve the machining efficiency through machining in the presence of suspended powder particles or through cryogenic treatment of electrodes. However, reports to analyze the machining efficiency using the hybrid approach of both types of modifications are scare in the literature.

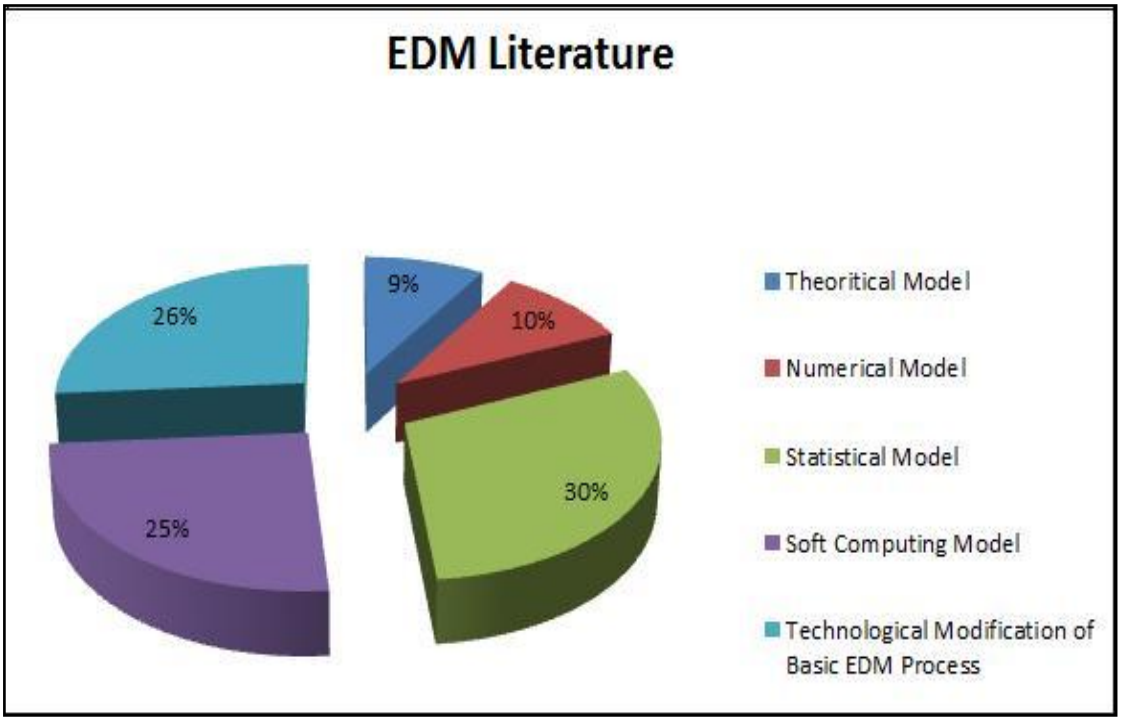

Figure 2.1 Literature appraisal in terms of percentage

2.3 Conclusions

After an exhaustive study made on the current literature, it is inferred that EDM is a rich and promising field of research with broad usage in production and manufacturing engineering. The study shows a change of interest in twenty first century by researchers from an experimental investigation to development of numerical and theoretical models in combination of statistical techniques with application of new heuristic, optimization algorithms for both single and multiple objectives responses. For multi objective problems, mostly researchers have used NSGA as an optimization strategy but applied to commonly used work piece-tool combination. It is also observed that, adequate research effort has not been paid to machining with a variety of electrodes, process modification both in cryo-treatment of electrodes and powder mixed with dielectric, numerical models and analyzing the machining efficiency with varied soaking duration during cryogenic treatment. Considering above limitations, a potential research opportunity is identified and an attempt has been made further to propose a robust frame work to enhance the machining efficiency of the process. In the recent decade, a large number of meta-heuristic algorithms have been proposed inspired by nature analogy. However, most of these algorithms do not always perform according to expectations even if having some special features. The success of these meta-heuristics algorithms depends on the exploration and exploitation ability of the algorithm. These abilities can be enhanced by using local search or global search methods or an incorporation of both global and local search approaches. The present research work uses an efficient multi-objective particle swarm optimization (MOPSO) algorithm which has gained much attention and been successfully applied to a wide range of applications.

CHAPTER 3

ASSESSMENT OF THE INFLUENCE OF DIFFERENT TOOL MATERIALS ON PERFORMANCE OF EDM PROCESS

3.1 Introduction

Generally metallic materials like copper and brass are used as electrode materials. However, non-metal like graphite can be used as a potential electrode material due to its high melting point and conductivity. The temperature resistance property makes graphite a preferable electrode material in compared to other electrodes. Literature reveals that performance of EDM process has not been dealt sufficiently with different tool materials viz. brass, copper and graphite using Inconel 718 as work piece material (Kuppan et al. 2011; Kumar et al. 2009; Kumar et al. 2012b; Lee and Li 2001). Furthermore, the studies on EDM are limited to analyse influence of various process parameters on performance measures using statistically designed experiments (Prabhu and Vinayagam 2013; Dewangan and Biswas 2013). In the past, numerous studies have been proposed to find out optimal process state for single objective either based on design of experiment (DOE) approach or empirical modeling followed by application of non-traditional optimization techniques like genetic algorithm (GA), differential evolution (DE) artificial bee colony (ABC) simulated annealing (SA) etc (Lin et al. 2000; Mahapatra and Patnaik 2007; Mandal et al. 2007; Kuriakose and Shunmugam 2005). Although optimization of multiple objectives is useful from practical point of view, limited attempt has been made in this direction using multiple attribute decision making(MADM) approaches for converting multiple performance measures into an equivalent performance measure in the framework of DOE approach (Prabhu and Vinayagam 2013; Dewangan and Biswas 2013). Joshi and Pande (2009) have proposed a non-dominated sorting genetic algorithm (NSGA) for optimizing multiple objectives in an electrical discharge machining process. However, particle swarm optimization is found to solve multi-objective optimization problems with less computation efforts requiring only few parameters to be tuned (Singh and Mahapatra 2012; Yoshida et al. 2001; Brandstatter and Baumgartner 2002). Usually, multi-objective optimization techniques generate large number of Pareto optimal solutions. Due to large number of non-dominated solutions, deciding the best one amongst the Pareto set is difficult due to subjective in judgment.

To address these issues, the present chapter proposes an experimental investigation on machinability of Inconel718 alloy in EDM process in which the performance characteristics are measured in terms of material removal rate (MRR), electrode wear ratio (EWR), surface roughness, radial overcut and white layer thickness under the influence of process variables viz. open circuit voltage, discharge current, pulse duration, duty factor, flushing pressure and electrode material. The experiments are planned as per Box-Behnken design of response

surface methodology (RSM) approach to obtain maximum information with limited number of experimental runs. Optimal parametric combination is found out using a proposed multi objective particle swarm optimization (MOPSO) algorithm for simultaneous optimization of more than one performance measures. Since particle swarm optimization (PSO) has an inherent drawback of getting trapped at local optimum due to large reduction in velocity values as iteration proceeds (Singh and Mahapatra 2012), a commonly used operator in genetic algorithm known as mutation operator has been introduced in this work for dealing with such a drawback and improving the solution quality. However, MOPSO results in a large number of non-dominated solutions. Therefore, maximum deviation theory proposed by Wang (1998) has been adopted for ranking the solution to ease the decision making process in choosing the best solution.

3.2 Particle swarm optimization

Particle swarm optimization algorithm, originally introduced by Kennedy and Eberhart (1995), is a population based evolutionary computation technique motivated by the behavior of organisms such as bird flocking and fish schooling. Due to its simple concept, easy implementation and rapid convergence, PSO has gained much attention and been successfully applied to a wide range of applications such as job scheduling, power and voltage control, mass spring system, supply chain network, vehicle routing, components placement inspection problems andnonlinear programming (Singh and Mahapatra 2012; Yoshida et al. 2001; Brandstatter and Baumgartner 2002; Bachlaus et al. 2008; Belmecheri 2013; Kim and Son 2012; Wu et al. 2009; Dong et al. 2005).In PSO, the initial population is generated randomly and parameters are initialized. After evaluation of the fitness function, the PSO algorithm repeats the following steps iteratively:

- Personal best (best value of each individual so far) is updated if a better value is discovered.
- Then, the velocities of all the particles are updated based on the experiences of personal best and the global best (best in the swarm) in order to update the position of each particle with the velocities currently updated.

After finding the personal best and global best values, velocities and positions of each particle are updated using equations 3.1 and 3.2 respectively.

$$v_{ij}^{t} = w^{t-1}v_{ij}^{t-1} + c_1 r_1\left(p_{ij}^{t-1} - x_{ij}^{t-1}\right) + c_2 r_2\left(g_{ij}^{t-1} - x_{ij}^{t-1}\right) \quad (3.1)$$

$$x_{ij}^{t} = x_{ij}^{t-1} + v_{ij}^{t} \quad (3.2)$$

where v_{ij}^{t} represents velocity of particle iat iteration t with respect to j^{th}dimension (j =1,2,……n). p_{ij}^{t} represents the position value of the i^{th} personal best with respect to the j^{th}dimension.g_{ij}^{t} represents the global best (g_{best}) i.e the best of personal best (p_{best}) among all the particles. x_{ij}^{t} is the position value of the i^{th} particle with respect to j^{th}dimension. c_1 andc_2 are positive acceleration parameters which provide the correct balance between exploration and exploitation and are called the cognitive parameter and the social parameter respectively. r_1 andr_2 are the random numbers provide a stochastic characteristic for the particles velocities in order to simulate the real behavior of the birds in a flock. The inertia weight parameter w is a control parameter which is used to control the impact of the previous velocities on the current velocity of each particle. Hence, the parameter w regulates the trade-off between global and local exploration ability of the swarm. The recommended value of the inertia weight w is to set it to a large value for the initial stages in order to enhance the global search of the search space and gradually decrease it to get more refined solutions facilitating the local search in the last stages. In general, the inertia weight is set according to the following equation 3.3 (Modares et al. 2011).

$$w = w_{\max} - \frac{w_{\max} - w_{\min}}{\text{iter}_{\max}} \times \text{iter} \qquad (3.3)$$

where $w_{\min}$ and $w_{\max}$ are initial and final weights and $\text{iter}_{\max}$ is the maximum number of iterations and $\text{iter}$is the current iteration number.

3.2.1 Proposed MOPSO algorithm

Real world problems involve simultaneous optimization of numerous contradistinctive and conflicting nature objectives. Multi-objective optimization (MOO) arises in many applications where two or more objective functions need to be optimized simultaneously. PSO has been extended for solving the MOO problems, which is generally known as the multi-objective particle swarm optimization (MOPSO) (Mostaghim and Teich 2003; Wang and Singh 2007; Coello et al. 2004). When all objectives are considered, these solutions are optimum in the sense that none of the other solutions in the search area are exceptionally good to another solution. These solutions are called as Pareto-optimal solutions. The image of the efficient set in the objective space is named as non-dominated set as each solution dominates the other solution. To identify the non-dominance, each solution is compared with every single solution and checked for satisfying the rules given below for the solution under consideration. Consider a minimization problem having two objectives:

$$Obj.1[l] > Obj.1[m] \quad \text{and} \quad Obj.2[l] \geq Obj.2[m], \qquad (3.4)$$

or $Obj.1[l] \geq Obj.1[m]$ and $Obj.2[l] > Obj.2[m]$ (3.5)

where l and m correspond to solution number in the population. Obj.1 and Obj.2 are two objective function values.

The multi-objective optimization aims at two objectives:

(a) Converging to the Pareto-optimal solution set;

(b) Maintaining diversity and distribution in solutions.

While solving single-objective optimization problems, the g_{best} that each particle uses to update its position is completely determined once a neighborhood topology is established. However, in the case of multi-objective optimizations problems, each particle might have a set of g_{best} from which just one can be selected in order to update its position. Such set of g_{best} is usually stored in a different place from the swarm known as external archive 'A_t'.This is a repository in which the non-dominated solutions found so far are stored. The MOPSO maintains an external archive 'A_t'of non-dominated solutions of the population which is updated after every iteration. The global archive 'A_t'is empty in the beginning and can store a user-specified maximum number of non-dominated solutions. In case the number of non-dominated solutions exceeds the maximum size of the archive, some individuals are cropped. There are several methods of controlling the external archive such as Maximin fitness based size control (Li. 2004), epsilon-dominance based size control (Mostaghim and Teich 2003) and crowding distance based size control (Raquel and Naval 2005). Archive size control is critical because the number of non-dominated solutions can grow very fast (Alvarez-Benitez et al. 2005; Fieldsendand Singh 2002).

Crowding distance technique has been extensively applied in evolutionary multi-objective algorithms to promote diversity. The use of crowding distance measure in MOPSO for g_{best} selection was first made in Raquel and Naval (2005). The approach is quite capable in converging towards the Pareto front and generating a well-distributed set of non-dominated solutions. In this study, crowding distance approach has only been applied to make g_{best} selection. Crowding distance factor is defined to show how much a non-dominated solution is crowded with other solutions. The crowding distance (CD) factor of a solution provides an estimate of the density of solutions surrounding that solution (Deb et al. 2002; Ebrahimipour et al. 2012). Figure 3.1 shows the calculation of the crowding distance of point k which is an estimate of the size of the largest cuboid enclosing k without including any other point. CD factor of boundary solutions which have the lowest and highest

objective function values (f_{max} and f_{min} respectively) are given an infinite crowding distance values. For other solutions, CD factor for the solution k is calculated by following relation.

$$CD_k = \frac{(f_{k+1} - f_{k-1})}{(f_{max} - f_{min})} \quad (3.6)$$

Finally, the overall crowding factor is computed by adding the entire individual crowding distance values in each objective function.

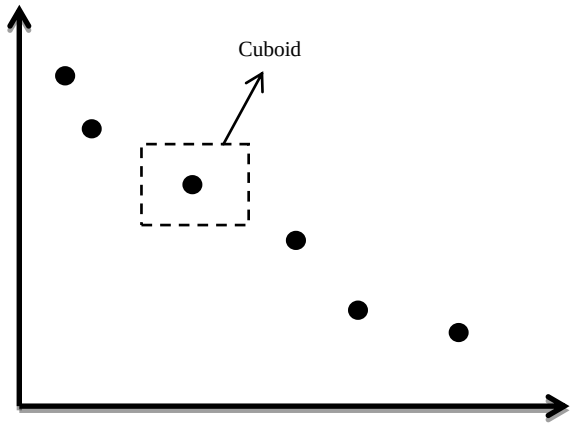

Figure3.1 The crowding distance

The non-dominated solutions in 'A_t'are sorted in descending crowding distance values and top 10% of them are randomly used as g_{best} guides

Particle swarm optimization typically converges relatively rapidly at the beginning of the search and then slows down or stagnates due to loss of diversity in the population (Pant et al. 2007; Singh and Mahapatra, 2012). To overcome this drawback, mutation, a widely used operator in genetic algorithm, is used to introduce diversity in the search procedure. When the change of the whole archive tends to decrease, the mutation process will begin (Tripathi et al. 2007). If the number of iteration is less than the product of maximum number of iteration and probability of mutation then only the mutation is performed on the position of the particle. Given a particle, a randomly chosen variable, say m_p, is mutated to assume a value m'_p as given by following equation.

$$m'_p = \begin{cases} m_p + \Delta(t, UB - m_p) & \text{if flip} = 0 \\ m_p - \Delta(t, m_p - LB) & \text{if flip} = 1 \end{cases} \quad (3.7)$$

when flip denotes the random event of returning 0 or 1. UB and LB denote the upper and lower bound of the variable $m_p$respectively. The function $\Delta(t, x)$ returns a value in the range [0,x] such that the probability of $\Delta(t, x)$ being close to 0 increases as t increases.

$$\Delta(t, x) = x \times \left(1 - r^{\left(1 - \frac{iter}{iter_{max}}\right)^b}\right) \quad (3.8)$$

where r is the random number generated in the range [0, 1], $\mathrm{iter}_{\max}$ is the maximum number of iterations and iter is the number of iteration. The parameter b determines the degree of dependence of mutation on the iteration number.

To summarize, the main difference between a basic PSO (single-objective) and MOPSO is the distribution of g_{best}. In single-objective problems, there is only one g_{best} exists. In MOPSO algorithm, g_{best} must be redefined in order to obtain a set of non-dominated solutions (Pareto front). Therefore, multiple numbers of non-dominated solutions are located on or near the Pareto front. Each non-dominated solution can be a g_{best}. The important feature of MOPSO is that the individuals also maintain a personal archive which is known as p_{best} archive with a maximum size. The p_{best}archive contains the most recent non-dominated positions a particle has encountered in the past. In every iteration t, each particle i is allocated with two guides p_{best} and g_{best} from its p_{best} archive and swarms global archive 'A_t'. After the guide selection, velocities and positions of particles are updated according to the equation3.9 and equation3.10 where v_{ij}^trepresents velocity and x_{ij}^t is the position value of the i^{th} particle with respect to j^{th}dimension. Maximum number of generations is set as termination criterion. The complete algorithm for MOPSO is shown as follows:

MOPSO Algorithm

1. For i= 1 to M (M is the population size)
    a. Initialize position of the particles randomly
    b. Initialize v_{ij}^t= 0 (v is the velocity of each particle)
    c. Evaluate each particle's fitness
    d. Compare each particle's fitness with the particle's p_{best}. Compare the fitness with the population's overall previous best
    e. Find out the personal best (p_{best}) and global best (g_{best}).
2. End For
3. Initialize the iteration counter t= 0
4. Store the non-dominated vectors found into archive 'A_t'
   ('A_t'is the external archive that stores non-dominated solutions found)
5. Repeat
    a. Compute the crowding distance values of each non-dominated solution in the archive 'A_t'

b. Sort the non-dominated solutions in 'A_t'in descending crowding distance values

c. For i= 1 to M

i. Randomly select the global best guide from a specified top 10% of the sorted archive 'A_t'and store its position to g_{best}.

ii. Compute the new velocity:

$$v_{ij}^{t} = w^{t-1}v_{ij}^{t-1} + c_1 r_1\left(p_{ij}^{t-1} - x_{ij}^{t-1}\right) + c_2 r_2\left((A_t)_{ij}^{t-1} - x_{ij}^{t-1}\right) \quad (3.9)$$

($(A_t)_{ij}^{t-1}$is the global best guide for each nondominated solution)

iii. Calculate the new position of $x_{ij}^{t} = x_{ij}^{t-1} + v_{ij}^{t}$ (3.10)

iv. If (t< (MAXT * PMUT), then perform mutation on x_{ij}^{t}

(MAXTis the maximum number of iterations and PMUT is the probability of mutation)

v. Evaluate x_{ij}^{t}

d. End For

e. Insert all new non-dominated solution into archive 'A_t' if they are not dominated by any of the stored solutions. All dominated solutions in the archive are removed by the new solution from the archive. If the archive is reached its maximum, the solution to be substituted is determined by the following steps:

i. Compute the crowding distance values of each non-dominated solution in the archive 'A_t'

ii. Sort the non-dominated solutions in archive 'A_t'in descending crowding distance values

iii. Randomly select a particle from a specified bottom 10% of the sorted archive 'A_t' and replace it with the new solution

f. Update the personal best solution of each particle. If the current p_{best} dominates the position in the memory, the particle position is updated.

g. Increment iteration counter t

6. Until maximum number of iterations is reached.

3.3 Solution ranking

Since MOPSO results in a large number of non-dominated solutions, choosing a best solution depends on decision maker's judgement and intuition. Usually, multi-attribute decision making (MADM) approaches are adopted to obtain scores for the solutions and the solution exhibiting maximum score is selected as the best one. However, the weights

assigned in multi-attribute decision making process for converting multiple objectives into a single equivalent objective score are reasonably subjective in nature and affect the decision of ranking the alternative solutions considerably. In order to avoid uncertainty of subjective assignment of weights by the experts and extract the accurate information from the available data, maximum deviation theory (MDT) suggested by Wang (1998) is adopted in this work**.** The basic idea of MDT rests on smaller weight should be assigned to the attribute having similar values in comparison to the attribute having larger deviations.

The non-dominated solutions obtained in MOPSO solutions are used as the decision matrix. Every element of the decision matrix denotes the value of j^{th} attribute for i^{th} alternative where i=1, 2 ...n, and j=1, 2...m. Normalization of each attribute is carried out to transform different scales and units among various attributes into a common measurable scale. The normalization of the attribute depends on its type such as “higher the better” and “lower the better”. The following equations are used for normalization of attributes.

$x_{ij}^{*} = \frac{\max_i\{x_{ij}\} - x_{ij}}{\max_i\{x_{ij}\} - \min_i\{x_{ij}\}}$, for lower the better attributes (3.11)

$x_{ij}^{*} = \frac{x_{ij} - \min\{x_{ij}\}}{\max_i\{x_{ij}\} - \min_i\{x_{ij}\}}$, for higher the better attributes (3.12)

The difference of performance values for each alternative is computed. For the attribute $\{A_j|\ j=1, 2\ldots m\}$, the deviation value of the alternative $\{S_i|\ i = 1, 2\ \ldots.n\}$ from all the other alternatives can be computed by the following equation

$$D_{ij}(w_j) = \sum_{i=1}^{N} d(\tilde{r}_{ij}, \tilde{r}_{lj}) w_j \quad (3.13)$$

wherew_j is the weight of the attributes to be calculated and $D_{ij}(w_j)$ is the deviation value of the alternatives.

The total deviation values of all alternatives with respect to other alternatives for the attribute $\{A_j|\ j =1, 2\ldots m\}$ can be computed by the following relation.

$$D_j(w_j) = \sum_{i=1}^{N} D_{ij}(w_j) = \sum_{i=1}^{N}\sum_{l=1}^{N} d(\tilde{r}_{ij}, \tilde{r}_{lj})\, w_j \quad (3.14)$$

where$D_j(w_j)$ is the total deviation value of all the alternatives.

The deviation of all the attributes along all the alternatives can be calculated by the relation

$$D(w_j) = \sum_{j=1}^{M} D_j(w_j) = \sum_{j=1}^{M}\sum_{i=1}^{N}\sum_{l=1}^{N} d(\tilde{r}_{ij}, \tilde{r}_{lj})\, w_j \quad (3.15)$$

where $D(w_j)$ is deviation of all the attributes along all the alternatives.

A linear programming model is constructed for finding out the weight vector w to maximize all deviation values for all the attributes and is given by

$$\begin{cases} D(w_j) = \sum_{j=1}^{M} \sum_{i=1}^{N} \sum_{l=1}^{N} d(\tilde{r}_{ij}, \tilde{r}_{lj})\, w_j \\ s.t \sum_{j=1}^{M} w_j^2 = 1, w_j \geq 0, j = 1,2, \dots \dots, M \end{cases} \quad (3.16)$$

A Lagrange function is constructed for solving the above model

$$L(w_j, \alpha) = \sum_{j=1}^{M} \sum_{i=1}^{N} \sum_{l=1}^{N} d(\tilde{r}_{ij}, \tilde{r}_{lj})\, w_j + \alpha\left(\sum_{j=1}^{M} w_j^2 - 1\right) \quad (3.17)$$

where α is the Lagrange multiplier. The partial derivative of L (w_j,α) with respect to w_j and α are

$$\begin{cases} \frac{\partial L}{dw_j} = \sum_{i=1}^{N} \sum_{l=1}^{N} d(\tilde{r}_{ij}, \tilde{r}_{lj}) + 2 \propto w_j = 0 \\ \frac{\partial L}{d\propto} = \sum_{j=1}^{M} w_j^2 - 1 = 0 \end{cases} \quad (3.18)$$

Further, w_j and α values are calculated from equation 3.17 and 3.18

$$\begin{cases} 2 \propto = -\sqrt{\sum_{j=1}^{M} \left(\sum_{i=1}^{N} \sum_{l=1}^{N} d(\tilde{r}_{ij}, \tilde{r}_{lj})\right)^2} \\ w_j = \frac{\sum_{i=1}^{N} \sum_{l=1}^{N} d(\tilde{r}_{ij}, \tilde{r}_{lj})}{\sqrt{\sum_{j=1}^{M} \left(\sum_{i=1}^{N} \sum_{l=1}^{N} d(\tilde{r}_{ij}, \tilde{r}_{lj})\right)^2}} \end{cases} \quad (3.19)$$

The normalized attribute weights can be further determined by the following relation

$$w_j = \frac{\sum_{i=1}^{N} \sum_{l=1}^{N} d(\tilde{r}_{ij}, \tilde{r}_{lj})}{\sum_{j=1}^{M} \sum_{i=1}^{N} \sum_{l=1}^{N} d(\tilde{r}_{ij}, \tilde{r}_{lj})} \quad (3.20)$$

The non-dominated solutions obtained through MOPSO algorithm are ranked by estimating the composite score of each solution by addition of the weighted performance of all attributes. Considering the ranking of the solutions, the tool engineer may choose suitable parametric setting from the top ranking solutions to justify the objectives set by the industry.

3.4 Materials

Inconel alloy 718, a nickel-chromium super alloy characterized by high-strength, high corrosion-resistant, good tensile and high creep rupture strength has been used as the work material in this study.A superalloy is an alloy which possesses several important features such as good mechanical strength, resistance to thermal creep deformation, good surface stability and resistance to corrosion.The super alloy is an aerospace material and has abundant usage in manufacturing of components for liquid fuled rockets, rings and casings, sheet metal parts for aircraft, land-based gas turbine engines, cryogenic tank fasteners and instrumentation parts. However, the material is extremely difficult to machine because of its low thermal conductivity, high hardness, high toughness, presence of highly abrasive

carbide particles and strong tendency to weld to the tool to form build up edge (Kuppan et al. 2008).

The work material was supplied by Manohar Metals Private Limited, Mumbai. The chemical composition of the material is been given in Table 3.1. Table 3.2 shows the thermal property of the work material. The X-ray diffraction plot of the Inconel 718 sample used in the present study is shown in Figure 3.2. It clearly shows that there are no peaks other than γ-phase (austenite) phase which corresponds to face-centred cubic Ni-based γ-phase of Inconel 718 alloy. The sharp peak of the diffraction patterns reveals the crystalline nature of the alloy. No other peaks are observed from the XRD pattern confirming highly pure nature of the alloy.

Table 3.1 Chemical composition of Inconel 718 sample used in the study

Chemical	C%	Si%	Mn%	S%	P%	Cr%	Fe%	Mo%	Co%	Nb%	Cu%	V%	Al%	Ti%	W%	Ni%
Amount	0.039	0.027	0.032	0.005	0.008	17.21	20.143	3.121	0.086	4.989	0.009	0.015	0.568	0.816	0.214	52.739

Table 3.2 Thermal property of the Inconel 718

Properties	Density	Melting Temperature	Thermal Conductivity	Thermal expansion	Possions ratio	Young's Modulus
Value	8190kg/m^3	1609^0 K	15 W/m.K	13.0 µm/m°C	0.27-0.3	205 G Pa

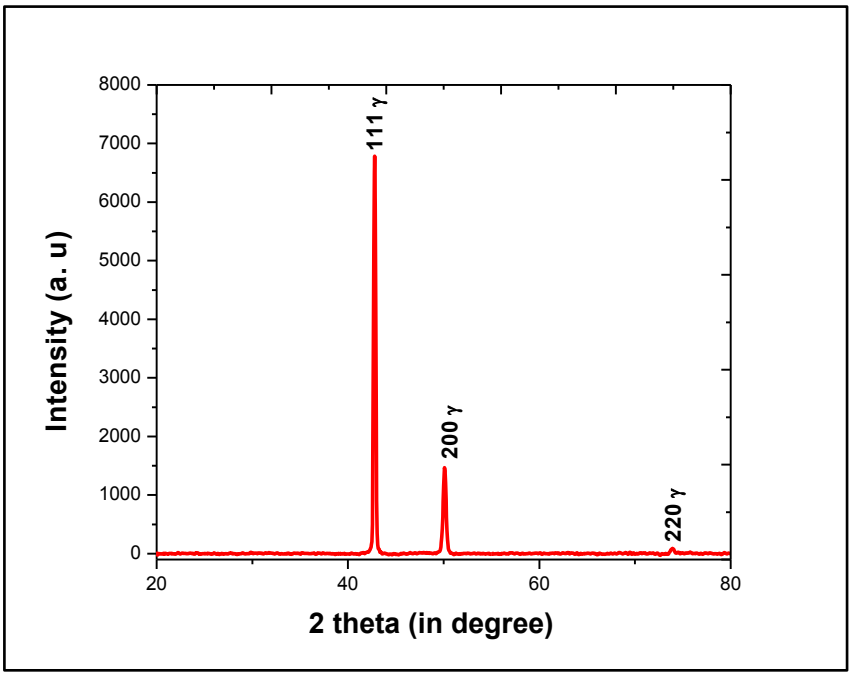

Figure 3.2 X-ray diffraction plot of the Inconel 718 work material

In EDM process the tool has to deal with a series of spark discharges. Hence, the tool must be of a good conductive material with high melting temperature, ability to withstand high temperature and dissipate the heat. Therefore, commercially available brass, copper, and graphite are used as the electrode material. The machining face of the three electrodes is cylindrical shape of diameter 13.5mm.

Experiments have been carried out in a die sinking CNC EDM machine (ECOWIN MIC-432C) with servo-head (constant gap) as shown in Figure 3.3. The specification of the machine is given in Table 3.3.Positive polarity for electrode and side flushing is used to conduct the experiments. The EDM process is performed on Inconel 718 plate having thickness 8mm and 10×11.5 cm^2 cross sectional area. A stopwatch is used to record each experimental run for 30 min. For weighing purpose, the work piece and the electrodes have been detached from the machine after each observation, cleaned and dried out. A precision electronic balance (accuracy 0.01g) is used for measuring the weights of the work piece and tool materials before and after machining. Surface roughness tester (Surftest SJ 210, Mitutoyo) is used for measuring the surface quality. A tool maker's microscope (Carl Zeiss) is used for measuring the crater diameter on the machined surface on the work material.

Table 3.3 Specification of the CNC Die sinker EDM machineECOWIN MIC-432C

Mechanism of process	Controlled erosion (melting and evaporation) through a series of electric spark
Spark gap	0.010- 0.500 mm
Spark frequency	200 – 500 kHz
Working Current	1-60A
Working voltage across the gap	30- 250 V
Maximum Flushing Pressure	0.5 Pa
Metal removal rate (max.)	680 mm^3/min
Specific power consumption	2-10 W/mm^3/min
Dielectric fluid	Liquid paraffin.
Dielectric tank Capacity	
Travel limit X-axis	400mm
Y-axis	400mm
Z-axis	400mm

3.5 Experimental strategy

The experiments have been conducted as per Box-Behnken design of response surface methodology (RSM) because it performs non-sequential experiments having fewer design points(Montgomery, 2008). It works in safe operating zone for the process as such a design does not have axial points. On the other hand, central composite designs have axial point outside the cube which may not be in the region of interest or may be impossible to run as they are beyond safe operating zone. Fifty four experimental runs need to be performed in Box-Behnken design with six factors each at three levels and six centre points. It helps to estimate a suitable functional relationship between input parameters and output. Generally, a second-order model shown in equation 3.21 is employed in response surface methodology.

$$y = \beta_0 + \sum_{i=1}^{k} \beta_i X_i + \sum_{i=1}^{k} \beta_{ii} X_i^2 + \sum_{kj} \sum \beta_{ij} X_i X_j + \varepsilon \quad (3.21)$$

where y is the output variable, X_i's are input parameters, X_i^2 and X_iX_j are the square and interaction terms of parameters respectively. β_0, β_i, β_{ii} and β_{ij} are the unknown regression coefficients and ε is the error. Experiments have been conducted to investigate the effect of open circuit voltage, discharge current, pulse-on-time, duty factor, flushing pressure and tool material on performance measures viz. material removal rate (MRR), electrode wear ratio (EWR),surface roughness, radial overcut and white layer thickness. Duty factor can be defined as $\tau = T_{on}/ (T_{on}+T_{off})$ in percentage where T_{off} is the pulse-off-time. The parametric levels are coded using the equation 3.22.

$$\text{Coded Value } (Z) = \frac{X - \frac{X_{max} + X_{min}}{2}}{\frac{X_{max} - X_{min}}{2}} \quad (3.22)$$

where Z is coded value (-1, 0, 1), X_{max} and X_{min} are maximum and minimum value of actual parameters and X is the actual value of corresponding parameter. Table 3.4 shows the levels of the process parameters.

Table 3.4 Process parameters and their levels

Process Parameters	Symbols	Levels		
		-1	0	1
Open circuit voltage in V	A	70	80	90
Discharge current in A	B	3	5	7
Pulse-on-time in µs	C	100	200	300
Duty factor in %	D	80	85	90
Flushing pressure in Bar	E	0.2	0.3	0.4
Tool	F	Brass	Copper	Graphite

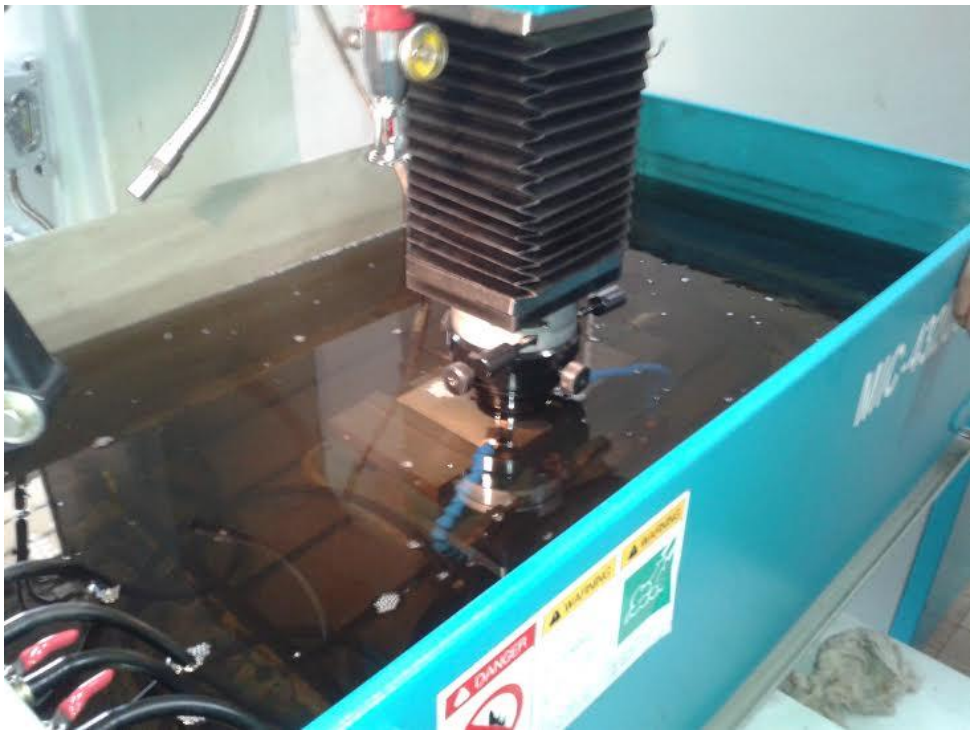

Figure 3.3 CNC die sinking EDM machine (ECOWIN PS 50ZNC) on experimental set up

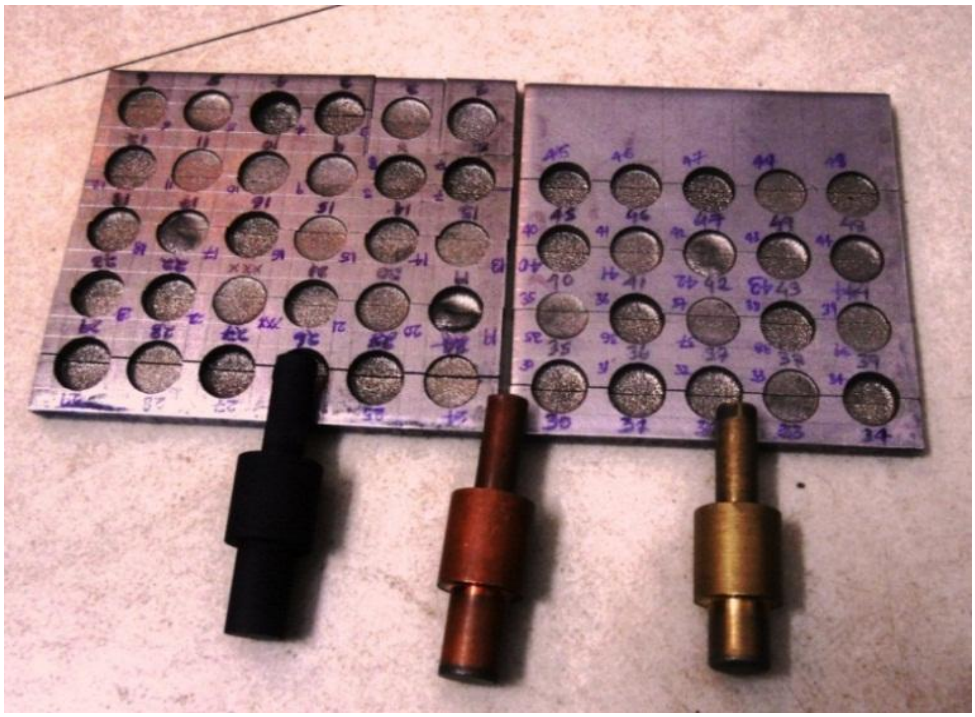

Figure 3.4 Wok material Inconel 718 after machining with three electrodes

3.5.1 Calculation of performance measures

(a) MRR

The work material after machining with three electrodes is shown in Figure 3.4.The weight of work piece before and after machining is recorded to calculate material removal rate (MRR) using following equations.

$$MRR = \frac{1000 \times \Delta Ww}{\rho_w \times T} \tag{3.23}$$

where ΔW_w is the work material weight loss during machining and $\rho_w$is the density of work material and T is the machining time.

(b) EWR

The weight of the tool material before and after machining is recorded to calculate the electrode wear ratio (EWR) in percentage the following equation

$$TWR = \frac{1000 \times \Delta Wt}{\rho_t \times T} \tag{3.24}$$

$$EWR = \frac{100 \times TWR}{MRR} \tag{3.25}$$

where TWR is the tool wear rate in mm^3/min, ΔW_t, istool weight loss during machining, $\rho_t$is the density of tool material (ρ_{brass}=8565 kg/m^3, ρ_{copper}=8960 kg/m^3 and $\rho_{graphite}$=2130 kg/m^3 and T is the machining time.

(c) Surface roughness

The surface roughness for machined surface of the work material is measured by a portable surface tester (Surftest SJ 210, Mitutoyo). Roughness measurements, in the transverse direction, on the work material are repeated five times and average of five readings of surface roughness values are noted down.

(d)Radial overcut

Radial overcut defined as the deviation between electrode diameter and the maximum diameter of the machined cavity. For precise and accurate machining minimization of over cut is essential. It is measured using the following relation

$$\text{Radial overcut} = \frac{d_w - d_t}{2} \quad (3.26)$$

where d_w is the maximum diameter of the crater cavity and d_t is the diameter of the tool.

(e)White layer thickness

The successive spark discharges, causes formation of molten metal pool and debris and later solidifies on the machined surface due to improper flushing. This leads to formation of recast layer or white layer on the machined surface and is easily distinguishable from parent metal. The layer consists of number of voids, micro cracks, globules, impurities and several microstructural defects which are responsible to weaken mechanical properties of the machined surface. A good machined surface should have minimum white layer thickness.

To measure the white layer thickness, the cross section of each the machined surface is was cut off is and polished on silicon carbide paper with grade sizes of 80, 120, 220, 320, 400, 800,1000,1200 respectively. Thereafter, the sample was polished a velvet cloth with diamond paste up to accuracy 1µm.The machined surface is etched with etchant Kalling's reagent to expose the white layer structure and the boundary line on the cross section. A scanning electron microscope (SEM) (Model, Joel JSM-6480LV, Japan) with a magnification of ×250 is employed to analyse the thickness of white layer. The thickness of white layer is calculated by measuring the area of deposited white layer by dividing the horizontal length of the micro graph. Table 3.5 shows the Box-Behnken design and performance measures for each experimental run.

Table 3.5 Box-behnken experimental design along with obtained performance measures

Run order	A	B	C	D	E	F	MRR mm^3/min	EWR %	Surface Roughness µm	Radial overcut mm	White layer thickness µm
1	-1	-1	0	-1	0	0	18.23	23.04	16.52	0.15	31.71
2	1	-1	0	-1	0	0	12.03	18.54	16.61	0.14	31.81
3	-1	1	0	-1	0	0	41.20	14.08	22.50	0.25	36.11
4	1	1	0	-1	0	0	32.50	18.12	22.80	0.25	36.01
5	-1	-1	0	1	0	0	26.90	15.95	16.57	0.16	33.70
6	1	-1	0	1	0	0	22.10	19.55	16.78	0.16	33.80
7	-1	1	0	1	0	0	36.10	16.23	22.59	0.28	36.30
8	1	1	0	1	0	0	31.20	18.94	22.72	0.26	36.20
9	0	-1	-1	0	-1	0	26.90	17.10	13.35	0.14	32.11
10	0	1	-1	0	-1	0	40.20	15.17	20.80	0.26	35.51
11	0	-1	1	0	-1	0	16.10	24.84	17.70	0.20	33.41
12	0	1	1	0	-1	0	30.50	16.43	23.50	0.30	36.41
13	0	-1	-1	0	1	0	24.10	19.29	14.00	0.15	32.21
14	0	1	-1	0	1	0	38.90	15.45	20.70	0.25	35.61
15	0	-1	1	0	1	0	16.50	24.85	15.60	0.21	33.61
16	0	1	1	0	1	0	29.80	17.08	21.30	0.31	36.31
17	0	0	-1	-1	0	-1	12.80	62.42	10.35	0.07	15.81
18	0	0	1	-1	0	-1	5.10	117.25	12.42	0.11	17.04
19	0	0	-1	1	0	-1	17.90	44.75	11.23	0.08	17.51
20	0	0	1	1	0	-1	12.50	56.16	13.31	0.11	18.92
21	0	0	-1	-1	0	1	33.80	9.76	21.60	0.39	46.14
22	0	0	1	-1	0	1	28.01	9.28	26.30	0.47	47.14
23	0	0	-1	1	0	1	44.50	7.53	22.60	0.40	46.43
24	0	0	1	1	0	1	36.10	7.34	27.20	0.48	47.42
25	-1	0	0	-1	-1	0	22.50	22.04	21.20	0.21	33.81
26	1	0	0	-1	-1	0	15.50	31.68	22.30	0.20	33.91
27	-1	0	0	1	-1	0	36.70	13.43	21.50	0.22	34.40
28	1	0	0	1	-1	0	23.50	21.15	22.35	0.21	34.42
29	-1	0	0	-1	1	0	26.30	18.94	21.30	0.22	33.96
30	1	0	0	-1	1	0	15.90	30.75	22.56	0.22	34.01
31	-1	0	0	1	1	0	31.90	15.64	22.00	0.23	34.41
32	1	0	0	1	1	0	24.70	20.24	22.59	0.23	34.80
33	0	-1	0	0	-1	-1	6.81	101.62	6.80	0.03	15.81
34	0	1	0	0	-1	-1	20.10	43.88	13.21	0.10	21.04
35	0	-1	0	0	1	-1	7.01	99.14	7.80	0.04	16.16
36	0	1	0	0	1	-1	20.20	44.06	13.95	0.11	21.24
37	0	-1	0	0	-1	1	20.05	11.42	19.80	0.35	45.14

38	0	1	0	0	-1	1	48.80	8.03	28.20	0.50	49.24
39	0	-1	0	0	1	1	26.12	9.00	20.10	0.36	45.24
40	0	1	0	0	1	1	48.90	8.08	28.50	0.52	48.94
41	-1	0	-1	0	0	-1	18.20	43.68	10.20	0.06	16.84
42	1	0	-1	0	0	-1	11.95	66.28	10.40	0.06	17.14
43	-1	0	1	0	0	-1	11.85	58.99	13.00	0.10	18.24
44	1	0	1	0	0	-1	5.92	118.41	13.30	0.10	18.34
45	-1	0	-1	0	0	1	43.10	9.03	21.80	0.40	47.04
46	1	0	-1	0	0	1	35.10	11.28	23.40	0.38	47.09
47	-1	0	1	0	0	1	35.90	7.52	26.50	0.51	48.04
48	1	0	1	0	0	1	27.10	10.15	27.80	0.48	48.14
49	0	0	0	0	0	0	18.50	25.95	22.50	0.25	35.11
50	0	0	0	0	0	0	21.50	21.86	24.00	0.20	34.91
51	0	0	0	0	0	0	16.70	30.54	21.00	0.26	35.41
52	0	0	0	0	0	0	20.40	22.55	22.20	0.20	34.86
53	0	0	0	0	0	0	18.30	27.87	23.45	0.25	35.46
54	0	0	0	0	0	0	19.60	23.21	21.80	0.21	35.06

3.6 Results and discussions

Table 3.5 shows the Box-Behnken design and performance measures for each experimental run.The experimental data collected as per Box-behnken design are analysed to establish the influence of various process parameters on the responses using analysis of variance (ANOVA) at significance level of 0.05.Table 3.6 shows the ANOVA table for MRR with percentage of contribution of each parameter and their interactions. The parameters such as tool material, discharge current, pulse-on-time, open circuit voltage and duty factor their square terms and interaction terms - discharge current×duty factor and discharge current×tool are found to be significant. The table also shows that tool material is the most influential parameter for MRR with highest percentage of contribution of 49.74% followed by discharge current, pulse-on-time, open circuit voltage and duty factor with percentage contribution of 24.76%, 5.48%, 5.40% and 4.16% respectively.Flushing pressure is found to an insignificant process parameter for MRR. The coefficient of determination (R^2) and adjusted (R^2) values are found to be 97.7% and 96.16% respectively. It is to be noted that the lack of fit is not significant for MRR.

Table 3.6 ANOVA for MRR

Source	Sum of Squares	Degrees of freedom	Mean Square	F-Value	Prob> F		% Contribution
Model	6289.4	22	285.882	61.38953	< 0.0001	significant	
A-Open circuit voltage	347.929	1	347.929	74.71341	< 0.0001		5.41
B-Discharge current	1593.33	1	1593.33	342.1463	< 0.0001		24.77
C-Pulse-on-time	353.204	1	353.204	75.84597	< 0.0001		5.49
D-Duty factor	268.202	1	268.202	57.59302	< 0.0001		4.17
E-Flushing pressure	0.29704	1	0.29704	0.063785	0.8023		0.00
F-Tool	3200.27	1	3200.27	687.2182	< 0.0001		49.74
A×B	0.845	1	0.845	0.181453	0.6731		0.01
A×E	0.845	1	0.845	0.181453	0.6731		0.01
A×F	2.66805	1	2.66805	0.57293	0.4548		0.04
B×D	79.0025	1	79.0025	16.96477	0.0003		1.23
B×E	2.00931	1	2.00931	0.431473	0.5161		0.03
B×F	78.4378	1	78.4378	16.84352	0.0003		1.22
C×E	1.805	1	1.805	0.387601	0.5381		0.03
C×F	0.95551	1	0.95551	0.205183	0.6537		0.01
D×E	7.605	1	7.605	1.633077	0.2108		0.12
D×F	4.94551	1	4.94551	1.061986	0.3107		0.08
E×F	4.30711	1	4.30711	0.924898	0.3436		0.07
A^2	39.1887	1	39.1887	8.415273	0.0068		0.61
B^2	205.154	1	205.154	44.05428	< 0.0001		3.19
C^2	86.2692	1	86.2692	18.52521	0.0002		1.34
D^2	47.6667	1	47.6667	10.23583	0.0032		0.74
E^2	24.028	1	24.028	5.159698	0.0302		0.37
Residual	144.362	31	4.65685				2.24
Lack of Fit	129.929	26	4.99727	1.731157	0.2834	Not significant	
Pure Error	14.4333	5	2.88667				
Cor Total	6433.77	53					

Table 3.7 shows the ANOVA table for EWRwith percentage of contribution of each parameter and their interactions. It shows that tool material, discharge current, pulse-on-time, open circuit voltage, duty factor and square terms of tool material and interaction terms -discharge current×tool, pulse-on-time×tool, open circuit voltage×tool, and duty factor×tool are significant parameters.The Table also shows that tool material is found to be the most influential parameter for EWR with highest percentage of contribution of 61.84% followed by discharge current, pulse-on-time, open circuit voltage and duty factor with percentage contribution of 2.44%, 2.37%, 1.76% and 1.56% respectively.Flushing pressure is found to

be an insignificant parameter for EWR. The coefficient of determination (R^2) and adjusted (R^2) values are found to be 93.55% and 90.51% respectively. It is to be noted that the lack of fit is not significant for EWR.

Table 3.7 ANOVA for EWR

Source	Sum of Squares	Degrees of freedom	Mean Square	F-Value	Prob> F	Source	% Contribution
Model	35218.0	17	2133.05	30.73	< 0.0001	significant	
A-Open circuit voltage	667.01	1	667.01	9.61	0.0037		1.77
B-Discharge Current	922.32	1	922.32	13.29	0.0008		2.45
C-Pulse-on-time	894.99	1	894.99	12.89	0.001		2.37
D-Duty Factor	590	1	590	8.5	0.0061		1.56
E-Flushing Pressure	0.76	1	0.76	0.011	0.9172		0.00
F-Tool	23326.53	1	23326.53	336.08	< 0.0001		61.85
A×C	172.98	1	172.98	2.49	0.1232		0.46
A×F	743.75	1	743.75	10.72	0.0024		1.97
B×C	13.56	1	13.56	0.2	0.6611		0.04
B×F	1471.84	1	1471.84	21.21	< 0.0001		3.90
C×D	232.5	1	232.5	3.35	0.0755		0.62
C×F	1172.96	1	1172.96	16.9	0.0002		3.11
D×F	695.48	1	695.48	10.02	0.0031		1.84
B^2	121.47	1	121.47	1.75	0.1942		0.32
C^2	59.22	1	59.22	0.85	0.3618		0.16
D^2	68.3	1	68.3	0.98	0.3278		0.18
F^2	4064.33	1	4064.33	58.56	< 0.0001		10.78
Residual	2498.69	36	69.41				6.62
Lack of Fit	2371.37	31	76.5	3	0.1108	not significant	
Pure Error	127.32	5	25.46				
Cor Total	37716.69	53					

Table 3.8 shows the ANOVA for surface roughnesswith percentage of contribution of each parameter and their interactions.It shows that tool material, discharge current, pulse-on-time,open-circuit voltage, square terms of discharge current, pulse-on-time,tool material and interaction terms-discharge current×tool, pulse-on-time×tool,pulse-on-time×flushing pressure are important parameters.The Table also shows that tool material is found to be the most influential parameter for surface roughness with highest percentage of contribution of 67.13% followed by discharge current, pulse-on-time and open circuit voltage with percentage contribution of 16.88%, 3.78% and 0.16% respectively.Duty factor and flushing pressure are found to be insignificant process parameters for surface roughness. The coefficient of determination (R^2) and adjusted (R^2) values are found to be 93.37% and

89.67% respectively. It is to be noted that the lack of fit is not significant for surface roughness

Table 3.8 ANOVA for surface roughness

Source	Sum of Squares	Degree of freedom	Mean Square	F Value	p-value Prob> F		% Contribution
Model	1530.104	17	91.17	206.85	< 0.0001	significant	
A-Open circuit voltage	2.62	1	2.62	5.95	0.0198		0.17
B-Discharge Current	260.96	1	260.96	592.1	< 0.0001		16.88
C-Pulse-on-time	58.59	1	58.59	132.94	< 0.0001		3.79
D-Duty Factor	1.03	1	1.03	2.34	0.1345		0.07
E-Flushing Pressure	4.00×10^{-3}	1	4.00×10^{-3}	9.09×10^{-3}	0.9246		0.00
F-Tool	1037.93	1	1037.93	2354.97	< 0.0001		67.14
A×F	0.72	1	0.72	1.63	0.2094		0.05
B×C	0.88	1	0.88	1.99	0.1667		0.06
B×F	2.25	1	2.25	5.1	0.0301		0.15
C×E	2.94	1	2.94	6.67	0.014		0.19
C×F	4.57	1	4.57	10.37	0.0027		0.30
E×F	0.16	1	0.16	0.37	0.5476		0.01
B^2	63.66	1	63.66	144.44	< 0.0001		4.12
C^2	23.41	1	23.41	53.11	< 0.0001		1.51
D^2	1.04	1	1.04	2.37	0.1325		0.07
E^2	0.16	1	0.16	0.36	0.5502		0.01
F^2	69.18	1	69.18	156.97	< 0.0001		4.47
Residual	15.87	36	0.44				1.03
Lack of Fit	9.88	31	0.32	0.27	0.991	not significant	
Pure Error	5.98	5	1.20				
Cor Total	1545.974	53					

Table 3.9 shows the ANOVA for radial overcut with percentage of contribution of each parameter and their interactions. It shows that tool material, discharge current, pulse-on-time, duty factor and square terms of tool material, discharge current, pulse-on-timeand interaction terms discharge current×tool, pulse-on-time×tool, are most influencing parameters.The Table also shows that that tool material is found to be the most influential parameter for radial overcut with highest percentage of contribution of 85.56%, followed by discharge current, pulse-on-time and duty factor with percentage contribution of 8%, 2.56% and 0.07% respectively.Open circuit voltage and flushing pressure are found to exhibit insignificant effect for radial overcut.The coefficient of determination (R^2) and adjusted (R^2) values are found to be 99.2% and 98.8% respectively. It is to be noted that the lack of fit is not significant for radial overcut.

Table 3.9 ANOVA for radial overcut

Source	Sum of Squares	Degree of freedom	Mean Square	F Value	p-value Prob> F		% Contribution
Model	0.89	16	0.056	376.67	< 0.0001	significant	
A-Open circuit voltage	5.13×10^{-4}	1	5.13×10^{-4}	3.46	0.0707		0.06
B-Discharge Current	0.072	1	0.072	485.42	< 0.0001		8.00
C-Pulse-on-time	0.023	1	0.023	158.14	< 0.0001		2.56
D-Duty Factor	6.62×10^{-4}	1	6.62×10^{-4}	4.46	0.0414		0.07
E-Flushing Pressure	5.51×10^{-4}	1	5.51×10^{-4}	3.72	0.0615		0.06
F-Tool	0.77	1	0.77	5162.1	< 0.0001		85.56
A×F	2.0×10^{-4}	1	2.00×10^{-4}	1.35	0.2528		0.02
B×C	2.81×10^{-5}	1	2.81×10^{-5}	0.19	0.6656		0.00
B×F	3.61×10^{-3}	1	3.61×10^{-3}	24.37	< 0.0001		0.40
C×E	7.81×10^{-5}	1	7.81×10^{-5}	0.53	0.4724		0.01
C×F	2.89×10^{-3}	1	2.89×10^{-3}	19.49	< 0.0001		0.32
A^2	4.97×10^{-4}	1	4.97×10^{-4}	3.35	0.0751		0.06
B^2	9.22×10^{-4}	1	9.22×10^{-4}	6.22	0.0172		0.10
C^2	6.99×10^{-4}	1	6.99×10^{-4}	4.72	0.0363		0.08
D^2	2.63×10^{-4}	1	2.63×10^{-4}	1.78	0.1909		0.03
F^2	0.011	1	0.011	75	< 0.0001		1.22
Residual	5.48×10^{-3}	37	1.48×10^{-4}				0.61
Lack of Fit	1.81×10^{-3}	32	5.67×10^{-5}	0.077	1	not significant	
Pure Error	3.67×10^{-3}	5	7.34×10^{-4}				
Cor Total	0.9	53					

Table 3.10 shows the ANOVA for white layer thicknesswith percentage of contribution of each parameter and their interactions. It shows that tool material,discharge current, pulse-on-time, duty factor, square terms of pulse-on-time, duty factor,flushing pressure, tool material and interaction terms-discharge current×duty factor, discharge current×tool, duty factor×tool are the most influential parameters.The Table also shows that tool material is found to be the most influential parameter for white layer thickness with highest percentage of contribution of 96.94% followed by discharge current, pulse-on-time and duty factor with percentage contribution of 1.53%, 0.14% and 0.09% respectively.Open circuit voltage and flushing pressure are found to be insignificant parameters for white layer thickness. The coefficient of determination (R^2) and adjusted (R^2) values are found to be 99.9% and 99.8% respectively. It is to be noted that the lack of fit is not significant for white layer thickness.

Table 3.10 ANOVA for white layer thickness

Source	Sum of Squares	Degree of freedom	Mean Square	F Value	p-value Prob> F		% Contribution
Model	5316.58	17	312.74	2279.02	< 0.0001	significant	
A-Open curcuit Voltage	0.051	1	0.051	0.37	0.5446		0.00
B-Discharge Current	81.44	1	81.44	593.46	< 0.0001		1.53
C-Pulse-on-time	7.65	1	7.65	55.75	< 0.0001		0.14
D-Duty Factor	4.88	1	4.88	35.55	< 0.0001		0.09
E-Flushing Pressure	0.069	1	0.069	0.51	0.4818		0.00
F-Tool	5159.15	1	5159.15	37596.06	< 0.0001		96.95
B×C	0.15	1	0.15	1.1	0.3008		0.00
B×D	1.62	1	1.62	11.81	0.0015		0.03
B×F	0.79	1	0.79	5.74	0.0219		0.01
C×F	0.086	1	0.086	0.62	0.4349		0.00
D×F	1.11	1	1.11	8.09	0.0073		0.02
E×F	0.07	1	0.07	0.51	0.4787		0.00
A^2	0.028	1	0.028	0.21	0.6522		0.00
C^2	2.22	1	2.22	16.21	0.0003		0.04
D^2	3.85	1	3.85	28.07	< 0.0001		0.07
E^2	0.77	1	0.77	5.62	0.0233		0.01
F^2	42.28	1	42.28	308.07	< 0.0001		0.79
Residual	4.94	36	0.14				0.09
Lack of Fit	4.63	31	0.15	2.38	0.1692	not significant	
Pure Error	0.31	5	0.063				
Cor Total	5321.52	53					

Process model for the responses obtained through regression analysis are given below:

MRR = +19.01 - 3.81 × A + 8.15 × B - 3.84 × C + 3.34 × D + 0.11 × E + 11.55 × F-0.58 × A × F -3.14 × B × D - 0.35 × B × E + 3.13 × B × F + 0.47 × C × E-0.98 × D × E + 0.79 × D × F + 0.73 × E × F + 1.93 × A^2+ 4.42 × B^2+2.78 × C^2+ 2.13 × D^2 + 1.51 × E^2 (Coded form) (3.27)

EWR = +31.93 + 5.27 × A - 6.20 × B + 6.11 × C - 4.96 × D - 0.18 × E - 31.18 × F + 4.65 × A × C - 9.64 × A × F - 1.30 × B × C + 13.56 × B × F - 5.39 × C × D - 8.56 × C × F + 9.32 × D × F - 3.29 × A^2 - 5.95 × B^2 - 4.93 × C^2 - 4.64 × D^2 - 2.27 × E^2 + 16.95 × F^2 (Coded form) (3.28)

Surface roughnes = +22.49+0.33× A+3.30× B+1.56× C+0.21×D-0.013×E+6.58×F+0.30×A×F-0.33× B× C+0.53× B×F-0.61 ×C × E+0.53×C×F-0.14×E×F-0.10×A^2-2.48×B^2-1.51×C^2-0.28×D^2-0.14×E^2-2.58×F^2(Codedform) (3.29)

Radial overcut = + 0.23 - 4.625 ×10^{-3} × A + 0.055 × B + 0.031 × C + 5.25 × 10^{-3}× D + 4.792 × 10^{-3} × E + 0.18 × F – 5 × 10^{-3} × A × F - 1.875 × 10^{-3} × B × C + 0.021 × B × F + 3.125 × 10^{-3} × C × E + 0.013 × C × F - 6.881 × 10^{-3} × A^2 - 9.071 × 10^{-3} × B^2 + 8.161 × 10^{-3} × C^2 - 5.006 × 10^{-3} × D^2 + 0.033 × F^2

(Coded form) (3.30)

White layer thickness= +35.13+0.046×A +1.84 × B+0.56×C+0.45 ×D+0.054× E+14.66×F-0.14×B×C-0.45×B ×D-0.31×B×F-0.073× C×F-0.37×D×F-0.094×E×F-0.052× A^2-0.46×C^2-0.61 ×D^2-0.26×E^2-2.01× F^2

(Coaded form) (3.31)

As discharge current is found to be a significant either as a parameter or in interaction with other parameters for all the responses, it is decided to observe the effect discharge current microscopically. Figure 3.5 and 3.6 shows the Scanning Electron Microscope (SEM) micrographs at parametric condition (A=80V B=3A C=100µs D=85% E=0.4bar F=copper electrode)experiment number 13 and (A=80V B=7A C=100µs D=85% E=0.4bar F=copper electrode)experiment number 14 respectively. From the SEM micrographs, it can be noted that size of the cracks and pores on the machined surface increases as discharge current increases from 3A to 7 A.

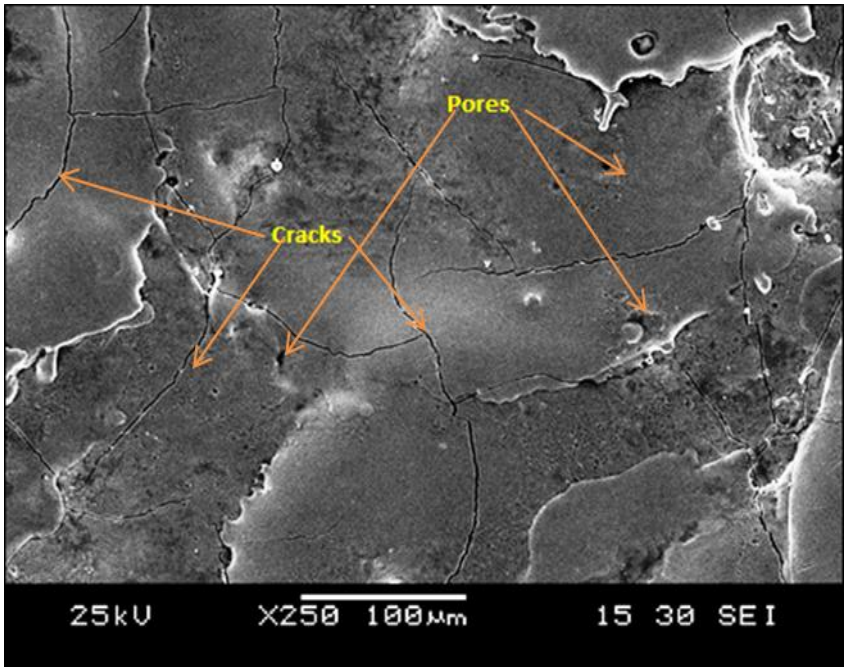

Figure 3.5 SEM Micrograph showing micro cracks and pores on the machined surface atA=80V B=3A C=100µs D=85% E=0.4bar F=copper electrode

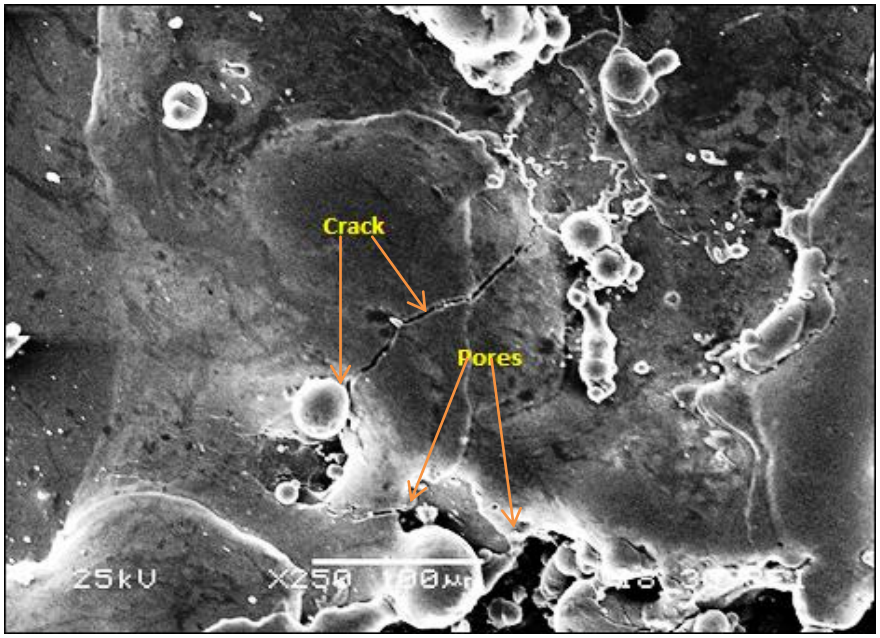

Figure 3.6 SEM Micrograph showing micro cracks and pores on the machined surface at A=80V B=7A C=100µs D=85% E=0.4bar F=copper electrode

Figure 3.7 (a-b-c) shows the SEM micrographs for the white layer thickness analysis taken with the parametric conditions at A=80V B=5A C=100µs D=80% E=0.3bar F=Brass tool, A=80V B=5A C=200µs D=85% E=0.3bar F=copper tool and A=80V B=5A C=300µs D=90% E=0.3bar F=Graphite tool respectively. The spark energy in EDM is primarily governed by discharge current, pulse-on-time and duty factor. Increase pulse-on-time and duty factor significantly improves the spark energy in between electrodes. From the micrographs, it can be clearly observed, that the white layer thickness increases with increase in spark energy and variation of tool material. It is can be clearly observed, that white layer formed on the machined surface with brass electrode is comparatively less as compared to copper and graphite electrode.

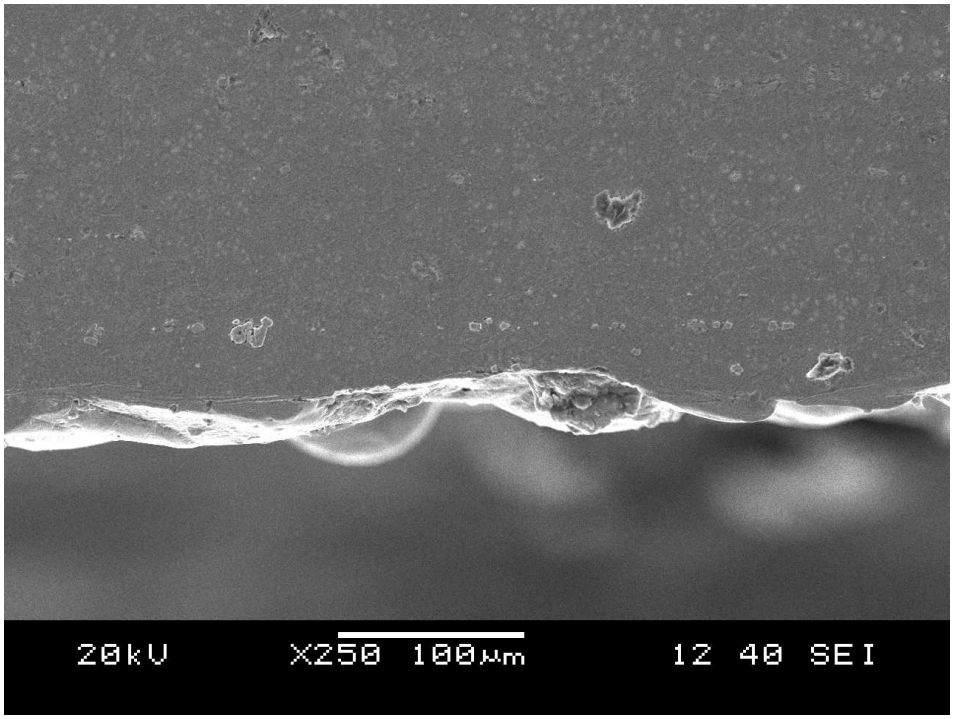

Figure 3.7(a) SEM Micrograph showing white layer on the cross section of machined surface at A=80V B=5A C=100µs D=80% E=0.3bar F=Brass tool

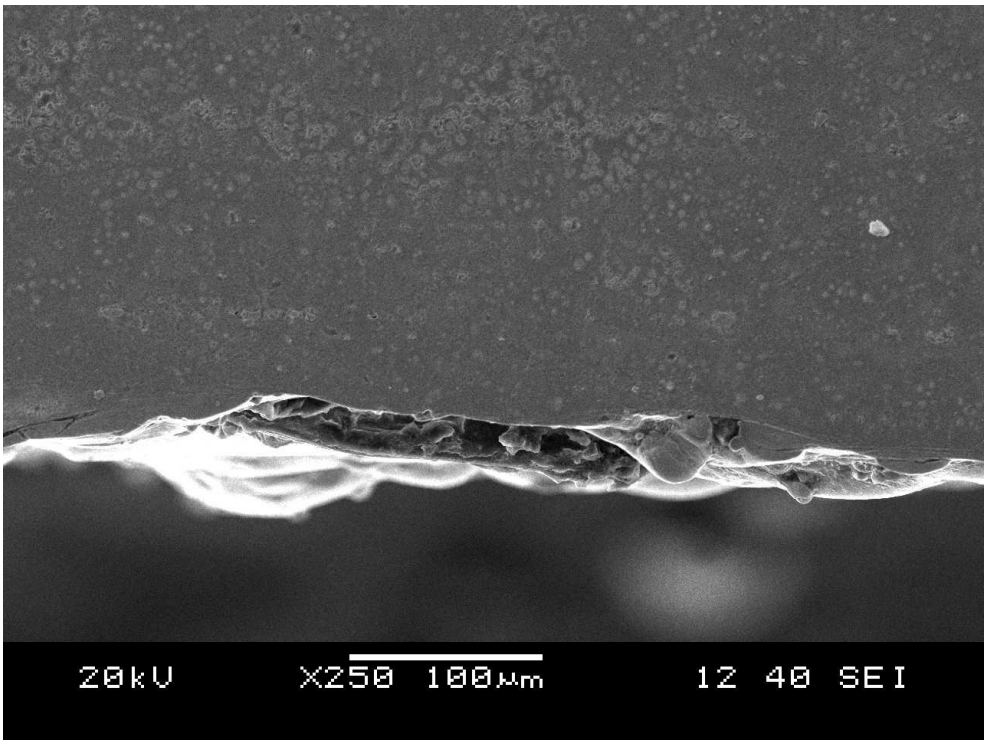

Figure 3.7(b) SEM Micrograph showing white layer on the cross section of machined surface at A=80V B=5A C=200µs D=85% E=0.3bar F=copper tool

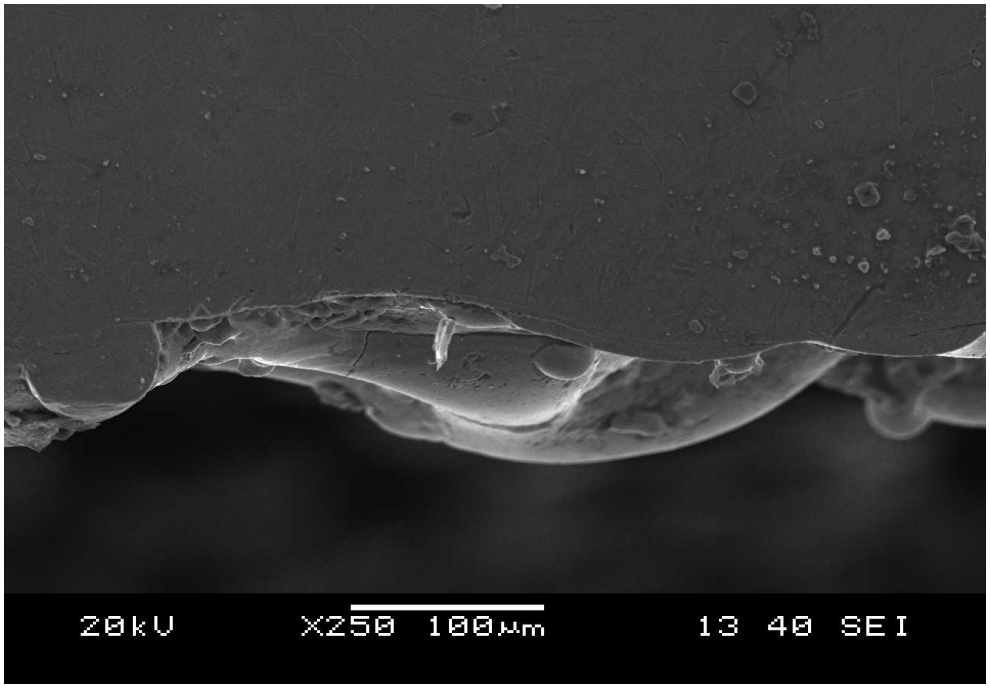

Figure 3.7(c) SEM Micrograph showing white layer on the cross sectionof machined surface at A=80V B=5A C=300µs D=90% E=0.3bar F=Graphite tool

Figure 3.8 shows the surface plot for variation of MRR with open circuit voltage and discharge current. The figure indicates that material removal rate increases with the increase of discharge current for all values of open circuit voltages. Increase in discharge current directly affects the discharge energy which in turn causes an increase in the crater dimension resulting in increased metal removal rate. The surface plot also shows that the MRR initially decreases with the increase of open circuit voltage for any value of discharge current but shows a slight increasing trend after reaching a minimum value. Low values of open circuit voltage can lead to increase in MRR whereas higher values of open circuit voltage can cause relatively lower material removal rates. This phenomenon is similar to experimental studies reported by Lee and Li (2001).

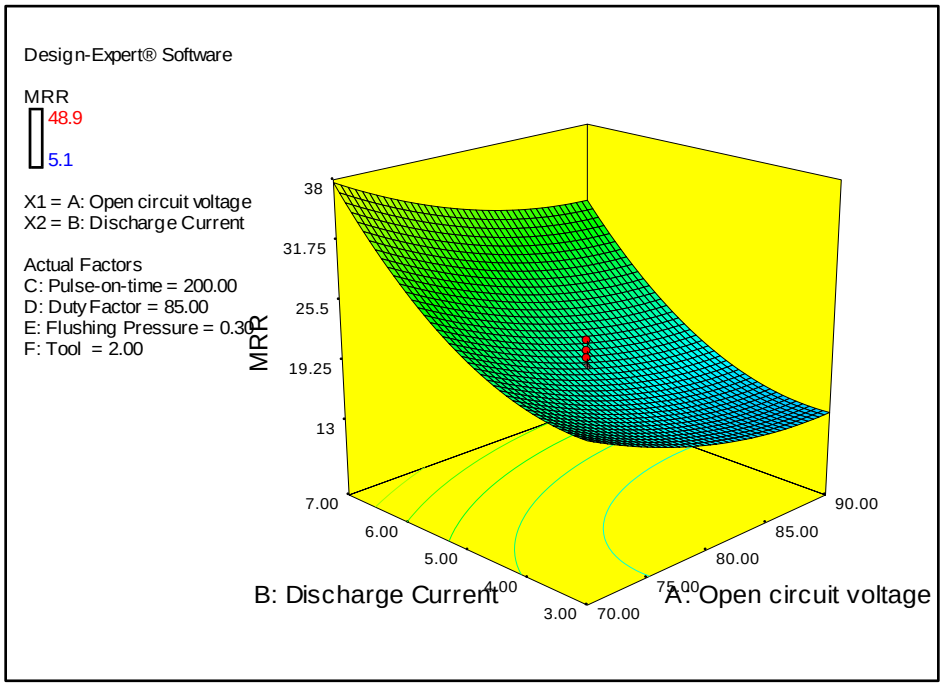

Figure 3.8 Surface plot of MRR with Discharge current and open circuit voltage

Figure 3.9 shows variation of MRR with discharge current and tool material. The Figure reveals that MRR increases monotonically with increase in discharge current with use of graphite and copper electrodes but increases slowly with the use of brass electrode. Material removal is higher while machining with graphite electrode followed by copper and brass respectively. As graphite and copper electrodes have higher thermal conductivities than brass electrode, the spark energy between the graphite and copper electrode is higher in comparison with brass, which in turn causes higher MRR in comparison with brass electrode.

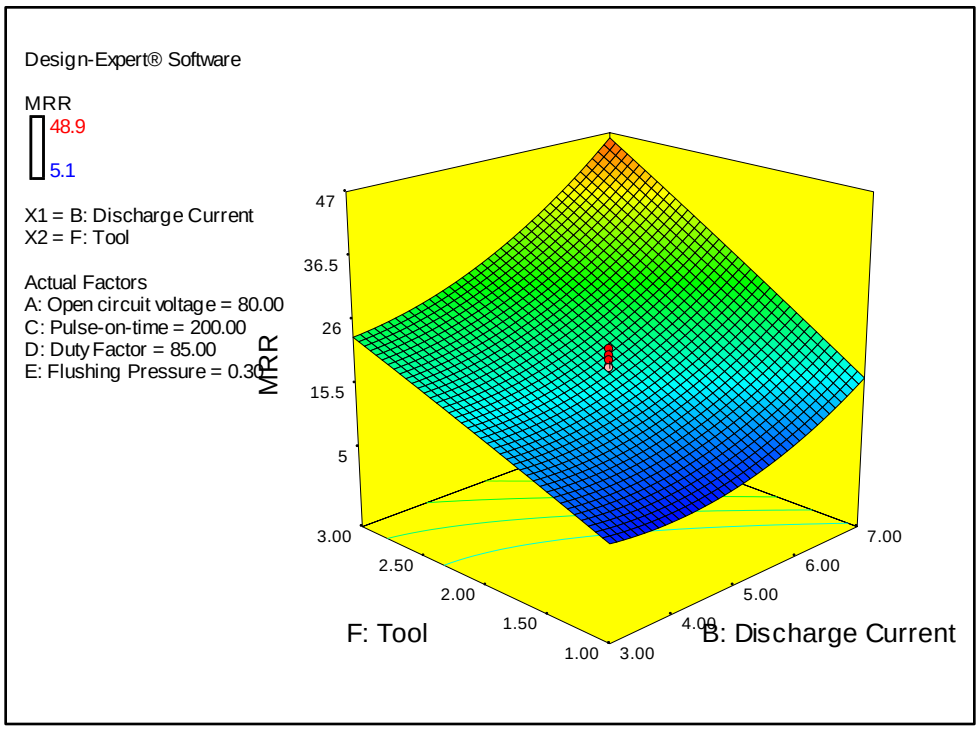

Figure 3.9 Surface plot of MRR with discharge current and tool material

Figure 3.10 shows the variation of MRR with tool material and pulse-on-time. It shows that MRR varies inversely with increase in pulse-on-time. Increase of pulse-on-time causes the heat flux to be conducted into the work piece in form of plasma channel for an extended time interval resulting in increase in the MRR (Panda 2008; Natsu et al. 2006). However, continuous application of the same heat flux for a longer duration decreases the pressure inside the plasma channel. As the volume of molten material remains unaffected, further increase in pulse-on-time results in decrease of MRR.A similar finding has been also observed in the experimental investigation of previous researchers (Pradhan and Biswas 2010).

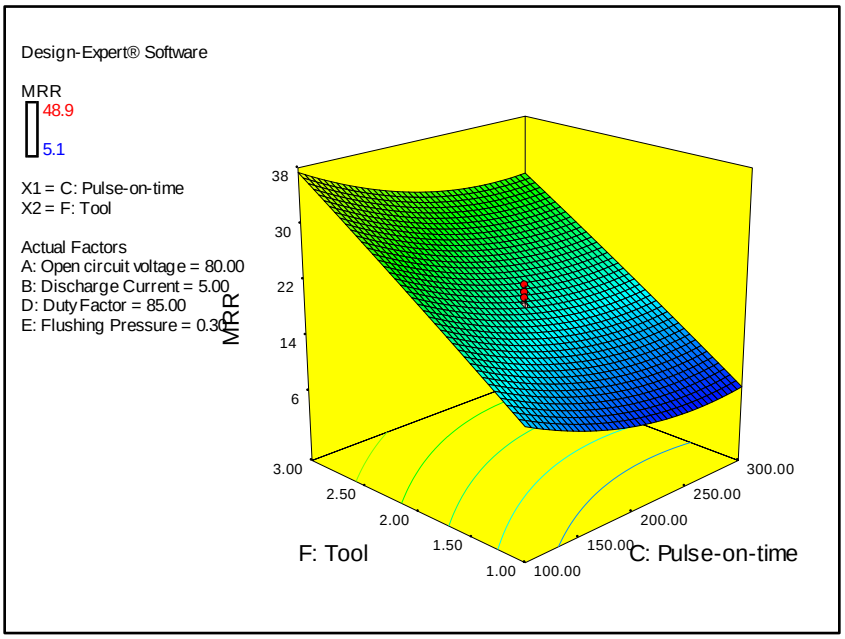

Figure 3.10 Surface plot of MRR with pulse-on-time and tool material

Figure 3.11 shows the variation of MRR with duty factor and tool material. It shows that for all three tool materials MRR shows a steady increase with increase in duty factor. However, the increase is more pronounced with graphite and copper tool. Increase in duty factor increases the number of sparks per unit time. As a result, the spark energy across the gap increases leading to increase in molten metal volume from the machined surface. This phenomenon influences increase in MRR.

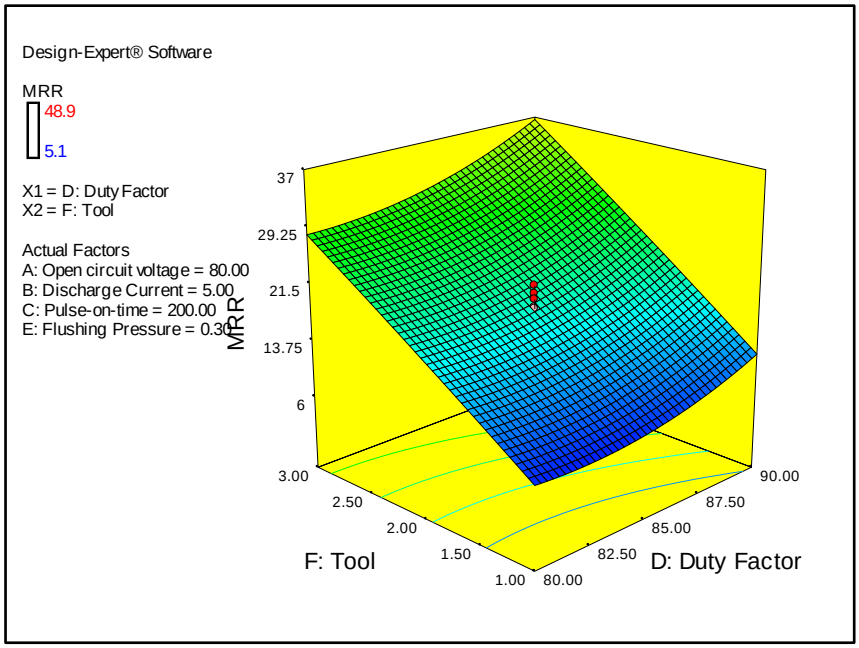

Figure 3.11 Surface plot of MRR with duty factor and tool material

Electrode wear ratio (EWR) is an important machining characteristic in EDM process as it directly affects the machining cost of the process. Figure 3.12 shows the surface plot of EWR with discharge current and tool material. The figure indicates that minimum electrode wear ratio can be obtained when machined with graphite electrode. Highest electrode wear ratio is observed when machined with brass electrode. Copper electrode exhibits wear ratio those between graphite and brass. The figure also indicates that EWR increases with increase in discharge current for all the electrodes. But increase of EWR in case of graphite electrode is relatively small.

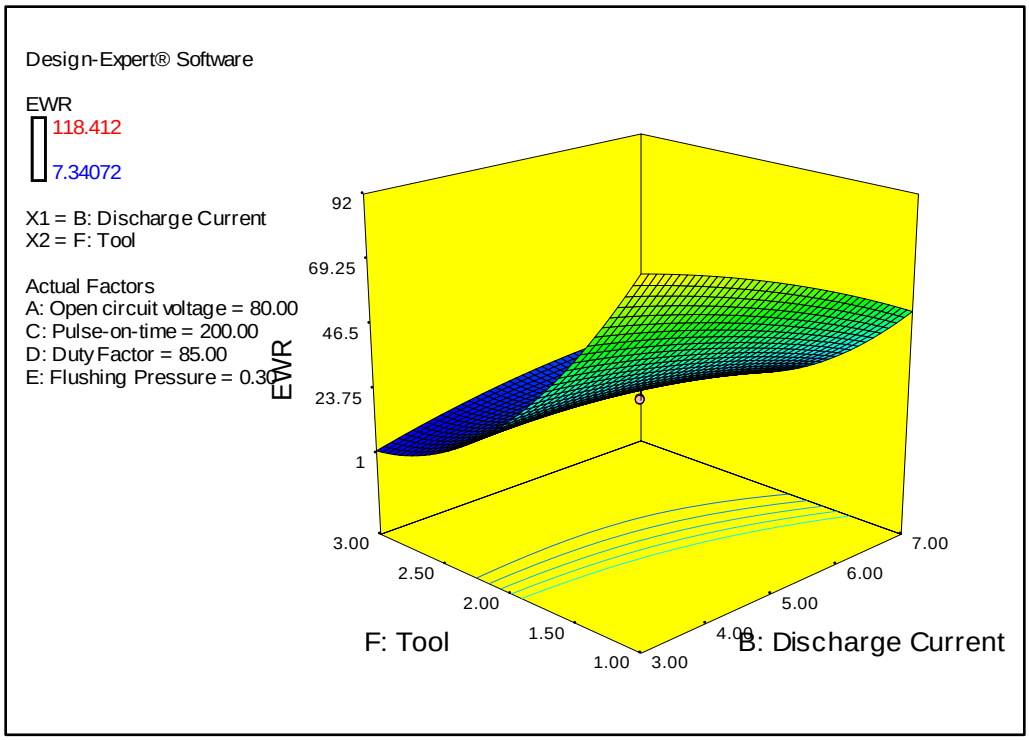

Figure 3.12 Surface plot of EWR with discharge current and tool material

Figure 3.13 shows the plot of pulse-on-time and open circuit voltage. It shows that EWR increases with increase in open circuit voltage. This obvious as, increase in open circuit voltage increases the spark energy, which in turn increases the molten metal volume from both the electrodes resulting in increase in EWR. The Figure also show that EWR increases with increase in pulse-on-time but shows a decreasing trend further when pulse-on time is set beyond 200µs. This may be due to decrease in spark energy density in the spark gap between electrodes as the diameter of the plasma channel expands with increase in pulse-on-time. Another reason for lower wear ratio at higher pulse-on-time is due to the attachment of carbon particles on to the electrode tip causing increase in the wearing resistance of tool and reducing EWR. A similar trend has been reported by previous researchers (Srivastava and Pandey 2012). Similarly, from the surface plot of EWR with pulse-on-time and duty factor it is observed that EWR increases slowly with increase in duty factor due to increase in spark energy.

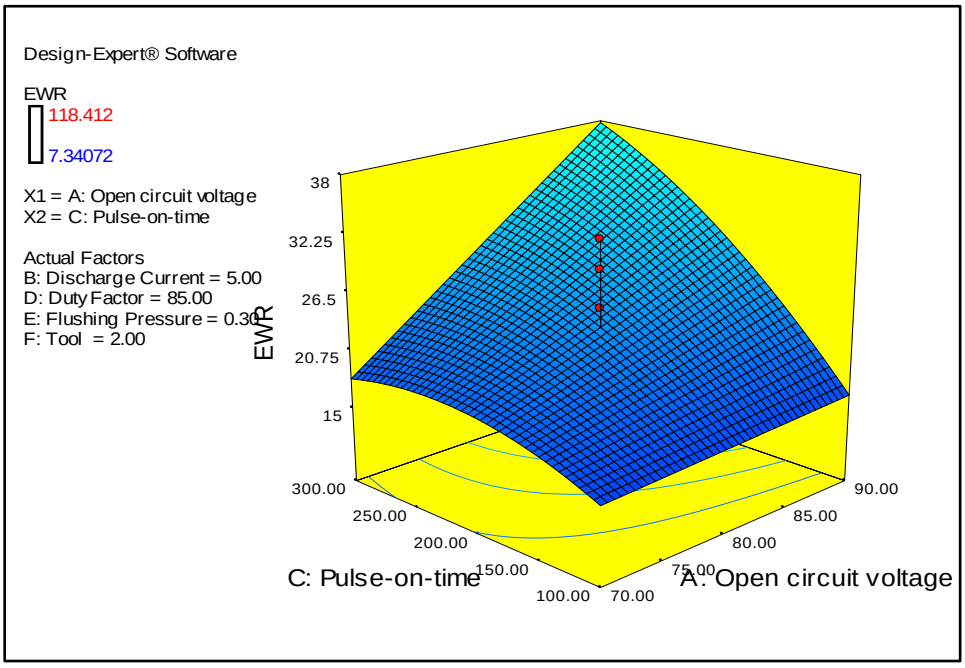

Figure 3.13 Surface plot of EWR with pulse-on-time and open circuit voltage

Figure 3.14 shows the variation of surface roughness with discharge current and tool material. It shows that surface quality deteriorates with increases in discharge current when graphite and copper electrodes are used. As discharge current increases, the spark energy also increases. Hence, more heat is produced resulting in larger size material to be removed from the work surface degrading the surface quality of the machined surface. Graphite electrode exhibits the poorest performance with regard to the surface finish. Brass electrode at smaller values of discharge current produces finest surface quality. Copper electrode produces Inconel 718 alloy work material with surface roughness value between those of copper and graphite.

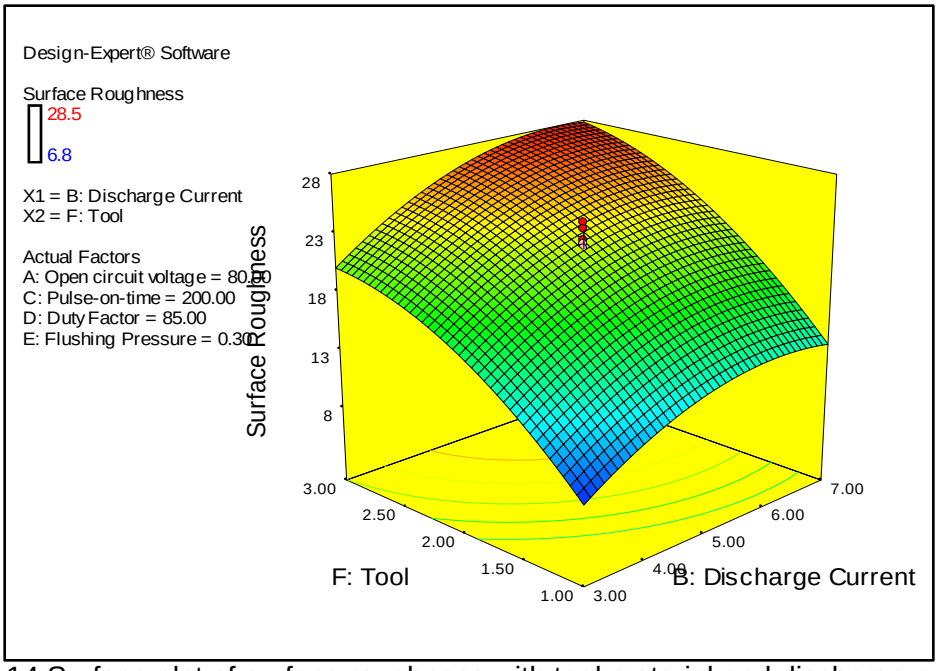

Figure 3.14 Surface plot of surface roughness with tool material and discharge current

Figure 3.15 shows the variation of surface roughness with tool material and pulse-on-time. It shows that surface roughness increases with increase in pulse-on-time. Increasing the pulse-on-time improves the spark energy which in turn causes larger size particle removed from the machined surface and in turn the machined surface quality is poor. Thus, it can be concluded that good surface quality can only be achieved at smaller value of discharge current with brass as the electrode material. Similarly, from the surface plot of surface roughness with tool material and open circuit voltage, it is observed that surface roughness increases slowly with increase in open circuit voltage.

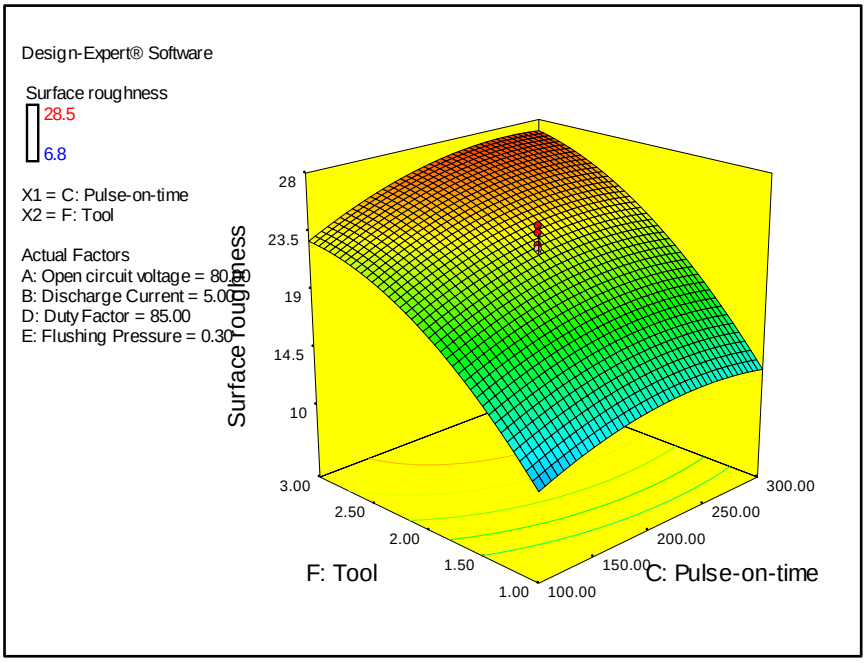

Figure 3.15 Surface plot of surface roughness with tool material and pulse-on-time

Figure 3.16 shows the variation of radial overcut with discharge current and tool material. It shows that radial overcut increases with increase in discharge current with the use of graphite and copper electrodes. The reason for this observation is that higher values discharge current causes increase in spark energy resulting in more heat to be produced and wider and larger craters are formed. Thus, it increases the overcut on the machined surface. Graphite electrode exhibits the poorest performance in regard to the overcut. Brass electrode at smaller values of discharge current minimizes overcut. Copper electrode produces Inconel 718 alloy work material with overcut values between those of copper and graphite. Thus, brass electrode and lower machining rate can be adopted for the smaller overcut on machining surface at the expense of tool erosion.

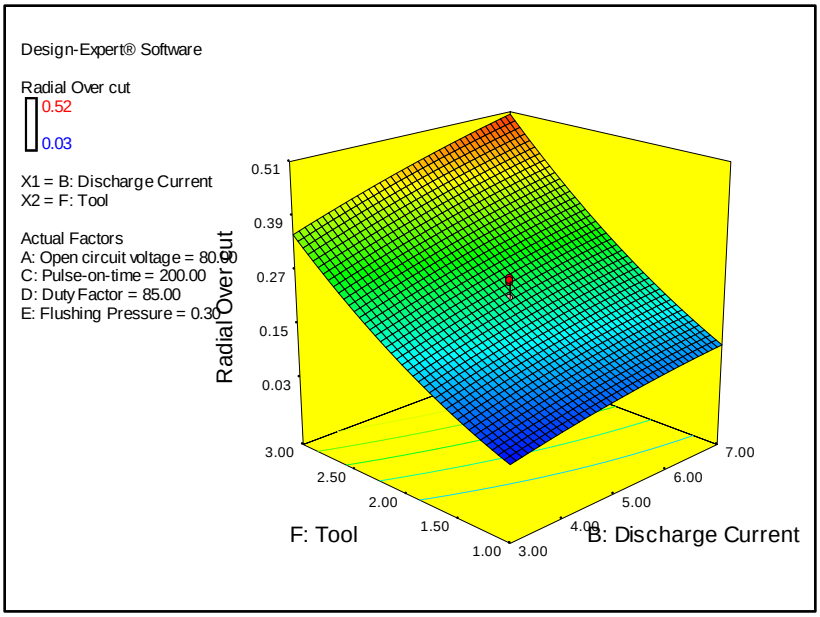

Figure 3.16 Surface plot of radial overcut with tool material and discharge current

Figure 3.17 shows the variation of radial over cut with pulse-on-time and tool material. Its shows that overcut increases gradually with increase of pulse-on-time. An increase in pulse-on-time increases the overcut on the machined surface due to prolonged occurrence of sparks causing an increase in energy per spark. However, it is observed that the effect of discharge current on over cut is higher as compared to pulse-on-time. Factors such as duty factor and open circuit voltage have little effect for variation of radial over cut, yet it is observed that over cut decreases very slowly with increase in open circuit voltage.

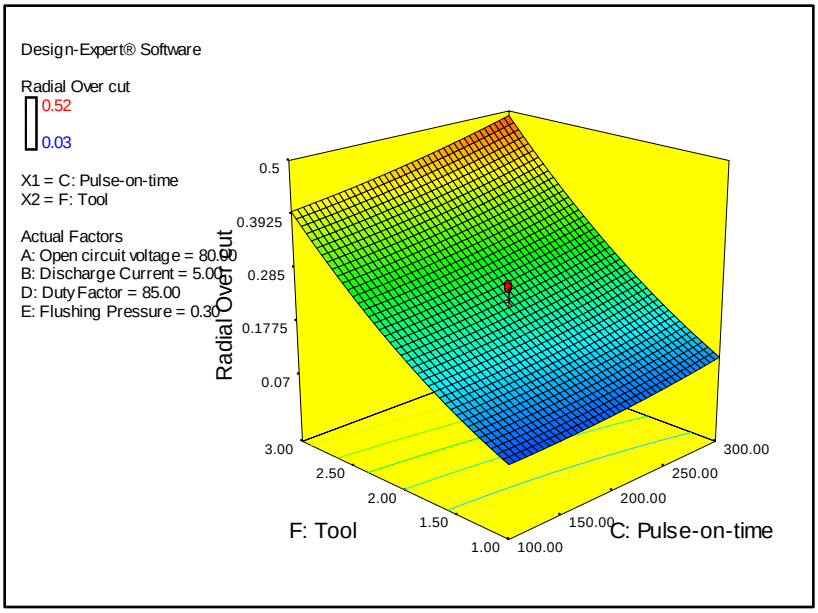

Figure 3.17 Surface plot of radial overcut with tool material and pulse-on-time

Figure 3.18 shows the variation of white layer thickness with discharge current and tool material. Its shows that white layer thickness increases briskly the use of graphite and copper electrodes, but in the increases is comparatively slower with the use of brass electrode. Increase in discharge current significantly improves the spark energy, which in turn increases the molten metal volume on the machined surface. As a result, owing to improper flushing larger volume of molten material is deposited on the machined surface and in turn the thickness of white layer is increased. Since, MRR produced in graphite and copper electrodes are higher than brass electrode the deposition of molten metal on the machined surface is also higher and in turn the white layer thickness is also higher.

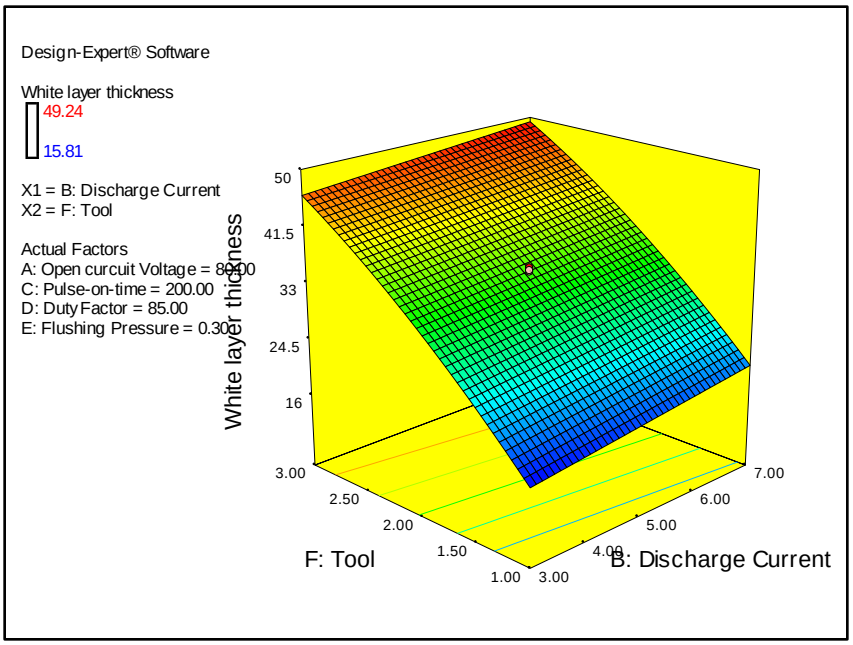

Figure 3.18 Surface plot of white layer thickness with discharge current and tool material

Figure 3.19 shows the variation of White layer thickness with pulse-on-timeand tool material. It shows that white layer thickness increases gradually with increase in pulse-on-time initially, but remains constant after reaching the pulse duration of 200 µs up to 300µs.Incrseing pulse on time means applying the same heat flux for an extended time interval. Continuous application of same heat flux decreases the pressure inside the plasma channel. Since, the molten metal volume remains constant, further increases in pulse-on time does not increase the deposition on the machined surfaceand the white layer thickness remains constant. The effect of duty factor on white layer thickness is not significant as compared to discharge current and pulse-on-time but still it is observed that white layer thinness increases very slowly with increase in duty factor due to increase in number of

sparks per unit time. Open circuit voltage and flushing pressure have little to offer for variation of white layer thickness.

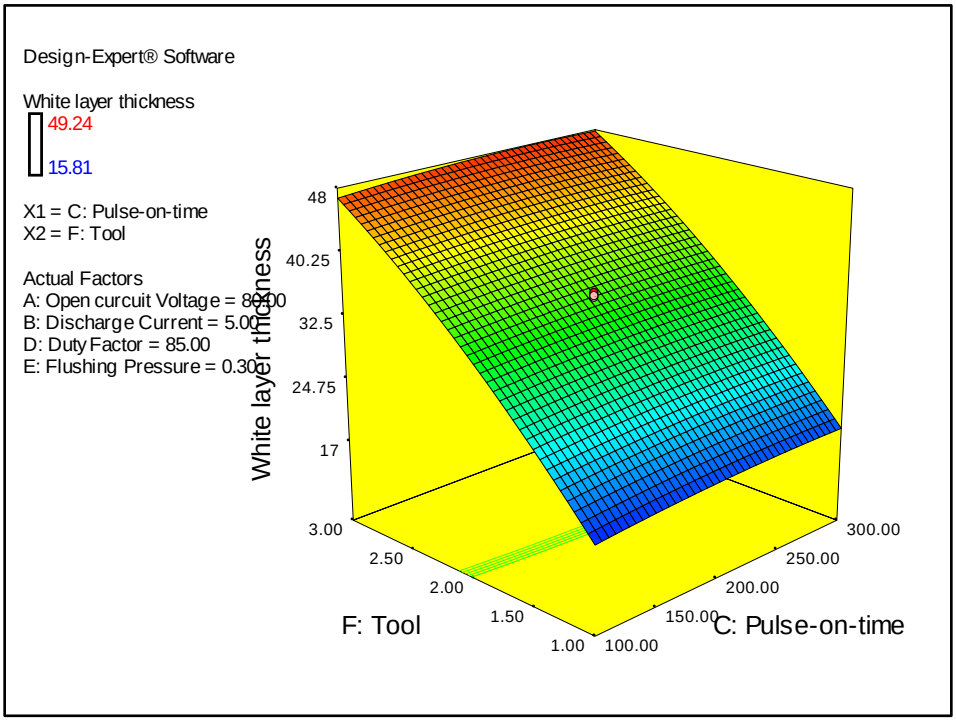

Figure 3.19 Surface plot of white layer thickness with pulse-on-time and tool material

In this study, five responses such as (MRR, EWR, surface roughness, radial overcut and white layer thickness) are considered. However, all the five responses may not be applicable simultaneously for industrial applications. The choice of responses purely depends on the requirement of process engineer and industries. Therefore, two responses are considered to be optimized treating other three responses are treated as constraints at a time. The constrained value is selected from the experimental observations. The empirical relation between the process parameters and process responses established from the RSM analysis is used as objective function for solving the multi-objective particle swarm optimization (MOPSO) problem. In the present work, the objectives are maximization of MRR and minimization of EWR, surface roughness, radial overcut and white layer thickness which are functions of process parameters viz. open circuit voltage, discharge current, pulse-on-time , duty factor, flushing pressure and tool material. Tool material is a qualitative process parameter whereas open circuit voltage, discharge current, pulse-on-time, duty factor, flushing pressure are quantitative process parameters. The quantitative parameters are real numbers that lies in the range [-1, 1]. For the qualitative parameters, the nearest

integer part of the real numbers has been considered. The ranges of the qualitative parameters (tool material) are considered in the manner if the values lie in the range [-1 to -0.3], it is treated as -1 or brass tool, [-0.29 to+0.3] as 0 or copper tool and [+0.31 to+1] as 1 or graphite tool.

Ten optimization problems are formed considering two responses as objectives and three as constraints. The empirical relation between input parameters and responses obtained in equations 27-30 are used as functional relations. MOPSO algorithm discussed in section 3.2 is coded MATLAB 13 for solving minimization problems.

Problem 1:

Maximize MRR

Minimize EWR

Subject to

Surface roughness $\leq$ 6.8

Radial overcut $\leq$ 0.03

White layer thickness $\leq$ 15.81

where 6.8 , 0.03 and 15.81 are the minimum values of surface roughness, radial over cut and white layer thickness obtained from the experimental table 3.5 respectively.

Problem 2:

Maximize MRR

Minimize surface roughness

Subject to

EWR $\leq$ 7.34

Radial overcut $\leq$ 0.03

White layer thinness $\leq$15.81

where 7.34 , 0.03 and 15.81 are the minimum values of EWR and radial overcut and white layer thickness obtained from the experimental table 3.5 respectively.

Problem 3:

Maximize MRR

Minimize radial overcut

Subject to

EWR $\leq$ 7.34

Surface roughness $\leq$ 6.8

White layer thinness $\leq$15.81

where 7.34, 6.8 and 15.81 are the minimum values of EWR, surface roughness and white layer thickness obtained from the experimental table 3.5 respectively.

Problem 4

Maximize MRR

Minimize white layer thickness

Subject to

EWR $\leq$ 7.34

Surface roughness $\leq$ 6.8

Radial overcut $\leq$ 0.03

Where 7.34, 6.8 and 0.03 are the minimum values of minimum values of EWR, surface roughness and radial over cut obtained from the experimental table 3.5 respectively

Problem 5:

Minimize EWR

Minimize Surface roughness

Subject to

MRR $\geq$ 48.9

Radial overcut $\leq$ 0.03

White layer thinness $\leq$15.81

where 48.9,0.03 and 15.81 are themaximum value of MRR and minimum values radial overcut and white layer thickness obtained from the experimental table 3.5 respectively.

Problem 6:

Minimize EWR

Minimize Radial overcut

Subject to

MRR $\geq$ 48.9

Surface roughness $\leq$ 6.8

White layer thinness $\leq$15.81

where 48.9, 6.8 and 15.81 are the maximum value of MRR and minimum values of surface roughness and white layer thickness obtained from the experimental Table 3.5 respectively.

Problem 7:

Minimize EWR

Minimize white layer thickness

Subject to

MRR ≥ 48.9

Surface roughness ≤ 6.8

Radial overcut ≤ 0.03

where, 48.9, 6.8 and 0.03 are the maximum value of MRR and minimum values of surface roughness and radial over cut obtained from the experimental Table 3.5 respectively.

Problem 8:

Minimize Surface roughness

Minimize Radial overcut

Subject to

MRR ≥ 48.9

EWR ≤ 7.34

White layer thinness ≤15.81

where 48.9, 7.34 and 15.81 are the maximum value of MRR and minimum values of EWR and white layer thickness obtained from the experimental Table 3.5 respectively.

Problem 9:

Minimize Surface roughness

Minimize white layer thickness

Subject to

MRR ≥ 48.9

EWR ≤ 7.34

Radial overcut ≤ 0.03

where 48.9, 7.34 and 0.03 are the maximum value of MRR and minimum values of EWR and radial over cut obtained from the experimental Table 3.5 respectively.

Problem 10:

Minimize radial over cut

Minimize white layer thickness

MRR ≥ 48.9

EWR ≤ 7.34

Surface roughness ≤ 6.8

where 48.9, 7.34 and 6.8 are the maximum value of MRR and minimum values of EWR and surface roughness obtained from the experimental Table 3.5 respectively

It is to be noted equivalent minimization function is used in the MATLAB program wherever an objective is maximized.

The optimization model was run on in a Pentium IV desktop. Simulation study is carried out to demonstrate the potentiality of MOPSO algorithm. The initial population chosen for the algorithms is 80. The parameters employed for MOPSO are as follows: the size of archive is 100, the inertia weight is 0.4 and both the cognitive and social parameters (c_1 and c_2) are taken as 2. This led to the development of ten sets Pareto-fronts viz. MRR and EWR, MRR and surface roughness, MRR and radial overcut, MRR and white layer thickness, EWR and surface roughness, EWR and radial overcut, EWR and white layer thickness, surface roughness and radial overcut, surface roughness and white layer thickness, radial over cut and white layer thickness generating optimal solution for the responses. Figure 3.20 shows the Pareto-front for MRR and EWR. A Sample set of the optimal solution for MRR and EWR has been given in Table 3.11.

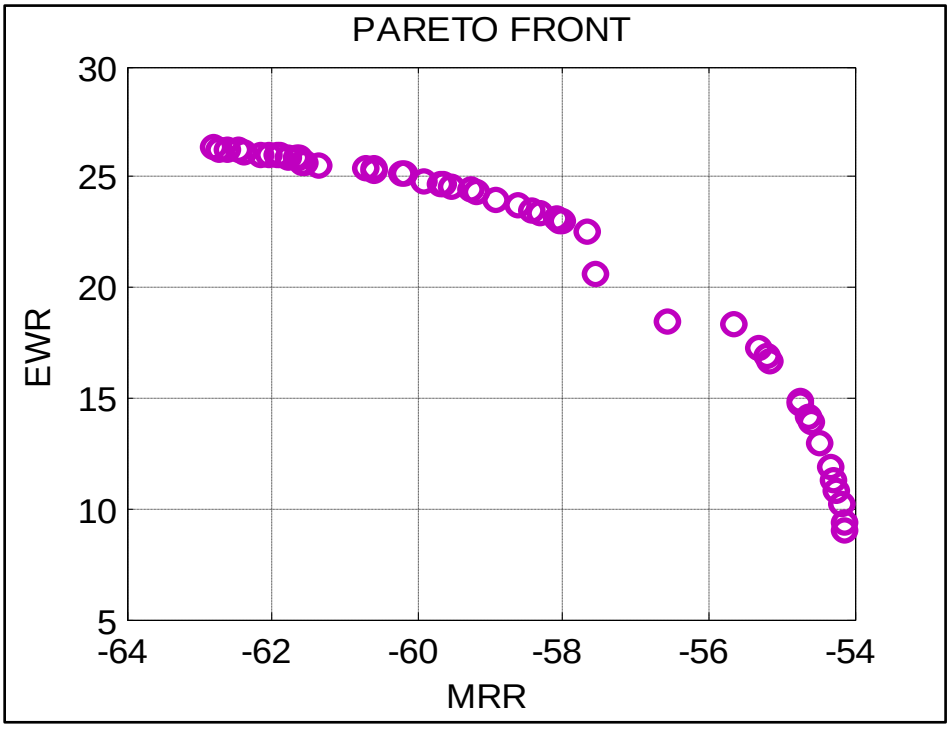

Figure 3.20 Pareto front objectives for MRR and EWR

Table 3.11Pareto optimal solution for MRR and EWR with corresponding variable setting

Run order	A (Volt)	B (Amp)	C (µs)	D (%)	E (bar)	F (tool)	MRR (mm^3/min)	EWR %
1	70.07	7.00	100.00	90.00	0.40	Graphite	62.80	26.30
2	70.19	7.00	100.00	90.00	0.40	Graphite	62.71	26.27
3	70.29	7.00	100.00	90.00	0.40	Graphite	62.63	26.24
4	70.50	7.00	100.00	90.00	0.40	Graphite	62.46	26.19
5	70.61	7.00	100.00	90.00	0.40	Graphite	62.37	26.16
6	70.29	7.00	105.36	90.00	0.40	Graphite	62.16	26.03
7	70.61	7.00	103.83	90.00	0.40	Graphite	62.03	26.01
8	71.15	7.00	100.00	90.00	0.40	Graphite	61.94	25.99
9	71.15	7.00	100.49	90.00	0.40	Graphite	61.90	25.98
10	71.36	7.00	100.00	90.00	0.40	Graphite	61.78	25.93
11	71.54	7.00	100.00	90.00	0.40	Graphite	61.64	25.87
12	71.59	7.00	100.00	90.00	0.40	Graphite	61.61	25.85
13	70.19	7.00	113.07	90.00	0.40	Graphite	61.59	25.68
14	70.29	7.00	112.79	90.00	0.40	Graphite	61.53	25.68
15	70.07	7.00	117.00	90.00	0.40	Graphite	61.37	25.50
16	71.36	7.00	112.44	90.00	0.40	Graphite	60.71	25.44
17	71.36	7.00	113.66	90.00	0.40	Graphite	60.61	25.38
18	72.95	7.00	100.00	90.00	0.40	Graphite	60.60	25.31
19	72.95	7.00	104.55	90.00	0.40	Graphite	60.20	25.19
20	71.65	7.00	116.35	90.00	0.40	Graphite	60.17	25.18
21	73.96	7.00	100.00	90.00	0.40	Graphite	59.90	24.84
22	71.00	7.00	126.24	90.00	0.40	Graphite	59.90	24.79
23	74.26	7.00	100.00	90.00	0.40	Graphite	59.70	24.68
24	74.37	7.00	100.00	90.00	0.40	Graphite	59.63	24.62
25	74.53	7.00	100.00	90.00	0.40	Graphite	59.53	24.54
26	74.53	7.00	103.05	90.00	0.40	Graphite	59.26	24.48
27	71.36	7.00	132.01	90.00	0.40	Graphite	59.21	24.37
28	75.48	7.00	100.00	90.00	0.40	Graphite	58.92	23.99
29	76.00	7.00	100.00	90.00	0.40	Graphite	58.61	23.67
30	76.01	7.00	100.00	90.00	0.40	Graphite	58.60	23.66
31	76.29	7.00	100.00	90.00	0.40	Graphite	58.44	23.48
32	76.51	7.00	100.00	90.00	0.40	Graphite	58.32	23.34
33	76.90	7.00	100.00	90.00	0.40	Graphite	58.09	23.07
34	77.01	7.00	100.00	90.00	0.40	Graphite	58.03	22.99
35	77.02	7.00	100.00	90.00	0.40	Graphite	58.03	22.98
36	77.68	7.00	100.00	90.00	0.40	Graphite	57.67	22.51
37	77.68	7.00	100.00	90.00	0.40	Graphite	57.67	22.50
38	70.19	7.00	175.55	90.00	0.40	Graphite	57.55	20.56

39	70.50	7.00	192.82	90.00	0.40	Graphite	56.56	18.51
40	82.31	7.00	100.00	90.00	0.40	Graphite	55.64	18.33
41	83.25	7.00	100.00	90.00	0.40	Graphite	55.33	17.30
42	83.61	7.00	100.00	90.00	0.40	Graphite	55.22	16.90
43	83.83	7.00	100.00	90.00	0.40	Graphite	55.15	16.65
44	85.33	7.00	100.00	90.00	0.40	Graphite	54.76	14.85
45	85.42	7.00	100.00	90.00	0.40	Graphite	54.74	14.73
46	85.86	7.00	100.00	90.00	0.40	Graphite	54.64	14.17
47	86.05	7.00	100.00	90.00	0.40	Graphite	54.60	13.92
48	86.10	7.00	100.00	90.00	0.40	Graphite	54.59	13.86
49	86.76	7.00	100.00	90.00	0.40	Graphite	54.46	12.98
50	87.56	7.00	100.00	90.00	0.40	Graphite	54.33	11.89
51	87.56	7.00	100.00	90.00	0.40	Graphite	54.33	11.88
52	87.96	7.00	100.00	90.00	0.40	Graphite	54.28	11.32
53	88.35	7.00	100.00	90.00	0.40	Graphite	54.23	10.76
54	88.77	7.00	100.00	90.00	0.40	Graphite	54.18	10.15
55	89.27	7.00	100.00	90.00	0.40	Graphite	54.14	9.39
56	89.54	7.00	100.00	90.00	0.40	Graphite	54.12	8.99
57	70.07	7.00	199.06	90.00	0.40	Graphite	56.69	17.61
58	70.07	7.00	199.96	90.00	0.40	Graphite	56.66	17.48
59	70.07	7.00	200.00	90.00	0.40	Graphite	56.65	17.48

However, application of MOPSO results in large number of non-dominated solutions for optimization of combination of responses viz. MRR and EWR, MRR and surface roughness, MRR and radial overcut, MRR and white layer thickness, EWR and surface roughness, EWR and radial overcut, EWR and white layer thickness, surface roughness and radial overcut, surface roughness and white layer thickness, radial over cut and white layer thickness. The Pareto-optimal solutions obtained through MOPSO have been ranked by the composite scores obtained through maximum deviation theory (MDT) to choose the best solution. The decision matrix is normalized using equation 3.11 and 3.12 appropriately. The objective weights are determined for the normalized values of objectives by applying maximum deviation method using equations 3.13-3.20. The weighted objective values are estimated by multiplying the normalized objective values and the objective weights. The best solution is selected depending upon the composite scores obtained by addition of the all the weighted objective function values for each alternative. The objectives with highest composite score are chosen as the best solution.Table 3.12 shows the best ranked solution forallthecombinationofmultipleresponses.

Table 3.12 Best ranked solution for multiple objectives

Multiple objectives	A (V)	B (A)	C (µs)	D (%)	E (Bar)	F Tool	Objective		Normalised objectives		Weighted Normalised		Compsite Score
MRR and EWR	89.54	7	100	90	0.4	Graphite	54.11	8.98	0.8306	0.693	0.3246	0.4221	0.7467
MRR and Surface roughness	71.54	7	100	80	0.2	Brass	32.32	10.01	0.3835	1	0.1572	0.5898	0.7471
MRR and Radial overcut	72.95	6.97	100	90	0.2	Brass	32.09	0.09	0.4363	0.7709	0.2118	0.3966	0.6084
MRR and White layer thickness	70.03	7	100	90	0.2	Graphite	64.76	42.20	1	0	0.6565	0.6565	0.6565
EWR and Surface roughness	71.74	3	100	80	0.29	Brass	2.10	6.76	1	0.5922	0.3519	0.3838	0.7357
EWR and Radial overcut	75.7	3	300	80	0.25	Copper	3.07	0.18	0.9816	0.9741	0.594	0.3846	0.9786
EWR and white Layer thickness	70	3	100	90	0.2	Brass	43.81	4.23	0.1029	1	0.0503	0.5112	0.5615
Surface roughness and Radial overcut	73.97	3	100	80	0.25	Brass	4.32	0.012	0.3817	0.8103	0.1787	0.4309	0.6096
Surface roughness and white layer thickness	74.26	3	300	80	0.4	Brass	4.78	7.01	1	0	0.3352	0.4212	0.7564
Radial over cut and white layer thickness	79.13	3	177.5	80	0.26	Brass	0.018	3.720	0.8131	0.58	0.2636	0.4436	0.7072

3.7 Conclusions

This chapter proposes a hybrid, integrated approach of response surface methodology (RSM) coupled with multi objective particle swarm optimization (MOPSO) for the optimisation of the machining parameters of EDM process on machinability of Inconel 718 alloy. In the second phase, maximum deviation theory (MDT) of objective weights determination is used to estimate the weights for the attributes. The composite score for all the non-dominated solutions is obtained through summing the weighted objective values. The best solution is selected from all the non-dominated solution considering the highest composite score to avoid subjectiveness and impreciseness in the decision making for the tool engineers. This research work offers an effective guideline to select optimum parameter settings for achieving the desired MRR, EWR, surface roughness, radial overcut and white layer thickness during EDM die sinking of Inconel 718 alloy to the experimenter and practitioners. Some important findings from the experimental investigation are discussed in the paragraphs below.

It is observed that tool material, discharge current and pulse-on-time are found to be the important process parameters for all the performance measures while machining Inconel 718. From analysis of variance of MRR, it is observed that tool material is the most influential parameter with highest percentage of contribution of 49.74% followed by discharge current, pulse-on-time, open circuit voltage and duty factor with percentage contribution of 24.76%, 5.48%, 5.40% and 4.16% respectively. Similarly, from analysis of variance of EWR, it is observed that tool material is found to be the most influential parameter with highest percentage of contribution of 61.84% followed by discharge current, pulse-on-time, open circuit voltage and duty factor with percentage contribution of 2.44%, 2.37%, 1.76% and 1.56% respectively. Similarly, from analysis of variance of surface roughness, it is observed that tool material is found to be the most influential parameter with highest percentage of contribution of 67.13% followed by discharge current, pulse-on-time and open circuit voltage with percentage contribution of 16.88%, 3.78% and 0.16% respectively. From analysis of variance of radial overcut, it is observed that tool material is found to be the most influential parameter with highest percentage of contribution of 85.56%, followed by discharge current, pulse-on-time and duty factor with percentage contribution of 8%, 2.56% and 0.07% respectively. From, analysis of variance of white layer thickness, it is observed that tool material is found to be the most influential parameter with highest percentage of contribution of 96.94% followed by discharge current, pulse-on-time

and duty factor with percentage contribution of 1.53%, 0.14% and 0.09% respectively. Material removal is comparatively high while machining with graphite tool followed by copper and brass. Due to high value of spark energy between electrodes, graphite and copper electrodes exhibit high MRR in comparison to brass electrode. EWR is comparatively less with the use of graphite electrode followed by copper electrode because low TWR and high MRR is observed. Brass electrode exhibits the poorest performance with regard to EWR due to high TWR. Brass tool at small values of discharge current produces fine surface quality followed by copper and graphite tools due to small spark energy between electrodes causing erosion of smaller size particle from machined surface. It is observed that MRR can be increased up to 449.21% whereas EWR can be reduced up to 92.08% while machining with graphite electrode when of experiment numbers 18 (brass tool) and 22 (graphite tool) shown in Table 3.5 were compared. It is also observed that surface roughness, radial overcut and white layer thickness can reduced up to 52.77%, 77.65% and 63.85% respectively while machining with brass electrode. Graphite electrode exhibits the poor performance in regard to the radial overcut followed by copper due to high MRR. Brass electrode at small values of discharge current produces precise and accurate EDMed components owing to small MRR suited for finishing operation. Owing to higher MRR, graphite electrode produces thicker white layer thickness on the machined surface. Brass electrode at small values of spark energy produces small value of white layer on the machined surface. Copper electrode produces white layer value those between graphite and brass. Hence, it can be concluded that graphite tool is more favorable than the copper and brass electrodes for machining of Inconel 718 work material if high material removal and low tool wear is desired, particularly in roughing operation.

CHAPTER 4

STUDY ON EFFECT OF SOAKING DURATION IN DEEP CRYOGENIC TREATMENT OF THE TOOL

4.1 Introduction

The major performance measure of the EDM process are evaluated in terms of material removal rate (MRR), tool wear rate (TWR), surface quality and dimensional accuracy of the machined surface (Ho and Newman 2003;Mahapatra and Patnaik 2007;Kumar et al.2009). For precise and cost effective machining it is essential to identify and estimate the changes those are taking place within electrode material. The electrode material life plays an important role in increasing productivity and, subsequently, is an important economic aspect of the process. However, high wear rate of electrode material leads to interruption during machining which in turn increases machining time and declines productivity of the process by increasing the machining cost. Although copper and graphite electrodes have been able to solve this issue to some extend yet their application severely limited to dimensional accuracy and surface finish of the machined surface (Lee and Li 2001; Kuppan et al. 2011; Kumar et al. 2009; Kumar et al. 2012;Mohanty et al.2014).In previous chapter it observed that brass electrode produces precise and accurate EDMed components while machining Inconel 718 super alloy. But the major concern while machining with brass electrode is the high erosion of tool and lower material removal due to poor thermal and mechanical properties. Hence, in this chapter an attempt has been made to improve the wearing resistance of brass electrode to enhance the machining efficiency of the process by improving the thermal and mechanical properties of the materialthrough deep cryogenic treatment of electrodes subjected to different soaking duration.

It is reported that brass exhibits low material removal rate and high wear ratio as EDM electrode due to poor thermal conductivity and low melting point temperature. Therefore, brass electrode is used in finishing machining condition as compared to copper and graphite electrodes (Mohanty et al. 2014; Lee and Li 2001; Kuppan et al. 2011). However, it is reported that brass can be cryogenically treated to improve wear resistance and material removal rate.Unlike coatings, cryogenic processing is an economical and everlasting treatment affecting the entire section of the material. The treatment is an supplementary process over the traditional heat treatment process in which the materials are cooled down to the particular cryogenic temperature at a controlled rate, retained at the stage for a longer duration and brought back to room temperature and tempered to ease the brittleness of the material. Cryogenic treatment brings some remarkable improvements to the mechanical properties like increasing the wear resistance, tensile strength, hardness and refining the microstructure of the materials (Jaswin and Lal 2010). In recent times, cryo-processing has been successfully applied in non-convention machining processes resulting in fruitful

application in EDM and wire EDM through treatment of electrodes and wires which are used for machining of toughened and high strength to weight ratio materials (Kumar et al. 2012; Jafferson and Hariharan 2013;Kapoor et al. 2012; Gill and Singh 2010). Some of the important parameters involved in cryogenic treatment of materials are cooling rate, soaking temperature, soaking duration and heating rate (Gill et al. 2010). Many studies have reported that soaking duration is an influential parameter than soaking temperature (Jaswin and Lal2010; Xu et al. 2007;Lal et al. 2001;Collins and Dormer 1997). However, studies on effect of cryogenic treatment of brass electrodes in electrical discharge in machining of Inconel 718 are limited in literature.

In view of this, present chapter investigates the effect of deep cryo-treated (-196^0 C) brass electrodes subjected to different soaking durations on the machinability of Inconel 718 work material. The machining performance of the process are evaluated in terms of material removal rate (MRR), electrode wear ratio (EWR), surface roughness, radial overcut and white layer thickness which are function of process variables viz. open circuit voltage, discharge current, pulse-on-time, duty factor, flushing pressure and cryogenic treatment soaking duration of electrodes. The experimental design is planned as per Box-Behnken design of response surface methodology (RSM). Regression analysis is conducted to relate the process variable with machining performance characteristics. An evolutionary multi-objective particle swarm optimization (MOPSO) algorithm has been applied for simultaneous optimization of performance characteristics. To deal with subjectiveness and impreciseness in the decision making, the non-dominated solutions obtained through MOPSO have been ranked further by applying maximum deviation theory(MDT).

4.2 Proposed MOPSO algorithm

The details of MOPSO algorithm have been already discussed in previous chapter section 3.2.

4.3 Solution ranking

The details of the Maximum deviation theory have been already discussed in previous chapter section 3.3.

4.4 Experimental strategy and materials

Experiments are carried out in a die sinking CNC EDM machine (Electronica Elektra S50 CNC) is shown in Figure 4.1. Positive polarity for electrode and side flushing is used to conduct the experiments. The specification of the machine is given in Table 4.1. The details of the work material and its properties have been already discussed in the previous chapter in section 3.4. The electrode material is the most critical part as it directly affects the machining cost of the process. Hence, commercially available brass has been chosen as the electrode material because of its lower electrical and thermal conductivity with an objective to improve its mechanical properties through deep cryogenic treatment and make the material suitable for industrial application. Three brass rods are brought in form of 20 mm diameter and 70 mm length. For suitable machining; the machining diameter is reduced to 13.5mm. Out of these three tool materials, one of the tool material is left untreated and other two tools are deep cryogenically treated varying soaking duration of 24-hr and 36-hr. The details of the experimental strategy have been discussed in the previous chapter 3.5. For suitable machining the parameters are coded using equation 3.22. Table 4.2 shows the levels of the process parameters.

Figure 4.1 CNC EDM machine (Electronica Elektra S50 CNC)

Table 4.1 Specification of the CNC die sinkerEDM machine Electronica ElektraS50 CNC

Mechanism of process	Controlled erosion (melting and evaporation) through a series of electric spark
Spark gap	0.010- 0.500 mm
Spark frequency	200 – 500 kHz
Working Current	1-50A
Working voltage across the gap	30- 200 V
Maximum Flushing Pressure	0.5 Pa
Metal removal rate (max.)	500 mm^3/min
Specific power consumption	2-10 W/mm^3/min
Dielectric fluid	Kerosene, liquid paraffin.
Dielectric tank Capacity	
Travel limit X-axis	300mm
Y-axis	300mm
Z-axis	250mm

Table 4.2 Process parameters and their levels

Process Parameters	Symbols	Levels		
		-1	0	1
Open circuit voltage in V	A	70	80	90
Discharge current in A	B	3	5	7
Pulse-on-time in µs	C	100	200	300
Duty factor in %	D	80	85	90
Flushing pressure in Bar	E	0.2	0.3	0.4
Cryogenic treatment soaking duration in Hrs.	F	0	24	36

4.4.1 Deep cryogenic treatment

To avoid thermal shock to the material, the cryogenic treatment is performed under dry condition where the material is not directly subjected to the liquid nitrogen. The cryogenic treatment for the brass electrodes is accomplished in cryogenic freezer Kryo 560-16 shown in Figure 4.2. The freezer consists of a treatment chamber coupled with a liquid nitrogen tank through an insulated tubular pipe. The liquid nitrogen flowing into the freezer is controlled by a solenoid valve. The thermocouple inside the chamber senses the temperature and provides information to the programmable digital temperature controller to operate the solenoid valve. Liquid nitrogen passes through the tubular pipe and enters into to freezer in gaseous state. The programmable digital temperature controller controls cryogenic treatment parameters viz. lowering temperature, soaking duration, cooling rate and heating rate. First, one tool material is placed inside the freezer and the temperature is slowly reduced to the temperature of liquid nitrogen -196^0 C by computerized programmable controller at the rate of 1^0C/min. At this temperature, the material is held constant for 24-hrs before the material is slowly brought to room temperature at rate of 1^0C/min. After reaching the room temperature, the material is subjected to two stages of tempering cycles for relievingthe stresses induced during cryogenic treatment. Tampering operation is executed by increasing the temperature up to $+196^0$ C at the rate of 1^0C/min and then slowly bringing back to the room temperature. Similar procedure is followed for the third tool material except that the soaking duration is kept constant for 36-hrs instead of 24-hrs. Figure 4.3 shows the graphical representation of deep cryogenic treatment and two stage tempering process for both the cycle followed in the study. UnithermTM 2022 is used for measuring the thermal conductivity of the tool material before and after cryogenic treatment. The micro hardness of the material is measured by Vaiseshika Micro Hardness tester. The mechanical properties of the tool material for the untreated and treated samples (with soaking durations of 24-hrs and 36-hrs) have been furnished in Table 4.3.

Figure 4.2Cryogenic freezer PLANER Kryo 560-16

Table 4.3 Mechanical property of brass tool before and after cryogenic treatment

Composition	Property	Untreated	Treated with soaking duration 24-hrs.	Treated with soaking duration 36-hrs.
Cu 62% Zn 38%	Thermal Conductivity (W/m.K)	108	121	129
	Micro Hardness (VHN)	202	241	265
	Average grain size (nm)	143.72	132.38	111.64

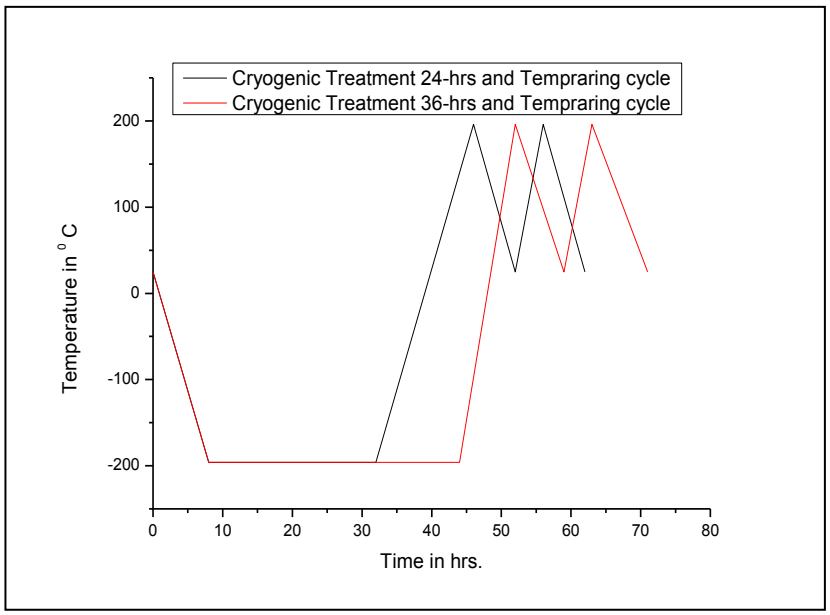

Figure 4.3Graphical representations of deep cryogenic treatment and two stage tempering process for both the cycle

4.4.2 Microstructural analysis and X-ray Diffraction analysis

The micro structural investigations for the brass samples were carried out using Olympus (model no-BX-5175E21P, Japan) optical microscope at 400X magnification.The optical micrograph images for the untreated and treated samples at identical magnifications have been shown in Figure 4.4 (a-b-c) below. From the optical images, it can be clearly visualized that the grain boundaries are interconnected and continuous within themselves in untreated samples whereas treated samples with soaking duration 24-hrs exhibit separate and distinct grain boundaries and the micro structure is densed with average grain size smaller than untreated samples. However, treated samples with soaking duration 36-hrs have more refined and smaller grains and microstructure is more densed due to longer soaking duration of cryogenic treatment when compared to other two samples.

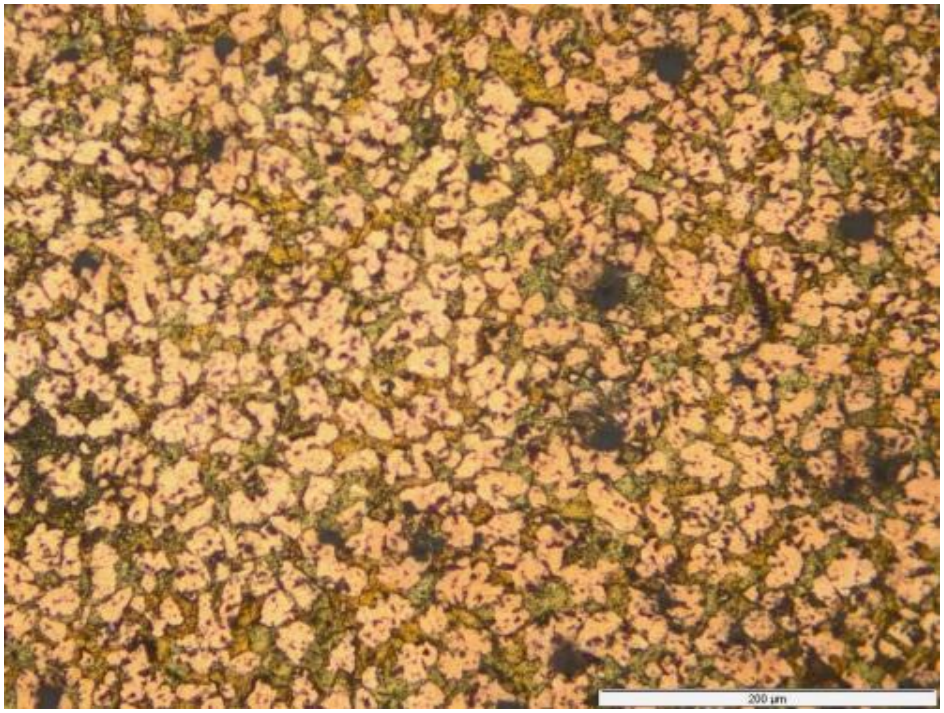

(a) Untreated brass

(b) Cryogenic-treated brass with soaking duration 24-hrs

(C)Cryogenic-treated brass with soaking duration 36-hrs

Figure 4.4(a, b and c) Microstructures of three electrode samples used in the study

These optical microscope images are further supported by the X-RD analysis reports. The X-RD analysis for the treated and untreated brass samples are carried out on an X-ray diffractometer (model no-X-Pert PRO, PANalytical, PW 3040/00, Netherland). The average grain size is calculated using the Debye Scherrer's relation

$$GS = \frac{0.89\alpha}{\beta \cos\theta} \quad (4.1)$$

where α is the wavelength of X-ray used, β-is the line broadening at half the maximum intensity (FWHM) in radians in the 2θ scale, θ is the Bragg angle, and GS is the grain size in nanometre. The calculated values of the average grain size are provided in the Table 4.3.

The X-RD analysis report reveals that due to deep cryogenic treatment the average grain size is reduced up to 7.78% and 25.43% for soaking duration of 24-hrs and 36-hrs respectively.

4.4.3 Calculation of performance measures

The EDM process is performed on Inconel 718 alloy rectangular plates having dimension of 5×105×110 mm^3 as shown in Figure 4.5. Each experiment is conducted for 20 minutes and the time is noted with a stopwatch. After each experimental run, the work piece and the electrodes are removed from the machine and are cleaned and dried out for weighing. A precision electronic balance (accuracy up to 0.001gm) is used for measuring the weights of the work and electrode materials before and after machining.The details of the calculation of the performance measures have been already discussed in the previous chapter in section 3.5.1.Table 4.4 shows the Box-Behnken experimental design along with obtained performance measures.

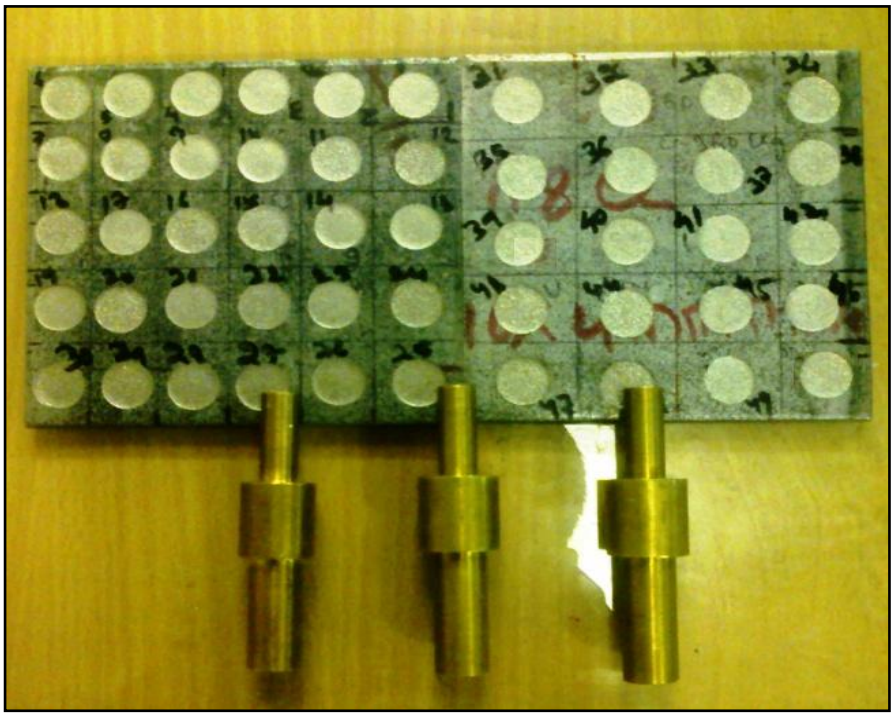

Figure 4.5 Work materials after machining with three brass electrodes

Table 4.4 Box-behnken experimental design along with obtained performance measures

Run order	A	B	C	D	E	F	MRR mm^3/min	EWR %	Surface Roughness µm	Over cut mm	White Layer Thickness µm
1	-1	-1	0	-1	0	0	2.50	92.12	8.40	0.15	24.30
2	1	-1	0	-1	0	0	2.00	97.03	8.43	0.14	24.40
3	-1	1	0	-1	0	0	6.20	119.10	9.50	0.25	28.70
4	1	1	0	-1	0	0	5.10	123.20	9.70	0.24	28.60
5	-1	-1	0	1	0	0	3.89	99.30	8.60	0.19	24.80
6	1	-1	0	1	0	0	2.55	105.21	8.67	0.20	24.90
7	-1	1	0	1	0	0	7.00	125.15	9.75	0.28	28.60
8	1	1	0	1	0	0	5.80	129.40	10.20	0.27	28.10
9	0	-1	-1	0	-1	0	2.40	89.31	7.90	0.14	24.70
10	0	1	-1	0	-1	0	5.30	118.26	9.60	0.26	28.10
11	0	-1	1	0	-1	0	1.90	105.19	9.50	0.24	26.00
12	0	1	1	0	-1	0	3.70	130.09	11.30	0.34	29.00
13	0	-1	-1	0	1	0	2.20	91.43	8.20	0.15	24.80
14	0	1	-1	0	1	0	5.40	121.37	9.75	0.25	28.20
15	0	-1	1	0	1	0	2.20	110.29	9.30	0.25	26.20
16	0	1	1	0	1	0	4.10	130.19	10.20	0.35	28.90
17	0	0	-1	-1	0	-1	3.60	132.18	10.30	0.39	38.38

18	0	0	1	-1	0	-1	2.90	136.17	11.90	0.47	39.38
19	0	0	-1	1	0	-1	4.20	142.36	10.60	0.45	39.10
20	0	0	1	1	0	-1	3.50	145.40	12.50	0.52	39.48
21	0	0	-1	-1	0	1	3.65	73.12	7.70	0.07	15.25
22	0	0	1	-1	0	1	2.92	85.33	8.90	0.11	16.45
23	0	0	-1	1	0	1	4.30	79.26	7.90	0.09	16.65
24	0	0	1	1	0	1	3.55	86.41	8.90	0.15	17.95
25	-1	0	0	-1	-1	0	5.30	111.10	9.10	0.21	26.40
26	1	0	0	-1	-1	0	4.40	115.23	9.20	0.19	26.50
27	-1	0	0	1	-1	0	6.10	125.12	9.40	0.25	26.80
28	1	0	0	1	-1	0	5.20	131.05	9.35	0.25	26.90
29	-1	0	0	-1	1	0	5.40	115.44	9.00	0.22	26.55
30	1	0	0	-1	1	0	4.40	121.37	8.95	0.19	26.60
31	-1	0	0	1	1	0	6.05	111.17	9.15	0.24	26.95
32	1	0	0	1	1	0	5.20	128.08	9.23	0.22	27.00
33	0	-1	0	0	-1	-1	2.90	127.06	8.90	0.39	37.38
34	0	1	0	0	-1	-1	5.40	152.42	12.20	0.54	41.48
35	0	-1	0	0	1	-1	2.99	130.19	9.30	0.36	37.48
36	0	1	0	0	1	-1	5.80	150.11	12.35	0.56	41.18
37	0	-1	0	0	-1	1	2.89	69.13	6.30	0.07	15.22
38	0	1	0	0	-1	1	5.91	79.23	8.50	0.14	20.45
39	0	-1	0	0	1	1	3.00	67.32	6.35	0.04	15.57
40	0	1	0	0	1	1	5.99	82.06	8.70	0.14	20.65
41	-1	0	-1	0	0	-1	5.40	135.37	11.10	0.39	39.28
42	1	0	-1	0	0	-1	4.60	141.39	10.90	0.34	39.33
43	-1	0	1	0	0	-1	3.99	145.42	12.70	0.37	40.28
44	1	0	1	0	0	-1	3.20	148.45	12.60	0.36	40.38
45	-1	0	-1	0	0	1	4.80	71.16	7.90	0.09	16.25
46	1	0	-1	0	0	1	4.20	73.13	7.70	0.06	16.55
47	-1	0	1	0	0	1	3.95	82.14	8.90	0.14	17.65
48	1	0	1	0	0	1	3.30	87.30	8.60	0.13	17.75
49	0	0	0	0	0	0	4.99	125.03	8.75	0.25	27.70
50	0	0	0	0	0	0	4.50	121.42	8.35	0.20	27.50
51	0	0	0	0	0	0	5.50	127.43	9.00	0.26	28.00
52	0	0	0	0	0	0	4.60	123.23	8.40	0.20	27.45
53	0	0	0	0	0	0	5.30	126.50	8.90	0.25	28.05
54	0	0	0	0	0	0	4.70	122.70	8.50	0.21	27.65

4.5 Results and discussions

The experiments have been conducted as per box-behnken design to analyze the effect of important process parameters on the performance measures viz. MRR, EWR, surface roughness, radial overcut and white layer thickness. Analysis of variance (ANOVA) is conducted for the performance measures and significance of each parameter is observed at the significance level of 0.05. Table 4.5 shows the ANOVA for MRR with percentage of contribution of each parameter and their interactions. It shows that parameters such as discharge current, pulse-on-time, open circuit voltage, duty factor, interaction terms such as discharge current×pulse-on-time and square terms of open circuit voltage, discharge current, pulse-on-time, duty factor, flushing pressure have significant effect on MRR. Soaking duration is found to be an insignificant parameter for MRR. The Table also indicates that discharge current happens to be the most influential parameter for MRR with a percentage contribution of 58.48% followed by pulse-on-time, open circuit voltage and duty factor with percentage contribution of 5.85%, 5.62% and 4% respectively. Flushing pressure is found to an insignificant process parameter for MRR. The coefficient of determination (R^2) and adjusted (R^2) values are found to be 97.28% and 95.49% respectively. It is to be noted that the lack of fit is not significant for MRR.

Table 4.5 ANOVA for MRR

Source	Sum of Squares	Degree of freedom	Mean Square	F Value	p-value Prob> F		% Contribution
Model	81.38	21	3.98	54.4	< 0.0001	significant	
A-Open circuit voltage	4.71	1	4.71	64.36	< 0.0001		5.63
B-Discharge Current	48.96	1	48.96	669.31	< 0.0001		58.48
C-Pulse-on-time	4.9	1	4.9	66.93	< 0.0001		5.85
D-Duty Factor	3.35	1	3.35	45.83	< 0.0001		4.00
E-Flushing Pressure	0.074	1	0.074	1.01	0.323		0.09
F-Soaking Duration	1.67E-05	1	1.67E-05	2.28E-04	0.9881		0.00
A×B	0.026	1	0.026	0.36	0.5519		0.03
A×D	0.039	1	0.039	0.53	0.4706		0.05
A×F	0.014	1	0.014	0.2	0.6597		0.02
B×C	0.72	1	0.72	9.84	0.0036		0.86
B×D	0.024	1	0.024	0.33	0.5692		0.03
B×E	0.029	1	0.029	0.4	0.5341		0.03
B×F	0.061	1	0.061	0.84	0.367		0.07
C×E	0.08	1	0.08	1.09	0.3035		0.10
C×F	0.06	1	0.06	0.82	0.3718		0.07
A^2	1.39	1	1.39	18.99	0.0001		1.66
B^2	4.81	1	4.81	65.81	< 0.0001		5.75
C^2	11.12	1	11.12	151.95	< 0.0001		13.28
D^2	0.57	1	0.57	7.76	0.0089		0.68
E^2	0.38	1	0.38	5.19	0.0296		0.45
F^2	0.065	1	0.065	0.89	0.3524		0.08
Residual	2.34	32	0.073				2.80
Lack of Fit	1.53	27	0.057	0.35	0.9666	not significant	
Pure Error	0.81	5	0.16				
Cor Total	83.72	53					

Table 4.6 shows the ANOVA table for EWR with percentage of contribution of each parameter and their interactions. The table shows that soaking duration, discharge current, pulse-on-time, duty factor, open circuit voltage, interaction terms-discharge current×soaking duration, duty factor×flushing pressure and square terms of discharge current, pulse-on-time, duty factor, soaking duration are important process parameters. The Table also shows that soaking duration is the most influential parameter for EWR with percentage contribution of 78.35% followed by discharge current, pulse-on-time, duty factor and open circuit voltage with percentage contribution of 10.66%, 2.13%, 1.04% and 0.64% respectively. Flushing pressure is found to be an insignificant parameter for EWR. The coefficient of determination (R^2) and adjusted (R^2) values are found to be 98.9% and 98.4% respectively. It is to be noted that the lack of fit is not significant for EWR.

Table 4.6 ANOVA for EWR

Source	Sum of Squares	Degree of freedom	Mean Square	F Value	p-value Prob> F		% Contribution
Model	29660.1	19	1561.06	162.8	< 0.0001	significant	
A-Open circuit voltage	194.09	1	194.09	20.24	< 0.0001		0.65
B-Discharge Current	3197.04	1	3197.04	333.42	< 0.0001		10.66
C-Pulse-on-time	641.08	1	641.08	66.86	< 0.0001		2.14
D-Duty Factor	311.9	1	311.9	32.53	< 0.0001		1.04
E-Flushing Pressure	1.42	1	1.42	0.15	0.7031		0.00
F-Soaking Duration	23495.7	1	23495.7	2450.39	< 0.0001		78.36
A×D	12.13	1	12.13	1.26	0.2686		0.04
A×E	20.42	1	20.42	2.13	0.1537		0.07
B×C	24.82	1	24.82	2.59	0.1169		0.08
B×F	52.22	1	52.22	5.45	0.0257		0.17
C×D	4.52	1	4.52	0.47	0.4972		0.02
C×F	25.93	1	25.93	2.7	0.1093		0.09
D×E	93.84	1	93.84	9.79	0.0036		0.31
D×F	18.57	1	18.57	1.94	0.173		0.06
A^2	38.68	1	38.68	4.03	0.0526		0.13
B^2	850.93	1	850.93	88.74	< 0.0001		2.84
C^2	129.52	1	129.52	13.51	0.0008		0.43
D^2	62.28	1	62.28	6.5	0.0155		0.21
F^2	730.06	1	730.06	76.14	< 0.0001		2.43
Residual	326.01	34	9.59				0.65
Lack of Fit	298.88	29	10.31	1.9	0.2457	not significant	
Pure Error	27.13	5	5.43				
Cor Total	29986.1	53					

Table 4.7 shows the ANOVA table for surface with percentage of contribution of each parameter and their interactions. From the table, it is observed that soaking duration, discharge current, pulse-on-time, duty factor, interaction terms-pulse-on-time×soaking duration and square terms of open circuit voltage, pulse-on-time, soaking duration are important process parameters. The Table also shows that soaking duration is the most influential parameter for surface roughness with percentage contribution of 58.99% followed by discharge current, pulse-on-time and duty factor with percentage contribution of 18.60%, 9.62% and 0.39% respectively. Open circuit voltage and flushing pressure are found to be insignificant process parameters for surface roughness. The coefficient of determination (R^2) and adjusted (R^2) values are found to be 96.1% and 94.1% respectively. It is to be noted that the lack of fit is not significant for surface roughness.

Table 4.7 ANOVA for Surface roughness

Source	Sum of Squares	Degree of freedom	Mean Square	F Value	p-value Prob> F		% Contribution
Model	103.592	18	5.87	53.33	< 0.0001	significant	
A-Open circuit voltage	3.75×10^{-5}	1	3.75×10^{-5}	3.41×10^{-4}	0.9854		0.00
B-Discharge Current	19.98	1	19.98	181.65	< 0.0001		18.60
C-Pulse-on-time	10.34	1	10.34	93.95	< 0.0001		9.62
D-Duty Factor	0.42	1	0.42	3.81	0.0591		0.39
E-Flushing Pressure	0.025	1	0.025	0.22	0.6385		0.02
F- Soaking Duration	63.38	1	63.38	576.07	< 0.0001		58.99
A×B	0.038	1	0.038	0.34	0.5615		0.04
B×C	0.038	1	0.038	0.34	0.5615		0.04
B×E	0.083	1	0.083	0.75	0.392		0.08
B×F	0.41	1	0.41	3.68	0.0632		0.38
C×E	0.38	1	0.38	3.48	0.0705		0.35
C×F	0.46	1	0.46	4.14	0.0495		0.43
D×F	0.061	1	0.061	0.56	0.4606		0.06
A^2	1.18	1	1.18	10.71	0.0024		1.10
C^2	5.46	1	5.46	49.65	< 0.0001		5.08
D^2	0.16	1	0.16	1.43	0.2394		0.15
E^2	0.047	1	0.047	0.43	0.5162		0.04
F^2	1.13	1	1.13	10.24	0.0029		1.05
Residual	3.85	35	0.11				3.58
Lack of Fit	3.48	30	0.12	1.57	0.3275	not significant	
Pure Error	0.37	5	0.074				
Cor Total	107.442	53					

Table 4.8 shows the ANOVA table for radial overcut with percentage of contribution of each parameter and their interactions. ANOVA for Radial overcut shows that soaking duration, discharge current, pulse-on-time, duty factor, interaction terms-discharge current×soaking duration and square terms of open circuit voltage, soaking duration are important process parameters. The Table also shows that soaking duration is the most influential parameter for radial overcut with percentage contribution of 79.01% followed by discharge current, pulse-on-time and duty factor with percentage contribution of 8.88%, 2.83% and1.18% respectively. Open circuit voltage and flushing pressure are found to exhibit insignificant effect for radial overcut. The coefficient of determination (R^2) and adjusted (R^2) values are found to be 97.5% and 96.6% respectively. It is to be noted that the lack of fit is not significant for radial overcut.

Table 4.8 ANOVA for radial overcut

Source	Sum of Squares	Degree of freedom	Mean Square	F Value	p-value Prob> F		% Contribution
Model	0.79	21	0.037	45.19	< 0.0001	significant	
A-Open circuit voltage	1.38×10^{-3}	1	1.38×10^{-3}	1.66	0.2062		0.17
B-Discharge Current	0.072	1	0.072	86.52	< 0.0001		8.89
C-Pulse-on-time	0.023	1	0.023	28.05	< 0.0001		2.84
D-Duty Factor	9.6×10^{-3}	1	9.60×10^{-3}	11.58	0.0018		1.19
E-Flushing Pressure	1.6×10^{-4}	1	1.60×10^{-4}	0.19	0.6632		0.02
F-Soaking Duration	0.64	1	0.64	770.82	< 0.0001		79.01
A×C	4.5×10^{-4}	1	4.50×10^{-4}	0.54	0.4666		0.06
A×D	1.56×10^{-4}	1	1.56×10^{-4}	0.19	0.6671		0.02
B×D	3×10^{-4}	1	3.00×10^{-4}	0.36	0.5516		0.04
B×E	2.48×10^{-4}	1	2.48×10^{-4}	0.3	0.5881		0.03
B×F	4.14×10^{-3}	1	4.14×10^{-3}	4.99	0.0325		0.51
C×D	5×10^{-5}	1	5.00×10^{-5}	0.06	0.8076		0.01
C×F	3.24×10^{-4}	1	3.24×10^{-4}	0.39	0.5363		0.04
D×E	4.35×10^{-4}	1	4.35×10^{-4}	0.52	0.474		0.05
D×F	3.13×10^{-4}	1	3.13×10^{-4}	0.38	0.5436		0.04
A^2	0.01	1	0.01	12.19	0.0014		1.23
B^2	2.82×10^{-4}	1	2.82×10^{-4}	0.34	0.5638		0.03
C^2	1.50×10^{-4}	1	1.50×10^{-4}	0.18	0.6733		0.02
D^2	1.99×10^{-3}	1	1.99×10^{-3}	2.4	0.1313		0.25
E^2	1.67×10^{-3}	1	1.67×10^{-3}	2.01	0.1656		0.21
F^2	0.014	1	0.014	16.48	0.0003		1.73
Residual	0.027	32	8.29×10^{-4}				3.33
Lack of Fit	0.023	27	8.47×10^{-4}	1.15	0.4843	not significant	
Pure Error	3.67×10^{-3}	5	7.34×10^{-4}				
Cor Total	0.81	53					

Table 4.9 shows the ANOVA table for white layer thickness with percentage of contribution of each parameter and their interactions. It shows that parameters such as discharge current, pulse-on-time, duty factor, soaking duration, interaction terms such as discharge current×soaking duration and square terms of pulse-on-time, duty factor, and soaking duration have significant effect on white layer thickness. The Table also shows that soaking duration is the most influential parameter for white layer thickness with percentage contribution of 95.55% followed by discharge current, pulse-on-time and duty factor with percentage contribution of 2.87%, 0.22% and 0.04% respectively. Open circuit voltage and flushing pressure are found to be insignificant parameters for white layer thickness. The coefficient of determination (R^2) and adjusted (R^2) values are found to be 99.83% and

99.72% respectively. It is to be noted that the lack of fit is not significant for white layer thickness.

Table 4.9 ANOVA for white layer thickness

Source	Sum of Squares	Degree of freedom	Mean Square	F Value	p-value Prob> F		% Contribution
Model	3097.37	20	154.87	948.97	< 0.0001	significant	
A-Open circuit Voltage	8.44×10^{-3}	1	8.44×10^{-3}	0.052	0.8215		0.00
B-Discharge Current	88.97	1	88.97	545.2	< 0.0001		2.87
C-Pulse-on-time	6.86	1	6.86	42.03	< 0.0001		0.22
D-Duty Factor	1.36	1	1.36	8.35	0.0068		0.04
E-Flushing Pressure	0.055	1	0.055	0.34	0.5651		0.00
F-Soaking Duration	2964.59	1	2964.59	18165.89	< 0.0001		95.55
A×B	0.08	1	0.08	0.49	0.4887		0.00
B×C	0.15	1	0.15	0.93	0.3427		0.00
B×D	0.32	1	0.32	1.96	0.1708		0.01
B×E	0.045	1	0.045	0.28	0.6024		0.00
B×F	0.79	1	0.79	4.83	0.0352		0.03
C×F	0.17	1	0.17	1.07	0.3089		0.01
D×F	0.54	1	0.54	3.31	0.0778		0.02
E×F	0.07	1	0.07	0.43	0.5161		0.00
A^2	0.27	1	0.27	1.67	0.2052		0.01
B^2	0.62	1	0.62	3.8	0.0596		0.02
C^2	1.72	1	1.72	10.52	0.0027		0.06
D^2	6.04	1	6.04	37.03	< 0.0001		0.19
E^2	0.071	1	0.071	0.44	0.5135		0.00
F^2	16.86	1	16.86	103.29	< 0.0001		0.54
Residual	5.39	33	0.16				0.19
Lack of Fit	5.07	28	0.18	2.89	0.1198	not significant	
Pure Error	0.31	5	0.063				
Cor Total	3102.76	53					

The process models for the performance measures obtained through regression analysis are given below:

MRR =+4.93-0.44×A+1.43×B-0.45×C+0.37×D+0.055×E-8.333×10^{-4}×F-0.057×A×B-0.049×A×D+0.043×A×F-0.30×B×C -0.055×B×D+0.042×B×E+0.087×B×F+0.100×C×E+0.061×C×F+0.37×A^2-0.68×B^2-1.04×$C^2$0.23×D^2+0.19×E^2-0.080×F^2(Coded form) (4.3)

EWR =+124.29 + 2.84 × A + 11.54 × B + 5.17 × C + 3.60 × D + 0.24 × E- 31.29 × F + 0.87 × A × D + 1.60 × A × E - 1.76 × B × C - 2.56 × B × F - 0.75 × C × D + 1.27 × C × F - 3.43× D × E-1.52 × D × F- 1.92 × A^2 - 8.72× B^2 - 3.51 × C^2 - 2.44 × D^2 - 8.34 × F^2 (Coded Form) (4.4)

Surface roughness =+8.67 + 1.25× 10-3 × A + 0.91 × B + 0.66 C+0.13× D-0.032× E - 1.63 × F + 0.069 ×A × B - 0.069 × B × C-0.072 × B × E - 0.22 ×B × F-0.22 × C × E-0.17 × C × F - 0.087 × D × F + 0.34 × A^2 + 0.72 × C^2+0.12 × D^2 + 0.065 × E^2 + 0.33 × F^2 (Coded Form) (4.5)

Radial overcut=+0.23 - 7.583 × 10^{-3} × A + 0.055 × B + 0.031 × C + 0.020 × D - 2.583 ×10^{-3} × E-0.16 × F + 7.5 × 10^{-3} × A × C + 3.125 × 10^{-3} × A × D - 6.125 × 10^{-3}× B × D + 3.937 × 10^{-3}× B × E- 0.023 × B × F + 4.5 × 10^{-3}× C × F -7.375 × 10^{-3} × D × E - 6.25 × 10^{-3}× D × F- 0.031 × A^2 + 5.236 ×10^{-3}× B^2 + 3.819 × 10^{-3} × C^2+ 0.014 × D^2+ 0.013 ×E^2 + 0.036 × F^2 (Coded Form) (4.6)

White layer thickness=+27.73+0.019 × A+1.93 × B+0.53 × C+0.24 × D+0.048 × E-11.11 × F-0.100 × A × B-0.14 B × C-0.20 × B × D-0.053× B × E+0.31 × B × F+0.10 × C × F+0.26 × D × F+0.094 × E × F-0.16 × A^2-0.25 × B^2-0.41 × C^2-0.77 × D^2-0.083 × E^2+1.28 × F^2(Coded Form) (4.7)

The machined surface of the tool is observed with the scanning electron microscope (SEM) (Model - JEOL JSM-6084LV) at 100 X magnification after completion of fifty four experimental runs as shown in Figure 4.6 (a,b and c). From the SEM micrographs, it can be clearly observed that the machined surface area is greatly damaged due to higher meting and evaporation from tool tip for the untreated electrode. However, improved machined surface is achieved due to less melting of the electrode from surface and tip for treated electrode with longer soaking duration (36-hrs). Electrode treated with 24-hrs soaking

duration exhibits a machined surface quality between untreated and treated with 36-hrs soaking duration. Hence, it can be concluded that improved machined surface and proper retention of tool shape can be achieved with longer duration of soaking period.

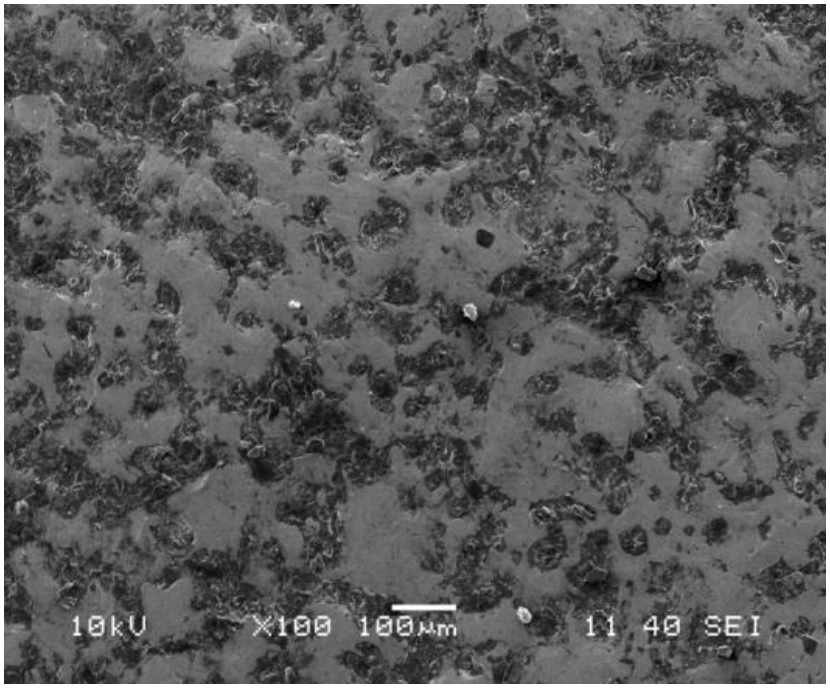

(a) Untreated brass

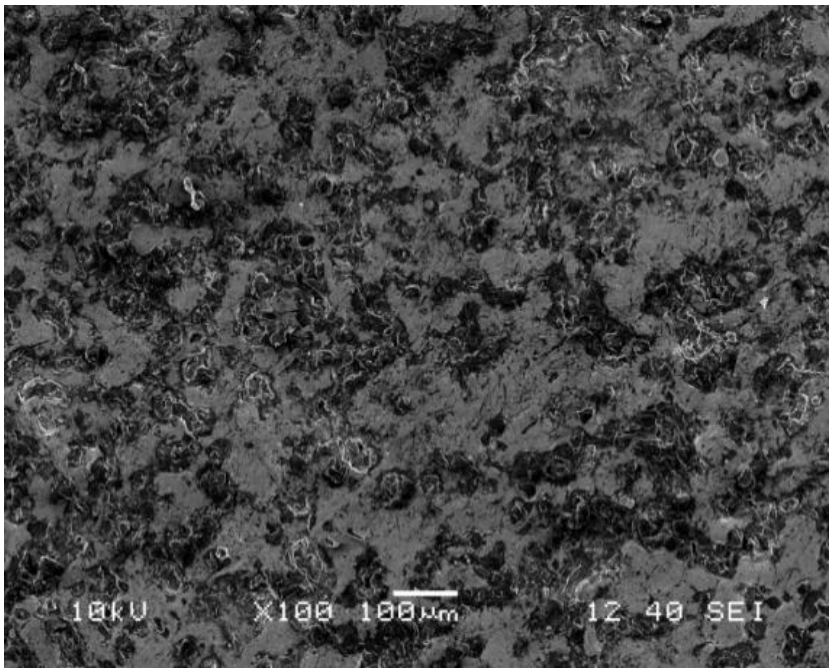

(b) Cryogenic-treated electrode with soaking duration of 24-hrs

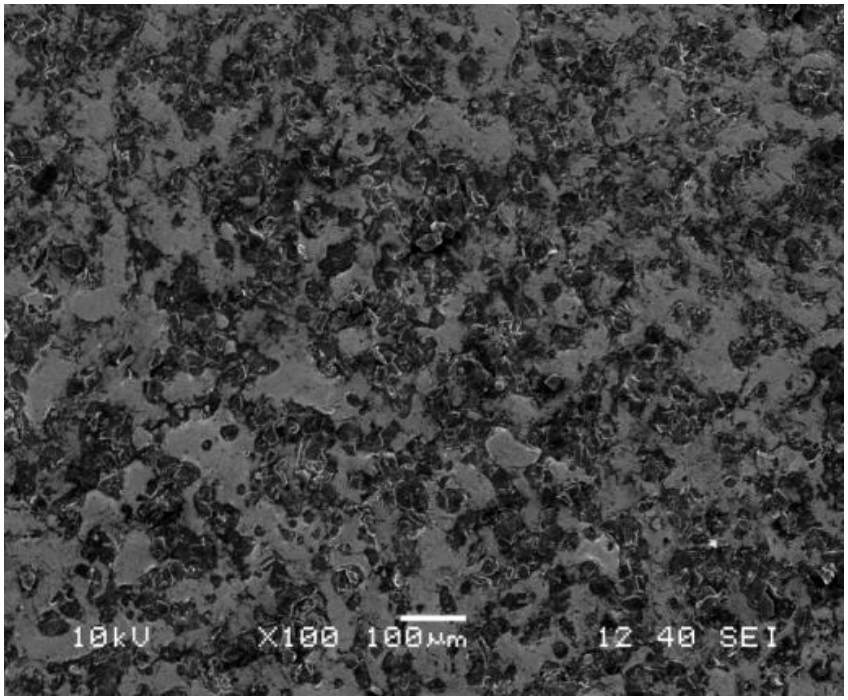

(c) Cryogenic-treated electrode with soaking duration of 36-hrs

Figure 4.6(a, b and c) SEM images of tool tip

Figure 4.7 (a and b) shows the SEM micrographs taken with the parametric conditions of A=80V, B=5A, C=300µs, D=80%, E=0.2bar, F=0-hrs and A=80V, B=5A, C=300µs, D=80%, E= 0.2bar, F=36-hrs respectively. From these figures, it is observed that the surface quality of the work piece improves because cracks and pores on the machined surface diminish as the soaking duration increases. From this, it can be concluded that machined surface quality heavily depends on proper retention of electrode shape. Cryo-treated tool with longer soaking duration produces finest surface quality on the machined surface due to proper retention of tool shape and uniform sparking.

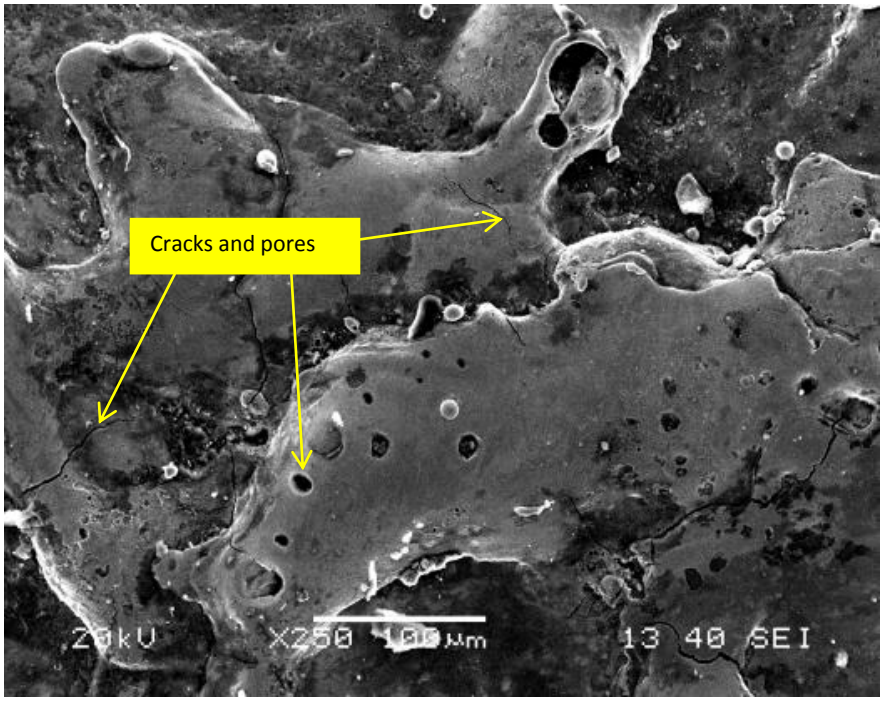

(a) SEM micrograph at A=80V, B=5A, C=300µs, D=80%, E=0.3bar, F=0-hrs

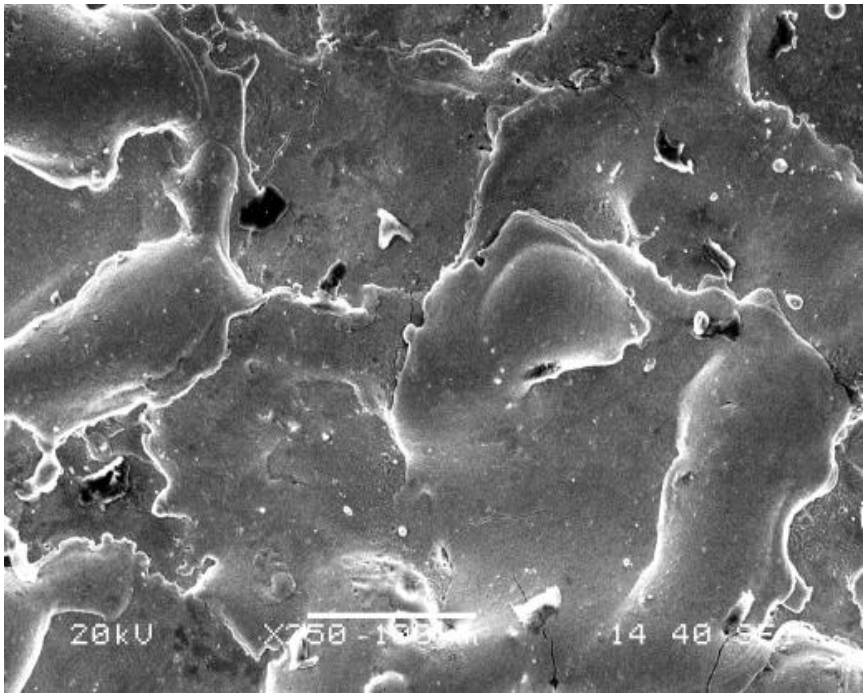

(b) SEM micrograph at A=80V, B=5A, C=300µs, D=80%, E=0.3bar, F=36-hrs

Figure 4.7(a and b) SEM images of the machined surface of the work piece

Figure 4.8(a) and (b) shows the SEM micrographs of white layer thickness taken at parametric condition at A=70V B=3A C=200µs D=80% E=0.3bar F=24 hrs and at A=70V B=7A C=200µs D=80% E=0.3bar F=24 hrs respectively. From the micrographs it can be clearly visible that white layer thickness increases with increase discharge current from 3A to 7A. Increase in discharge current significantly improves the spark energy which in turn increases the volume of molten material eroded both the electrodes. As a result, it becomes difficult to be flushed away by the dielectric fluid and settles down on the machined surface in turn increases the white layer thickness.

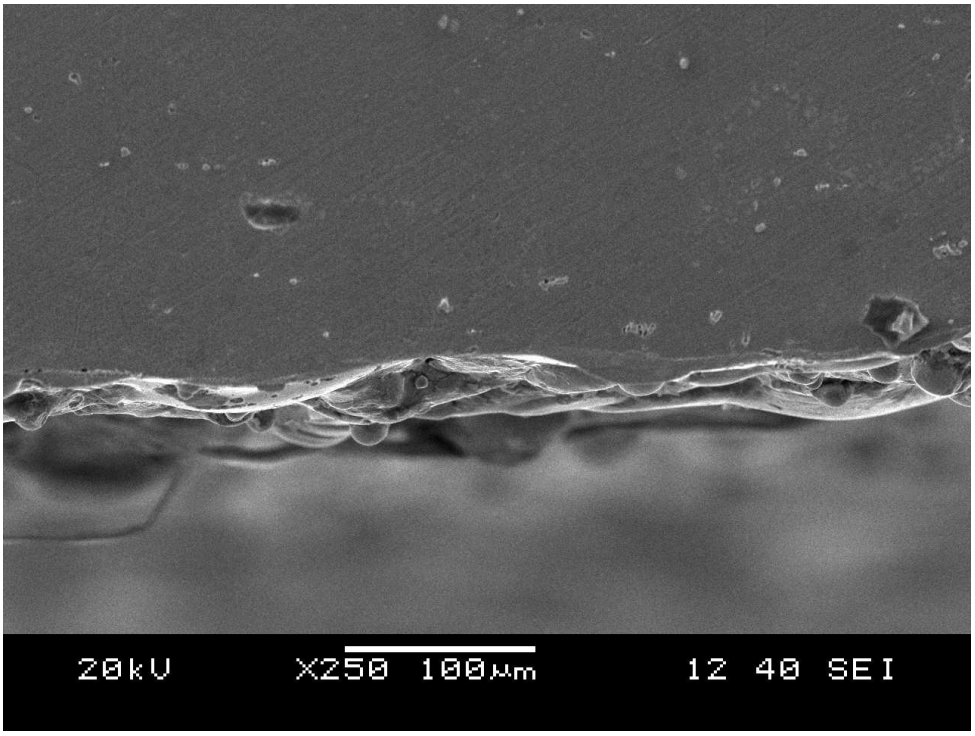

(a) Micrograph at A=70V B=3A C=200µs D=80% E=0.3bar F=24hrs

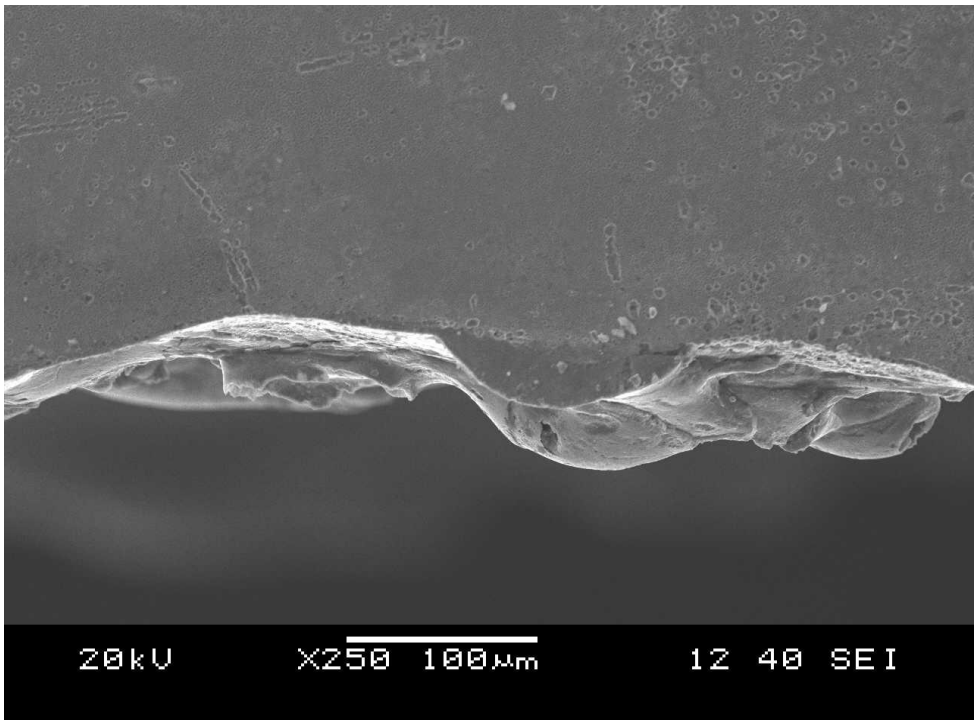

(b)Micrograph at A=70V B=7A C=200µs D=80% E=0.3bar F=24 hrs

Figure 4.8(a) and (b) SEM micrograph showing white layer at on the cross section of the machined surface

Figure 4.9 (a) and (b) shows the SEM micrographs of white layer thickness taken at parametric condition at A=80V B=5A C=100µs D=80% E=0.3bar F=0-hrs and at A=80V B=5A C=100µs D=80% E=0.3bar F=36-hrsrespectively. From the micro graphs, it can be observed that white layer thickness decreases with increase in cryogenic treatment soaking duration from 0-hrs to 36-hrs.Owing to deep cryogenic treatment the thermal and mechanical properties such as thermal conductivity and micro hardness of the tool material improves. This phenomenon permits easy dissipation of heat from tool material which results in better retention in tool shape, uniform sparking and superior surface quality on the machined surface. This phenomenon improves the flushing efficiency of the machined surface and reduces deposition of molten metal and thus reduces the white layer thickness.

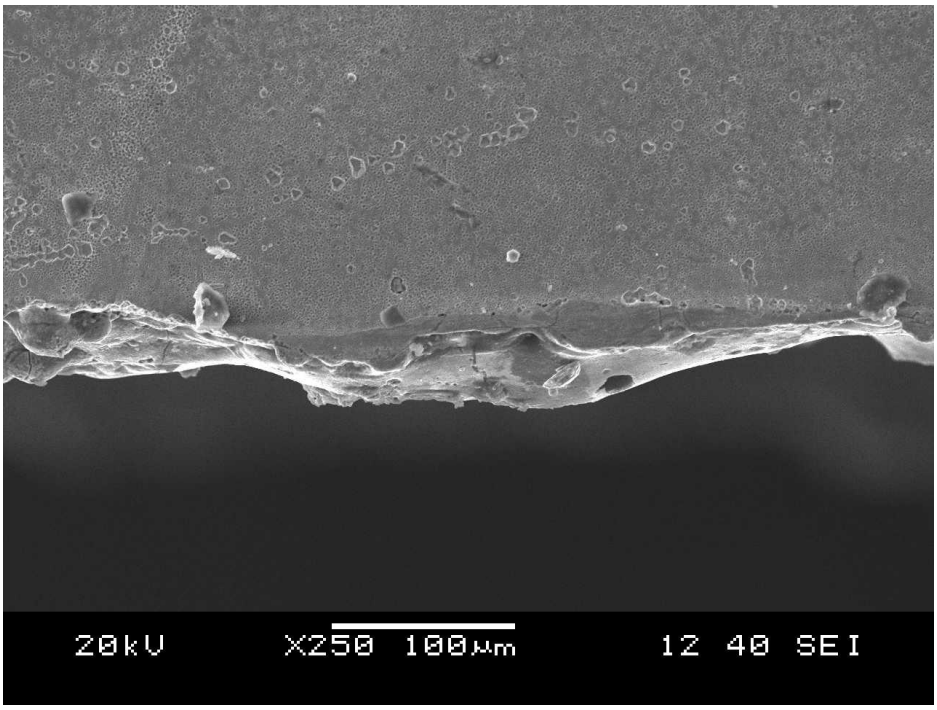

(a) Micrograph at A=80V B=5A C=100µs D=80% E=0.3bar F=0 hrs

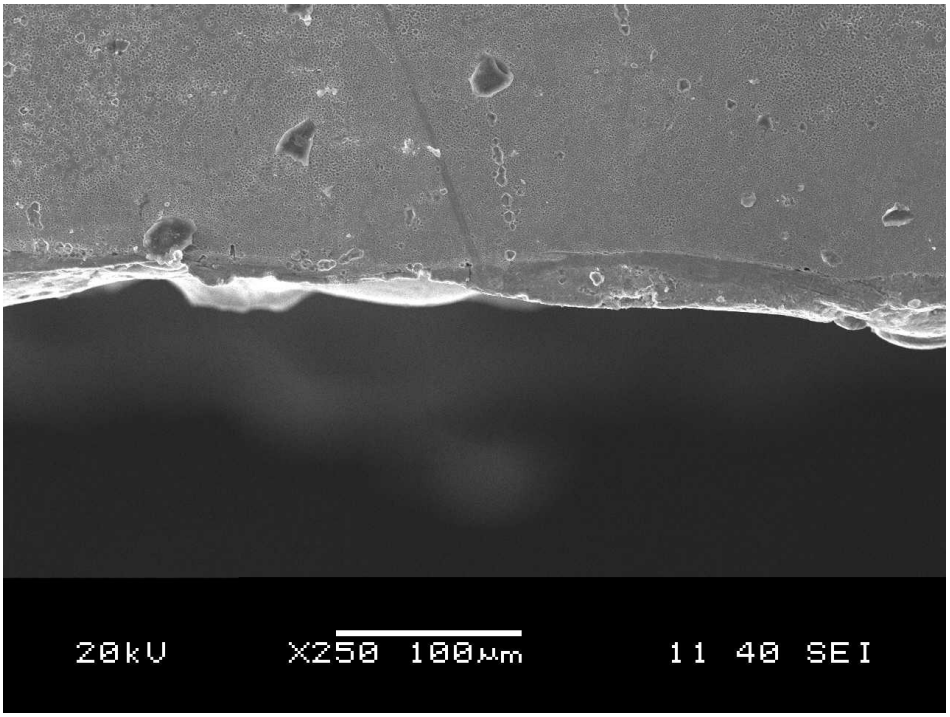

(b) Micrograph at A=80V B=5A C=100µs D=80% E=0.3bar F=36hrs

Figure 4.9(a) and (b) SEM micrograph showing white layer on the cross section of the machined surface

The machining efficiency of the EDM process is directly evaluated in terms of material removal rate (MRR). Hence it is the most important performance measure of the process. Figure 4.10 shows the variation of MRR discharge current and open circuit voltage. It shows that MRR increases briskly with increase in discharge current. Discharge current happens to be the most dominant process parameter and directly governs the spark energy. Increase in discharge current significantly increases the spark energy higher volume of material is removed from the machined surface. The figure also shows that MRR initially decreases with the increase of open circuit voltage for any value of discharge current but shows a slight increasing trend after reaching a minimum value. A similar trend has been also reported in the experimental investigation of Lee and Li (2001).

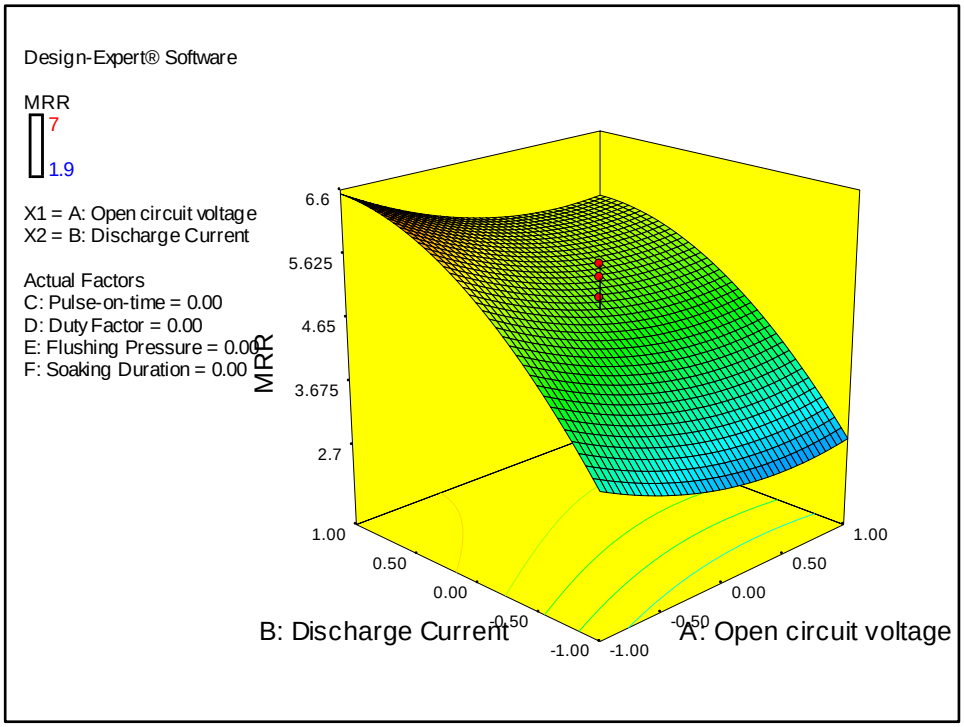

Figure 4.10 Surface plot of MRR with open circuit voltage and discharge current

Figure 4.11 shows the variation of MRR with pulse-on-time and discharge current. It shows that for all value of discharge current MRR increases with increase in pulse-on-time initially but shows a decreasing after reaching a pulse-on-time of 200µs.Increasing the pulse-on-time increases the spark energy and in turn higher MRR is produced. But continuous application of same heat flux decreases the pressure inside the plasma channel and since the molten metal volume remains constant, further increase in pulse-on-time causes decrease in MRR. Similarly, from the surface plot of MRR discharge current and duty factor it is observed that MRR increases with increase in briskly with increase in

discharge current and duty factor except at the lower values of the both parameters due to smaller value of spark energy. It was expected that MRR will improve due to deep cryogenic treatment of the brass electrode. However, the low thermal conductivity and high micro hardness of Inconel 718 work material does not allow higher volume of material to be eroded from the work surface. As a result, MRR remains constant with increase in soaking duration. Hence, parameters such as soaking duration and flushing pressure have no effect on MRR.

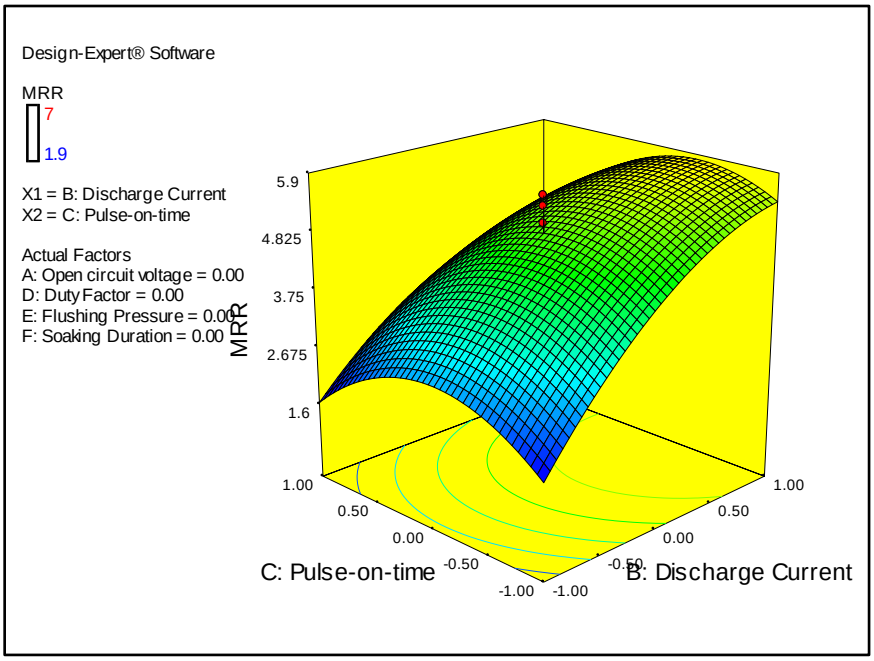

Figure 4.11Surface plot of MRR with pulse-on time and discharge current

EWR is an important performance measure in EDM as it directly affects the machining cost and time. Figure 4.12 shows the surface plot of EWR with discharge current and soaking duration. Figure shows that EWR increases briskly with increases in discharge current at lower level of soaking duration. Higher values of discharge current leads to significant increase in spark energy, which in turn influences increases in the volume of the molten metal from both the electrodes causing increase in EWR. The figure also shows that EWR varies inversely with soaking duration. At the cryogenic temperature, the thermal vibration of atoms in a metal becomes weaker resulting in easy movement of electrons inside the metal. This phenomenon increases the electrical conductivity of the metal. As per Wiedemann-Franz-Lorenz Law, increase in electrical conductivity increases the thermal conductivity of the material. The increase in thermal conductivity decreases the local temperature rise of the material due to faster heat transfer away from metal surface reducing tool wear. As the soaking duration increases, the increase in wear resistance property of

electrode increases due to improvement in thermal conductivity and micro hardness. The heat dissipation capacity of the electrodes increases due to increase in thermal conductivity which in turn declines TWR and EWR. Increasing soaking duration up to 36-hrs further reduces the grain size of the electrodes and the microstructure becomes refined leading to considerable increase in micro hardness of the material. Hence, the resistance against penetration of heat for the treated electrodes is increased. Therefore, vaporization and melting of material in treated tools are reduced causing reduction in EWR at higher value soaking duration.

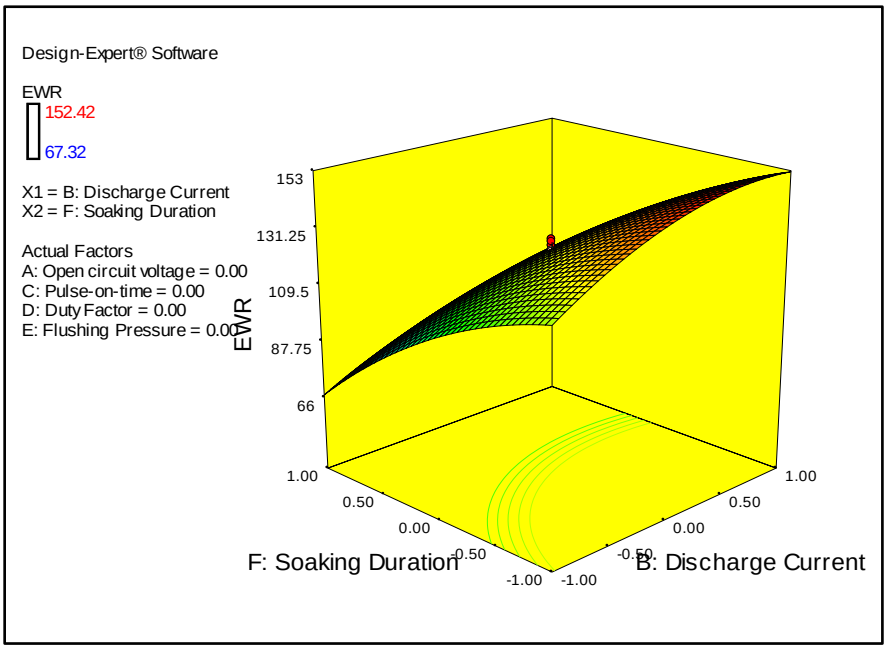

Figure 4.12Surface plot of EWR with discharge current and soaking duration

Figure 4.13 shows variation of EWR with pulse-on-time and duty factor. It shows that EWR increases with increase in pulse-on-time initially but shows a decreasing trend at higher value of pulse-on-time. This is caused due to decrease in spark energy density in the spark gap between electrodes because the diameter of the plasma channel expands with increase in pulse-on-time. Another reason for lower wear ratio at higher pulse-on-time is due to the attachment of carbon particles on to the electrode tip causing increase in the wearing resistance of tool and reducing EWR. A similar trend has been also observed by previous researchers (Srivastava and Pandey 2012). Figure also shows that EWR increases with increase in the duty factor. Increase in duty factor causes increase in the spark energy across the gap between the electrodes which increases EWR. Similarly, EWR increases with increase in open circuit voltage and duty factor observed from the surface plot of EWR with open circuit voltage and duty factor.

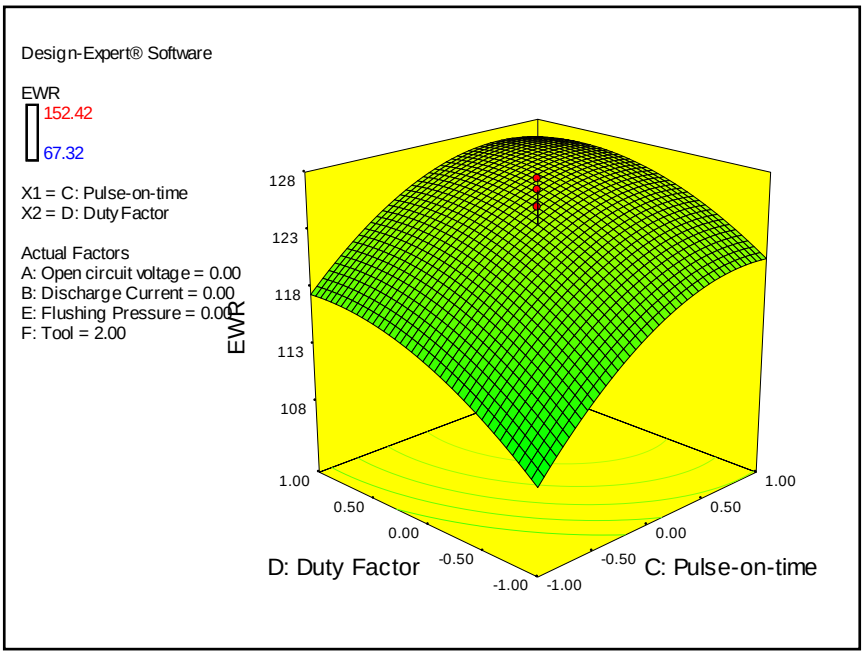

Figure 4.13 Surface plot of EWR with Duty factor and pulse-on-time

Figure 4.14 shows the surface plot of surface roughness with discharge current and soaking duration. Figure shows that surface quality deteriorate with increase in discharge current at lower value of soaking duration. As discharge current increases, the spark energy between the electrodes increases resulting in removal of lager size material from the machined surface and hence produces poor surface quality. The figure also indicates that surface quality improves gradually as soaking duration increases. At the lower level of soaking duration, heat generated during EDM cannot dissipate from the electrode due to poor thermal conductivity of the untreated tool. This leads to vaporizing and melting of the machined surface of tool tip and the machined surface gets damaged. Due to non-uniform sparking between the electrodes, the surface produced is of poor quality. As the soaking duration increases, the wear resistance property of electrode increases due to improvement in thermal conductivity and micro hardness. This allows easy dissipation of heat from electrodes which in turn results in improvement in surface integrity, better retention in tool shape, uniform sparking and superior surface quality.

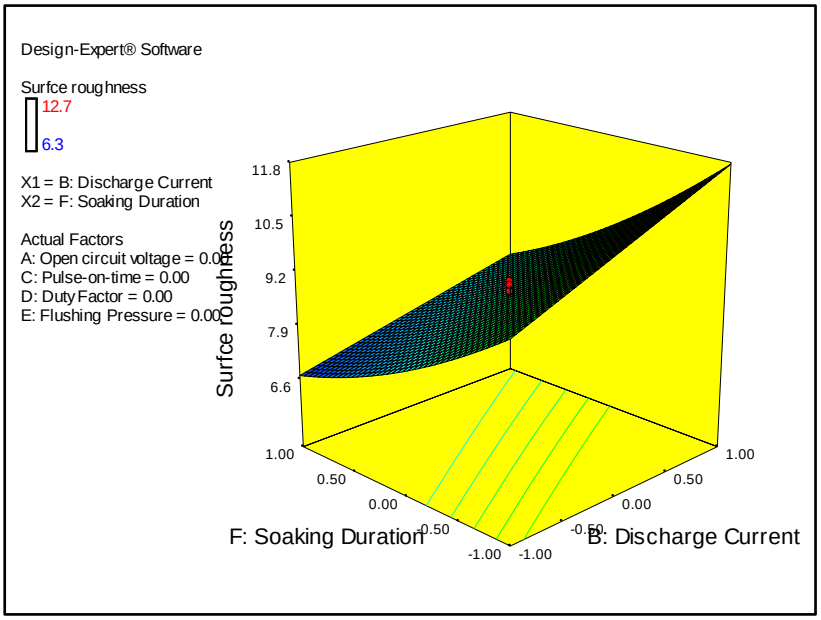

Figure 4.14 Surface plot of surface roughness with discharge current and soaking duration

Figure 4.15 shows the surface plot of surface roughness with pulse-on-time and soaking duration. It shows that surface roughness increases with increase in pulse-on-time for all values of soaking duration. Increase in pulse-on-time causes high spark energy which enables detachment of large sized particle from the machined surface and the surface becomes rough. Similarly the surface plot of duty factor and soaking duration indicates that surface roughness increases slowly with increase in duty factor. Open-circuit voltage and flushing pressure have little effect on surface roughness.

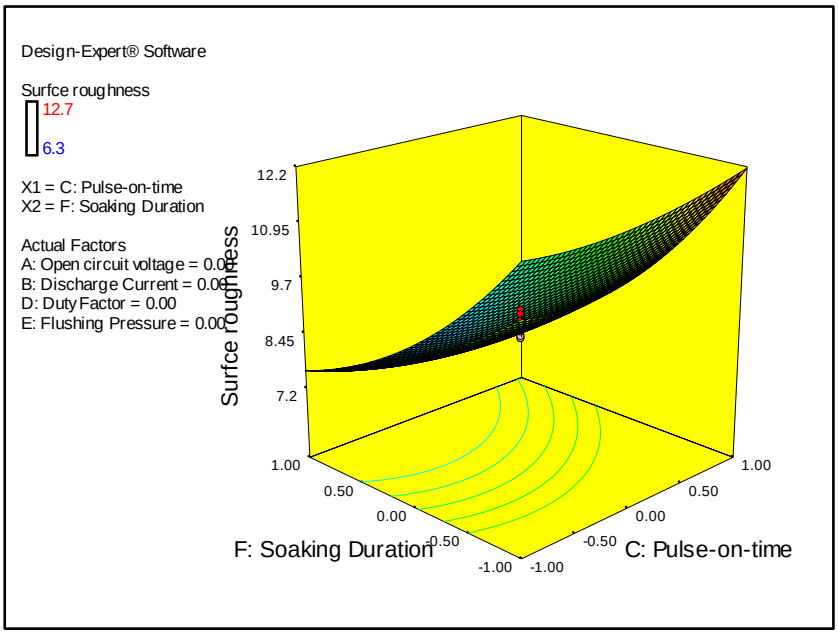

Figure 4.15 Surface plot of surface roughness with pulse-on-time and soaking duration

For precise and accurate machining minimization of over cut is vital. Figure 4.16 shows the surface plot of Radial overcut with discharge current and soaking duration. The figure indicates that over cut increases briskly with the increase in discharge current at lower level of soaking duration. As discharge current increases, the spark energy across the gap between electrodes increases resulting in more material to be vaporized from work surface and increase in overcut. The figure also indicates that over cut decreases with increase in soaking duration. At the lower level of soaking duration, heat generated during EDM cannot dissipate through the electrode due to poor thermal conductivity of the untreated tool. This causes vaporization and melting of material due to increase in the local temperature rise of the material disturbing the roundness of electrode. This results in non-uniform sparking and hence production accuracy of the drilled holes is poorer. However, for the treated electrodes with soaking duration 24-hrs the thermal conductivity and micro hardness of the material is higher in comparison with untreated electrodes. Increasing the soaking duration, further improves the thermal conductivity and micro harness and the microstructure become refined. This reduces vaporization and melting of material from the tool tip and roundness of electrode material is maintained. As a result, the production accuracy of the drilled holes is increased due to uniform sparking and proper retention in tool shape.

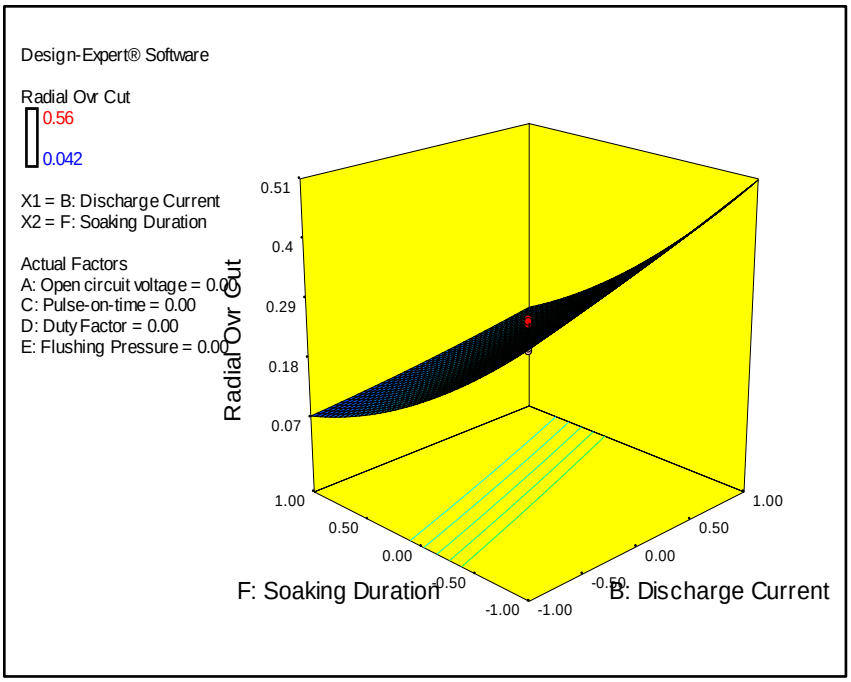

Figure 4.16 Surface plot of radial overcut with discharge current and soaking duration

Figure 4.17 shows the surface plot of Radial overcut with duty factor and pulse-on-time. The surface plot shows that overcut increases gradually with increase in duty factor and pulse-on-time. Increasing duty factor increases the number of sparks per unit time. This results in increase in material removal rate and in turn influences increases in over cut. Increasing pulse-on-time also increases the over cut on the machined surface due to prolonged occurrence of spark discharges.

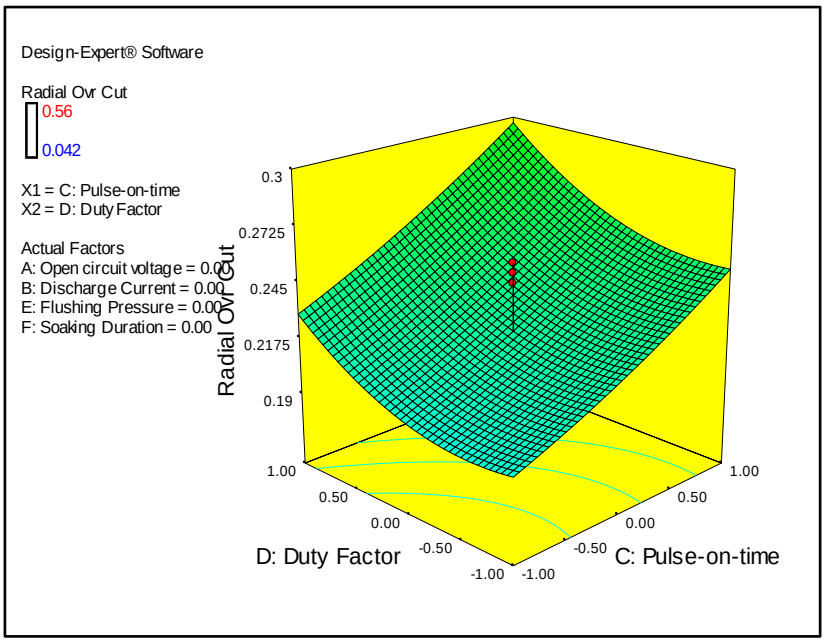

Figure 4.17 Surface plot of Radial overcut with duty factor and pulse-on-time

Figure 4.18 shows the variation of white layer thickness with discharge current and soaking duration. It shows that white layer thickness increases rapidly with increase in discharge current. This is obvious, as increase in discharge current significantly improves the spark energy higher volume of molten material is eroded from electrodes. As a result, it becomes difficult to be flushed away by the dielectric fluid and gets deposited on the machined surface in turn increases the white layer thickness. The figure also shows that white layer thickness varies inversely with increase in soaking duration. Deep cryogenic treatment improves the thermal conductivity and micro hardness of the tool material. This allows easy dissipation of heat from tool material which results in better retention in tool shape, uniform sparking and superior surface quality on the machined surface. This phenomenon improves the flushing efficiency of the machined surface and reduces deposition of molten metal and thus reduces the white layer thickness. As the molten metal volume remains unaffected with increasing the soaking duration further increase in soaking duration reduces the white layer thickness.

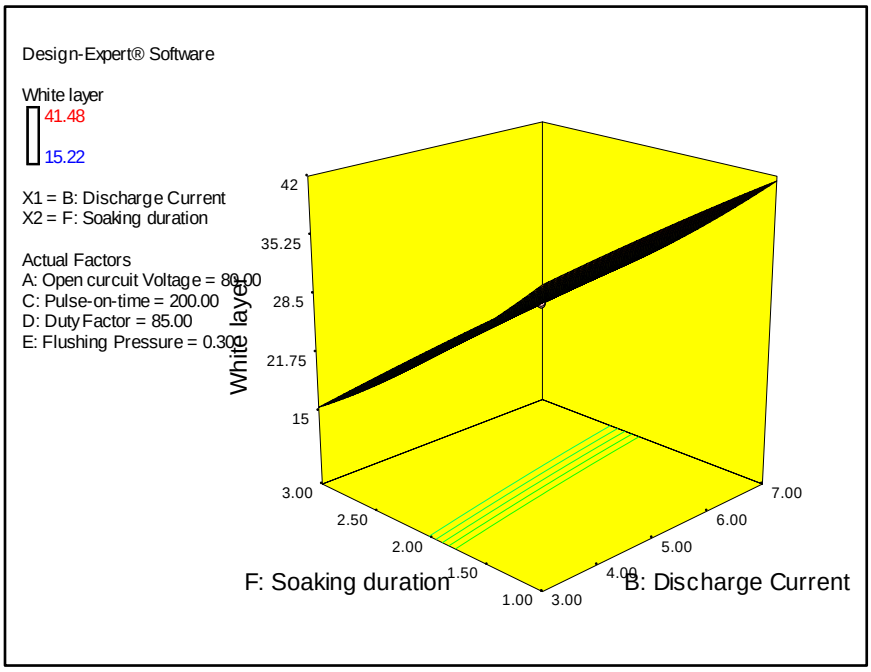

Figure 4.18Surface plot of white layer thickness with soaking duration and discharge current

Figure 4.19 shows the variation of white layer thickness with pulse-on-time and soaking duration. It shows that white layer thickness increases with increase in pulse-on-time. Increase in pulse-on-time increases the spark energy between the electrodes. The molten metal volume increases due to prolonged occurrence of spark discharges. Due to improper flushing action higher volume of molten metal gets deposited on the machined surface and thus increases the white layer thinness on the machined surface. Similarly, from the surface plot of white layer thickness soaking duration and duty factor it is observed, that white layer thickness increases with increase in duty factor. Increases in duty factor, increases the no of sparks per unit time which in turn, increases the molten metal volume and as a result the white layer thinness on the machined surface is increased. It was expected that flushing pressure would have played a vital role in reducing the white layer thickness, but within the scope this experiment it was observed that flushing pressure and open circuit voltage have subtle effect on white layer thickness.

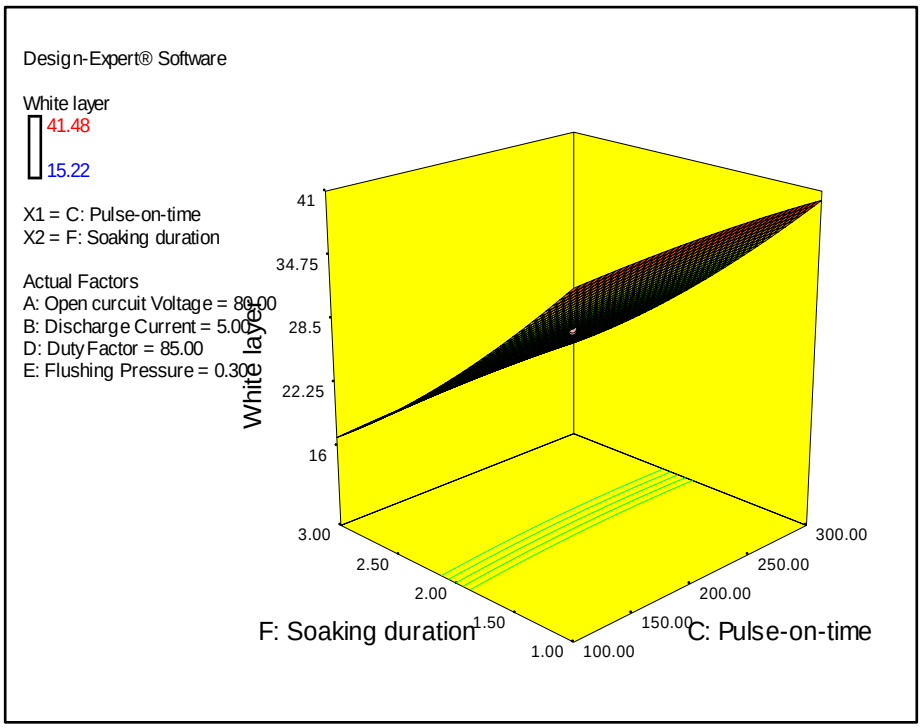

Figure 4.19 Surface plot of white layer thickness with pulse-on-time and soaking duration

In this study, five responses such as (MRR, EWR, surface roughness, radial overcut and white layer thickness) are considered. However, all the five responses may not be applicable simultaneously for industrial applications. Therefore, two responses are considered to be optimized treating other three responses are treated as constraints at a time. The constrained value is selected from the experimental observations. The empirical relation between the process parameters and process responses established from the RSM analysis is used as objective function for solving the multi-objective particle swarm optimization (MOPSO) problem. In the present work, the objectives are maximization of MRR and minimization of EWR, surface roughness, radial overcut and white layer thickness which are functions of process parameters viz. open circuit voltage, discharge current, pulse-on-time , duty factor, flushing pressure and soaking duration.

Ten optimization problems are formed considering two responses as objectives and three as constraints. The empirical relation between input parameters and responses obtained in equations 4.3-4.7 are used as functional relations. MOPSO algorithm discussed in section 3.2 is coded MATLAB 13 for solving minimization problems.

Problem 1:

Maximize MRR

Minimize EWR

Subject to

Surface roughness $\leq$ 6.3

Radial overcut $\leq$ 0.042

White layer thickness $\leq$ 15.22

where 6.3, 0.042 and 15.22are the minimum values of surface roughness, Radial overcut and white layer thickness obtained from the experimental table 4.4 respectively.

Problem 2:

Maximize MRR

Minimize surface roughness

Subject to

EWR $\leq$67.32

Radial overcut $\leq$ 0.042

White layer thinness $\leq$15.22

where 67.32, 0.042 and 15.22 are the minimum values of EWR and radial overcut and white layer thickness obtained from the experimental table 4.4 respectively.

Problem 3:

Maximize MRR

Minimize radial overcut

Subject to

EWR $\leq$67.32

Surface roughness $\leq$ 6.3

White layer thinness $\leq$15.22

where 67.32, 6.3and 15.22are the minimum values of EWR, surface roughness and white layer thickness obtained from the experimental table 4.4 respectively.

Problem 4

Maximize MRR

Minimize white layer thickness

Subject to

EWR $\leq$67.32

Surface roughness $\leq$ 6.3

Radial overcut $\leq$ 0.042

where 67.32, 6.3 and 0.042 are the minimum values of EWR, surface roughness and Radial overcut obtained from the experimental table 4.4 respectively

Problem 5:

Minimize EWR

Minimize Surface roughness

Subject to

MRR ≥ 7

Radial overcut $\leq$ 0.042

White layer thinness ≤ 15.22

where 7,0.042 and 15.22 are the maximum value of MRR and minimum values radial overcut and white layer thickness obtained from the experimental table 4.4 respectively.

Problem 6:

Minimize EWR

Minimize Radial overcut

Subject to

MRR ≥ 7

Surface roughness ≤ 6.3

White layer thinness ≤ 15.22

where 7, 6.3 and 15.22 are the maximum value of MRR and minimum values of surface roughness and white layer thickness obtained from the experimental Table 4.4 respectively.

Problem 7:

Minimize EWR

Minimize white layer thickness

Subject to

MRR ≥ 7

Surface roughness ≤ 6.3

Radial overcut $\leq$ 0.042

where 7, 6.3 and 0.042 are the maximum value of MRR and minimum values of surface roughness and Radial overcut obtained from the experimental Table 4.4 respectively.

Problem 8:

Minimize Surface roughness

Minimize Radial overcut

Subject to

MRR ≥ 7

EWR ≤67.32

White layer thinness ≤15.22

where7, 67.32 and 15.22 are the maximum value of MRR and minimum values of EWR and white layer thickness obtained from the experimental Table 4.4 respectively.

Problem 9:

Minimize Surface roughness

Minimize white layer thickness

Subject to

MRR ≥7

EWR ≤67.32

Radial overcut ≤ 0.042

where 7, 67.32 and 0.042 are the maximum value of MRR and minimum values of EWR and Radial overcut obtained from the experimental Table 4.4 respectively.

Problem 10:

Minimize Radial overcut

Minimize white layer thickness

Subject to

MRR ≥7

EWR ≤67.32

Surface roughness ≤ 6.3

where 7, 67.32 and 6.3 are the maximum value of MRR and minimum values of EWR and surface roughness obtained from the experimental Table4.4 respectively

It is to be noted equivalent minimization function is used in the MATLAB program wherever an objective is maximized.

The optimization model was run on in a Pentium IV desktop. Simulation study is carried out to demonstrate the potentiality of MOPSO algorithm. The initial population chosen for the algorithms is 120. The parameters employed for MOPSO are as follows: the size of archive is 100, the inertia weight is 0.4 and both the cognitive and social parameters (c_1 and c_2) are taken as 1.2. This led to the development of ten sets Pareto-fronts viz. MRR and EWR, MRR and surface roughness, MRR and radial overcut, MRR and white layer thickness, EWR and surface roughness, EWR and radial overcut, EWR and white layer thickness, surface roughness and radial overcut, surface roughness and white layer thickness, radial overcut and white layer thickness generating optimal solution for the

responses. Figure 4.20 shows the Pareto-front for MRR and EWR. A Sample set of the optimal solution for MRR and EWR has been given in Table 4.10.

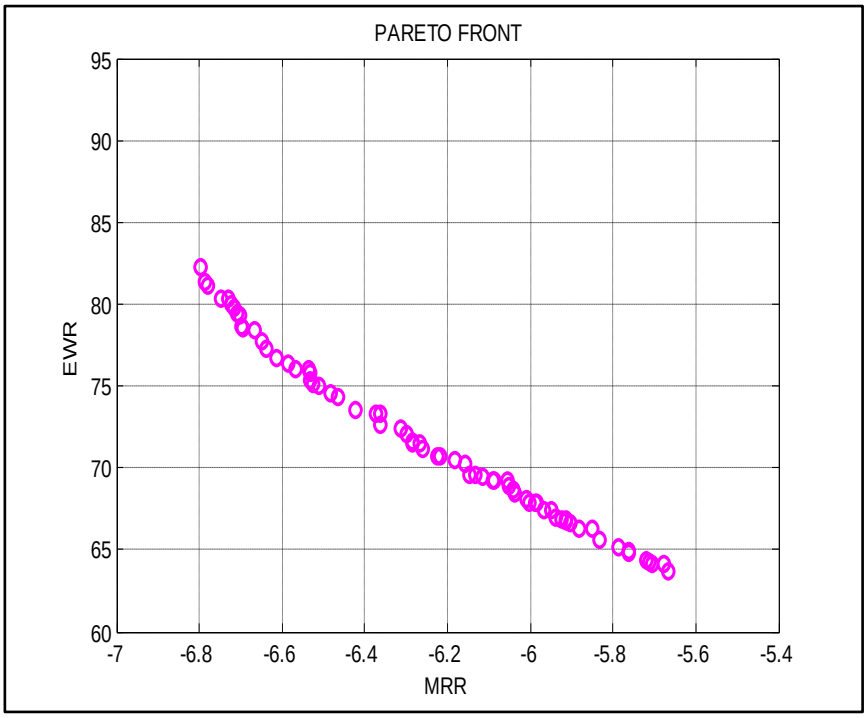

Figure 4.20 Pareto front objectives for MRR and EWR

Table 4.10Pareto optimal solution for MRR and EWR with corresponding variable setting

Run order	A (V)	B (A)	C (µs)	D (%)	E (bar)	F Hrs.	MRR mm^3/min	EWR %
1	70.81	7.00	161.97	88.46	0.20	36	6.80	82.27
2	70.81	7.00	154.63	88.07	0.20	36	6.79	81.38
3	70.81	7.00	150.89	88.13	0.20	36	6.78	81.14
4	70.81	7.00	140.44	88.22	0.20	36	6.75	80.32
5	70.99	7.00	143.18	87.82	0.20	36	6.73	80.30
6	71.02	7.00	154.96	86.61	0.20	36	6.72	80.05
7	71.02	7.00	149.90	86.68	0.20	36	6.71	79.72
8	70.99	7.00	145.97	86.70	0.20	36	6.71	79.38
9	70.99	7.00	144.21	86.75	0.20	36	6.70	79.28
10	70.81	7.00	138.97	86.69	0.20	36	6.70	78.60
11	70.81	7.00	140.46	86.48	0.20	36	6.70	78.51
12	70.99	7.00	139.76	86.33	0.20	36	6.67	78.39
13	70.81	7.00	131.72	86.51	0.20	36	6.65	77.68
14	70.81	7.00	144.33	85.19	0.20	36	6.64	77.31
15	70.81	7.00	136.70	85.33	0.20	36	6.61	76.75
16	70.81	7.00	126.13	85.94	0.20	36	6.58	76.42
17	70.81	7.00	126.30	85.65	0.20	36	6.57	76.07
18	71.02	7.00	125.01	85.64	0.20	36	6.53	76.07
19	71.02	7.00	137.36	84.50	0.20	36	6.53	75.85
20	70.81	7.00	126.70	85.03	0.20	36	6.53	75.33
21	70.81	7.00	135.37	84.25	0.20	36	6.52	75.17
22	70.81	7.00	125.45	84.90	0.20	36	6.51	75.01
23	70.81	7.00	122.61	84.81	0.20	36	6.48	74.57
24	70.81	7.00	120.30	84.82	0.20	36	6.46	74.32
25	70.81	7.00	120.61	84.26	0.20	36	6.42	73.58
26	70.99	7.00	117.14	84.28	0.20	36	6.37	73.31
27	70.99	7.00	113.46	84.60	0.20	36	6.36	73.30
28	70.81	7.00	118.14	83.84	0.20	36	6.36	72.67
29	70.99	7.00	117.07	83.65	0.20	36	6.31	72.37
30	70.99	7.00	118.72	83.35	0.20	36	6.30	72.12
31	70.81	7.00	112.55	83.59	0.20	36	6.28	71.61
32	70.81	7.00	116.01	83.25	0.20	36	6.28	71.52
33	70.81	7.00	108.97	83.80	0.20	36	6.27	71.47
34	70.81	7.00	117.02	82.95	0.20	36	6.26	71.17
35	70.81	7.00	111.80	83.09	0.20	36	6.22	70.74
36	70.99	7.00	100.00	90.00	0.35	36	6.22	70.72
37	70.99	7.00	111.78	82.87	0.20	36	6.18	70.51
38	70.99	7.00	110.24	82.82	0.20	36	6.16	70.23
39	70.81	7.00	113.25	82.28	0.20	36	6.15	69.61

40	70.81	7.00	105.66	82.86	0.20	36	6.13	69.59
41	70.81	7.00	103.85	82.92	0.20	36	6.12	69.42
42	70.81	7.00	100.00	83.13	0.20	36	6.09	69.24
43	70.81	7.00	100.00	83.11	0.20	36	6.09	69.21
44	71.02	7.00	100.00	83.01	0.20	36	6.06	69.18
45	71.02	7.00	104.91	82.44	0.20	36	6.05	68.92
46	71.02	7.00	107.57	82.09	0.20	36	6.04	68.69
47	70.81	7.00	100.00	82.65	0.20	36	6.04	68.47

In the present investigation, application of MOPSO results in large number of non-dominated solutions for optimization of objectives. The Pareto-optimal solutions obtained through MOPSO have been ranked by the composite scores obtained through maximum deviation theory (MDT) to choose the best solution. The decision matrix is normalized using the equations 3.11 and 3.12 appropriately. The objective weights are determined for the normalized values of objectives by applying maximum deviation method using equation 3.13-3.20. The weighted objective values are estimated by multiplying the normalized objective values and the objective weights. The best solution is selected depending upon the composite scores obtained by addition of the all the weighted objective function values for each alternative. The objectives with highest composite score are chosen as the best solution. Table 4.11 shows the best ranked solution for all combination of responses obtained through maximum deviation theory.

Table 4.11 Best ranked solution for multiple objectives

Multiple objectives	A (Volt)	B (Amp)	C (µs)	D (%)	E (Bar)	F (Hrs.)	Objective		Normalized objectives		Weighted Normalized		Composite Score
MRR and EWR	70.81	7	136.6	85.3	0.2	36	6.61	76.75	0.8232	0.3153	0.4282	0.1513	0.5795
MRR and Surface roughness	72.13	5.2	179.8	86.7	0.3	36	5.88	7.75	0.7776	0.3767	0.4069	0.1796	0.5865
MRR and Radial overcut	70.03	5.2	108.5	85.0	0.3	36	5.45	0.03	0.7599	0.4107	0.3997	0.1947	0.5944
MRRand White layer thickness	72.76	7	125.3	86.6	0.4	36	6.44	19.29	0.9453	0.4188	0.5799	0.1619	0.7418
EWR and Surface roughness	70.17	3	100	80	0.2	36	44.25	7.38	1	0	0.5047	0	0.5047
EWR and Radial overcut	89.53	7	100	82.4	0.2	36	65.76	0.06	0.2589	0.7456	0.1294	0.3728	0.5022
EWR and white Layer thickness	70.19	3	100	80	0.2	36	44.26	12.21	0.1798	0.1374	0.3459	0.2864	0.6323
Surface roughness and Radial overcut	85.92	3	161.5	84.39	0.26	36	6.77	0.023	0.688	0.385	0.3437	0.1927	0.5364
Surface roughness and white layer thickness	75.31	3	100	80	0.2	36	7.09	12.39	0.7199	0.3582	0.3561	0.181	0.5371
White layer thickness and Radial overcut	70.03	3	100	80	0.2	36	12.22	0.002	0.5268	0.4820	0.2634	0.2407	0.5042

4.6 Conclusions

In this work, a hybrid approach of responses surface methodology (RSM) combined with a novel multi-objective particle swarm optimization algorithm (MOPSO) has been proposed for the optimization of various machining parameters in electrical discharge machining using cryo-treated brass tool. It shows that brass can be used as a potential electrode material for EDM after deep cryogenic treatment with longer soaking duration. In the second phase, maximum deviation theory (MDT) of objective weights determination is used to estimate the weights for the attributes. The composite score for all the non-dominated solutions is obtained through summing the weighted objective values. The best solution is selected from all the non-dominated solution considering the highest composite score to avoid subjectiveness and impreciseness in the decision making. Some of the major findings of the research work are discussed in the paragraph below.

It is observed that soaking duration, discharge current, pulse-on-time and duty factor exhibit significant influence on the performance measures. The thermal conductivity and micro-hardness of brass electrode improves with increase in soaking duration (Table 4.3). The treated tools help in effective heat transfer away from the electrode increasing the wearing resistance of the tool. From analysis of variance for MRR, it is observed that discharge current is found to be the most influential parameter with a percentage contribution of 58.48% followed by pulse-on-time, open circuit voltage and duty factor with percentage contribution of 5.85%, 5.62% and 4% respectively. From analysis of variance for EWR it is observed that soaking duration is found to be the most influential parameter with percentage contribution of 78.35% followed by discharge current, pulse-on-time, duty factor and open circuit voltage with percentage contribution of 10.66%, 2.13%, 1.04% and 0.64% respectively. From analysis of variance for surface roughness, it is observed that soaking duration is found to be the most influential parameter with percentage contribution of 58.99% followed by discharge current, pulse-on-time and duty factor with percentage contribution of 18.60%, 9.62% and 0.39% respectively. From analysis of variance for radial overcut, it is observed that soaking duration is found to be the most influential parameter with percentage contribution of 79.01% followed by discharge current, pulse-on-time and duty factor with percentage contribution of 8.88%, 2.83% and 1.18% respectively. From analysis of variance for white layer thickness, it is observed that soaking duration is found to be the most influential parameter with percentage contribution of 95.55% followed by discharge current, pulse-on-time and duty factor with percentage contribution of 2.87%, 0.22% and 0.04% respectively. The study confirms that significant reduction in EWR, surface roughness, radial overcut and white layer thickness can be achieved if the tools are subjected to longer soaking

duration (treated up to 36 hrs.). It is observed that EWR, surface roughness, radial overcut and white layer thickness can be reduced upto 48.29%, 31.72%, 88.33% and 58.45% respectively due to longer treatment of soaking duration when experiment numbers 35 (untreated brass tool) and 39 (cryo-treated brass tool for soaking duration of 36 hrs.) shown in (Table 4.4) were compared. This indicates that soaking duration is an important parameter to improve performance measures in EDM. Scanning electron microscope (SEM) micrograph (Figures 4.6 a-b-c) show that electrodes treated with longer soaking duration can maintain good surface integrity of the machined surface and retain initial shape of the tool. The improvement in thermal properties of brass electrode allows easy dissipation of heat from tool material. As a result, better retention in tool shape, uniform sparking and superior quality of the machined surface is achieved. The flushing efficiency of the machined surface improves owing to improved machined surface quality which in turn reduces the deposition of molten material on the machined surface and decreases the white layer thickness. Cryogenic treatment soaking duration hardly influence MRR. It was expected that deep cryogenic treatment of the brass electrode will result in higher MRR. But, the high micro-hardness and low thermal conductivity of Inconel 718 work material does not allow higher volume of material to be eroded from the work surface. With improved thermal conductivity and micro-hardness, brass can be used as potential electrode material to produce precise and accurate EDMed components, particularly in finishing operation.

CHAPTER 5

PERFORMANCE ANALYSIS OF THE EDM PROCESS THROUGH POWDER MIXED DIELECTRIC AND CRYOGENICALLY TREATED ELECTRODES

5.1 Introduction

In the previous chapter, it is observed that brass can be used as a potential tool material after deep cryogenic treatment with longer soaking duration. Moreover, it was expected that deep cryogenic treatment to brass tool will enhance material removal from machined surface. But the high micro-hardness and poor thermal conductivity of Inconel 718 does not allow higher volume of material to be eroded from machined surface. However, few studies have reported that deep cryogenic treatment to work piece can enhance material removal from machined surface (Gill and Singh 2010).Hence, in this chapter, an attempt has been made to analyze the machining efficiency of the process through deep cryogenic of both the electrodes.

The material removal, surface quality and dimensional accuracy of the machined surface on the work material are related to the amount of spark energy used to erode material during machining. Increase in spark energy improves the material removal but creates numerous adverse effect such as increasing cracks, pores, heat affected jones (HAZ) and inducing residual stresses on the machined surface (Das et al. 2003; Kumar et al. 2009). Owing to the complex nature of the process involving the physics of series of spark discharges, it is difficult to observe the process experimentally and find suitable parametric setting to improve the machining efficiency. Thus, low machining efficiency, poor surface finish and dimensional accuracy of the machined surface are the major concerns for tool engineers working on EDM. To overcome these difficulties, machining in the presence of suspended powders known as powder mixed EDM (PMEDM) is attempted (Padhee et al. 2012). The presence of electrically conductive powders increases the spark gap between the electrodes and decreases the insulating strength of the dielectric fluid during machining (Padhee et al.2012; Wong et al.1998; Ming and He 1995; Chow et al.2000). Therefore, the process becomes more stable and results in improved material removal and surface quality on the machined surface.

It has been already discussed in the previous chapter that deep cryogenic treatment brings some remarkable improvements in the mechanical properties like increasing the wear resistance, thermal conductivity, hardness and refining the microstructure of the materials (Jaswin and Lal 2010). In recent times, cryogenic treatment has been successfully applied to non-convention machining processes resulting in fruitful application in EDM and wire EDM through treatment of electrodes and wires which are used for machining of toughened and low conductive materials (Kumar et al.2012; Jafferson and Hariharan2012; Kapoor et al. 2012). This results in effective heat transfer away from the electrodes and in turn improves

the wear resistance property and improved machining characteristics of the EDM process. As far as, PMEDM is concerned, a good amount of work is reported in the literature to use suspended powders in the dielectric medium for enhancing the machining efficiency (Peças and Henriques 2008; Kansal et al. 2005;Kansal et al. 2007a; Patel et al. 2009). However, reports to analyze the machining efficiency of the process by the hybrid approach of both type of modifications have been scarce in the literature.

In view of this, present work has been undertaken to compare the machining efficiency of different cryo-treated (-196^0 C) work-tool pair (Inconel 718 super alloy and brass electrode) in the presence of suspended fine graphite powder particles with an objective to enhance the machining efficiency and fulfill minimum surface damage. Hence, commercially available Inconel 718 and brass are used as the work piece and tool material respectively owing to their poor thermal and electrical conductivities. The objective is to make both the materials suitable for industrial application by enhancing their mechanical properties and analyzing the machining efficiency of different work-tool pair through cryogenic treatment. The machining efficiency of the process has been evaluated in terms of material removal rate (MRR), electrode wear ratio (EWR), surface roughness, radial overcut and white layer thickness which are function of process parameters viz. open circuit voltage, discharge current, pulse-on-time, duty factor, concentration of fine graphite powder and cryogenically treated work-tool pair. Regression analysis is carried out to relate the performance measures with process variable. A multi-objective particle swarm optimization algorithm (MOPSO) is used to obtain the optimal Pareto front and compared with popular multi-objective optimization algorithm, NSGA II. Finally, non-dominated solutions obtained through MOPSO algorithm is further ranked by applying maximum deviation theory (MDT).

5.2 Powder-mixed EDM

In PMEDM process, a suitable fine powdered particle is mixed into the dielectric fluid either in the same tank or in a different tank. A stirring device is employed inside the machining tank for better movement of the powder particles inside the dielectric fluid. For proper circulation of fine powdered particles inside the machining tank a small circulation pump of capacity 0.25 hp is employed. The suction head distance from the outlet of the tank to the pump usually kept short so as to ensure proper suction of dielectric and powdered particles into the spark gap. In order to separate the debris from the dielectric fluid, two permanent magnets are positioned at the bottom of machining tank. The presence of conductive powder particles promotes the breakdown of dielectric within the spark gap and

increases the spark gap between electrodes. The conductive powder particles come close to each other and organize themselves to form the shape of a chain under the sparking area. The powder particles interlocked within themselves in the direction of flow of current. The interlocking forms a chain and works as a bridge in between electrodes. This phenomenon declines the insulating strength of the dielectric fluid. Early explosion in the gap occurs due to easy short circuit between electrodes. This allows faster sparking discharges and increase in material removal rate due to rapid erosion of work material. Simultaneously, the suspended powder particles modify the plasma channel to become widen (Kansal et al. 2007b). The powder particles uniformly distribute the spark discharges and reduce the spark density on the machining spot. As a result, tiny particles are eroded from the machined surface and thus the machined surface quality is improved.

5.2.1Experiment set up

Experiments are carried out in a die sinking EDM machine (ELECTRONICA-ELECTRAPULS PS 50ZNC) with servo-head (constant gap). The specification of machine is provided in Table 5.1. Positive polarity for electrode and side flushing was used to conduct the experiments.

Table 5.1 Specification of the EDM machine ELECTRONICA- ELECTRAPLUSPS 50ZNC

Mechanism of process	Controlled erosion (melting and evaporation) through a series of electric spark
Spark gap	0.010- 0.500 mm
Spark frequency	200 – 500 kHz
Working Current	1-70A
Working voltage across the gap	30- 250 V
Maximum Flushing Pressure	0.5 Pa
Metal removal rate (max.)	5000 mm^3/min
Specific power consumption	2-10 W/mm^3/min
Dielectric fluid	EDM oil, Kerosene, liquid paraffin.
Dielectric tank Capacity	
Travel limit X-axis	400mm
Y-axis	400mm
Z-axis	400mm

The conventional EDM machining tank is replaced with a fabricated tin tank of 300×300×300 mm^3 dimension. A circulation pump (TULLU green 50) of capacity 0.25 hp is employed to the same tank where machining is performed. A stirring device is employed

inside the tank so as to avoid particle settling inside the tank during machining. The outlet of the machining tank is connected to the suction head of the pump and the inlet of the tank is connected to the flushing nozzles through delivery head. The outlet and inlet of the tank is provided with two pressure gauges and control valves so as to control flow of dielectric into the machining tank. The control valve helps in maintaining a constant height of liquid inside the tank. Two permanent magnets are placed inside the tank to separate the debris from the dielectric fluid. The front elevation of the fabricated tank along with the pump, stirring devices and other accessories has been shown in Figure 5.1 (a-b). Figure (a) shows the front elevation and Figure (b) shows the top view of the machining tank along with the accessories.

(a) PMEDM experimental set up (Front view)

(b) PMEDM experimental set up (Top view)

Figure 5.1 (a-b) PMEDM experimental set up

Graphite powder is suspended into the commercial available kerosene oil (specific gravity 0.817). The size of the powder particle is from 10 to 20µm. Each experimental run is conducted for 20 minutes and weight of the work and tool materials were recorded. Positive polarity for electrode and side flushing is used to conduct the experiments.

5.3 Experimental strategy and materials

The details of the work material and its properties have been already discussed in section 3.4. Commercially available Inconel 718 and brass were considered as the work piece and tool material respectively owing to their poor thermal and electrical conductivities. Three brass rods are brought in form of 20 mm diameter and 70 mm length. For suitable machining, the machining diameter is reduced to 13.5mm. Inconel 718 were brought in form of plate thickness of 5mm and area (100×100) mm^2 and are reduced to number of small pieces for suitable machining. In this work, both work piece and tool materials were cryogenically treated at low temperature to enhance the mechanical properties of materials. The work piece and electrode materials were cryogenically treated to the temperature of -196^{0}C at the rate of 1^{0}C/min. At this temperature, the material is held constant for 36-hrs (as better result is achieved at longer soaking duration) before the material is slowly brought back to the room temperature at rate of 1^{0}C/min. After reaching the room temperature, the

work material is subjected to two stages of tempering cycles for relieving the stresses induced during cryogenic treatment. Tampering operation is executed by increasing the temperature up to $+196^0$C at the rate of 1^0/min and then slowly bringing back to the room temperature. Tampering is only essential for nickel based alloys, not for copper and its alloys. The details of the cryogenic treatment and its accessories have been already discussed in chapter 4.4.1. For machining purpose, representation is made as: deep cryo-treated work piece and tool material are written as treated work piece (TW) and treated tool (TT) respectively. Similarly, non- treated work piece and tool material are written as non-treated work piece (NW) and non-treated tool (NT) respectively. The details of the experimental strategy have been discussed in the previous chapter 3.5. For suitable machining the parameters are coded using equation 3.22.

5.3.1 Scanning electron microscopic analysis and X-ray diffraction analysis

A scanning electron microscope (SEM) and X-ray diffraction (XRD) study were carried out to distinguish the likely changes brought into the electrodes by the deep cryogenic treatment. The micrographs were analyzed in a high resolution analytical SEM (Model - JEOL JSM-6084LV) at 500X magnification. The micrographs with identical magnifications for each treated and untreated electrodes are shown in Figures 5.2 (a-b) and 5.3 (a-b). From the micrographs 5.2 (a-b), it can be clearly visualized that the micro structure is more refined and densed due to smaller particles size owing to deep cryogenic treatment when compared to untreated brass sample. Similarly, from Figures 5.3 (a-b), it can be observed that the micro structure is more refined and denser due to smaller particle sizes in comparison with untreated Inconel 718 sample. The figure also shows that micro holes in the micro-structure are filled with few carbide fillers owing to deep cryogenic treatment.

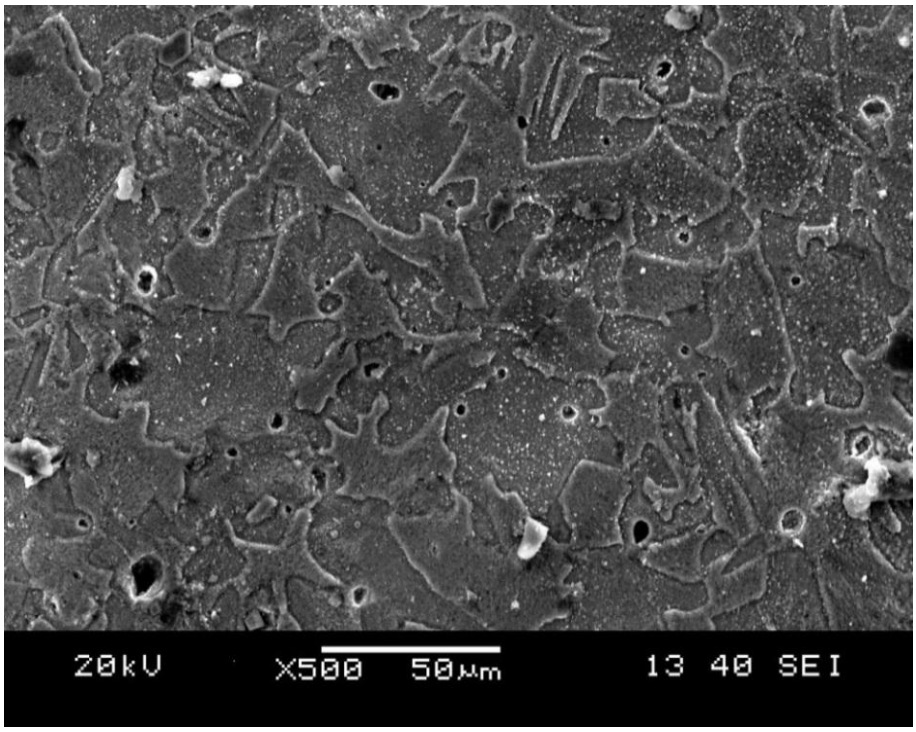

(a) Untreated brass

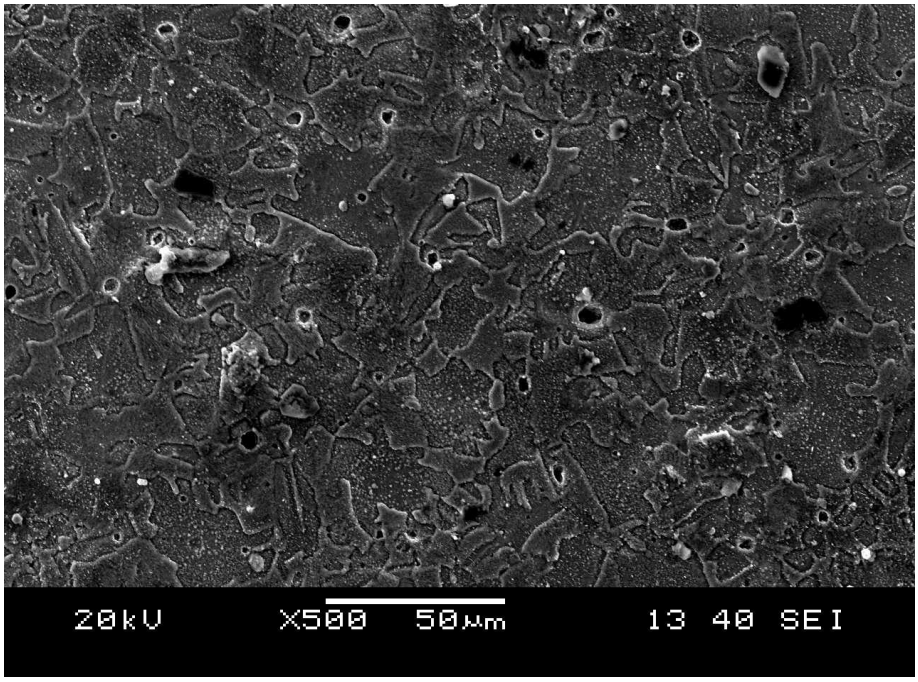

(b) Cryogenic treated brass

Figure 5. 2 (a and b) Microstructure of brass electrodes samples used in the present study

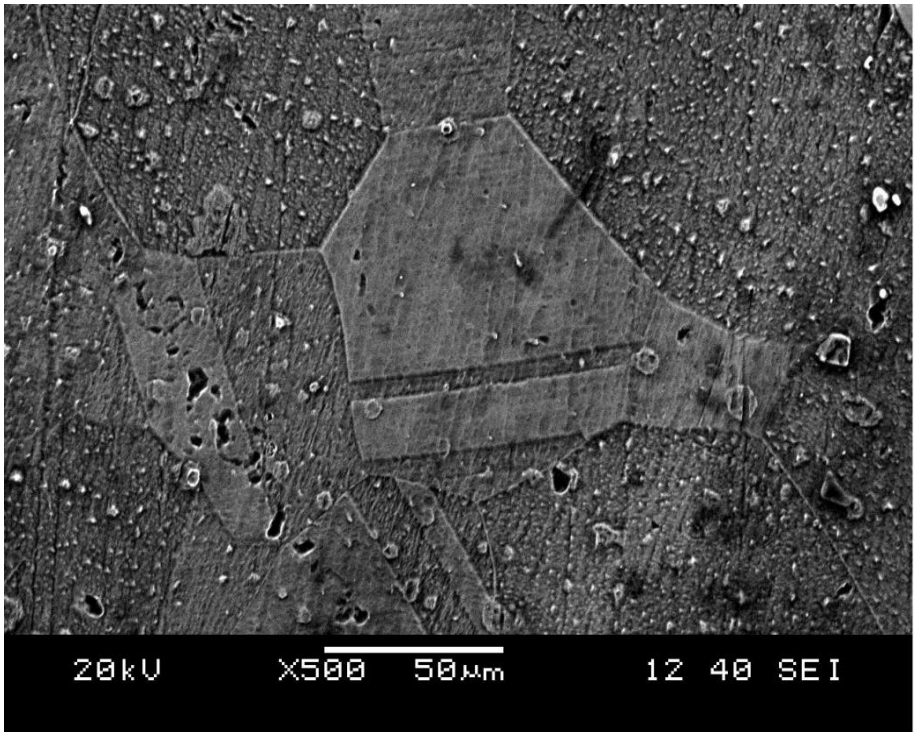

(a)Untreated Inconel 718

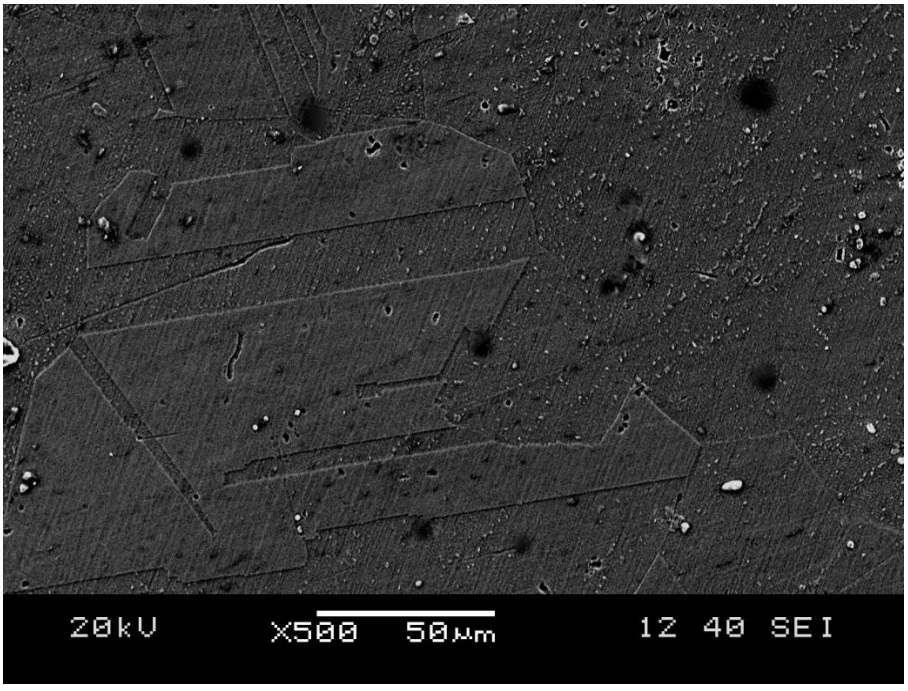

(b) Cryogenic treated Inconel 718

Figure 5.3 (a and b) Microstructure of work piece Inconel 718 samples used in the present study

These scanning electron microscope (SEM) images are further supported by the XRD analysis. The XRD analysis for the treated and untreated brass and Inconel 718 samples are carried out on an X-ray diffractometer (model no-X-Pert PRO, PANalytical, PW 3040/00, Netherland). The average grain size is calculated using the Debye Scherrer's relation(equation 4.1). The calculated values of the average grain size are provided in the Table 5.2.

The XRD analysis report reveals that the average grain size is reduced upto 23.44% and 6.06% for treated brass and Inconel 718 samples respectivelydue to deep cryogenic treatment. Table 5.2 shows the properties of the tool and work piece before and after cryogenic treatment.Table 5.3 shows the levels of the process parameters.

Table 5.2Properties of the tool and work piece before and after cryogenic treatment

Property	Untreated Brass	Cryogenic treated Brass	Untreated Inconel 718	Cryogenic treated Inconel 718
Thermal Conductivity (W/m.K)	108	122	6.7	10.3
Micro Hardness (VHN)	212	276	382	385
Average grain size (nm)	65.72	50.31	125.54	117.92

Table 5.3 Process parameters and their levels

Process Parameters	Symbols	Levels		
		-1	0	1
Open circuit voltage in V	A	70	80	90
Discharge current in A	B	3	5	7
Pulse-on-time in µs	C	100	200	300
Duty factor in %	D	80	85	90
Concentration of graphite powder in gm./lit	E	0	2	4
Work-Tool pair	F	NW-TT	TW-NT	TW-TT

5.3.2 Calculation of performance measures

The details of the calculation of the performance measures have been already discussed in the previous chapter in section 3.5.1. Table 5.4 shows the Box-Behnken experimental design along with obtained performance measures. Figure 5.4 shows the three combinations of work-tool pair after machining.

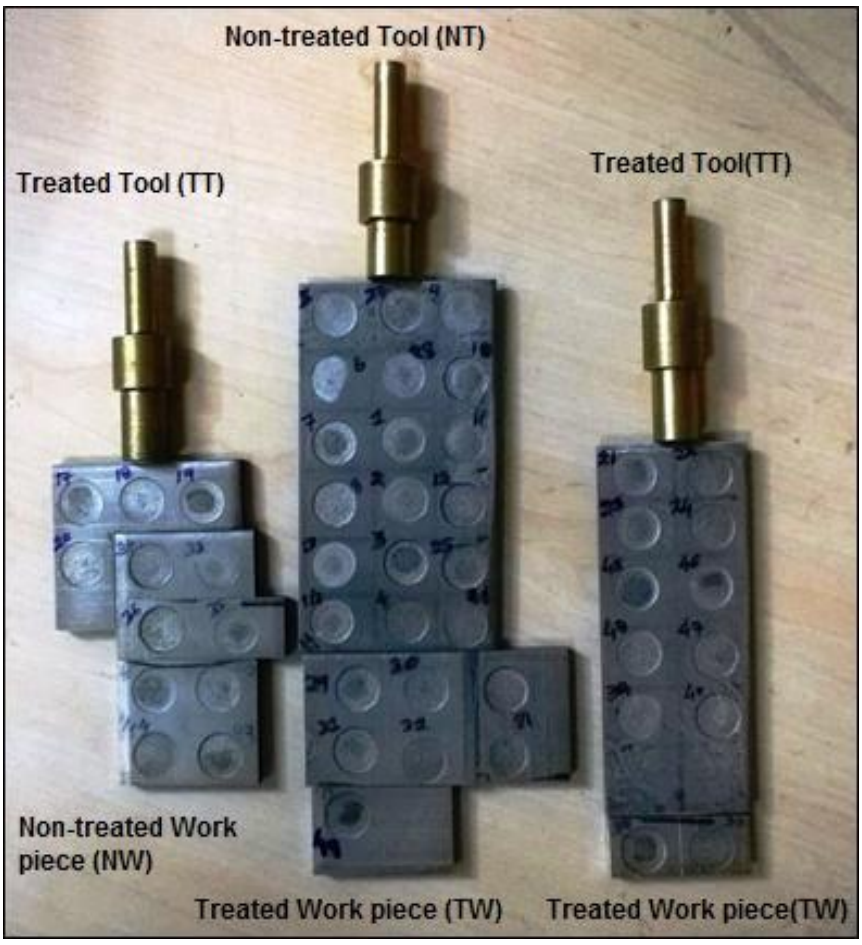

Figure 5.4 Three combinations of work-tool pair after machining

Table 5.4 Box-behnken experimental design along with obtained performance measures

Run order	A	B	C	D	E	F	MRR mm^3/min	EWR %	Surface Roughness µm	Radial overcut mm	White Layer Thickness µm
1	-1	-1	0	-1	0	0	3.44	80.12	6.40	0.17	31.50
2	1	-1	0	-1	0	0	1.80	87.58	6.43	0.14	31.60
3	-1	1	0	-1	0	0	6.59	106.77	8.50	0.36	35.90
4	1	1	0	-1	0	0	4.89	109.05	8.70	0.33	35.80
5	-1	-1	0	1	0	0	2.85	84.74	6.80	0.18	31.60
6	1	-1	0	1	0	0	1.70	90.43	6.62	0.17	31.70
7	-1	1	0	1	0	0	7.10	106.13	8.80	0.35	35.40
8	1	1	0	1	0	0	5.10	113.21	9.10	0.33	34.90
9	0	-1	-1	0	-1	0	1.50	97.56	5.90	0.14	32.40
10	0	1	-1	0	-1	0	5.04	122.02	8.60	0.33	35.80
11	0	-1	1	0	-1	0	1.70	101.32	7.50	0.24	33.70
12	0	1	1	0	-1	0	4.40	126.56	10.35	0.42	36.70
13	0	-1	-1	0	1	0	2.27	82.02	5.70	0.13	30.80
14	0	1	-1	0	1	0	6.80	97.78	8.30	0.32	34.10
15	0	-1	1	0	1	0	1.75	89.78	6.72	0.15	32.10
16	0	1	1	0	1	0	6.35	96.05	8.80	0.34	34.80
17	0	0	-1	-1	0	-1	3.62	109.99	8.20	0.38	38.84
18	0	0	1	-1	0	-1	2.54	116.01	9.80	0.46	39.84
19	0	0	-1	1	0	-1	3.85	118.98	8.50	0.41	39.26
20	0	0	1	1	0	-1	2.85	122.78	10.40	0.47	39.64
21	0	0	-1	-1	0	1	3.80	78.91	5.70	0.07	23.12
22	0	0	1	-1	0	1	3.40	84.04	6.80	0.11	24.23
23	0	0	-1	1	0	1	3.90	80.06	5.80	0.07	24.12
24	0	0	1	1	0	1	4.90	81.04	6.70	0.13	25.42
25	-1	0	0	-1	-1	0	4.10	113.87	9.10	0.24	34.10
26	1	0	0	-1	-1	0	2.99	117.56	9.20	0.20	34.20
27	-1	0	0	1	-1	0	4.30	110.12	9.40	0.25	34.10
28	1	0	0	1	-1	0	3.15	119.42	9.35	0.24	34.20
29	-1	0	0	-1	1	0	4.75	96.45	6.50	0.16	32.50
30	1	0	0	-1	1	0	2.81	101.24	6.45	0.11	32.45
31	-1	0	0	1	1	0	4.95	101.34	6.61	0.14	32.50
32	1	0	0	1	1	0	2.95	105.36	6.71	0.11	32.50
33	0	-1	0	0	-1	-1	2.20	110.95	8.90	0.39	38.34
34	0	1	0	0	-1	-1	5.56	132.53	13.20	0.63	40.44
35	0	-1	0	0	1	-1	2.40	98.97	6.71	0.25	36.62
36	0	1	0	0	1	-1	6.18	122.95	10.81	0.54	38.32
37	0	-1	0	0	-1	1	2.50	79.15	6.30	0.10	23.09
38	0	1	0	0	-1	1	5.99	90.41	9.50	0.25	27.32

39	0	-1	0	0	1	1	2.75	69.08	3.81	0.04	23.44
40	0	1	0	0	1	1	7.10	79.23	7.20	0.20	28.14
41	-1	0	-1	0	0	-1	3.90	94.95	9.10	0.42	39.74
42	1	0	-1	0	0	-1	2.80	102.05	8.90	0.34	39.79
43	-1	0	1	0	0	-1	2.99	102.56	10.60	0.38	38.78
44	1	0	1	0	0	-1	2.50	107.65	10.50	0.36	38.75
45	-1	0	-1	0	0	1	4.80	77.15	5.60	0.11	22.12
46	1	0	-1	0	0	1	4.10	84.01	5.55	0.06	22.42
47	-1	0	1	0	0	1	3.40	82.99	6.80	0.16	23.52
48	1	0	1	0	0	1	2.90	89.12	6.59	0.13	23.62
49	0	0	0	0	0	0	3.90	104.41	6.72	0.24	34.90
50	0	0	0	0	0	0	3.75	100.05	6.35	0.19	33.72
51	0	0	0	0	0	0	4.30	106.76	7.10	0.25	35.20
52	0	0	0	0	0	0	3.60	101.16	6.20	0.19	32.00
53	0	0	0	0	0	0	4.40	108.43	6.70	0.24	35.15
54	0	0	0	0	0	0	3.40	100.51	6.40	0.20	33.85

5.4 Results and discussions

The experimental data collected as per Box-behnken design are analysed to establish the influence of various process parameters on the performance measures using analysis of variance (ANOVA) at significance level of 0.05.Table 5.5 shows the ANOVA for MRR with percentage of contribution of each parameters and their interactions. It shows that open circuit voltage, discharge current, pulse-on-time, powder concentration, work-tool pair, interaction terms discharge current×powder concentration and square terms of discharge current, pulse-on-time are important parameters.The table also shows that discharge current is the most influential parameter for MRR with a percentage contribution of 70.98% followed by open circuit voltage, work-tool pair, powder concentration and pulse-on-time with percentage contribution of 8.68%, 3.03%, 2.11% and 1.17% respectively.It is also observed that comparatively higher percentage of variation is explained by treatment of work piece-tool combination than suspended powder particles on MRR.Duty factor is found to be an insignificant parameter for MRR.The coefficient of determination (R^2) and adjusted (R^2) values are found to be 95.15% and 91.51% respectively. It is to be noted that the lack of fit is not significant for MRR.

Table 5.5 ANOVA for MRR

Source	Sum of Squares	Degree of freedom	Mean Square	F Value	p-value Prob> F		% Contribution
Model	107.64	23	4.68	19.39	< 0.0001	significant	
A-Voltage	9.98	1	9.98	41.38	< 0.0001		8.69
B-Discharge current	81.55	1	81.55	337.94	< 0.0001		70.99
C-Pulse-on-time	1.35	1	1.35	5.61	0.0245		1.18
D-Duty Factor	0.62	1	0.62	2.59	0.1183		0.54
E-Powder concentration	2.43	1	2.43	10.05	0.0035		2.12
F-Work-Tool pair	3.49	1	3.49	14.46	0.0007		3.04
A×B	0.1	1	0.1	0.43	0.5175		0.09
A×C	0.082	1	0.082	0.34	0.5643		0.07
A×E	0.35	1	0.35	1.46	0.2361		0.30
B×C	0.074	1	0.074	0.31	0.5836		0.06
B×D	0.25	1	0.25	1.03	0.3183		0.22
B×E	1.09	1	1.09	4.5	0.0422		0.95
B×F	0.061	1	0.061	0.25	0.6181		0.05
C×D	0.77	1	0.77	3.19	0.0844		0.67
C×F	0.33	1	0.33	1.36	0.253		0.29
D×F	0.53	1	0.53	2.2	0.1486		0.46
E×F	0.036	1	0.036	0.15	0.7003		0.03
A^2	0.36	1	0.36	1.49	0.2325		0.31
B^2	1.31	1	1.31	5.42	0.0268		1.14
C^2	2.04	1	2.04	8.44	0.0068		1.78
D^2	0.15	1	0.15	0.64	0.4317		0.13
E^2	0.061	1	0.061	0.25	0.6185		0.05
F^2	0.28	1	0.28	1.14	0.2936		0.24
Residual	7.24	30	0.24				6.30
Lack of Fit	6.47	25	0.26	1.68	0.2974	not significant	
Pure Error	0.77	5	0.15				
Cor Total	114.88	53					

Table 5.6 shows the ANOVA for EWR with percentage of contribution of each parameter and their interactions. It shows that open circuit voltage, discharge current, pulse-on-time, powder concentration, work-tool pair and square terms of open circuit voltage, discharge current, powder concentration, work-tool pair are important process parameters. The Table also shows that work-tool pair is the most influential parameter for EWR with a percentage contribution of 47.84% followed by discharge current, powder concentration open circuit voltage and pulse-on-time with percentage contribution of 19.17%, 11.78%, 1.73%, 1.06% respectively. When machining is done in the presence of suspended powder particles with

cryogenically treated electrodes, the influence of cryogenic treatment of work-tool pair is much higher on EWR than the suspended powder particles. Duty factor is found to be an insignificant parameter for EWR. The coefficient of determination (R^2) and adjusted (R^2) values are found to be 93.61% and 90.59% respectively. It is to be noted that the lack of fit is not significant for EWR.

Table 5.6 ANOVA for EWR

Source	Sum of Squares	Degree of freedom	Mean Square	F Value	p-value Prob> F		% Contribution
Model	10871.76	17	639.52	31.01	< 0.0001	significant	
A-Voltage	201.2	1	201.2	9.76	0.0035		1.73
B-Discharge current	2223.18	1	2223.18	107.81	< 0.0001		19.14
C-Pulse-on-time	123.4	1	123.4	5.98	0.0195		1.06
D-Duty Factor	42.72	1	42.72	2.07	0.1587		0.37
E-Powder concentration	1368.36	1	1368.36	66.36	< 0.0001		11.78
F-Work-Tool pair	5556.52	1	5556.52	269.45	< 0.0001		47.84
B×C	9.48	1	9.48	0.46	0.502		0.08
B×E	43.49	1	43.49	2.11	0.1551		0.37
B×F	72.9	1	72.9	3.54	0.0682		0.63
D×E	14.85	1	14.85	0.72	0.4017		0.13
D×F	38.76	1	38.76	1.88	0.1788		0.33
A^2	133.82	1	133.82	6.49	0.0153		1.15
B^2	311.36	1	311.36	15.1	0.0004		2.68
C^2	34.42	1	34.42	1.67	0.2046		0.30
D^2	81.18	1	81.18	3.94	0.0549		0.70
E^2	301.52	1	301.52	14.62	0.0005		2.60
F^2	317.62	1	317.62	15.4	0.0004		2.73
Residual	742.37	36	20.62				6.39
Lack of Fit	680.31	31	21.95	1.77	0.2744	not significant	
Pure Error	62.06	5	12.41				
Cor Total	11614.14	53					

Table 5.7 shows the ANOVA for surface roughness with percentage of contribution of each parameter and their interactions. It shows that discharge current, pulse-on-time, powder concentration, work-tool pair and square terms of open circuit voltage, discharge current, powder concentration, work-tool pair are important process parameters. It is observed that work-tool pair is found to be the most influential parameter for surface roughness with a percentage contribution of 37.97% followed by discharge current, powder concentration and pulse-on-time with percentage contribution of 28.58%, 12.99% and 6.07% respectively. It is to be noted that influence of cryogenic treatment of work-tool pair is higher

on surface quality of the machined surface than the suspended powder particles. Duty factor and open circuit voltage are found to be insignificant parameters for surface roughness. The coefficient of determination (R^2) and adjusted (R^2) values are found to be 94.94% and 92.34% respectively. It is to be noted that the lack of fit is not significant for surface roughness.

Table 5.7 ANOVA for surface roughness

Source	Sum of Squares	Degree of freedom	Mean Square	F Value	p-value Prob> F		% Contribution
Model	160.81	18	8.78	36.48	< 0.0001	significant	
A-Voltage	5.04×10^{-4}	1	5.04×10^{-4}	2.1×10^{-3}	0.9637		0.00
B-Discharge current	48.37	1	48.37	201.05	< 0.0001		28.58
C-Pulse-on-time	10.28	1	10.28	42.75	< 0.0001		6.07
D-Duty Factor	0.38	1	0.38	1.57	0.2186		0.22
E-Powder concentration	22	1	22	91.46	< 0.0001		13.00
F-Work-Tool pair	64.26	1	64.26	267.1	< 0.0001		37.97
A×B	0.053	1	0.053	0.22	0.6423		0.03
B×E	0.048	1	0.048	0.2	0.6565		0.03
B×F	0.41	1	0.41	1.7	0.2005		0.24
C×E	0.42	1	0.42	1.74	0.1957		0.25
C×F	0.35	1	0.35	1.45	0.2371		0.21
D×F	0.1	1	0.1	0.42	0.5207		0.06
A^2	2.26	1	2.26	9.4	0.0042		1.34
B^2	1.41	1	1.41	5.86	0.0208		0.83
C^2	0.29	1	0.29	1.22	0.277		0.17
D^2	0.65	1	0.65	2.7	0.1092		0.38
E^2	3.91	1	3.91	16.24	0.0003		2.31
F^2	5.62	1	5.62	23.34	< 0.0001		3.32
Residual	8.42	35	0.24				4.98
Lack of Fit	7.89	30	0.26	2.46	0.1595	not significant	
Pure Error	0.53	5	0.11				
Cor Total	169.2315	53					

Table 5.8 shows the ANOVA for radial overcut with percentage of contribution of each parameter and their interactions. It shows that open circuit voltage, discharge current, pulse-on-time, powder concentration, work-tool pair, interaction terms discharge current×work-tool pair, pulse-on-time×powder concentration and square termsof open circuit voltage, discharge current, powder concentration, work-tool pair are important process parameters. It is observed that work-tool pair is found to be the most influential parameter for radial overcut with a percentage contribution of 58.70% followed by discharge current, powder

concentration and pulse-on-time with percentage contribution of 23.91%, 3.91% and 1.52% respectively. When machining is done in the presence of suspended powder particles with cryogenically treated electrodes, the influence of cryogenic treatment of work-tool pair is higher on radial overcut than the suspended powder particles. Duty factor is found to be insignificant parameters for surface roughness. The coefficient of determination (R^2) and adjusted (R^2) values are found to be 97.9% and 96.7% respectively. It is to be noted that the lack of fit is not significant for radial overcut.

Table 5.8 ANOVA for radial overcut

Source	Sum of Squares	Degree of freedom	Mean Square	F Value	p-value Prob> F		% Contribution
Model	0.9	19	0.047	84.56	< 0.0001	significant	
A-Voltage	6.83×10^{-3}	1	6.83×10^{-3}	12.18	0.0014		0.74
B-Discharge current	0.22	1	0.22	398.06	< 0.0001		23.91
C-Pulse-on-time	0.014	1	0.014	24.13	< 0.0001		1.52
D-Duty Factor	5.23×10^{-4}	1	5.23×10^{-4}	0.93	0.3412		0.06
E-Powder concentration	0.036	1	0.036	64.79	< 0.0001		3.91
F-Work-Tool pair	0.54	1	0.54	964.22	< 0.0001		58.70
A×C	6.48×10^{-4}	1	6.48×10^{-4}	1.16	0.29		0.07
A×D	3.90×10^{-4}	1	3.9×10^{-4}	0.7	0.4102		0.04
B×D	4.21×10^{-4}	1	4.21×10^{-4}	0.75	0.3927		0.05
B×E	3.15×10^{-4}	1	3.15×10^{-4}	0.56	0.4588		0.03
B×F	6.16×10^{-3}	1	6.16×10^{-3}	10.98	0.0022		0.67
C×E	2.78×10^{-3}	1	2.78×10^{-3}	4.95	0.0329		0.30
C×F	4.73×10^{-4}	1	4.73×10^{-4}	0.84	0.3649		0.05
D×E	4.96×10^{-4}	1	4.96×10^{-4}	0.88	0.3536		0.05
E×F	1.86×10^{-3}	1	1.86×10^{-3}	3.32	0.0774		0.20
A^2	4.02×10^{-3}	1	4.02×10^{-3}	7.17	0.0113		0.44
B^2	0.033	1	0.033	59.05	< 0.0001		3.59
E^2	2.53×10^{-3}	1	2.53×10^{-3}	4.51	0.0411		0.28
F^2	0.024	1	0.024	42.77	< 0.0001		2.61
Residual	0.019	34	5.61×10^{-4}				2.07
Lack of Fit	0.015	29	5.25×10^{-4}	0.68	0.769	not significant	
Pure Error	3.85×10^{-3}	5	7.70×10^{-4}				
Cor Total	0.92	53					

Table 5.9 shows the ANOVA for white layer thickness with percentage of contribution of each parameter and their interactions. It shows that discharge current, pulse-on-time, powder concentration, work-tool pair, interaction terms discharge current×work tool pair, powder concentration×work-tool pair and square terms open circuit voltage, work-tool pair

are important parameters.It is observed that work-tool pair is found to be the most influential parameter for white layer thickness with a percentage contribution of 88.02% followed by discharge current, powder concentration and pulse-on-time with percentage contribution of 4.62%, 0.72% and 0.21% respectively. The table also shows that when machining is done in the presence of suspended powder particles with cryogenically treated electrodes the influence of cryogenic treatment work-tool pair is much higher on white layer thickness than the suspended powder particles.Duty factor and open circuit voltage are found to be an insignificant parameter for white layer thickness. The coefficient of determination (R^2) and adjusted (R^2) values are found to be 98.3% and 97.6% respectively. It is to be noted that the lack of fit is not significant for white layer thickness.

Table 5.9 ANOVA for white layer thickness

Source	Sum of Squares	Degree of freedom	Mean Square	F Value	p-value Prob> F		% Contribution
Model	1471.64	16	91.98	137.03	< 0.0001	significant	
A-Voltage	1.20×10^{-3}	1	1.20×10^{-3}	1.79×10^{-3}	0.9664		0.00
B-Discharge current	69.12	1	69.12	102.98	< 0.0001		4.62
C-Pulse-on-time	3.07	1	3.07	4.58	0.039		0.21
D-Duty Factor	0.066	1	0.066	0.099	0.7553		0.00
E-Powder concentration	10.83	1	10.83	16.13	0.0003		0.72
F-Work-Tool pair	1317.2	1	1317.2	1962.35	< 0.0001		88.02
B×C	0.13	1	0.13	0.19	0.6686		0.01
B×D	0.32	1	0.32	0.48	0.4942		0.02
B×F	3.29	1	3.29	4.9	0.0331		0.22
C×F	1.98	1	1.98	2.95	0.0942		0.13
D×F	0.49	1	0.49	0.72	0.4007		0.03
E×F	3.14	1	3.14	4.67	0.0372		0.21
A^2	5.64	1	5.64	8.4	0.0063		0.38
C^2	0.79	1	0.79	1.18	0.2854		0.05
E^2	0.21	1	0.21	0.32	0.5763		0.01
F^2	47.41	1	47.41	70.63	< 0.0001		3.17
Residual	24.84	37	0.67				1.66
Lack of Fit	17.27	32	0.54	0.36	0.967	not significant	
Pure Error	7.56	5	1.51				
Cor Total	1496.47	53					

The process models for the responses obtained through regression analysis are given below:

MRR= + 3.89 - 0.65 × A + 1.84 × B - 0.28 × C + 0.12 × D + 0.32 × E + 0.34 × F -0.11 × A × B + 0.10 × A × C - 0.21 × A × E - 0.096 × B × C + 0.18 × B × D + 0.26 × B × E + 0.088 × B × F + 0.19 × C × D + 0.081 × C × F + 0.13 × D × F + 0.067 × E × F - 0.13 × A^2 + 0.37 × B^2 - 0.47 × C^2 + 0.053 × D^2 - 0.063 × E^2 + 0.14 × F^2

(Coded form) (5.1)

EWR = + 103.55 + 2.90 × A + 9.62 × B + 2.27 × C + 1.33 × D - 7.55 × E - 15.22 × F - 1.09 × B × C - 1.65 × B × E - 3.02 × B × F + 1.36 × D × E - 2.20 × D × F - 3.61 × A^2-5.50 × B^2 -1.83 × C^2 + 2.81 × D^2 + 5.41 × E^2 - 5.56 × F^2

(Coded form) (5.2)

Surface

roughness = + 6.58 - 4.583 × 10^{-3}×A+1.42×B+0.65×C+0.13×D-0.96×E-1.64×F+0.081×A×B-0.055 × B × E - 0.23 × B × F - 0.23 × C × E - 0.15 × C × F - 0.11 × D × F + 0.47 × A^2 + 0.37 B^2 + 0.17 × C^2 + 0.25 × D^2 + 0.62 × E^2 + 0.74 × F^2

(Coded form) (5.3)

Radial

overcut = + 0.22 - 0.017 × A + 0.096 × B + 0.024 × C + 4.667 × 10^{-3} × D - 0.039 × E - 0.15 × F + 9.000 × A× C + 4.938 × 10^{-3} × A × D - 7.250 × 10^{-3} × B × D + 4.438 × B × E-0.028 × B × F - 0.019 × C × E + 5.437 × 10^{-3} × C× F - 7.875 × 10^{-3}× D × E+0.015 × E × F-0.019 × A^2+0.056 × B^2-0.015 × E^2+0.045 × F^2

(Coded form) (5.4)

White layer

Thickness = + 34.19 + 7.083 × 10^{-3} × A + 1.70 × B + 0.36 × C + 0.052 × D - 0.67 × E-7.41 × F - 0.13 × B × C - 0.20 × B × D + 0.64 × B × F + 0.35 × C × F + 0.25 × D × F + 0.63 × E × F - 0.70 × A^2 - 0.27 × C^2 - 0.14 × E^2-2.11 × F^2

(Coded form) (5.5)

Figure 5.5 (a and b) shows the Scanning Electron Microscope (SEM) micrographs of the machined surface of the work piece at parametric condition at A=80V, B=7A, C=200µs, D=85%, E=0gm/liter, F= NW-TT and at A=80V, B=7A, C=200µs, D=85%, E=4gm/liter, F= NW-TT respectively. From the micrographs, it can be clearly observed that machined surface quality improves as the cracks and voids on the machined surface reduce with increase in powder concentration from 0gm/liter to 4gm/liter.

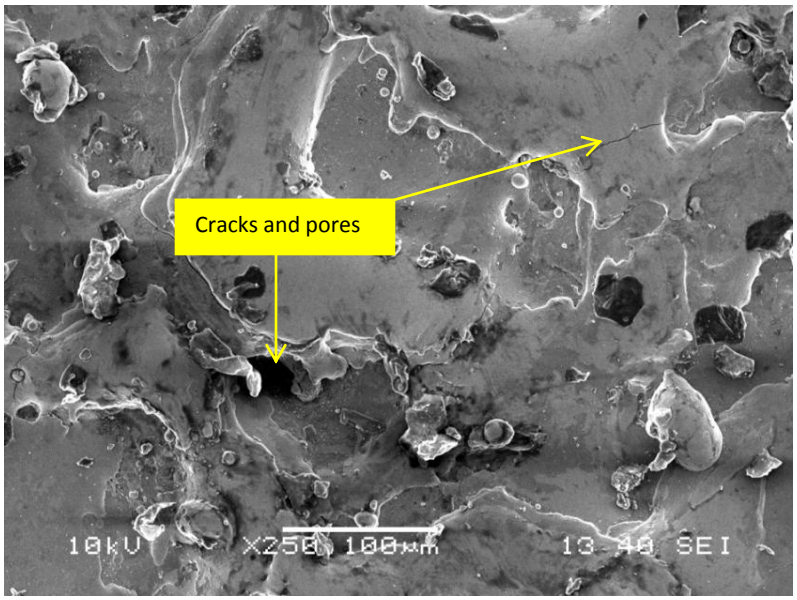

(a) SEM micrograph at A=80V, B=7A, C=200µs, D=85%, E=0gm/liter, F=NW-TT

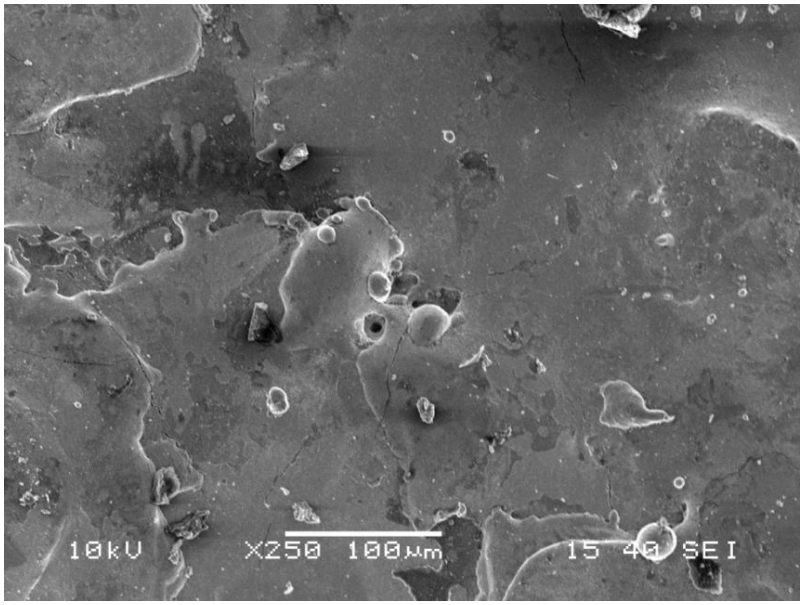

(b) SEM micrograph at A=80V, B=7A, C=200µs, D=85%, E=4gm/liter, F= NW-TT

Figure 5.5 (a and b) SEM images of the machined surface of the work piece

Figure 5.6 (aand b) shows the SEM micrographs of the machined surface of the work piece at parametric condition A=80V, B=5A, C=300µs, D=80%, E=2gm/liter, F=NT-TT and at A=80V, B=5A, C=300µs, D=80%, E=2gm/liter, F= TW-TT. From the micrographs, it can be clearly observed that machined surface quality improves significantly while the work-tool pair is varied from NT-TT toTW-TT. Hence, it can be concluded that the surface qualityproduced,is superior when both the electrodes arecryogenically treated in comparison to that when only tool is treated.

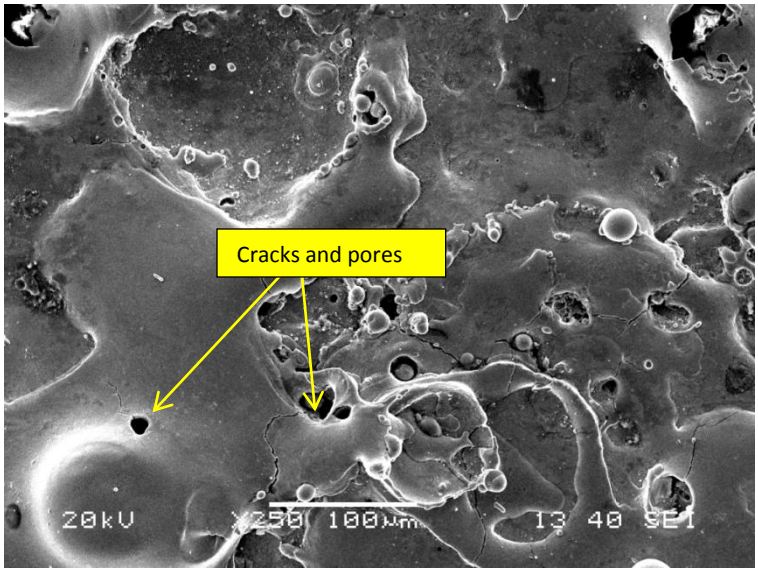

(a) SEM micrograph at A=80V, B=5A, C=300µs, D=80%, E=2gm/liter, F= NW-TT

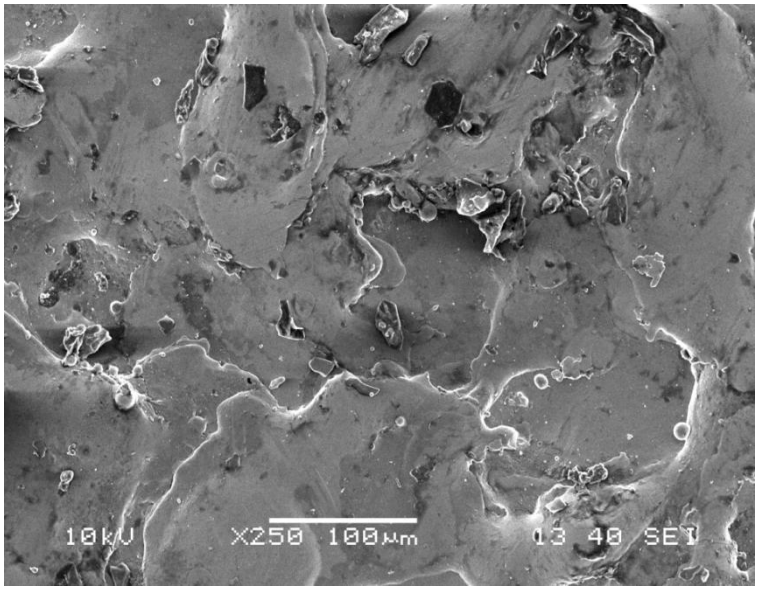

(b) SEM micrograph at A=80V, B=5A, C=300µs, D=80%, E=2gm/liter, F= TW-TT

Figure 5.6 (a and b) SEM images of the machined surface of the work piece

Figure 5.7 (a and b) shows the SEM micrographs of the white layer thickness on the cross section of the work piece at parametric condition at A=80V, B=7A, C=200µs, D=85%, E=0gm/liter, F= NW-TT and at A=80V, B=7A, C=200µs, D=85%, E=4gm/liter, F= NW-TT respectively. From the micrographs it can be clearly observed that white layer thickness decreases with increase with increase in powder concentration from 0gm/liter to 4gm/liter.

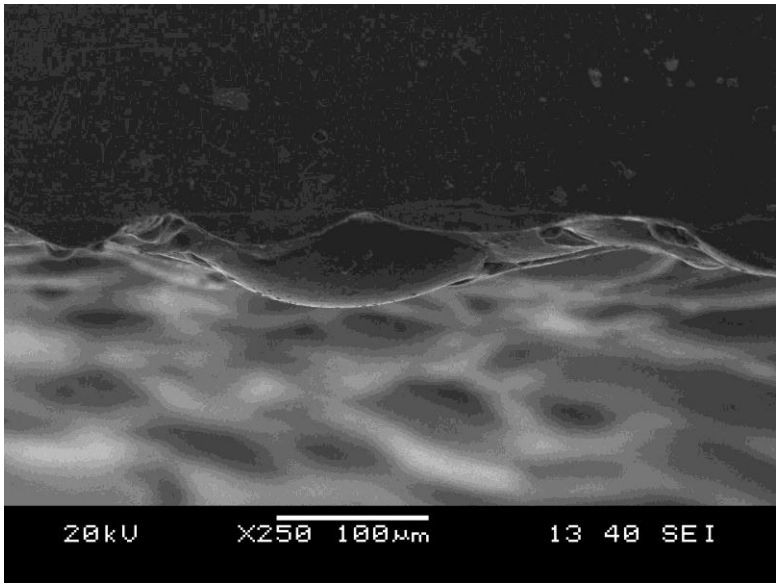

(a) SEM micrograph at A=80V, B=7A, C=200µs, D=85%, E=0gm/liter, F= NW-TT

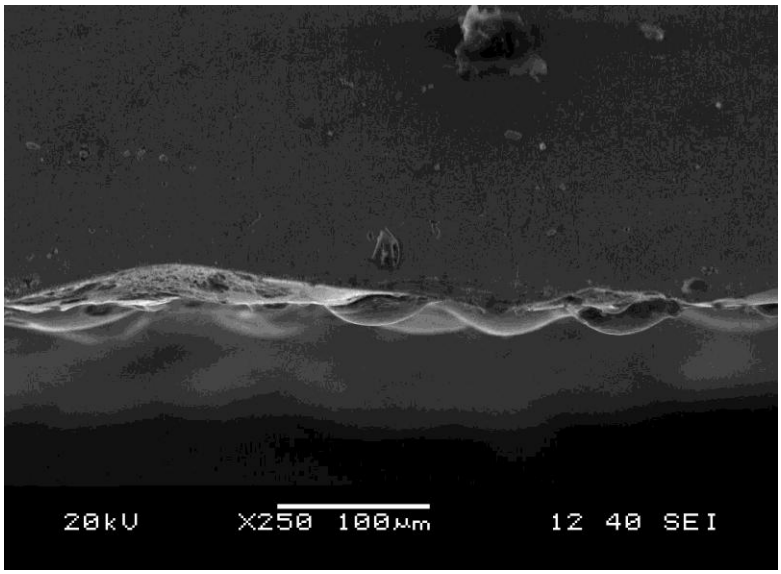

(b) SEM micrograph at A=80V, B=7A, C=200µs, D=85%, E=4gm/liter, F= NW-TT

Figure 5.7 (a and b) SEM micrograph showing whitelayer on the cross section of the machined surface

Figure 5.8 (a and b) shows the SEM micrographs of the white layer thickness on the cross section of the work piece at parametric A=80V, B=5A, C=300µs, D=80%, E=2gm/liter, F= NW-TT and at A=80V, B=5A, C=300µs, D=80%, E=2gm/liter, F=TW-TT. From the micrographs, it can be clearly observed that the white layer thickness on the cross section of the work piece decreases significantly when the work-tool pair is varied from NW-TT to TW-TT. Thus, it can be concluded that the white layer thickness produced, is smaller when both the electrodes are cryogenically treated in comparison to that when only tool is treated.

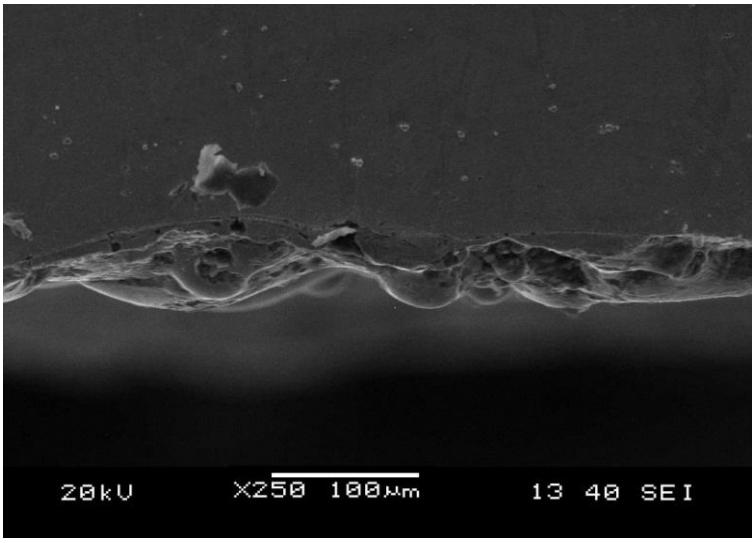

(a) SEM micrograph at A=80V, B=5A, C=300µs, D=80%, E=2gm/liter, F= NW-TT

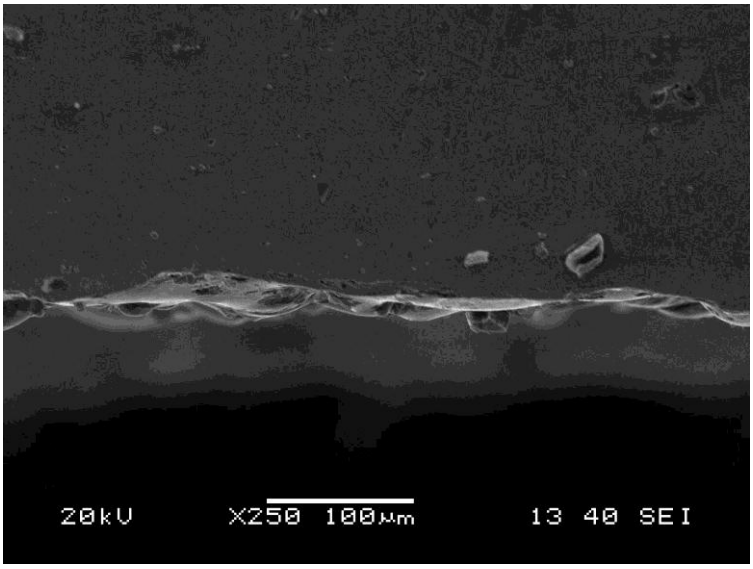

(b) SEM micrograph at A=80V, B=5A, C=300µs, D=80%, E=2gm/liter, F= TW-TT

Figure 5.8 (a and b) SEM micrograph showing white layer on the cross section of the machined surface

In EDM, material removal rate (MRR) is the most important performance measure. For cost effective machining, maximization of MRR is vital. Figure 5.9 shows the variation of MRR with discharge current and open circuit voltage. It shows that MRR increase monotonically with increase in discharge current. Increase in discharge current significantly improves the spark energy. As a result, higher volume of material is eroded from the machined surface and in turn, it influences increase in MRR. The figure also shows that MRR decreases with increase in open circuit voltage for all value of discharge current. This phenomenon matches the studies reported by previous researchers Pradhan and Biswas (2010) and Lee and Li (2001).

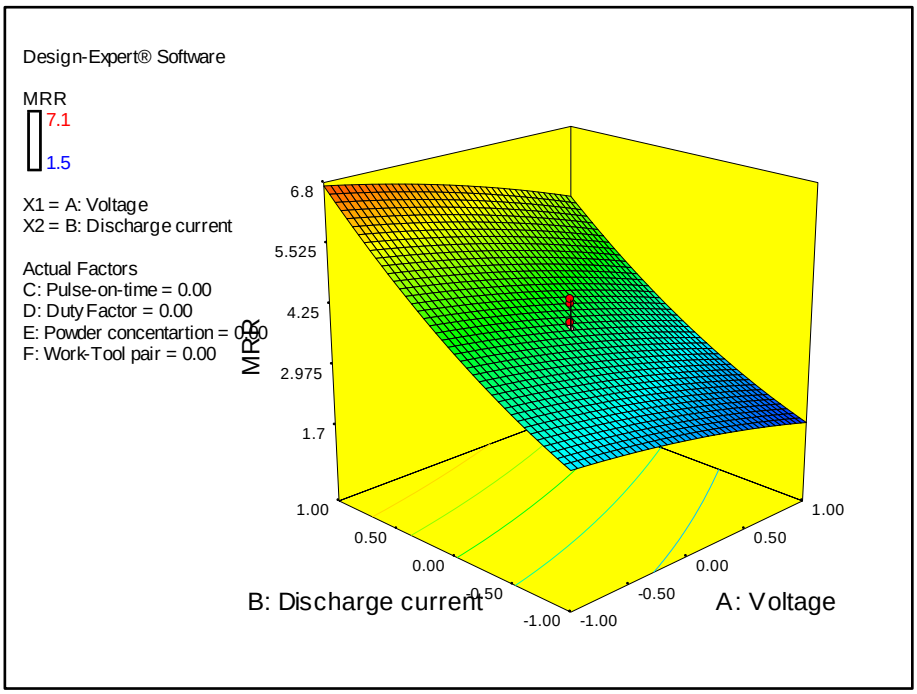

Figure 5.9 Surface plot of MRR with discharge current and open circuit voltage

Figure 5.10 shows the variation of MRR with discharge current and pulse-on-time. It shows that MRR increases with increase in pulse-on-time initially but shows a decreasing beyond a pulse-on-time of 200µsfor all value of discharge current. Increasing the pulse-on-time increases the spark energy and in turn influences increase in MRR. But continuous application of same heat flux decreases the pressure inside the plasma channel. Since the molten metal volume remains constant, further increase in pulse-on-time causes reduction in MRR.

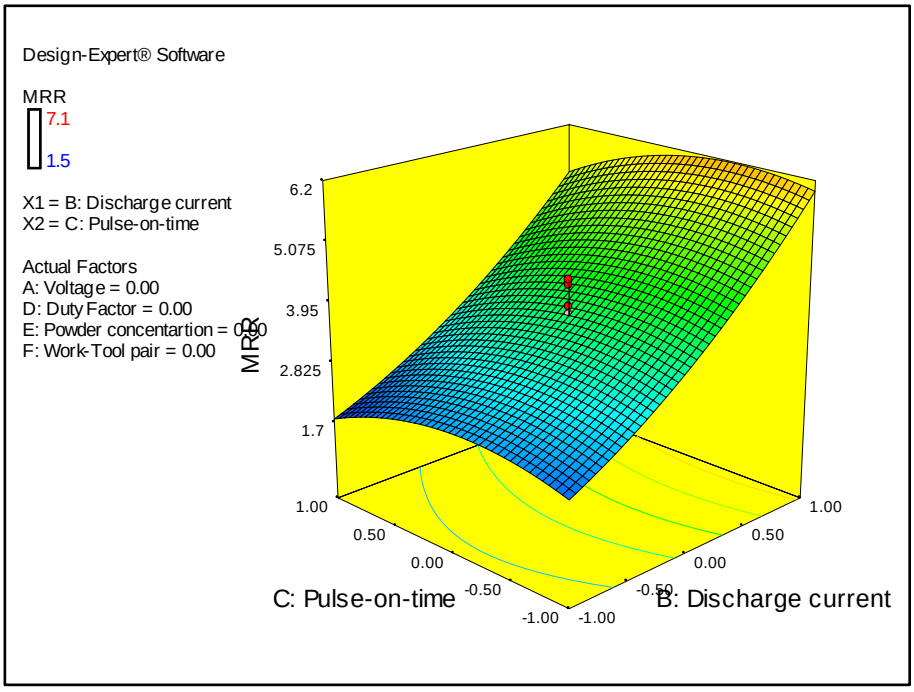

Figure 5.10 Surface plot of MRR with discharge current pulse-on-time

Figure 5.11 shows the variation of MRR with powder concentration and work-tool pair. Form the figure its can clearly observed that for all the combination of work-tool pair MRR increases with increase in powder concentration. This is because the powder mixed in the dielectric fluid forms bridging effect in between the electrodes. This phenomenon enables the dispersion of spark discharge into numerous increments which in turn increases the volume of eroded material from work piece and hence increases the MRR. The figure also shows that treated work piece (TW) and treated tool (TT) work-tool pair exhibits the highest MRR. Non-treated work piece (NW) and treated tool (TT) work-tool pair exhibits the lowest MRR. Treated work piece (TW) and non-treated tool (NT) work-tool pair exhibits MRR value those between TW-TT and NW-TT work-tool pairs. Hence, it is very much evident that deep cryogenic treatment of work piece can increase the MRR leading to productivity of the process. The material removal mechanism in EDM is primarily dependent up on the work material's ability to absorb and dissipate heat. The poor thermal and electrical conductivity of Inconel 718 super alloy does not permit easy absorption of heat deep inside in to work piece. As a result, the local temperature rise on the machined surface is low and in turn declines MRR. Due to deep cryogenic treatment, the thermal and electrical conductivity of work piece improves. At the cryogenic temperature, the thermal vibration of atoms in a metal becomes weaker resulting in easy movement of electrons inside the metal. This phenomenon increases the electrical conductivity of the metal. As per Wiedemann-Franz-

Lorenz Law, increase in electrical conductivity increases the thermal conductivity of the material. Due to improvement in thermal conductivity, the heat penetration and dissipation capacity of the work piece improves, which eventually increases the MRR. However, it is observed that treatment to work piece does not have any impact in increasing wearing resistance of tool. As reflected from the surface plot, the maximum value of MRR is obtained at the highest level of powder concentration while TW is machined with TT. This is because, when both the electrodes are treated, the spark energy generated between them is higher in comparison to other two work-tool pair due to improvement in thermal conductivities, which eventually results in higher MRR. Duty factor has little effect for variation of MRR, but still it is observed that MRR increases very slowly with increase of duty factor.

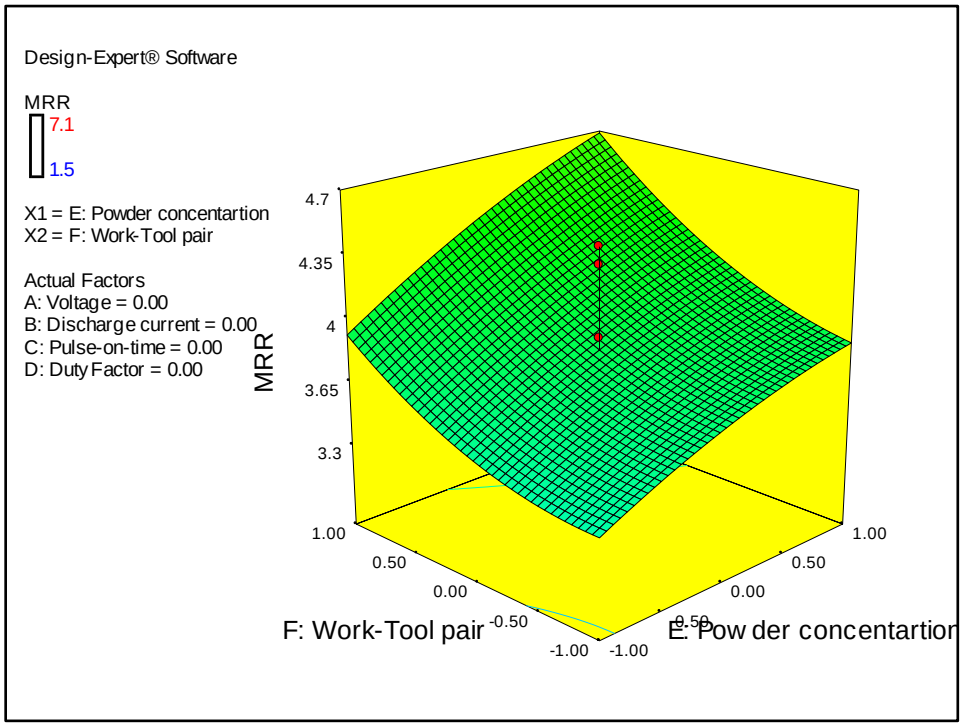

Figure 5.11 Surface plot of MRR with powder concentration and work-tool pair

For suitable industrial applications maximizing MRR is not always desirable as tool wear also increases along with increases of MRR. Therefore, minimization of wear ratio of electrodes is of greatest importance, as it directly affects the cost of machining of the process. Figure 5.12 show the surface plot of EWR with discharge current and open circuit voltage. Figure shows that EWR increases briskly along with increase in discharge current and open circuit voltage except at smaller value of both the parameters. This is obvious, as an increase in both parameters significantly improves the spark energy, which in turn

increases the molten metal volume eroded from both the electrodes and influences increase in MRR.

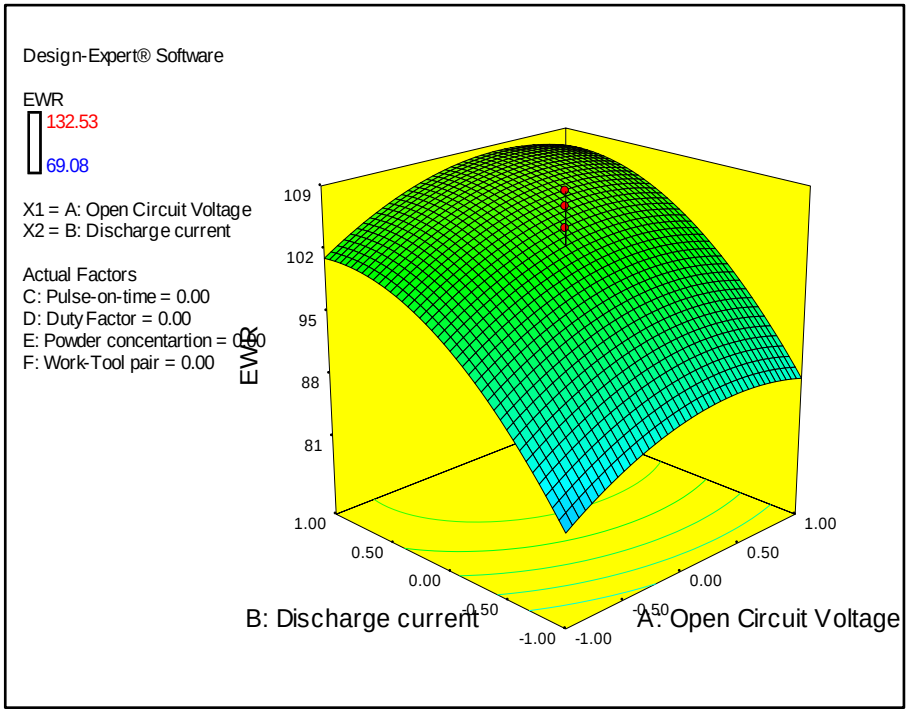

Figure 5.12 Surface plot of EWR with open circuit voltage and discharge current

Figure 5.13 shows the variation of EWR with powder concentration and work-tool pair. The figure indicates that EWR varies inversely with increase in powder concentration. EWR ratio refers to ratio of, weight loss of tool material to weight loss of work material due to machining. It has been already discussed, that the MRR increases with increases in powder concentration due to bridging effect in between the electrodes. This phenomenon ultimately reduces EWR with increase in powder concentration. Another reason for decrease of EWR with increase in powder concentration is due to attachment of carbon particles to the tool tip which eventually reduces tool wear and in turn declines EWR. The figure also shows that TW-TT work-tool pair exhibits the best performance with respect to EWR. NW-TT work-tool pair exhibits the highest EWR.TW-NT work-tool pair exhibits EWR value those between TW-TT and NW-TT work-tool pairs. Due to deep cryogenic treatment the thermal conductivity and micro hardness of tool improves which in turn decreases the local temperature rise of the tool material due to faster heat transfer away from metal surface and thus reducing tool wear. Hence, for NW-TT work-tool pair only tool wear is reduced without out causing any significant improvement to MRR. In this work, it has been already observed that treatment to work piece only increases the MRR. Hence, for TW-NT work-tool pair only MRR is increased

without causing any significant decreases to tool wear. However, it is observed that treatment to both the electrodes significantly improves MRR and declines tool wear due to improvement in thermal conductivities, which ultimately influences decrease in EWR. Hence, it is very much evident that deep cryogenic treatment of both work piece and tool material can increase the MRR and reduce tool erosion resulting beneficial for both the electrodes leading to productivity of the process.

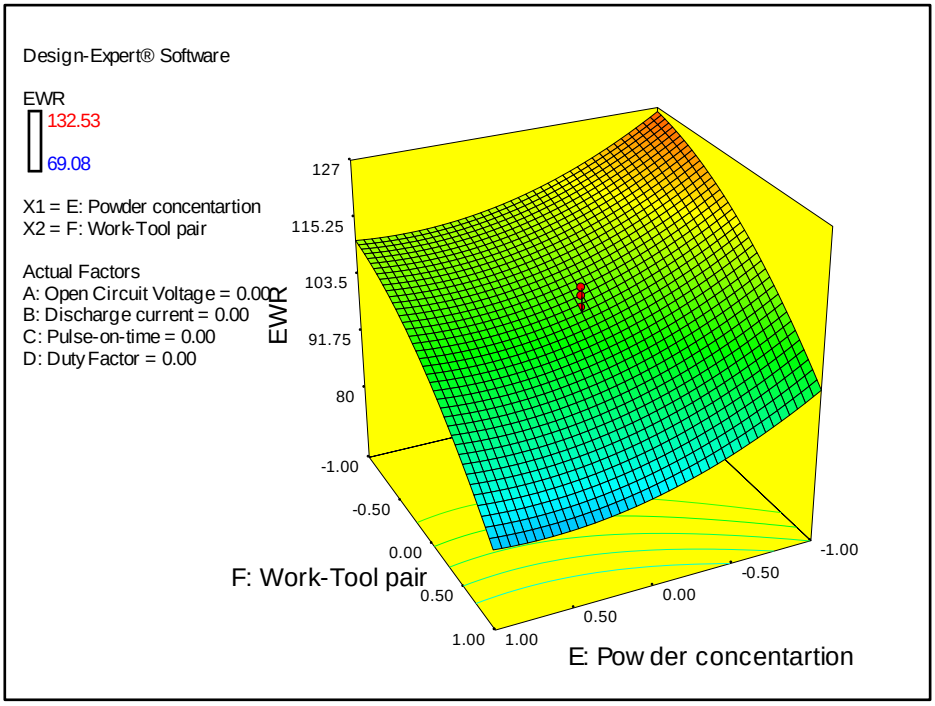

Figure 5.13Surface plot of EWR with powder concentration and work-tool pair

Figure 5.14 shows the variation of EWR with discharge current and pulse-on-time. Figure shows that EWR increases briskly for all the value of discharge current and pulse-on-time except at lower value of both the parameters. This is obvious, as discharge current and pulse-on time significantly improves the spark energy higher volume of material is eroded from both the electrodes resulting in increasing EWR. Effect of duty factor for variation of EWR is minimal, but still it is observed that at higher value of duty factor EWR shows a slight increasing trend due to increase in spark energy.

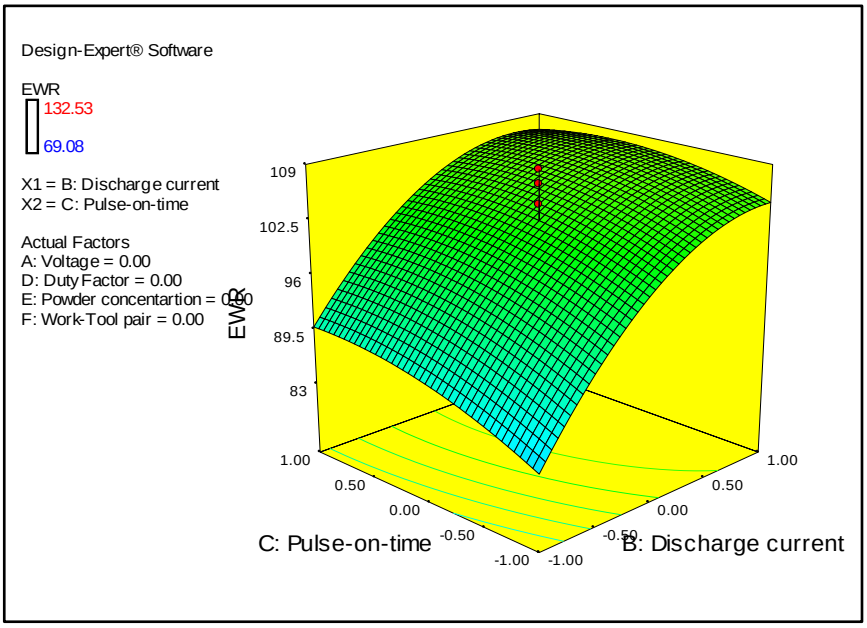

Figure 5.14 Surface plot of EWR with discharge current and pulse-on-time

The surface quality and integrity of the machined parts are the important performance measure to determine the machining efficiency of the process. Figure 5.15 shows the variation of surface roughness with discharge current and pulse-on-time. As reflected from the figure, the surface quality deteriorates heavily with increase in discharge current and pulse-on-time. Increasing discharge current and pulse on time significantly improves the spark energy resulting in lager size particle to be eroded from machined surface and thus degrading the surface quality.

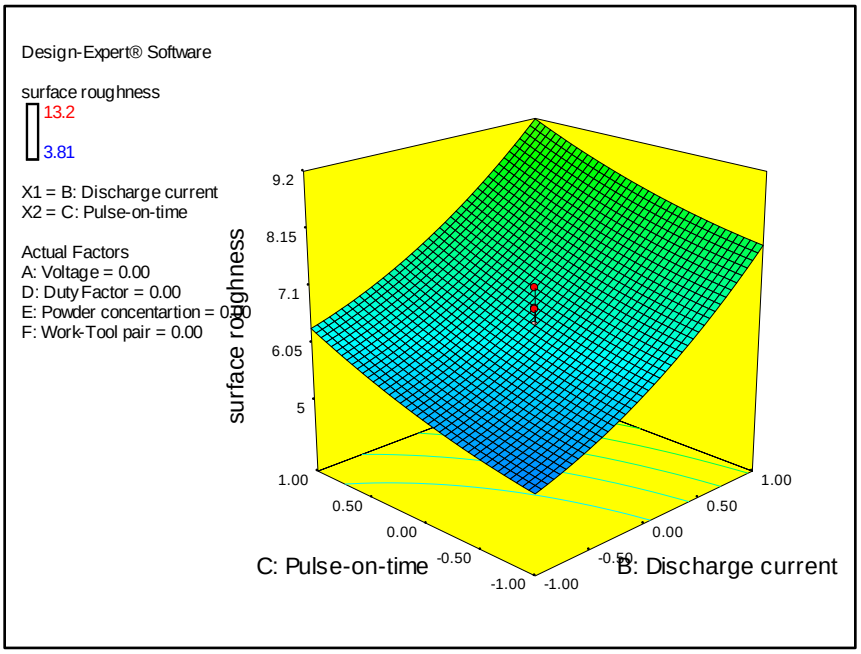

Figure 5.15 Surface plot of surface roughness with discharge current and pulse-on-time

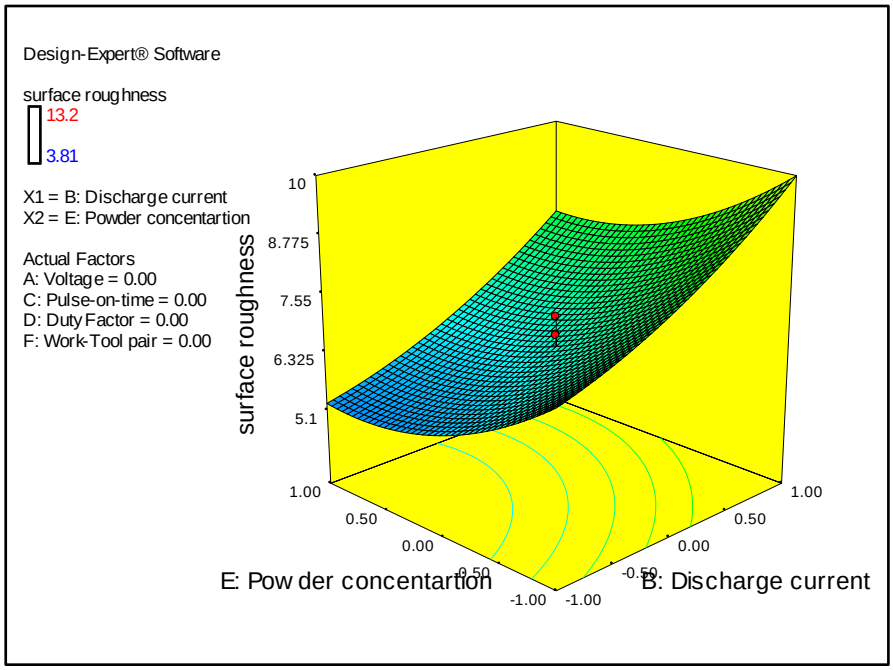

Figure 5.16 Surface plot of surface roughness with discharge current with powder concentration

Figure 5.16 shows the variation of surface roughness with discharge current and powder concentration. Figure shows that for all values of discharge current surface roughness decreases with increases in powder concentration. From this it is quite evident, that powder added to the dielectric fluid improves the surface quality due to modification of plasma channel. The powder particles uniformly distribute the spark discharge as the plasma channel is widened. This phenomenon reduces the spark density on the machining spot. As a result, tiny particles are eroded from the machined surface and thus the machined surface quality is improved.

Figure 5.17 shows the surface plot of surface roughness with discharge current and work-tool pair. Figure shows that for all combination of work-tool pair surface roughness increases with increase in discharge current. As reflected from the figure, TW-TT work-tool pair exhibits the best performance with respect to surface quality. NW-TT work-tool pair exhibits the worst performance with respect to surface quality.TW-NT work-tool pair exhibits the surface quality value those between TW-TT and NW-TT work-tool pairs. Hence, it is quite evident that the surface quality of the machined surface is better when both the electrodes treated in comparison with either treatment of tool or treatment of work piece. Treatment to both the electrodes improves the thermal conductivities of both the electrodes. As a result, the heat absorption and dissipation capacity of both the electrodes improves. This phenomenon reduces the excessive vaporization and melting of both the electrodes.

Consequently, the initial shape retention is better in comparison with other work-tool pair. Hence, the sparking is more uniform and evenly distributed spark discharges takes place; which ultimately results in superior quality of the machined surface. Another reason of achieving improved surface quality when both the electrodes are treated is due to improvement in flushing efficiency. In EDM, the machined surface quality and integrity are closely related to recast layer formation. Higher value of surface roughness leads to higher value of recast layer thickness and vice-versa. Owing to deep cryogenic treatment of both the electrodes, the excessive heating and vaporization of electrodes are reduced due to improvement in thermal conductivities. As a result, the volume of debris formed during machining is also reduced. The smaller volume of molten metal pool gets flushed away easily without being accumulated on the machined surface and thus improving the surface quality of the machined surface. Parameters such as open circuit voltage and duty factor have little effect for variation of surface roughness.

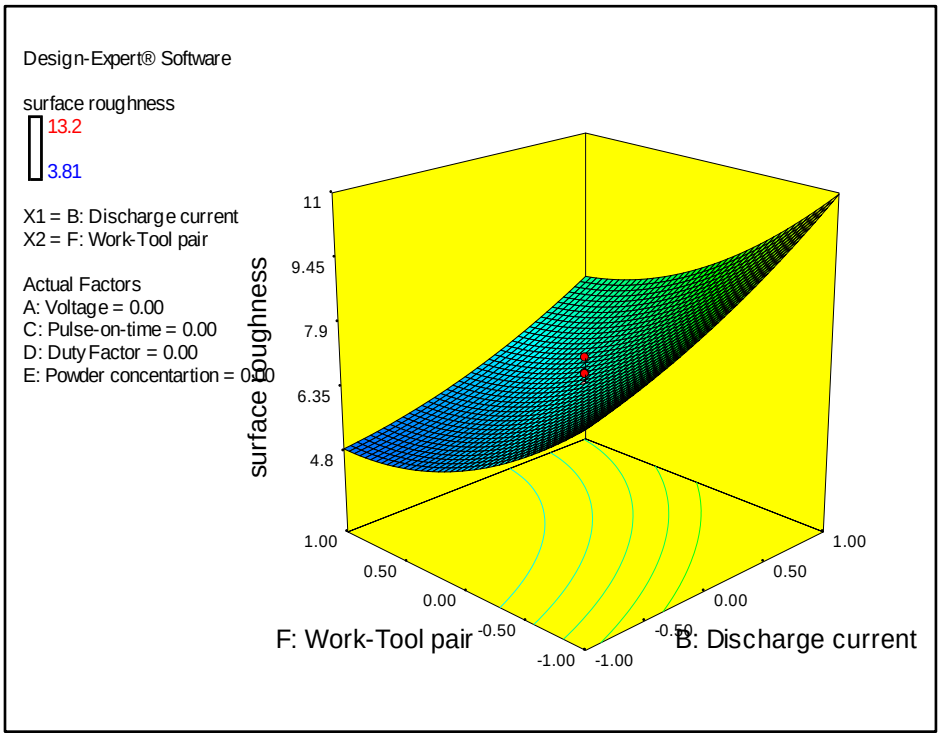

Figure 5.17 Surface plot of surface roughness with discharge current and work-tool pair

In EDM, the dimensional accuracy of the drilled holes is evaluated in terms of radial overcut. Therefore, for precise and accurate machining minimization of over cut is vital. Figure 5.18 shows the variation of radial over cut with discharge current and pulse-on-time. Figure shows that overcut increases with increase in discharge current and pulse-on-time. This is obvious as increase in both the parameters significantly improves the spark energy. As a result, the molten metal volume increases and wider craters are produced on the machined surface which intern influence increase in over cut.

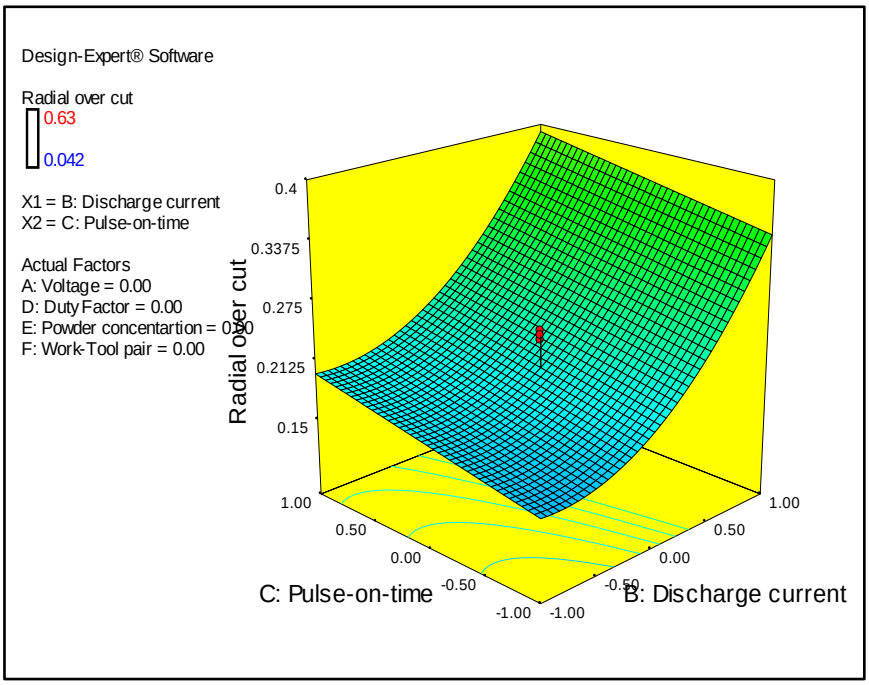

Figure 5.18 Surface plot of radial overcut with discharge current and pule-on-time

Figure 5.19 shows the variation of radial overcut with powder concentration and work-tool pair. Figure shows that for all combination of work-tool pair radial overcut decreases with increases in powder concentration. The presence of suspended powder particle increases the spark gap and forms a bridging effect in between electrodes. As a result, the plasma channel gets widened and reduces the electrical spark density on the machining spot. This phenomenon reduces the spark energy and distributes the discharges more evenly throughout the machined surface, which in turn produces shallow craters and over cut is minimized. The figure also shows that TW-TT work-tool pair exhibits the best performance with respect to overcut. NW-TT work tool pair exhibits the worst performance with respect overcut.TW-NT work tool pair exhibits overcut value those between TW-TT and NW-TT work tool pairs. Hence, it is quite evident that preciseness and accuracy of the drilled holes is better when both the electrodes are treated as compared to when either work piece

is treated or tool is treated. This is because, treatment to either tool or work piece reduces vaporization and melting of that particular electrode due to improvement in its thermal conductivity and micro hardness. The roundness of the untreated electrodes gets damaged due to local temperature rise and excessive heating owing to poor mechanical properties. However, treatment to both the electrodes allows easy absorption and dissipation of heat of both the electrodes due to improvement in their thermal conductivities. As a result, the initial shape and roundness retention for the electrodes is better as before. The spark is uniformly distributed on the machined surface which ultimately improves the accuracy of the drilled holes improving productivity of the process.

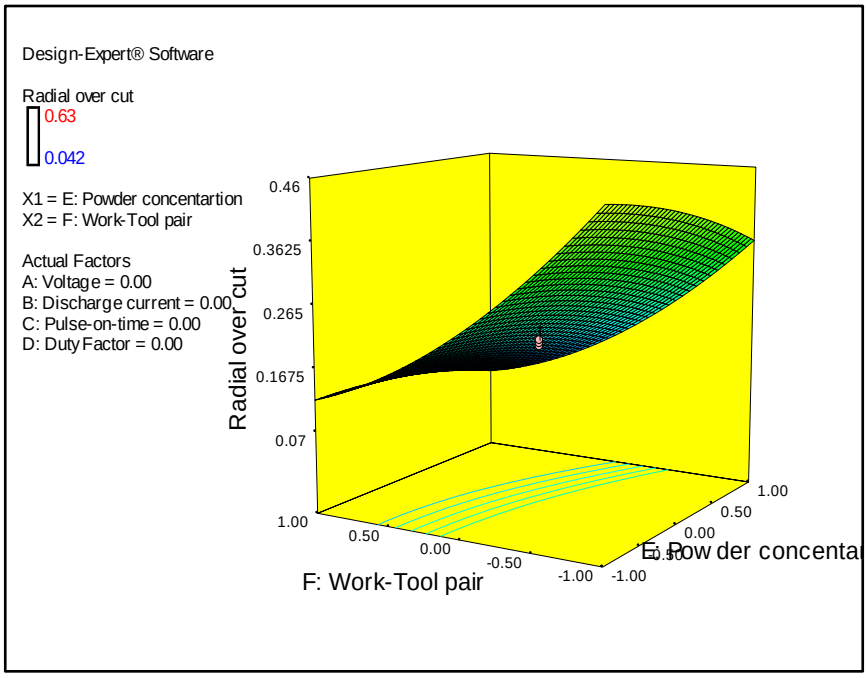

Figure 5.19 Surface plot of radial overcut with powder concentration and work-tool pair

The White layer is formed due to improper flushing of molten metal pool by the dielectric and later solidifies on the machined surface after cooling. Formation of white layer severely damages the surface integrity of the machined surface, increasing number of cracks and voids. Therefore, it is important to minimize white layer thickness to achieve improved surface quality. Figure 5.20 shows the variation of white layer thickness with discharge current and pulse-on-time. Figure shows that white layer thickness increases briskly with increase in discharge current for all the levels of pulse-on-time. But the increase is more pronounced up to a pulse-on-time of 200µs, beyond which the white layer thickness shows a slight decreasing trend due to decrease in MRR. This is obvious, as increasing discharge current and pulse-on-time significantly improves the spark energy which in turn increases

the molten metal volume. The debris solidifies on the machined surface due to improper flushing and thus increasing the white layer thickness.

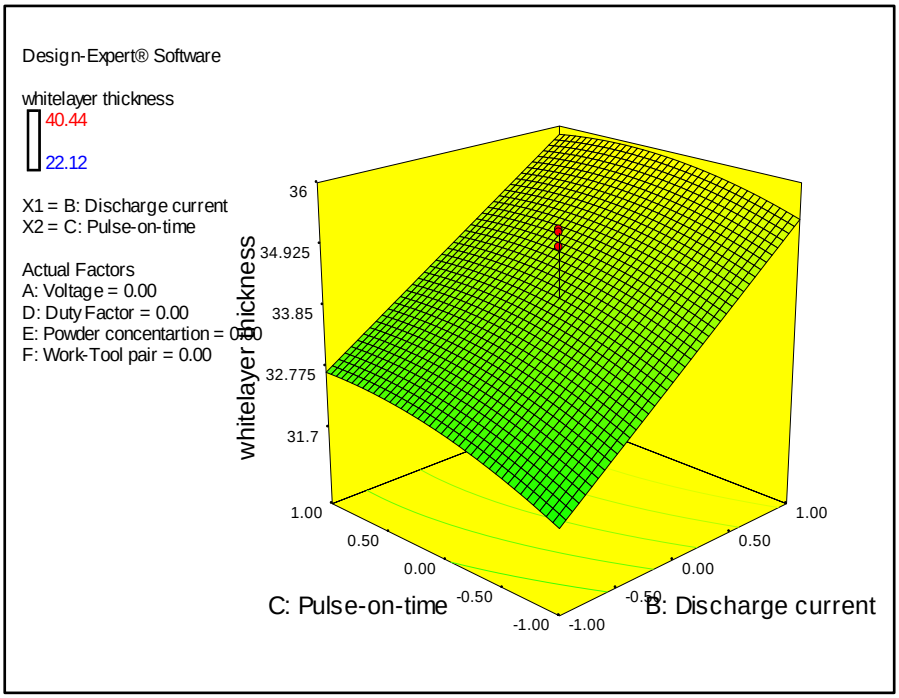

Figure 5.20 Surface plot of white layer thickness with discharge current and pulse-on-time

Figure 5.21 shows variation of white layer thickness with powder concentration and work-tool pair. As reflected from figure, for all the combination of work-tool pair white layer thickness decreases with increase in powder concentration. The presence of conductive powder particles promotes the breakdown of dielectric within the spark gap and increases the spark gap between electrodes. Thus, the plasma channel gets widened and enlarged. The powder particles uniformly distribute the spark discharges, and reduce the spark density on the machining spot. As a result, tiny particles are eroded from the machined surface and the surface quality is improved. Consequently, the formation of surface cracks, micro holes, micro voids and surface roughness are reduced. Due to improved surface quality the flushing efficiency increases and the molten metal pool gets flushed away easily without being accumulated on the machined surface. This phenomenon reduces the white layer thickness. The figure also shows that TW-TT work tool pair exhibits the best performance with respect to white layer thickness. NW-TT work-tool pair exhibits the worst performance with respect to white layer thickness.TW-NT work-tool pair exhibits white layer thickness value those between TW-TT and NW-TT work-tool pair. Therefore, it can be concluded that treatment to both the electrodes produces thinner white layer as compared to either treatment of work piece or treatment of tool. It has been already discussed that treatment to

both the electrodes significantly improves the surface quality of the machined surface. Again, when both the electrodes are treated the excessive melting and vaporization is reduced due improvement in thermal properties which in turn reduces the molten metal pool on the machined surface. These phenomenon, allows easy flushing of debris from the machined surface and reducing the white layer thickness.

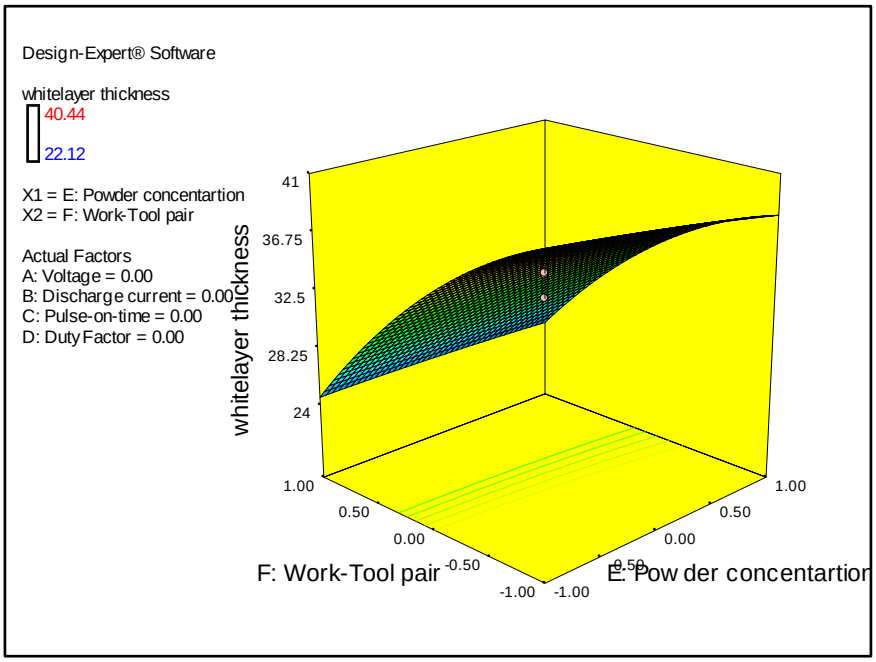

Figure 5.21 Surface plot of white layer thickness with powder concentration and work-tool pair

In this chapter, a novel multi-objective particle swarm optimization (MOPSO) technique is proposed with the goal of finding approximations of the optimal Pareto front and is compared with another popular multi-objective algorithm known as non-dominated sorting genetic algorithm II (NSGA-II) proposed by Deb et al.(2002)which has been fruitfully applied for solving many problems. The algorithms are compared in terms of in terms of four performance metrics. In this study, five responses such as (MRR, EWR, surface roughness, radial overcut and white layer thickness) are considered. However, all the five responses may not be applicable simultaneously for industrial applications. Therefore, two responses are considered to be optimized treating other three responses are treated as constraints at a time. The constrained value is selected from the experimental observations. The empirical relation between the process parameters and process responses established from the RSM analysis is used as objective function for solving in MOPSO and NSGA II algorithms. In the present work, the objectives are maximization of MRR and minimization of EWR, surface roughness, radial overcut and white layer thickness which are functions of process

parameters viz. open circuit voltage, discharge current, pulse-on-time , duty factor, concentration of fine graphite powder and work-tool pair. Work-tool pair is a qualitative process parameter whereas, open circuit voltage, discharge current, pulse-on-time, duty factor, flushing pressure are quantitative process parameters. The quantitative parameters are real numbers that lies in the range [-1, 1]. For the qualitative parameters, the nearest integer part of the real numbers has been considered. The ranges of the qualitative parameters (work-tool pair) are considered in the manner if the values lie in the range [-1 to -0.3], it is treated as -1 or non-treated work piece-treated tool (NW-TT), [-0.29 to+0.3] as 0 or treated work piece-non treated tool (TW-NT) and [+0.31 to+1] as 1 or treated work piece-treated tool (TW-TT).

Ten optimization problems are formed considering two responses as objectives and three as constraints. The empirical relation between input parameters and responses obtained in equations 5.1-5.5 are used as functional relations. MOPSO and NSGA-II algorithms are coded MATLAB 13 for solving minimization problems.

Problem 1:

Maximize MRR

Minimize EWR

Subject to

Surface roughness $\leq$3.81

Radial overcut $\leq$ 0.042

White layer thickness $\leq$22.12

where 3.81, 0.042 and 22.12 are the minimum values of surface roughness, radial overcut and white layer thickness obtained from the experimental Table 5.4 respectively.

Problem 2:

Maximize MRR

Minimize surface roughness

Subject to

EWR $\leq$ 69.08

Radial overcut $\leq$ 0.042

White layer thinness $\leq$22.12

where 69.08, 0.042 and 22.12 are the minimum values of EWR and radial overcut and white layer thickness obtained from the experimental table 5.4 respectively.

Problem 3:

Maximize MRR

Minimize radial overcut

Subject to

EWR $\leq$ 69.08

Surface roughness $\leq$3.81

White layer thinness $\leq$22.12

where 69.08, 3.81 and 22.12 are the minimum values of EWR, surface roughness and white layer thickness obtained from the experimental table 5.4 respectively.

Problem 4

Maximize MRR

Minimize white layer thickness

Subject to

EWR $\leq$ 69.08

Surface roughness $\leq$3.81

Radial overcut $\leq$ 0.042

where 69.08, 3.81 and 0.042 are the minimum values of EWR, surface roughness and radial overcut obtained from the experimental table 5.4 respectively

Problem 5:

Minimize EWR

Minimize Surface roughness

Subject to

MRR $\geq$ 7.1

Radial overcut $\leq$ 0.042

White layer thinness $\leq$22.12

where 7.1,0.042 and 22.12 are the maximum value of MRR and minimum values radial overcut and white layer thickness obtained from the experimental table 5.4 respectively.

Problem 6:

Minimize EWR

Minimize Radial overcut

Subject to

MRR $\geq$ 7.1

Surface roughness $\leq$3.81

White layer thinness $\leq$22.12

where 7.1, 3.81 and 22.12 are the maximum value of MRR and minimum values of surface roughness and white layer thickness obtained from the experimental Table 5.4 respectively.

Problem 7:

Minimize EWR

Minimize white layer thickness

Subject to

MRR $\geq$ 7.1

Surface roughness $\leq$3.81

Radial overcut $\leq$ 0.042

where 7.1, 3.81 and 0.042 are the maximum value of MRR and minimum values of surface roughness and radial over cut obtained from the experimental Table 5.4 respectively.

Problem 8:

Minimize Surface roughness

Minimize Radial overcut

Subject to

MRR $\geq$ 7.1

EWR $\leq$ 69.08

White layer thinness $\leq$22.12

where 7.1, 69.08 and 22.12 are the maximum value of MRR and minimum values of EWR and white layer thickness obtained from the experimental Table 5.4 respectively.

Problem 9:

Minimize Surface roughness

Minimize white layer thickness

Subject to

MRR $\geq$ 7.1

EWR $\leq$ 69.08

Radial overcut $\leq$ 0.042

where 7.1, 69.08 and 0.042 are the maximum value of MRR and minimum values of EWR and radial overcut obtained from the experimental Table 5.4 respectively.

Problem 10:

Minimize radial overcut

Minimize white layer thickness

Subject to

MRR ≥ 7.1

EWR ≤ 69.08

Surface roughness ≤3.81

where 7.1, 69.08 and 3.81 are the maximum value of MRR and minimum values of EWR and surface roughness obtained from the experimental Table 5.4 respectively

It is to be noted equivalent minimization function is used in the MATLAB program wherever an objective is maximized.

5.5 Performance estimation of Pareto frontiers obtained through MOPSO and NSGA II

The effectiveness of the proposed MOPSO algorithm is compared with another popular multi-objective algorithm known as non-dominated sorting genetic algorithm II (NSGA-II) which was first introduced by Deb et al.(2002) and successfully applied in many multi-objective problems(Basu 2008; Ghiasi et al.2011).

Based on exhaustive experimentation, Figures 5.22-5.25 are drawn to compare the Pareto front between objectives MRR-EWR, MRR-surface roughness, MRR-radial overcut and MRR-white layer thickness respectively. The Pareto fronts reveals that a small decrease of one objective value can cause a large increase in the other conflicting objective value. The results convey two messages: (1) Focusing on optimizing a single objective may result in bad performance of the other objective (2) The trade-off relationship between the objectives is not always easy to predict.

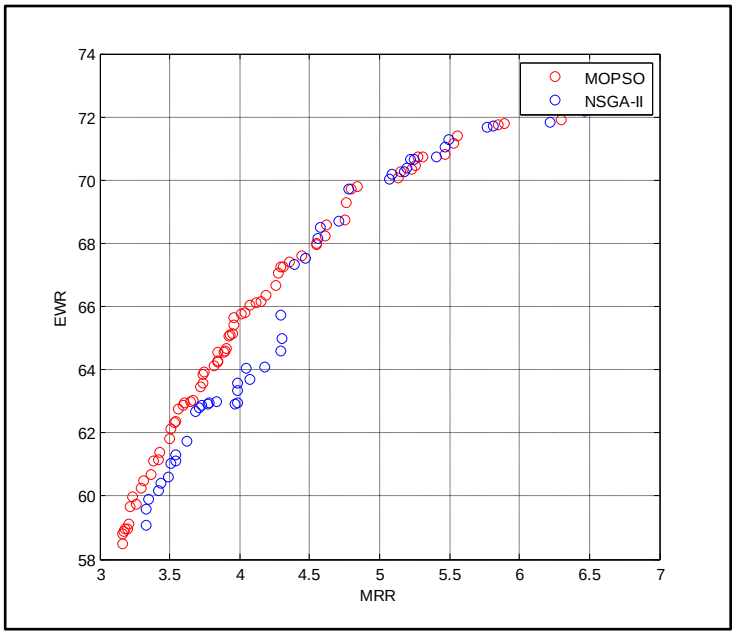

Figure 5.22 Pareto front for objectives MRR and EWR

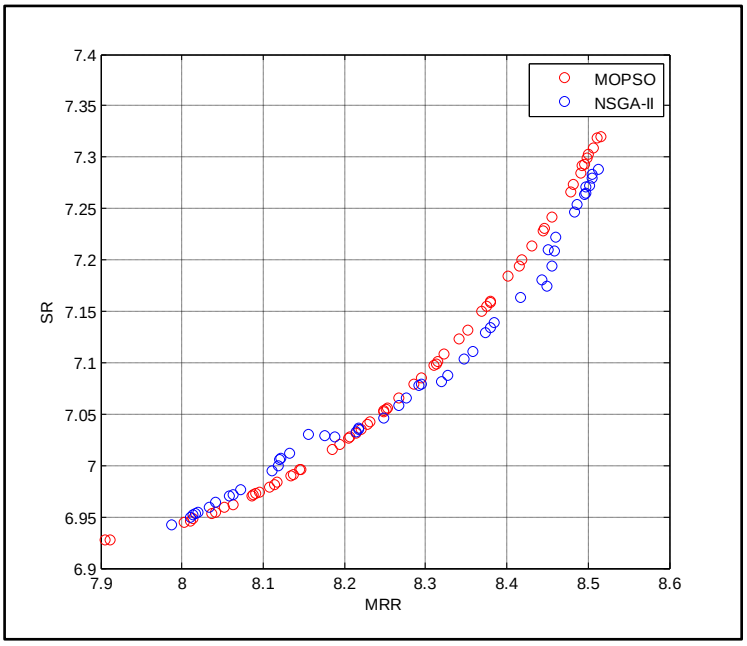

Figure 5.23 Pareto front for objectives MRR and Surface roughness

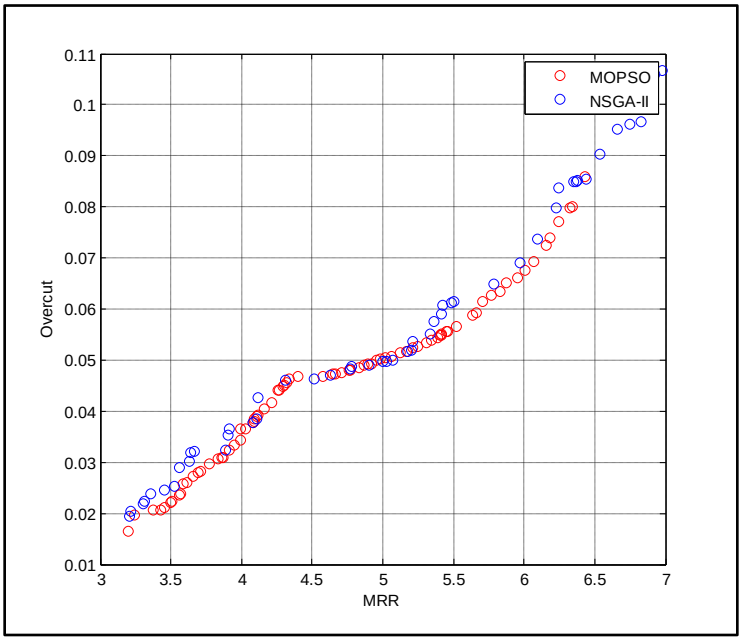

Figure 5.24 Pareto front for objectives MRR and Radial overcut

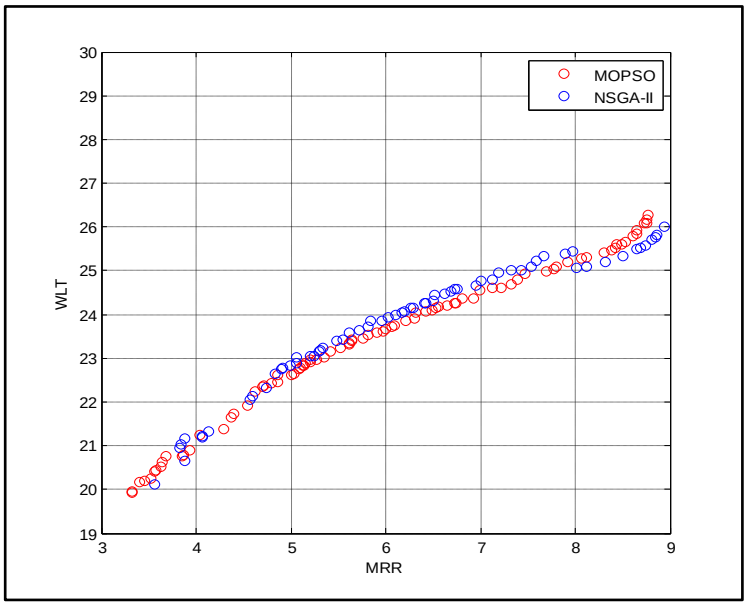

Figure 5.25 Pareto front for objectives MRR and white layer thickness

There are two goals in a multi-objective optimization: (i) convergence to the Pareto-optimal set (ii) maintenance of diversity in solutions of the Pareto-optimal set. These two tasks cannot be measured adequately with one performance metric. Many performance metrics have been suggested to evaluate the non-dominated solutions (Deb et al. 2002; Karimi et al. 2010). To evaluate comprehensively the non-dominated solutions obtained by the MOPSO and NSGA-II algorithm, four performance metrics are considered in this work. The following performance measures are used to compare the results of non-dominated solutions obtained by multi-objective algorithms.

Mean ideal distance (MID): The MID measurement presents the proximity between non-dominated solutions and ideal point (0, 0). Algorithm A is considered to have more opportunity to reach the Pareto frontier than algorithm B if A has the lower value of MID than B. MID of algorithm can be obtained by the following formulation.

$$\mathrm{MID} = \frac{\sum_{i=1}^{n} C_i}{n} \tag{5.6}$$

where n is the number of non-dominated solutions and $C_i = \sqrt{f_{1i}^2 + f_{2i}^2}$

f_{1i} and f_{2i} are the objective function values for solution i. The performance of the algorithm will be better if the value of MID is lower.

The rate of achievement to two objectives simultaneously (RAS): The value of this measure is calculated from the following relation. Smaller value of this criterion indicates a higher quality solution.

$$RAS = \frac{\sum_{i=1}^{n} |f_{1i} - f_1^{best}| + |f_{2i} - f_2^{best}|}{n} \quad (5.7)$$

f_1^{best} and f_2^{best} are the best solutions in the non-dominated sets for objectives 1 and 2.

Spread of non-dominance solutions (SNS): The spacing metric aims at assessing the spread (distribution) of vectors throughout the set of non-dominated solutions. This criterion, which is known as an indicator of diversity, is calculated from the following relation:

$$SNS = \sqrt{\frac{\sum_{i=1}^{n} (MID - C_i)^2}{n-1}} \quad (5.8)$$

Diversification matrix (DM): This performance measure gives an indication of the diversity of solutions obtained from a given algorithm.

$$DM = \sqrt{(\max f_1 - \min f_1)^2 + (\max f_2 - \min f_2)^2} \quad (5.9)$$

where $\max f_1$ and $\max f_2$ is the maximum objective functions value of the of non-dominated solutions and $\min f_1$ and $\min f_2$ is the minimum objective functions value of the of non-dominated solutions. Larger values of SNS and DM are indicative of higher quality solutions.

The results obtained by the proposed algorithms are compared in terms of the performance metrics with the NSGA-II. Table 5.10 presents the comparative results of two algorithms with respect to four performance measures. Table 5.10 indicates that MOPSO results are superior to the NSGA-II in most of the case with respect to MID, RAS, SNS and DM performance measures.

Table 5.10 Performance metrics of Pareto frontiers

Problem	MID		RAS		SNS		Diversity (DM)	
	MOPSO	NSGA-II	MOPSO	NSGA-II	MOPSO	NSGA-II	MOPSO	NSGA-II
MRR-EWR	**65.7498**	65.8022	8.3503	**7.6495**	**4.2534**	4.23872	**15.6689**	13.4729
MRR-Surface roughness	**10.893**	10.9044	**0.3287**	0.4462	**0.2072**	0.2032	**0.72495**	0.6289
MRR-Radial overcut	**4.689**	5.067	**1.521**	1.9004	**1.887**	1.1717	**4.231**	3.775
MRR-White layer thickness	**24.188**	26.124	**6.1521**	6.5721	**2.0758**	1.749	**8.35711**	8.1579
EWR-Surface roughness	**61.561**	62.756	**4.1892**	5.193	**2.052**	1.8695	**7.7894**	7.2128
EWR-Radial overcut	**61.781**	62.439	**4.1926**	5.0568	**2.9254**	1.761	**7.983**	7.5412
EWR-White layer thickness	62.5583	**62.824**	1.808	**1.2593**	**0.72351**	0.6783	**3.2694**	2.3854
Surface roughness-radial overcut	4.5821	**4.556**	0.135667	0.**11834**	**0.1048**	0.09157	**0.374852**	0.32598
Surface roughness-White layer thickness	**20.939**	21.6522	**0.9013**	1.47	**0.2833**	0.2813	**1.514**	1.092
Radial overcut-White layer thickness	20.089	**19.571**	**0.2704**	0.2719	**0.19017**	0.1072	**0.7894**	0.4215

*

The best obtained values are marked in bold letter

In the present investigation, application of MOPSO results in large number of non-dominated solutions for optimization of objectives. The Pareto-optimal solutions obtained through MOPSO have been ranked by the composite scores obtained through maximum deviation theory (MDT) to choose the best solution. The decision matrix is normalized using the equations 3.11 and 3.12 appropriately. The objective weights are determined for the normalized values of objectives by applying maximum deviation method using equation 3.13-3.20. The weighted objective values are estimated by multiplying the normalized objective values and the objective weights. The best solution is selected depending upon the composite scores obtained by addition of the all the weighted objective function values for each alternative. The objectives with highest composite score are chosen as the best solution. Table 5.11 shows the pareto optimal solution set for objectives MRR and EWR with corresponding variable setting. Table 5.12 shows the best ranked solution for all combination of responses obtained through maximum deviation theory.

Table 5.11 Pareto optimal solution for MRR and EWR with corresponding variable setting

Run Order	A V	B A	C µs	D %	E gm/lit.	F (work-tool)	MRR (mm^3/min)	EWR %
1	74.80	6.85	100	88.80	3.94	TW-TT	7.57	76.85
2	74.54	6.83	100	88.39	3.95	TW-TT	7.53	76.35
3	70.75	6.65	100	88.12	3.90	TW-TT	7.50	73.27
4	70.37	6.49	100	87.72	3.92	TW-TT	7.26	72.83
5	70.37	6.17	100	87.24	3.91	TW-TT	6.75	72.71
6	70.04	6.02	100	87.06	3.90	TW-TT	6.54	72.25
7	70.04	5.87	100	86.57	3.87	TW-TT	6.30	71.90
8	70.08	5.55	100	86.71	3.97	TW-TT	5.90	71.79
9	70.30	5.55	100	86.39	3.90	TW-TT	5.85	71.76
10	70.50	5.35	100	85.65	3.91	TW-TT	5.56	71.38
11	70.20	5.29	100	86.28	3.91	TW-TT	5.53	71.15
12	70.04	5.24	100	85.98	3.94	TW-TT	5.47	70.82
13	70.30	5.13	100	85.75	3.94	TW-TT	5.31	70.73
14	70.24	5.09	100	86.22	3.96	TW-TT	5.28	70.73
15	70.20	5.09	100	85.76	3.88	TW-TT	5.25	70.44
16	70.04	5.05	100	86.01	3.95	TW-TT	5.23	70.33
17	70.20	4.99	100	85.81	3.94	TW-TT	5.15	70.25
18	70.04	4.97	100	86.03	3.95	TW-TT	5.13	70.09
19	70.61	4.76	100	85.57	3.94	TW-TT	4.84	69.80
20	70.51	4.70	100	86.26	3.97	TW-TT	4.80	69.73
21	70.50	4.71	100	84.90	3.85	TW-TT	4.76	69.29
22	70.08	4.69	100	84.78	3.83	TW-TT	4.75	68.76
23	70.20	4.55	100	85.54	3.95	TW-TT	4.62	68.57
24	70.08	4.56	100	84.78	3.85	TW-TT	4.61	68.24
25	70.08	4.50	100	84.65	3.84	TW-TT	4.55	67.98
26	70.04	4.49	100	84.93	3.88	TW-TT	4.55	67.94
27	70.08	4.38	100	85.23	3.93	TW-TT	4.44	67.61
28	70.24	4.32	100	84.66	3.90	TW-TT	4.36	67.39
29	70.24	4.26	100	85.37	3.96	TW-TT	4.31	67.26
30	70.30	4.26	100	85.24	3.95	TW-TT	4.30	67.24
31	70.24	4.23	100	85.43	3.94	TW-TT	4.27	67.06
32	70.04	4.22	100	84.69	3.88	TW-TT	4.26	66.66
33	70.08	4.16	100	84.72	3.85	TW-TT	4.19	66.34
34	70.04	4.11	100	84.97	3.95	TW-TT	4.15	66.16
35	70.20	4.09	100	84.63	3.90	TW-TT	4.12	66.13
36	70.30	4.05	100	84.59	3.90	TW-TT	4.08	66.03
37	70.24	4.01	100	83.39	0.39	TW-TT	4.03	65.82
38	70.39	4.00	100	84.13	0.39	TW-TT	4.01	65.75
39	70.51	3.94	100	84.70	0.40	TW-TT	3.96	65.63
40	70.37	3.94	100	84.13	0.39	TW-TT	3.95	65.42

Table 5.12 Best ranked solution for multiple objectives

Multiple objectives	A (Volt)	B (Amp)	C (µs)	D (%)	E (gm/l)	F Tool	Objective		Normalized objectives		Weighted Normalized		Composite Score
MRR and EWR	70.75	6.65	100	88.12	3.90	TW-TT	7.50	73.27	0.5158	0.5509	0.2596	0.2736	0.5333
MRR and Surface roughness	71.15	6.84	181.9	89.9	4	TW-TT	8.44	7.23	0.8430	0.6827	0.4204	0.3421	0.7626
MRR and Radial overcut	70.07	7	112.2	90	4	TW-TT	8.42	25.51	0.6710	0.5518	0.3725	0.2455	0.6180
MRR and White layer thickness	70.07	7	112.26	90	4	TW-TT	8.42	25.51	0.9366	0.1168	0.4938	0.0552	0.5490
EWR and Surface roughness	74.80	3	100	85.07	3.09	TW-TT	61.38	4.51	0.3847	0.6889	0.1923	0.3444	0.5368
EWR and Radial overcut	70.07	3	100	85.0	4	TW-TT	58.55	0.056	0.7808	0.9165	0.3894	0.4594	0.8488
EWR and white Layer thickness	70.07	3	100	83.05	3.09	TW-TT	57.96	20.23	0.8487	0.3658	0.4711	0.1627	0.6338
Surface roughness and Radial overcut	86.05	3	100	84.74	4	TW-TT	4.59	0.026	0.6670	0.4787	0.3230	0.2468	0.5699
Surface roughness and white layer thickness	89.54	3	100	80	3.09	TW-TT	4.93	19.99	0.3548	0.8743	0.1713	0.4522	0.6235
Radial over cut and white layer thickness	88.35	3.16	100	80	4	TW-TT	20.27	0.003	0.6281	0.4384	0.3161	0.2177	0.5339

5.6 Conclusions

The work implemented in this Chapter is novel in the sense of application of an hybrid approach of investigation on powder-mixed EDM of cryogenically treated electrodes on Inconel 718 super alloy. It is observed that the process is quite effective to machine Inconel 718 work material with cryogenically treated brass electrode. In the second stage, a novel multi-objective particle swarm optimization algorithm (MOPSO) has been proposed and compared with another popular multi-objective algorithm NSGA II in order to achieve the optimal Pareto front. From the study, it is observed that MOPSO algorithm is superior to NSGA II algorithm. To end with, the best solution is identified from a large number of non-dominated solutions using maximum deviation theory (MDT) to avoid subjectiveness and impreciseness in the decision making. Some of the most significant conclusions from the extensive experimental analysis are discussed in the paragraph below.

It is observed that discharge current, pulse-on-time, powder concentration and work-tool pair exhibit significant effect on performance measures. The thermal conductivity and micro-hardness of brass electrode improves due to deep cryogenic treatment. As a result, the wearing resistance of the tool increases due to easy dissipation of heat. Due to deep cryogenic treatment, the heat dissipation capacity of Inconel 718 work material improves and helps in decreasing local temperature rise on the work piece surface owing to improvement in thermal conductivity. Consequently, the ability of the work piece to absorb and dissipate heat increases which eventually increases the MRR. The study confirms that significant improvement on material removal rate and reduction in EWR, surface roughness, radial overcut and white layer thickness can be achieved if both the electrodes are cryogenically treated. It is observed that MRR can be increased up to 71.92% and EWR, surface roughness, radial overcut and white layer thickness can be reduced up to 33.99%, 35.57%, 72.82% and 35.87% respectively when both the electrodes are cryogenically treated and worked in a powder mixed dielectric condition when experiment numbers 20 (untreated work piece and treated tool) and 24 (both tool and work piece treated) shown in (Table 5.4) were compared. This shows that treatment to both the electrodes results in better EDM performance measures in comparison to either treatment of the tool or treatment of the work piece. It is also observed that the presence of suspended powder particles can enhance the machining efficiency of the process. Comparison of experiment numbers 12 (no suspended particles in dielectric, treated work piece and untreated tool) and 16 (highest concentration of suspended particles in dielectric, treated work piece and untreated tool) (Table 5.4) indicates that MRR can be increased up to 44.31% and EWR, surface

roughness, radial overcut and white layer thickness can be reduced up to 24.10%, 14.97%, 19.04% and 5.17% respectively when machining is done in the presence of suspended powder particles. From analysis of variance for MRR, it is observed that discharge current is found to be the most influential parameter with a percentage contribution of 70.98% followed by open circuit voltage, work-tool pair, powder concentration and pulse-on-time with percentage contribution of 8.68%, 3.03%, 2.11% and 1.17% respectively. From analysis of variance for EWR, it is observed that work-tool pair is found to be the most influential parameter with a percentage contribution of 47.84% followed by discharge current, powder concentration open circuit voltage and pulse-on-time with percentage contribution of 19.17%, 11.78%, 1.73%, 1.06% respectively. From analysis of variance for surface roughness, it is observed that work-tool pair is found to be the most influential parameter with a percentage contribution of 37.97% followed by discharge current, powder concentration and pulse-on-time with percentage contribution of 28.58%, 12.99% and 6.07% respectively. From analysis of variance for radial overcut, it is observed that work-tool pair is found to be the most influential parameter with a percentage contribution of 58.70% followed by discharge current, powder concentration and pulse-on-time with percentage contribution of 23.91%, 3.91% and 1.52% respectively. From analysis of variance for white layer thickness, it is observed that work-tool pair is found to be the most influential parameter with a percentage contribution of 88.02% followed by discharge current, powder concentration and pulse-on-time with percentage contribution of 4.62%, 0.72% and 0.21% respectively. When machining is done in the presence of suspended powder particles with cryogenically treated electrodes, the influence of cryogenic treatment work-tool pair is relatively higher on performance measures than the suspended powder particles. SEM micrographs (Figures 5.6, 5.7, 5.8 (a and b)) show that machined surface quality and surface integrity is superior when machining is done in the presence of suspended powder particles and both the electrodes are cryogenically treated.

CHAPTER 6

PERFORMANCE ASSESSMENT OF EDM PROCESS THROUGH THERMO-STRUCTURAL MODEL

6.1 Introduction

Electrical discharge machining (EDM) process is a popular method amongst non-traditional machining processes finding an extensive application in industries such as die and mould making, aerospace, automotive and other industrial usages. The machining process involves controlled erosion of electrically conductive materials by the initiation of repetitive electrical spark discharge between the tool and the work piece separated by dielectric fluid. The complicated nature of the process involving physics of spark discharges makes the process difficult to analyse the process experimentally and to evaluate the performance measures.EDM literature reveals that a good number of experimental investigations have been reported until now but they could be severely limited by work piece-tool combinations and time constraint for experimentation. It is also observed that only a few studies have been reported until now to analyse the process numerically (Saleh 2006; Kansal 2008; Joshi and Pande 2009;Joshi and Pande 2010; Mohanty et al.2013; Allen and Chen 2007;Izquierdo et al. 2009).Furthermore, experimental approaches could be error prone, time consuming and expensive. Therefore, there exists a vital needto propose a numerical model for precise and accurate prediction of performance measures, which can effect considerable saving in time as well as reduce the experimentation cost.

To address these important issues, in this chapter,a thermal model based on finite element analysis has been proposed to predict the MRR and TWR when work piece Inconel 718 is machined with a variety of electrodes viz. copper, graphite and brass. A coupled thermo-structural model has been also proposed to estimate the induced residual stresses on work piece. The numerical model is validated by comparing the experimental results obtained from the Chapter 3. Numerical model for estimating various performance measures under different work-tool combination have been developed. Parametric analysis is carried out on the proposed model to investigate the effect of important process parameters on theperformance measures.

6.2 Proposed integrated process model for EDM

The procedural steps of the process model for the EDM process model has been shown Figure 6.1. The model principally consists of two stages such as the numerical modelconsidering the thermo-structural characteristics of the process and an experimental model to validate the numerical model when work material Inconel 718 is machined with variety electrodes such as brass, copper and graphite. The approach has definite advantages for tool engineers, since it can be adoptedfor prediction of important performance measures of the EDM process before going for actual cutting operation.

The model provides an inexpensive and time saving alternative to study the performance of machiningbefore going for actual cutting operation.

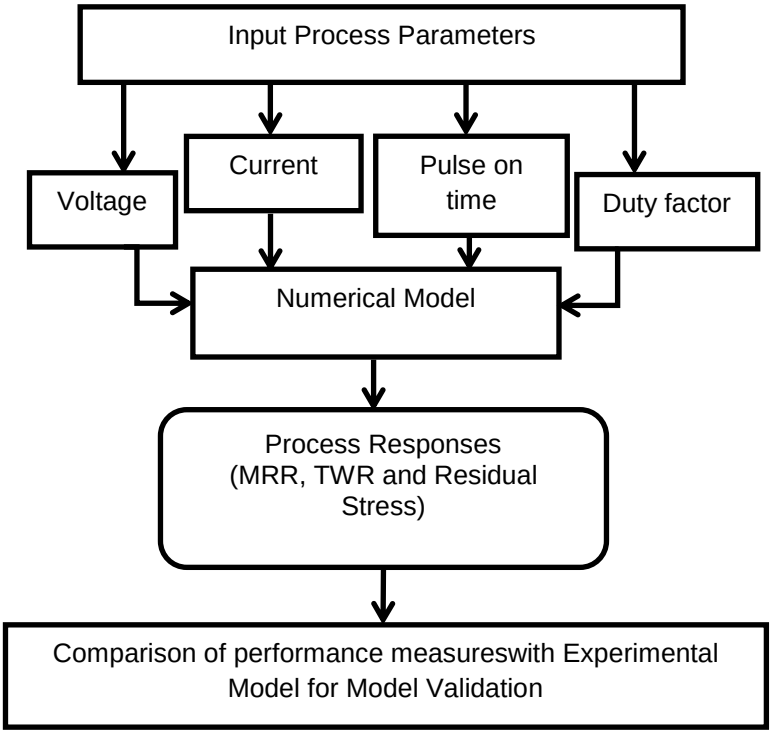

Figure 6.1 Proposed integrated process model for EDM

6.3Simulation of EDM process

6.3.1Thermal modelling of the process

In EDM process, the dielectric medium ionizes due to high electric potential resulting in plasma arc to be produced. The primary mechanism of material removal in EDM process isdue to extreme heat generated by the plasma spark in erosion process which causes melting of material from both work piece as well as tool. The highly ionized chargedparticles of the plasma raise the temperature of thework piece and tool material past theirmelting point, occasionally even higher thanthatofboilingpoint of the electrodes. Therefore, for thermal analysis of the process, conduction is considered as primary mode of heat transfer. Transient nonlinear analysis of the single spark operation of EDM process has been carried out in ANSYS 10 software.

6.3.2Assumptions in the analysis

- Homogeneous and isotropic material is assumed both for the work piece and tool.
- The material properties of both the tool and work piece depend on temperature.

- There is only one mode of heat transfer i.e. conduction. Other heat losses are ignored.
- It is assumed that spark radius is a function of discharge current and time.
- The analysis is made for a single spark.
- Flushingefficiency is considered as 100%
- Ambient temperature is assumed to be room temperature i.e. 298K.

6.3.3 Governing equation required for the analysis

Fourier heat conduction equation is considered as governing equation for the thermal analysis of the EDM process. ANSYS solves the differential equation for the heat transfer of the two dimensional axisymmetric model. The equation is given by

$$\rho c\frac{\partial T}{\partial t} = \frac{1}{r}\frac{\partial}{\partial r}\left(k_r\frac{\partial T}{\partial r}\right) + \frac{\partial}{\partial z}\left(k\frac{\partial T}{\partial Z}\right) \quad (6.1)$$

wherer and zdenote cylindrical coordinates of the work and tool material,T-Temperature in kelvin,k-Thermal conductivity in W/m.k, ρ-Density in kg/m^3, t-Timein seconds,c-Specific heat in J/kgk of the work and tool material,

6.3.4 Desired boundary conditions

The boundary conditions associated with the EDM process are shown in Figure 6.2. The work piece is submerged in dielectric medium.AD is an axi-symmetric boundary. Insulated boundary condition is assumed for the boundaries away from the spark radius i.e. for CD and BC and heat flux is applied at the top surface of the boundary AB.

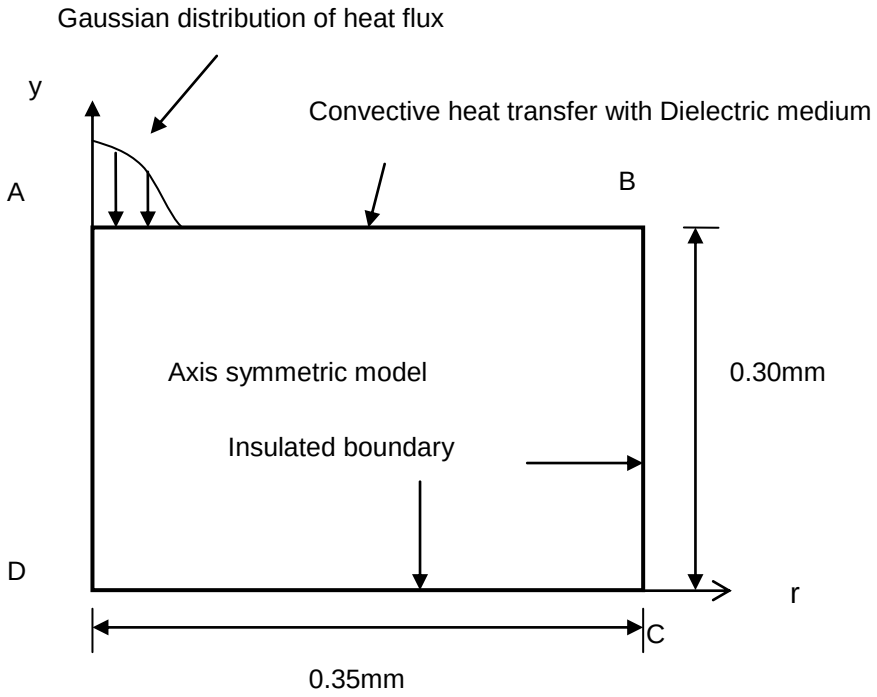

Figure 6.2 Anaxi-symmetric two dimensional model for the EDM process analysis

6.3.5 Heat input required for analysis

Heat input, materialproperties and radius of spark are the significant factors which affect considerablyfor theprecise calculation of responses in single spark EDM analysis.In this model, Gaussian distribution of heat flux is assumed with quantity of heat entering into the two-dimensional domain is given by relation

$$q_w(r) = \frac{4.56PVI}{\pi R_s^2} \exp\left\{-4.5\left(\frac{r}{R_s}\right)^2\right\} \quad (6.2)$$

where q_w- Heat entering into the work and tool material, P-Fraction of heat going to work and tool material, V-Discharge voltage in (V),I-discharge current in (A),R_s-Spark radius (μm).

6.3.6 Spark radiuscalculation

Different methodshave been proposed in the literature for calculation of spark radius. Erden (1983) has proposed an empirical relation for calculation of spark radius in which spark radius is a function of discharge power and time. A methodology suggested by Pandey and Jilani (1986) based on the boiling point temperature, energy density and the thermal diffusivity of work material finds limited applications.The semi-empirical relation derived by Ikaiand Hashiguchi (1995) has been adopted by Joshi and Pande (2009)known as “equivalent heat input radius” which a function is of discharge current and pulseontime has been adopted in this model. It is given as follows

$$R_s = (2.04\exp - 3)I^{0.43}T_{on}^{0.44} \quad (6.3)$$

where $R_s$is spark radius in (μm), I discharge current in (Amp) and T_{on} is the pulse-on-time in (μs).

6.3.7 Discharge energy

In EDM process, the current produced by the pulse generator develops an equilateral triangle as shown in Figure 6.3. If the average working voltage is V, then the single discharge energy is given by the following relation

$$\Delta E = \int V(\tau)\, i(\tau) d\tau = V \times K \times T_{on}^2 \quad (6.4)$$

where ΔE is total discharge energy in (mJ) and K denotes the rising slope of the electrical current, measured in terms of$\mathrm{Amp}/\mu s$.

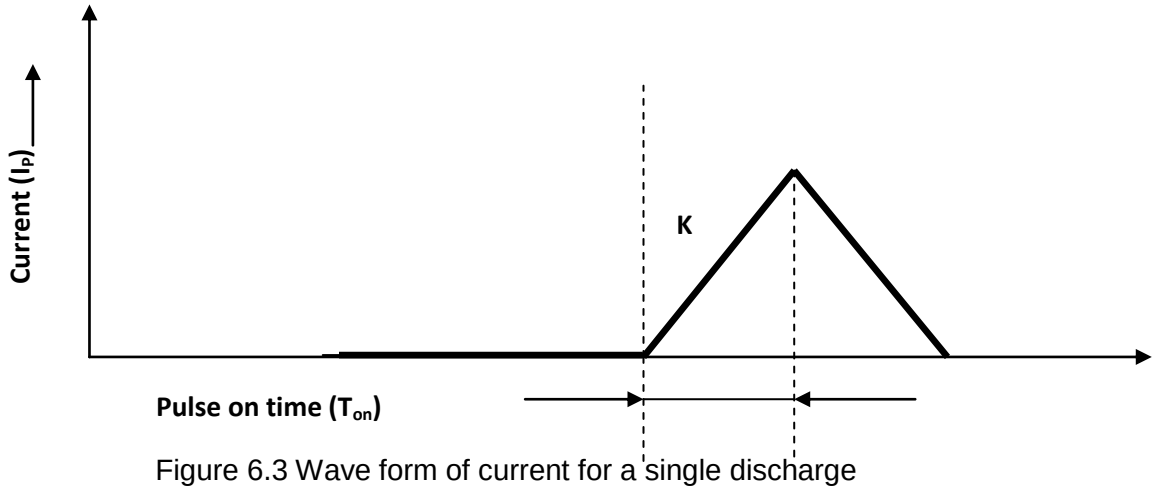

Figure 6.3 Wave form of current for a single discharge

6.3.8 Total dischargeenergy distribution

The total energy developedduring spark discharge gets scattered into three sections, a portion of it is absorbed by work piece, a portion of it is carried away by the tool and the rest is being dissolved in the dielectric liquid(Joshi and Pande 2009). Shankar et al.(1997) have recommended that 40-45% of the heat is absorbed by the work piece. Joshi and Pande (2009) have suggested an energy distribution of 1-8% for work piece and 18.3% for tool material.In this work, comparing theexperimental and numerical analysis,an energy distribution of 1.7-4.5% for work piece, 3.2-7.5% for brass tool,8.5-18% for copper tool and 8.1-14.8% for graphite tool is suggested.

6.3.9 Solution methodology of thermal analysis in ANSYS software

ANSYS^{TM} 10.0 has been employed to solve the governing equation (Equation6.1) with boundary conditions as shown in Figure 6.2 by finite element method to compute the temperature distribution. The two-dimensional, axisymmetric, thermal solid element (PLANE 55), continuum of size 0.35×0.3 mm has been considered for the thermal analysis. Model geometry is created and meshing is done with element size of 1µm. Material property such as density, specific heat and thermal conductivity is employed along with initial bulk temperature is set at 298 K. The heat flux equation is introduced (Equation6.2) and applied to the spark location on the centre of the two dimensional continuum. Temperature distribution is obtained. The node having temperature more than melting point temperature is identified and killed to eliminate from mesh. The MRR and TWR are calculated using coordinate data of the craters of work and tool material respectively.

6.3.10Solution methodology for coupled thermal-structural analysis

The extreme temperature gradient produced on the work material due to sequence of spark discharges causes residual stresses to develop on work surface.This leads to structural disorder affecting the surface integrity and reducing the fatigue life of the

machined surfaces. Therefore, it is important to know the exact value induced residual stress on the machined parts so that it can be minimized. To estimate the residual stress distribution on the work piece, a coupled thermal-structural analysis has been employed in sequence to predict the residual stresses with ANSYS 10 as the FEM solver considering two planes PLANE 55 for thermal analysis and PLANE 42 for structural analysis. After killing the elements above the melting temperature of the work piece, the residual stress distribution is estimated by solving the previously obtained temperature profiles in structural environment applying structural boundary conditions. The relation between the thermal stress analysis and thermal loading is given by

$$\{\sigma\} = [D]\{e\} - \{m\}, \tag{6.5}$$

where

$$\{\sigma\} = \{\sigma_{rr}, \sigma_{\theta\theta}, \sigma_{yy}, \sigma_{ry}\}^T, \tag{6.6}$$

$$[D] = \frac{E}{(1+\upsilon)(1-2\upsilon)} \begin{bmatrix} 1-\upsilon & \upsilon & \upsilon & 0 \\ \upsilon & 1-\upsilon & \upsilon & 0 \\ \upsilon & \upsilon & 1-\upsilon & 0 \\ 0 & 0 & 0 & \frac{1-2\upsilon}{2} \end{bmatrix}, \tag{6.7}$$

$$\{e\} = \{e_{rr}, e_{\theta\theta}, e_{yy}, e_{ry}\}^T, \tag{6.8}$$

$$\{m\} = \frac{E\alpha\Delta T}{1-2\upsilon}\{1110\}^T, \tag{6.9}$$

where D is the elasticity matrix, σ is the stress matrix, e is the strain matrix, E is the Young's modulus, v the Poisson's ratio, α the coefficient of thermal expansion, ΔT the thermal loading because of temperature change and m is the latent heat of fusion.

The structural boundary conditions (as shown in Figure 2) are given by

- $u_r = 0$and $t_y = 0$ on boundary AD;
- $u_y = 0$and $t_r = 0$ on boundary CD;
- $t_y = 0$and$t_r = 0$ on boundaries AB and BC.

6.4Modelvalidation through experimentation

The thermo-structural model determines performance parameters considering the occurrence of a single spark analysis. In actual practice the material removal in EDM during machining is influenced by many factors viz. flushing efficiency, presence of debris in dielectric fluid, ignition delay and phase change of electrode materials. However,it is utmost difficult to include these factors into the process model.In this work, thecalculation of MRR (for process parameters shown in Table 6.2) is done assuming that all sparks are equally effective with 100% flushing efficiency of dielectric fluid. To validate the above proposed numerical model the obtained results from the analysis are

compared with the experimental study carried out in chapter 3. Table 6.1 shows the temperature dependant properties of work material Inconel 718. Table 6.2 shows the comparison of the predicted results of the numerical analysis with experimental results obtained from Chapter 3.

Table 6.1 Temperature dependant material properties of Inconel 718

Temperature in ^{O}C (T)	20	100	300	500	700	900	1350
Density in kg/m^3 (ρ)	8146	8120	8052	7979	7899	7803	7300
Thermal conductivity in W/m.K (k)	11.4	12.5	14.0	15.5	21.5	26	31.3
Specific heat in J/kg.K (C)	427.14	441.74	481.74	521.74	561.74	601.74	691.74

Table 6.2 Comparison of the predicted results of the numerical analysis with experimental results from chapter 3

Run order	A	B	C	D	E	F	Numerical MRR mm^3/min	Experimental MRR mm^3/min	Numerical TWR mm^3/min	Experimental TWR mm^3/min	Numerical Residualstressin radial direction (MPa)
1	-1	-1	0	-1	0	0	19.50	18.23	4.50	4.19	1710.00
2	1	-1	0	-1	0	0	12.48	12.03	2.45	2.22	1808.00
3	-1	1	0	-1	0	0	43.20	41.20	6.20	5.79	1914.00
4	1	1	0	-1	0	0	33.10	32.50	6.10	5.88	1850.00
5	-1	-1	0	1	0	0	27.50	26.90	4.40	4.28	1747.00
6	1	-1	0	1	0	0	23.10	22.10	4.50	4.31	1808.00
7	-1	1	0	1	0	0	37.40	36.10	6.50	5.85	1835.00
8	1	1	0	1	0	0	31.90	31.20	6.10	5.90	1905.00
9	0	-1	-1	0	-1	0	27.70	26.90	4.70	4.59	1685.00
10	0	1	-1	0	-1	0	41.00	40.20	6.43	6.09	1889.00
11	0	-1	1	0	-1	0	17.40	16.10	4.10	3.99	1690.00
12	0	1	1	0	-1	0	32.00	30.50	5.50	5.00	1911.00
13	0	-1	-1	0	1	0	25.10	24.10	5.10	4.64	1729.00
14	0	1	-1	0	1	0	41.00	38.90	6.43	6.00	1861.00
15	0	-1	1	0	1	0	18.00	16.50	4.10	4.09	1742.00
16	0	1	1	0	1	0	31.10	29.80	5.50	5.08	1860.00
17	0	0	-1	-1	0	-1	13.51	12.80	8.33	7.98	1590.00
18	0	0	1	-1	0	-1	5.25	5.10	6.33	5.97	1660.00
19	0	0	-1	1	0	-1	19.00	17.90	8.50	8.00	1785.00
20	0	0	1	1	0	-1	13.50	12.50	7.50	7.02	1711.00
21	0	0	-1	-1	0	1	34.10	33.80	3.50	3.29	1845.00
22	0	0	1	-1	0	1	28.49	28.01	2.80	2.59	1820.00
23	0	0	-1	1	0	1	45.00	44.50	3.40	3.34	1800.00
24	0	0	1	1	0	1	37.00	36.10	2.80	2.64	1750.00
25	-1	0	0	-1	-1	0	22.76	22.50	5.01	4.95	1750.00
26	1	0	0	-1	-1	0	16.50	15.50	5.50	4.90	1826.00
27	-1	0	0	1	-1	0	38.10	36.70	5.05	4.92	1800.00
28	1	0	0	1	-1	0	23.70	23.50	5.15	4.96	1772.00
29	-1	0	0	-1	1	0	27.10	26.30	5.40	4.97	1780.00
30	1	0	0	-1	1	0	16.50	15.90	5.30	4.88	1826.00
31	-1	0	0	1	1	0	32.10	31.90	5.25	4.98	1800.00
32	1	0	0	1	1	0	25.10	24.70	5.30	4.99	1772.00
33	0	-1	0	0	-1	-1	7.10	6.81	7.00	6.91	1469.00
34	0	1	0	0	-1	-1	21.50	20.10	9.00	8.81	1794.00
35	0	-1	0	0	1	-1	7.10	7.01	7.10	6.94	1469.00
36	0	1	0	0	1	-1	21.30	20.20	9.10	8.89	1794.00
37	0	-1	0	0	-1	1	21.00	20.05	2.40	2.28	1800.00
38	0	1	0	0	-1	1	50.10	48.80	3.98	3.91	1920.00

39	0	-1	0	0	1	1	26.20	26.12	2.40	2.34	1800.00
40	0	1	0	0	1	1	50.10	48.90	3.98	3.94	1920.00
41	-1	0	-1	0	0	-1	19.00	18.20	8.33	7.94	1725.00
42	1	0	-1	0	0	-1	13.00	11.95	8.01	7.91	1681.00
43	-1	0	1	0	0	-1	13.10	11.85	7.20	6.98	1714.00
44	1	0	1	0	0	-1	6.50	5.92	7.50	7.00	1535.00
45	-1	0	-1	0	0	1	44.02	43.10	4.00	3.88	1798.00
46	1	0	-1	0	0	1	35.72	35.10	4.01	3.95	1777.00
47	-1	0	1	0	0	1	35.96	35.90	2.80	2.69	1879.00
48	1	0	1	0	0	1	27.50	27.10	2.75	2.74	1829.00
49	0	0	0	0	0	0	21.00	18.50	4.90	4.79	1757.00
50	0	0	0	0	0	0	21.00	21.50	4.90	4.69	1757.00
51	0	0	0	0	0	0	21.00	16.70	4.90	5.09	1757.00
52	0	0	0	0	0	0	21.00	20.40	4.90	4.59	1757.00
53	0	0	0	0	0	0	21.00	18.30	4.90	5.09	1757.00
54	0	0	0	0	0	0	21.00	19.60	4.90	4.54	1757.00

From Table 6.2, it is clear that the values of the responses predicted by numerical model are closer to the experimental results for MRR, TWR and residual stress (RS) in radial direction. Thus, it can be concluded that the numerical model providesaccurate prediction of responses which confirms the validation of the numerical model. Figures 6.4-6.6 showscraters predicted by the numerical analysis while machining with brass, copper and graphite tool respectively. It is easily noticeable that craters produced with graphite electrode are wider and deeper which leading to higher MRR whereas craters produced with brass electrode are narrow and smaller having less MRR. Craters predicted through copper tool are slightly smaller in radius and depth in comparison to graphite tool. The higher thermal conductivity of graphite and copper electrode generates higher value of spark energy in between electrodes in comparison to brass tool causing higher amount of material to be removed while machining with graphite and copper tool.

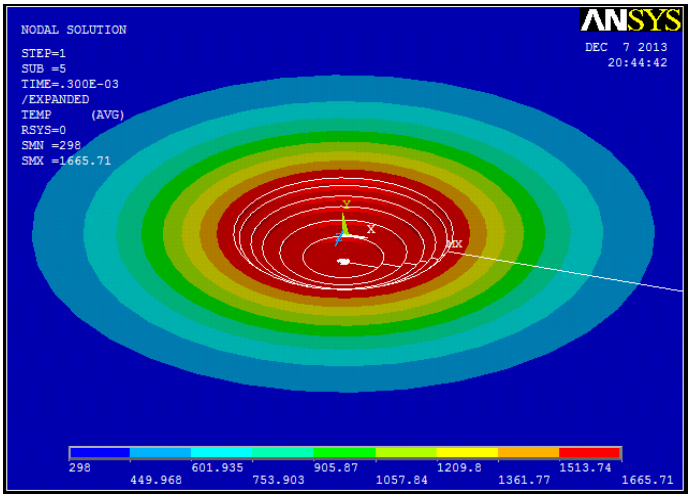

Figure 6.4 Predicted crater of MRR 5.25 mm^3/min at open circuit voltage 80V, discharge current 5 A, pulse-on-time 300µs, duty factor 80% flushing pressure 0.3 bar machined with brass toolfor 18th reading

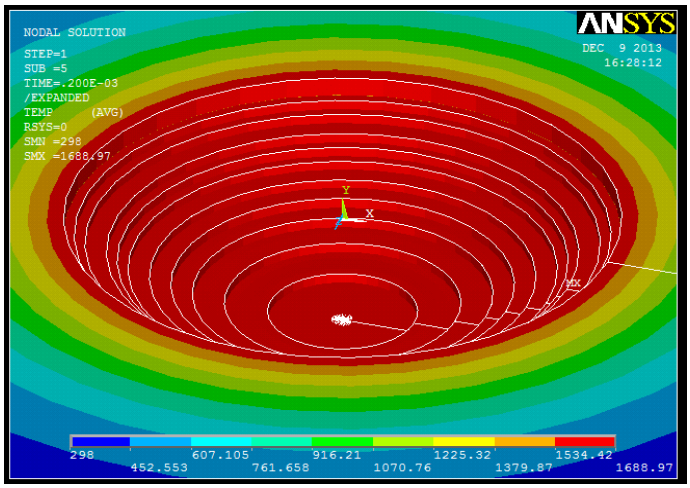

Figure 6.5 Predicted crater of MRR 38.1 mm^3/min at open circuit voltage 70V, discharge current 5 A, pulse-on-time 300µs, duty factor 90%flushing pressure 0.2 bar machined with copper tool for 27th reading

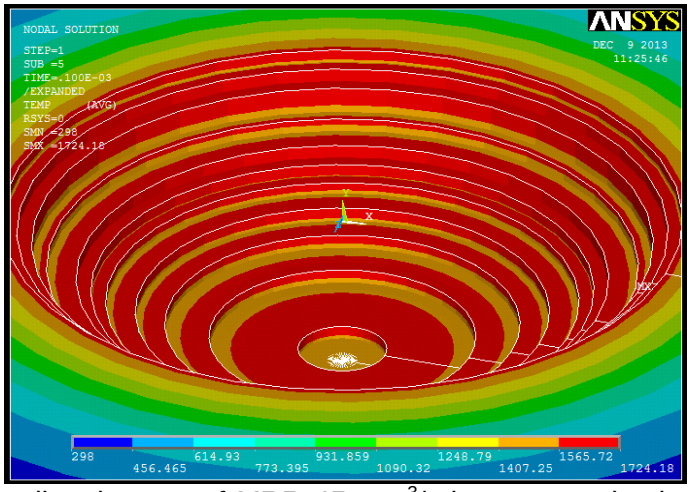

Figure 6.6 Predicted crater of MRR 45 mm^3/min at open circuit voltage 80V, discharge current 5 A, pulse-on-time 100µs, duty factor 90% flushing pressure 0.3 bar machined with graphite tool for 23th reading

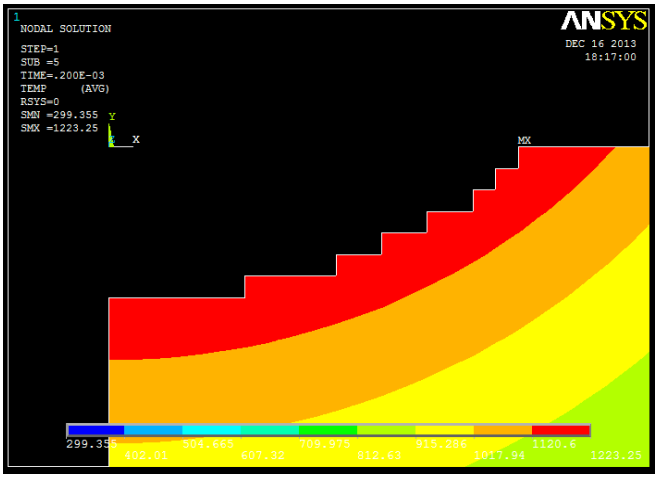

Figure 6.7 Predicted TWR of 9 mm^3/min at open circuit voltage 80V, discharge current 7A, pulse-on-time 200µs, duty factor 85%,flushing pressure 0.2 bar,brass tool for 34th reading

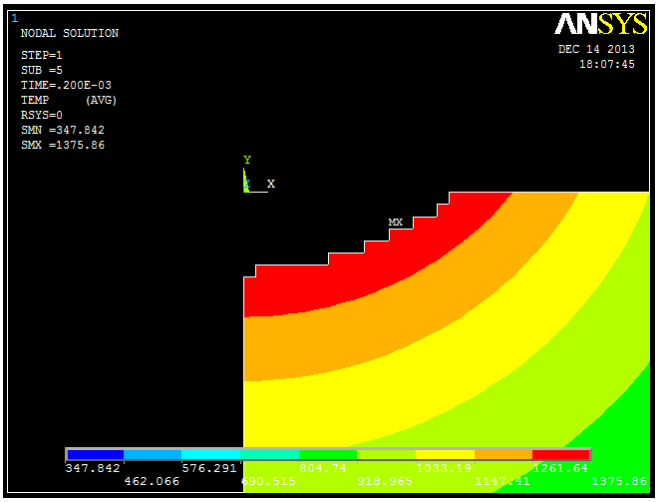

Figure 6.8 Predicted TWR of 6.1 mm^3/min at open circuit voltage 90V, discharge current 7A, pulse-on-time 200µs, duty factor 80%,flushing pressure 0.3 bar, copper tool for 4th reading

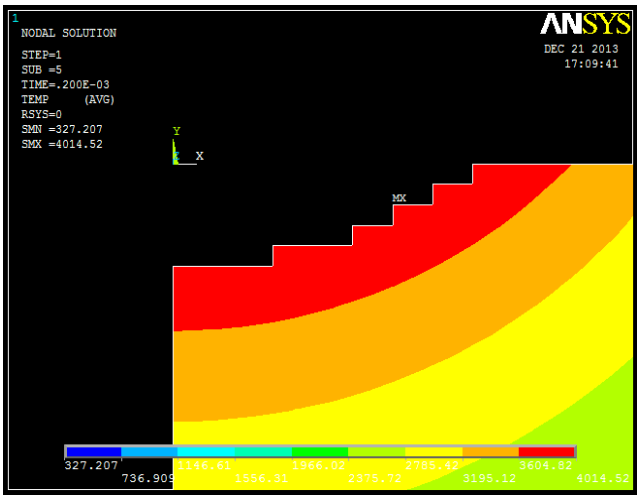

Figure 6.9 Predicted TWR of 3.98 mm^3/min at open circuit voltage 80V, discharge current 7A, pulse-on-time 200µs, duty factor 85%,flushing pressure 0.2 bar, graphite tool for 38th reading

Figures 6.7-6.9 shows tool wear occurred on a two dimensional axisymmetric model in brass, copper and graphite tool respectively. It is quite clear that tool wear on brass tool is higher while machining Inconel 718 in comparison to copper tool and graphite tool. This is probably due to high melting point temperature and high thermal conductivity of graphite and copper tool material leading to minimal tool wear in comparison with brass tool.

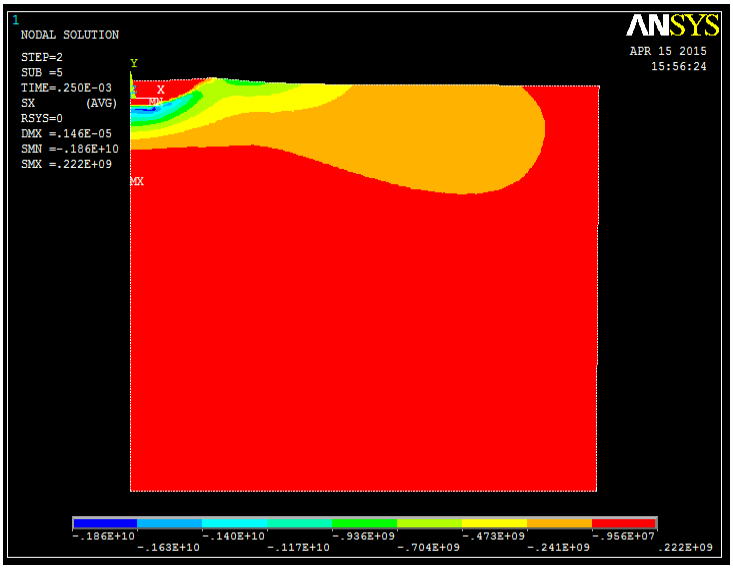

Figure 6.10 Thermal stress directly after heat flux in radial directionat open circuit voltage 90V, discharge current 7A, pulse-on-time 200µs, duty factor 80%, flushing pressure 0.3 bar, copper tool for 4th reading

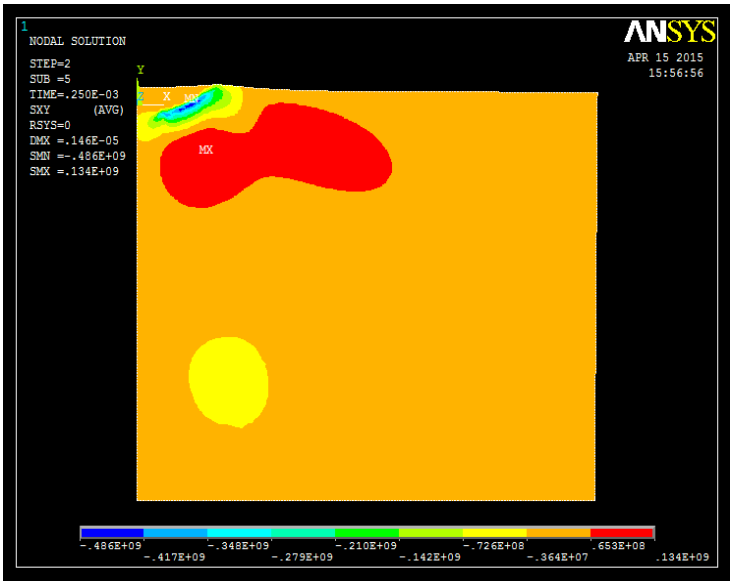

Figure 6.11 Thermal stress directly after heat flux in circumferential directionat open circuit voltage 90V, discharge current 7A, pulse-on-time 200µs, duty factor 80%, flushing pressure 0.3 bar, copper tool for 4th reading

Figures 6.10 and 6.11 shows the finite element stress distribution of the thermal stress directly after the heat flux in radial and circumferential direction respectively. It is

to be noted that the stresses being developed just below the spark is compressive whereas the stresses away from the spark is tensile.This is obvious, as the work piece heats up after application of heatflux; it unable to expand immediatelyleading to generation of compressive thermal stresses in beneath the crater. Similar trend of thermal stress distribution has been also observed in the structural model of Alen and Chen (2007).

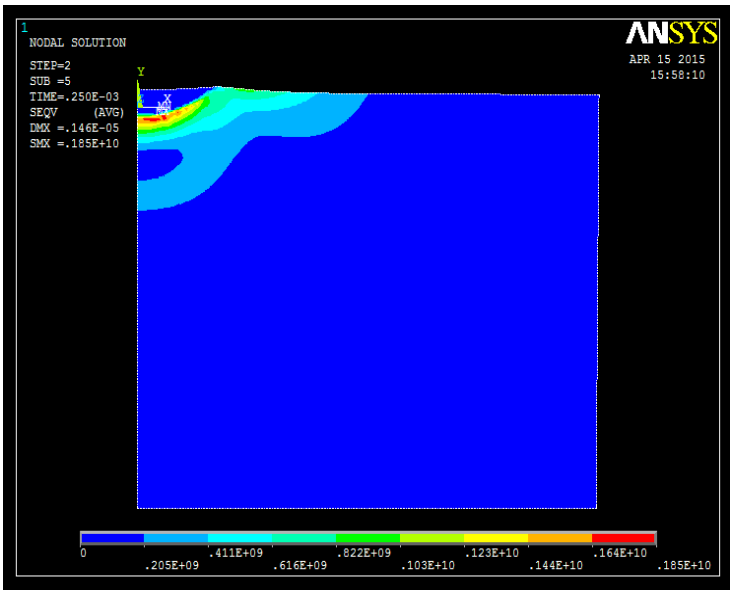

Figure 6.12 Residual thermal stress in radial directionat open circuit voltage 90V, discharge current 7A, pulse-on-time 200µs, duty factor 80%, flushing pressure 0.3 bar, copper tool for 4th reading

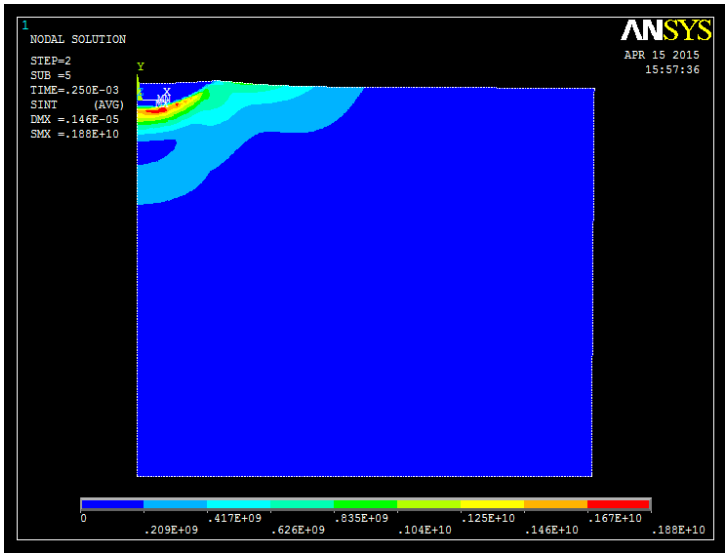

Figure 6.13 Residual thermal stress in circumferential directionat open circuit voltage 90V, discharge current 7A, pulse-on-time 200µs, duty factor 80%, flushing pressure 0.3 bar, copper tool for 4th reading

Figures 6.12 and 6.13 shows the residual stress remaining in the work piece in radial and circumferential direction respectively after the work piece reaches to the room

temperature. The compressive stress beneath the crater changes to tensile stress after completion of cooling period. The tensile stresses are at their highest near the crater of the work material and moving away from crater the value decreases gradually. It is to be noted that stress distribution of radial and circumferential stress components are similar after the completion of cooling period. A similar trend has been also reported in the numerical investigation of Alen and Chen (2007) which confirms the validation of the structural model.

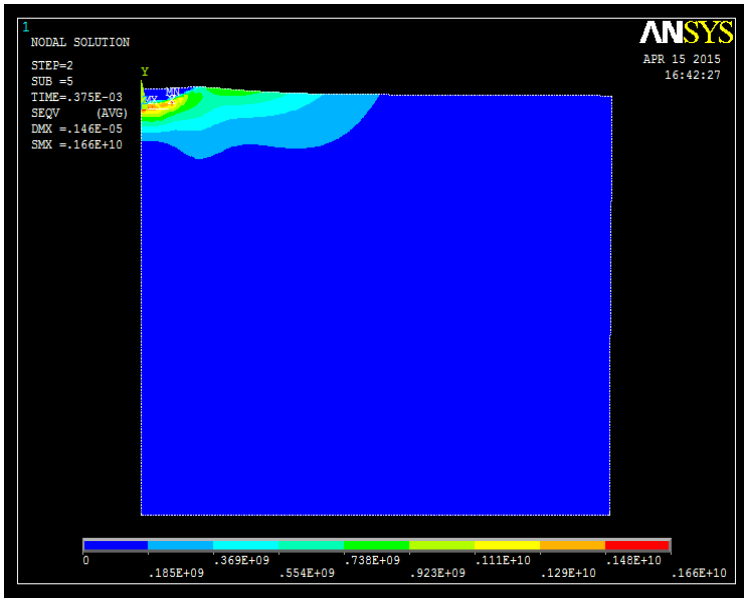

Figure 6.14 Predicted residual thermal stress of 1660MPa in radial direction at open circuit voltage 80V, discharge current 5 A, pulse-on-time 300µs, duty factor 80% flushing pressure 0.3 bar machined with brass tool for 18th reading

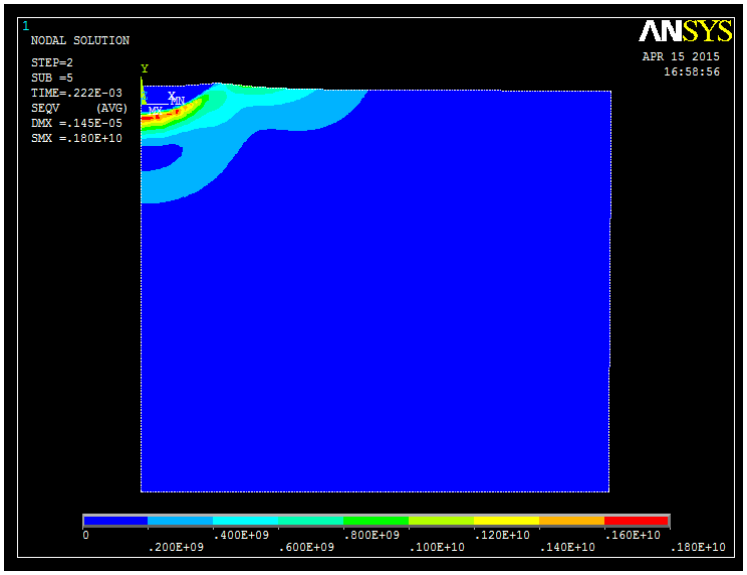

Figure 6.15 Predicted residual thermal stress of 1800MPa in radial direction at open circuit voltage 70V, discharge current 5 A, pulse-on-time 200µs, duty factor 90%flushing pressure 0.2 bar machined with copper tool for 27th reading

Figures 6.14-6.16 shows the residual stresses developed on work piece in radial direction while machining with brass, copper and graphite tool respectively. From the figures it can be observed that the residual stress developed on work material Inconel 718 is comparatively higher while machining with graphite and copper electrode in comparison to brass electrode. Due to higher thermal conductivity of the graphite and copper electrode the spark energy in between electrodes is higher in comparison to brass. This induces higher value of residual stress on the work surface. However,owing to poor thermal conductivity of brass electrode smaller value of material is eroded from the machined surface, which induces smaller residual stress on the machined surface.

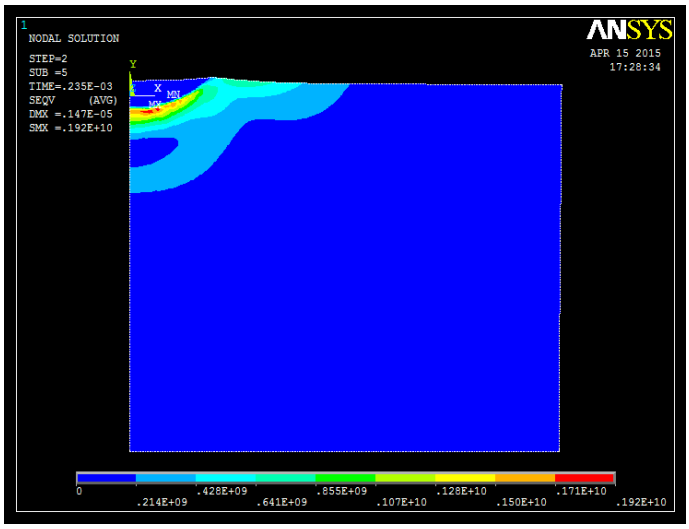

Figure 6.16Predicted residual thermal stress1920MPain radial direction at open circuit voltage 80V, discharge current 7 A, pulse-on-time 200µs, duty factor 85%flushing pressure 0.2 bar machined with graphite tool for 38th reading

In this work, the predicted values of residual stress are compared with earlier studies reported by researchers Das et al. (2003) and Allen and Chen (2007).The figures indicate that higher value of residual stress is near to the spark locality. This particular stress is primarily responsible for the formation of micro-cracks and voids which are observed so often on machined surface during SEM analysis.It is to be noted that using L_6 steel work piece Das et al. (2003) have found residual stress value higher than the ultimate tensile strength of the material. In this work, Inconel 718 is used as work material which possesses an ultimate tensile strength of about 1300 MPa. From Table 6.2 it can clearly observed, that the predicted values of the residual stress are higher than ultimate tensile strength of Inconel 718 work piece. This is clear indication that micro cracks and voids will definitely occur on the machined surface. To relate this phenomenon with the experimental analysis, the microcracks and voids are clearly visible on the machined surface thorough SEM analysis in chapter 3 figures 3.5 and 3.6. Even if, theorders of magnitude of stresses do not match, the distribution of stress

matches well with studies reported by previous researchers (Das et al. 2003;Allen and Chen 2007). The difference in stress value is due to the difference in thermal and mechanical properties and different machining condition of both the materials. However,the largest value of residual stress obtained by Allen and Chen (2007) using molybdenum work piece is only 376Pa. This is due to the higher thermal conductivity of molybdenum work piece (138 W/m.K), which is much higher than thermal conductivity of Inconel 718(11 W/m.K) which allows easy dissipation of heat and induces smaller value of residual stress on the machined surface.

6.4.1 Experimental Validation of Residual Stress

It is not easy tovalidatethe residual stress resultsobtained from a single spark analysis by comparing the same with experimentally obtained results from the multi-spark analysis (Das et al. 2003). However, in this work the work material used in Chapter 3(Inconel 718) after machining is subjected to the X-Ray Diffraction analysis to estimate the induced residual stressexperimentally and is compared with predicted results of the thermo-structural model. The X-ray diffraction measurement is performed in an advanced X-ray Diffraction System BRUKER D8 Discover operating at 40 kV and 40 mA is shown in Figure 6.17(a). Figure 6.17(b) shows the work material on experimental set up.

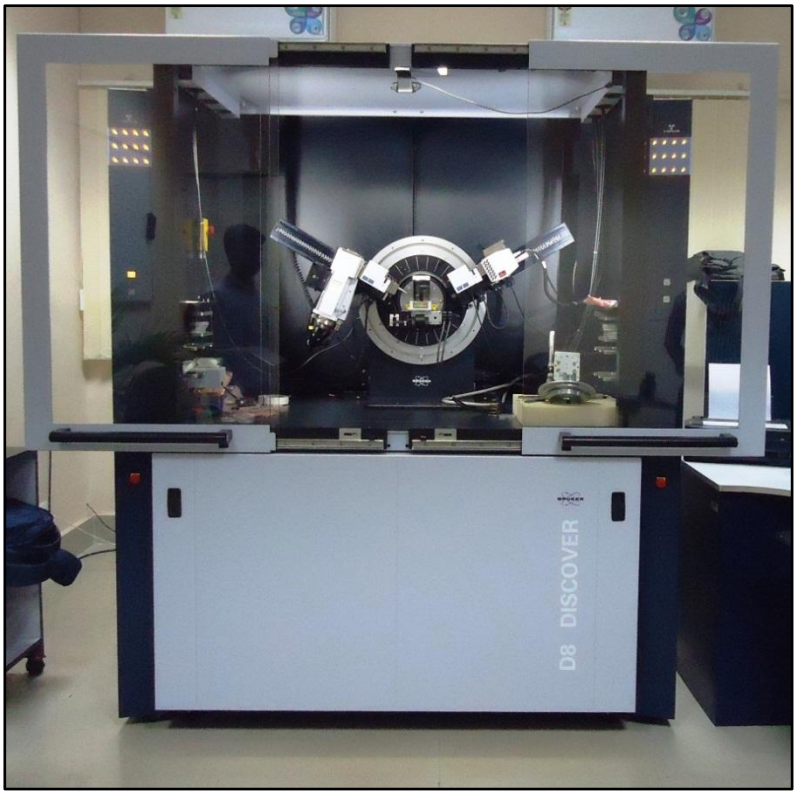

(a) X-ray Diffraction machineBRUKER D8 Discover

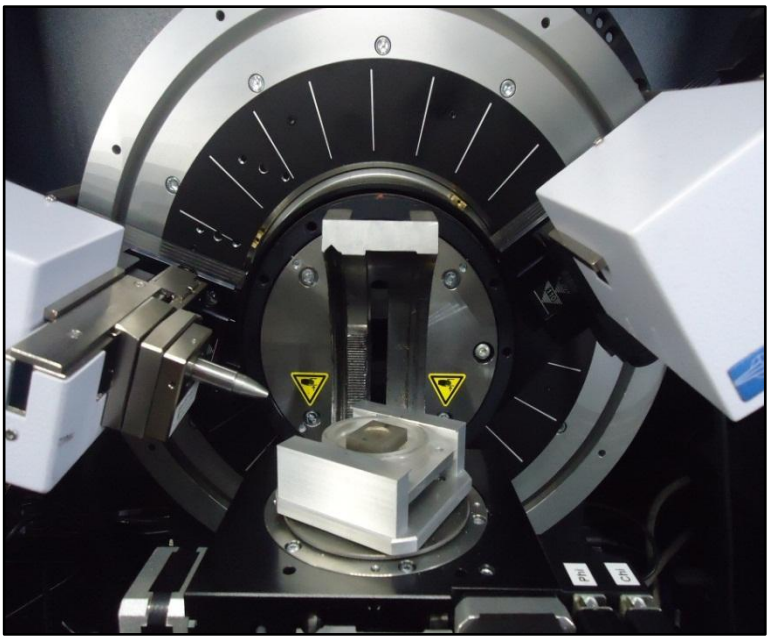

(b) Work material Inconel 718 on Experimental set up

Figure 6.17 X-ray Diffraction machine BRUKER D8 Discover

For experimental stress measurement the work material is cut in to number of small pieces so as to fit in the holder of the machine. The X-ray Diffraction System is provided with a vertical goniometer equipped with a Cu-radiation source, $\lambda_{CuK\alpha}$= 1.54 A.The plane considered for the analysis was (3 1 1) andtilt angle 'ψ' was varied from ± 45^{o}.The residual stress profiles are conventionally analysed using sin^{2}ψ method. Peak positions were calculated using the conventional Gaussian curve fitting and the slope of the line represents the magnitude of the residual stress for a given Sin^{2}ψ. This calculation was performed usingthe commercial software Leptos 7 by BRUKER. Figure 6.18 shows the strain versussin^{2}ψ plot of Inconel 718.The X-ray diffraction patterns of the measure peak of thework material Inconel 718 at different tiltangles (ψ) is shown in Figure 6.19. Boththe figures shown here are meant for a particularsample i.e. for experiment no 1 only. Similar procedure was adopted tomeasure the residual stresses for other sample.

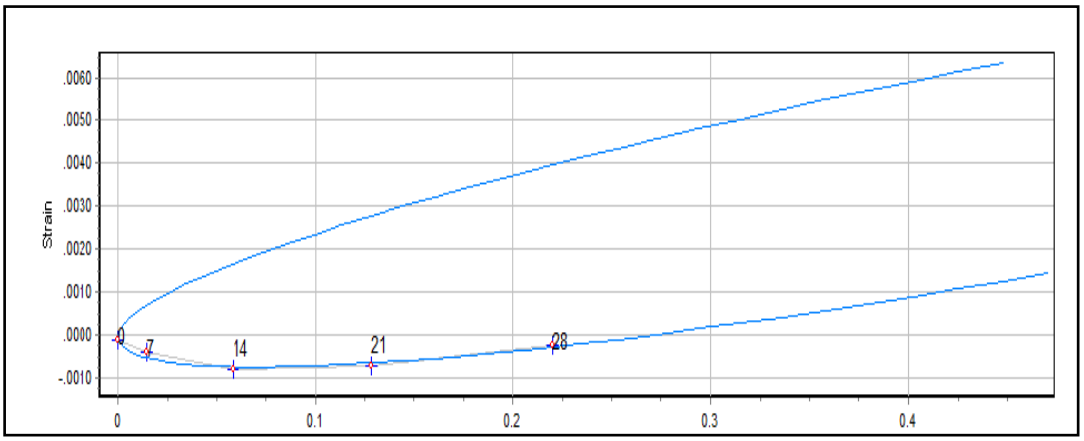

Figure 6.18 Strain Versus Sin^{2}ψ plot

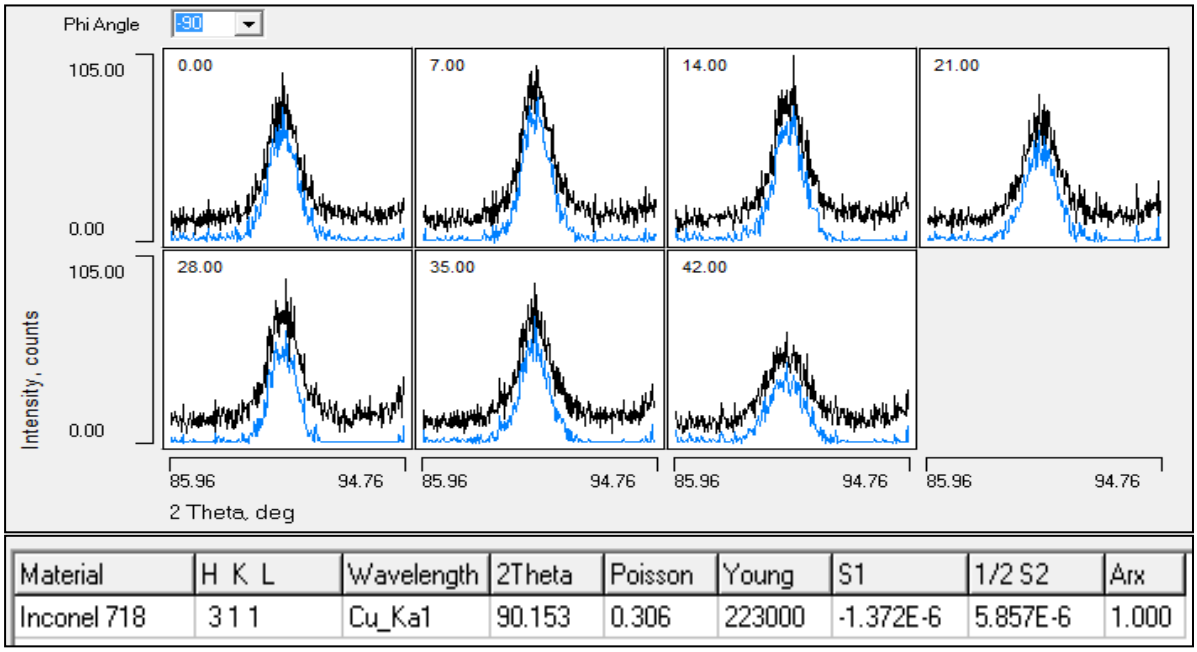

Material	H K L	Wavelength	2Theta	Poisson	Young	S1	1/2 S2	Arx
Inconel 718	3 1 1	Cu_Ka1	90.153	0.306	223000	-1.372E-6	5.857E-6	1.000

Figure 6.19X-ray diffraction peak of Inconel 718 at different tilt (ψ) angles

Table 6.3 shows calculated values of the residual stress obtained through experimental investigationin radial and circumferential directionsin comparison with numerical results along with machining conditions. From the table it can be observed thatalthough the exact values of experimental and numerical results of stresses do not match, the order of magnitude of the predicted values of stress obtained through the thermo-structural model isexistingwithin the results of the experimental investigation. Hence, it can be concluded that the thermo-structural model provides reasonably accurate prediction of responses.

Table 6.3 Residual stress value obtained through experimental investigation in comparison with numerical results along with machining conditions

Run order	A in Volt	B in Amp	C in µs	D in %	E in Bar	F Tool	Expt. Stress in radial direction (MPa)	Num. Stress in radial direction (MPa)	Expt. Stressin circumferential direction (MPa)	Num. Stress in circumferential direction (MPa)
1	70	3	200	80	0.3	Copper	1650±210	1780	-468±80	-486
2	90	3	200	80	0.3	Copper	1686±250	1808	-480±92	-505
3	70	7	200	80	0.3	Copper	1805±210	1914	-585±115	-562

6.5 Parametric study on the proposed model

Parametric investigations were conducted by the proposed numerical EDM process model with an objective to realize the impact of input process parameters on the responses.The input parameters such as discharge current is varied from 3 to 13 Amp in the steps of 2 Amp, pulseontime is varied from 100 to 400µs in steps of 100µs, duty factor is varied from 80 to 90% in steps of 5%, and break down voltage is varied from 40

to 50V in steps of 5V. More than one hundred twenty numerical simulations were conducted to investigate the influence of selected processes parameters on the responses.

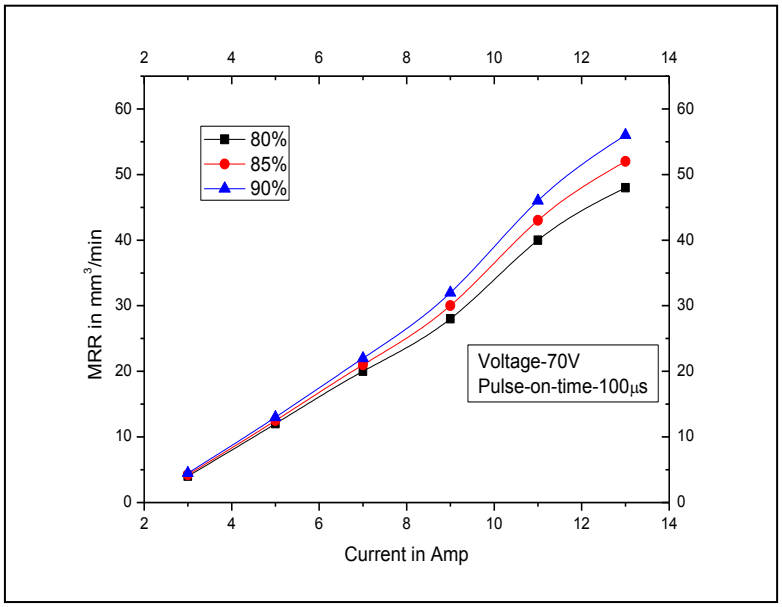

Figure 6.20 Variation of MRR with discharge current

6.5.1 Effect of discharge current on MRR, TWR and residual stress

The mostdominant process parameters in EDM process is discharge current as it significantly affects the total discharge energy. Figure 6.20shows the variation of MRR with discharge current. It is clearly evident that MRR increases briskly with increaseindischargecurrentfor any value of dutyfactor. As the duty factor increases, the increase of MRR with increase of discharge current is more pronounced. Smaller values of discharge current and duty factor lead to better surface finish during machiningwhile greater values are suggested for rough and course machining.

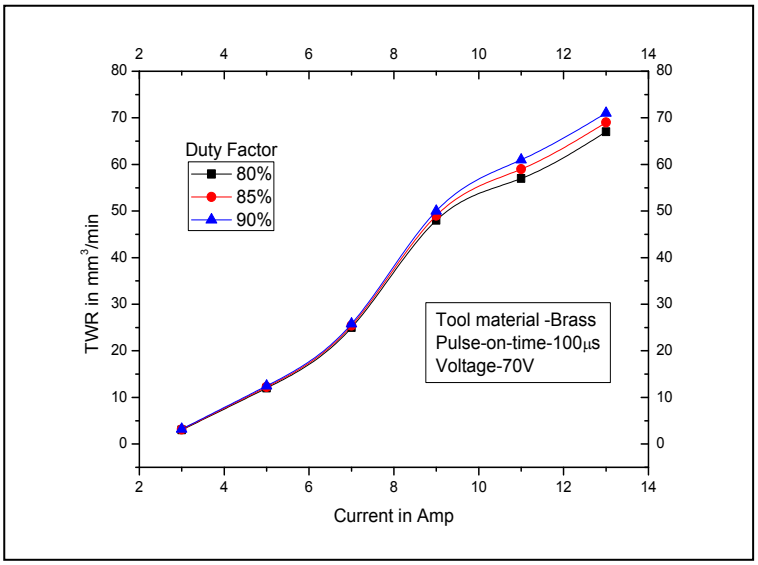

Figure 6.21 Variation of TWR with discharge current

Figure 6.21 shows the variation tool wear rate with discharge current. Figure shows thaterosion of tool is faster at higher values of discharge current and duty factor which results decreasingproductivity and increasing the cost of machining of the EDM process. So, smaller value of discharge current and duty factor are suggested with minute tool wear for increasing productivity of the process.

Figure 6.22 shows the variation of residual stress with discharge current. Residual stress increases rapidly with increase in discharge current and voltage affecting the surface integrity and reducing the fatigue life of the machined surfaces. Hence, moderate ranges of discharge current and voltage can be adopted for least stresses to be developed on machined surface with an objective to maximize the material removal rate.

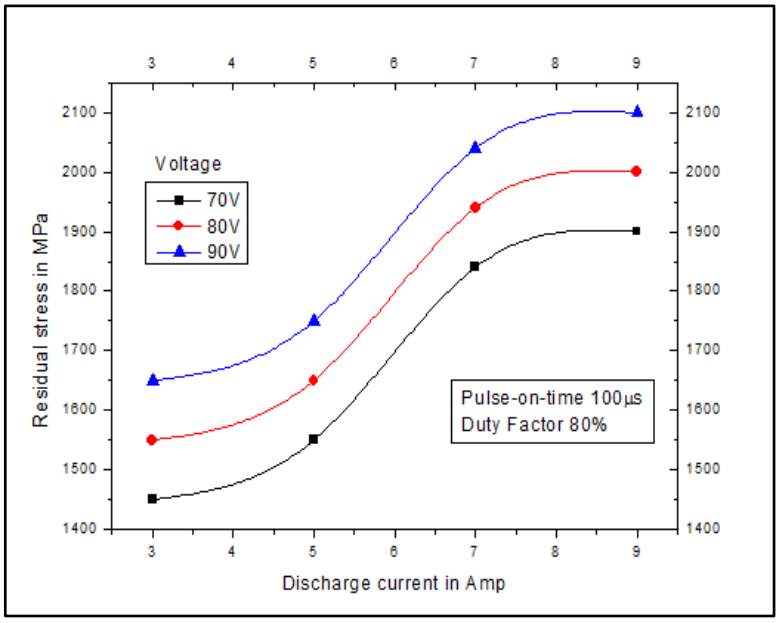

Figure 6.22 Variation of residual stress with discharge current

Figures 6.23 and 6.24shows the variation in crater radius and crater depth with discharge current. It is quite clearly evident that both crater radius and depth increase monotonically with increase in discharge current. Therefore, higher value of discharge current produces wider and deeper holes which will lead to higher material removal but causes rough machining. For finishing machining operation, smaller ranges of discharge current can be suggested subjected to smaller and narrow craters.

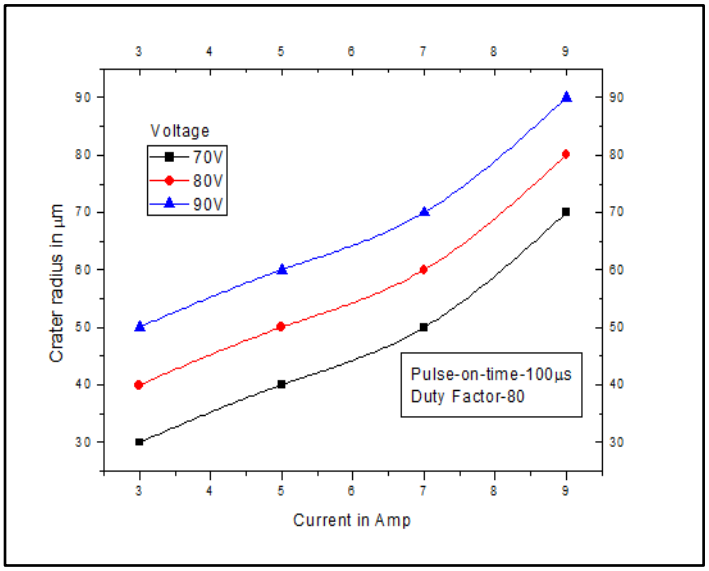

Figure 6.23 Variation of crater radius with discharge current

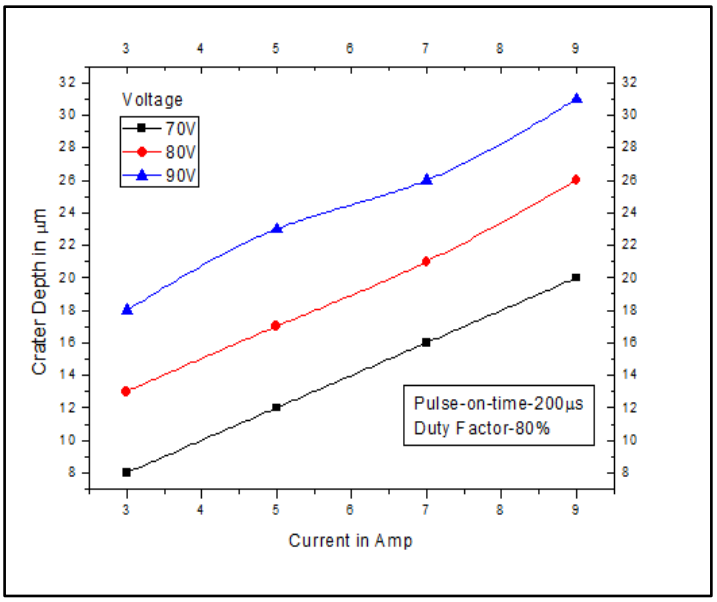

Figure 6.24 Variation of crater depth with discharge current

6.5.2Effect of pulse-on-time on MRR, TWR and residual stress

The interval for which the total discharge energy is to be applied on the work surface is called as pulseontime. It is an important process parameter in EDM process as it decides spark duration. Figure6.25 shows the variation of MRR with pulseontime.It shows an increasing trend with increase in pulseontime initially and then shows a reducing trend before reaching an extreme value. This is perhaps due to constant duty factorwhich is causing a reduction in flux density due to lack of sparks. Similar observations have also been observed by Joshi and Pande (2009)and experimental

investigation of Panda and Bhoi (2005).Smaller value of pulseontime usually (100-250)µscan be adopted for improved MRR which might cause rough machining while, higher value of pulseontime greater than 250µsare suggested for finishing machining operation.

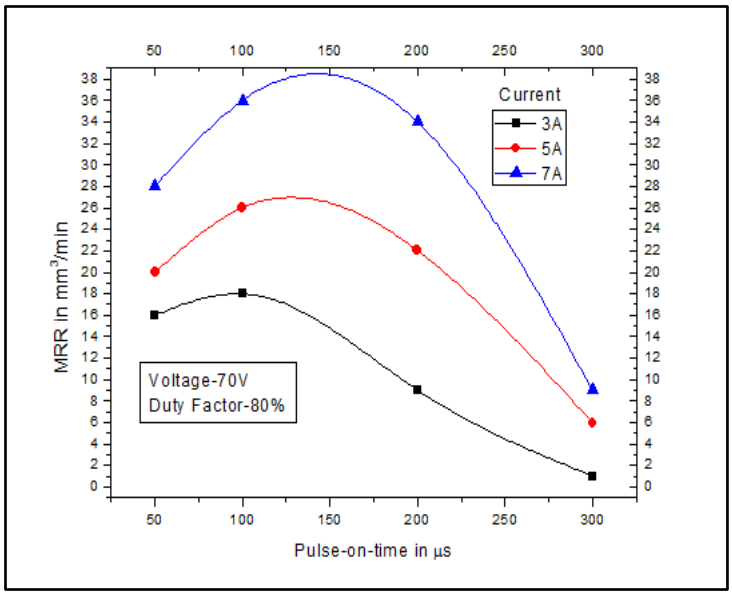

Figure 6.25 Variation of MRR with pulse-on-time

Figure 6.26 shows the variation of residual stress with pulse on time. It shows a decreasing trend with increase in pulse on time. Constant duty factor is causing a reduction in flux density decreasing the heat affected zones leading to fall in residual stress. Hence, moderate range of current and higher value of pulse on time, usually greater than 300µs, is recommended for increased MRR and small residual stresses on wok piece during machining.

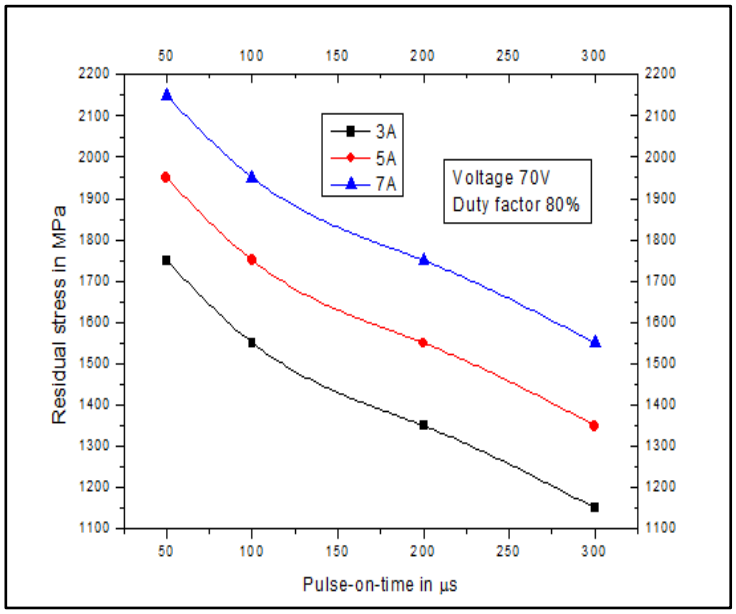

Figure 6.26 Variation of residual stress with pulse-on-time

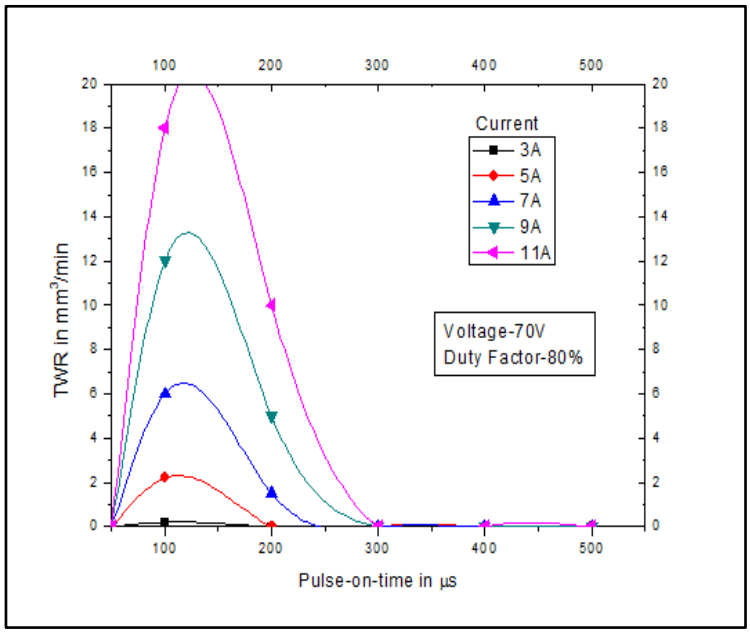

Figure 6.27 Variation of TWR with pulse-on-time brass tool

Figure 6.27 show the variation in tool wear with pulseontime on the copper tool. Following the trend of material removal rate, tool wear also increases with increase in pulseontime initially but shows a decreasing trend further before reaching an extreme value matching to the numerical analysis of Joshi and Pande (2009). This is perhaps due to constant duty factor which is causing a reduction in flux density due to lack of sparks. Spark duration of greater than 300µs is convenient for finishing machining condition as tool wear is minimal.

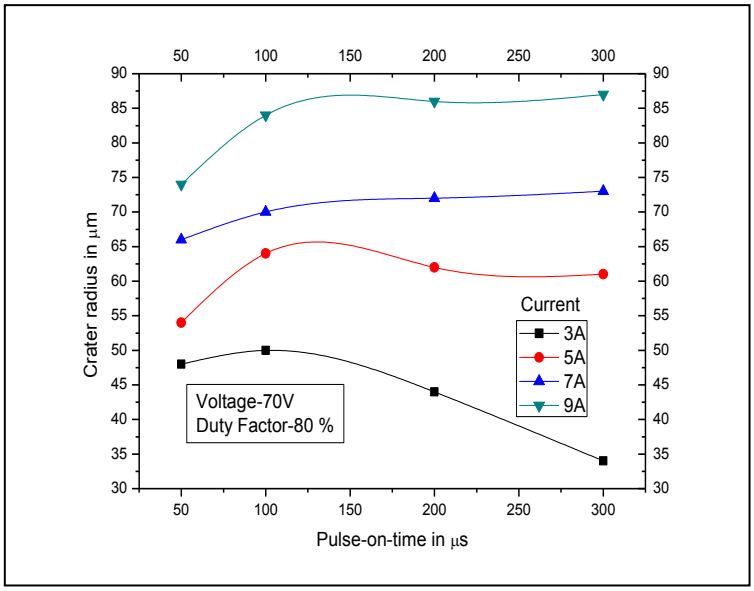

Figure 6.28 Variation of crater radius with pulse-on-time

Figures6.28 and 6.29 shows the variation in crater radius and crater depth with pulseontime respectively. Crater radius increases slightly with increase in pulseontime and remains constant at higher values of current but tends to decrease for lower value of current (5 amp.). However, crater depth shows a decreasing trend with increase in pulse-on-time. Since duty factor is remaining constant, number of sparks per unit time decreases with the increase of pulse-on-time causing decrease in crater radius and crater depth. As a result, MRR per pulse gets reduced.

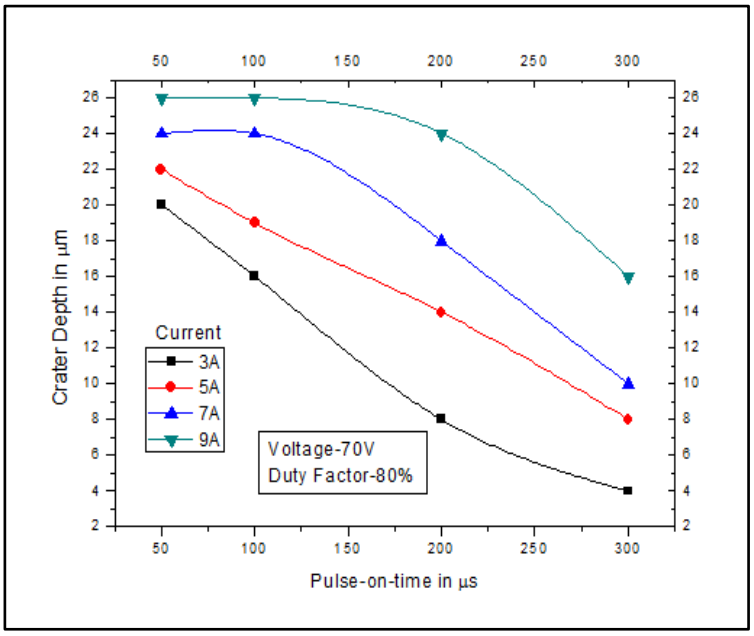

Figure 6.29 Variation of crater depth with pulse-on-time

5.3 Effect of duty factor on MRR, TWR and residual stress

The important process parameter which controls the number of sparks per unit time is the duty factor. It is defined as the ratio of pulseontime to total spark time. Higher values of duty factor indicateincrease in number of sparks per unit time. It can be observed from Figures 6.17 and 6.18 that increase in duty factor results in increase of MRR and TWR. For finishing machining condition, smaller valuesof duty factor can be suggested while upper ranges can be recommended for higher MRR with more tool wear.However, duty factor doesnot contribute much to the variation of residual stresses.

6.6 Conclusions

A numerical approach of modelling of electrical discharge machining on Inconel 718 super alloy has been presented in this chapter.The results obtained by numerical analysis are validated through extensiveexperimentation on a die-sinking EDM machine. It can be concluded, that numerical method provides reasonably accurate estimation of responses. The proposed model provides an inexpensive time saving alternative to study

the performance of machining before going for actual cutting operation.Parametric study is carried out on important process parameters to study their effects on responses. The proposed model can be used for selecting ideal process states to improve EDM process efficiency and finishing capability.The approach can be extended to study machining behaviour of other work-tool piece combinations. Therefore, prediction of residual stresses helps the tool engineers to go for robust machining operation. Some of the major findings from the model are discussed in the paragraph below.

The parametric study carried on proposed model indicates that discharge current, open circuit voltage, and pulse-on-time exhibit significant effect on performance measures. It is observed that craters produced with graphite and copper electrodes are wider and deeper in comparisontocrater produced withbrass electrode leading to higher MRRfor copper and graphite electrode. Owing to higher thermal conductivity tool wear is minimal while machining with graphite and copper electrode in comparison to brass electrodes. The thermo-structural model proposed in the study, shows that compressive stresses developed beneath the crater and moving away from crater both radially and axially the stress becomes tensile.On comparison of experiment numbers 18 (brass tool) and 22 (graphite tool) shown in Table 6.2, it is observed that residual stress can be reduced up to 8.97% if machined with brass tool.

CHAPTER 7

EXECUTIVE SUMMERY AND CONCLUSIONS

7.1 Introduction

This work explores the influence of different tools, deep cryogenic treatment of tools subjected to different soaking duration and a hybrid approach of powder mixed EDM of cryogenically treated electrodes on machinability of Inconel 718 super alloy through extensive experimentation and analysis. The data collected for the study is based on a Box-Behnken design, a popular response surface methodology. Regression analysis is conducted to relate the machining parameters with the performance measures. A novel multi-objective particle swarm optimization (MOPSO) algorithm has been adopted for simultaneous optimization of multiple objectives.The best ranked solution is identified from a large number of non-dominated solutions applying maximum deviation theory.Finally, a thermal model based on finite element method has been proposed to predict the MRR and TWR when work piece is machined with different electrode materials. A coupled thermo-structural model has been also proposed to estimate the residual stresses.

7.2 Summary of finding

Extensive experimental and numerical simulationsare carried out to analyze theinfluence of important process parameters on performance measures of the EDM process. Some of the major findings from this research work are discussed in the paragraphs below:

From the exhaustive study of different tool materials (Chapter 3), it is observed that tool material, discharge current and pulse-on-time are found to be the important process parameters for all the performance measures while machining Inconel 718. From ANOVA table (Table 3.6), it is observed that tool material is the most influential parameter for MRR with highest percentage of contribution of 49.74% followed by discharge current, pulse-on-time, open circuit voltage and duty factor with percentage contribution of 24.76%, 5.48%, 5.40% and 4.16% respectively. From Table 3.7, it is observed that tool material is found to be the most influential parameter for EWR with highest percentage of contribution of 61.84% followed by discharge current, pulse-on-time, open circuit voltage and duty factor with percentage contribution of 2.44%, 2.37%, 1.76% and 1.56% respectively.From Table 3.8, it is observed that tool material is found to be the most influential parameter for surface roughness with highest percentage of contribution of 67.13% followed by discharge current, pulse-on-time and open circuit voltage with percentage contribution of 16.88%, 3.78% and0.16% respectively.From Table 3.9, it is observed that tool material is found to be the most influential parameter for radial overcut with highest percentage of contribution of 85.56%, followed by discharge current, pulse-on-time and duty factor with percentage

contribution of 8%, 2.56% and 0.07% respectively. From Table 3.10, it is observed that tool material is found to be the most influential parameter for white layer thickness with highest percentage of contribution of 96.94% followed by discharge current, pulse-on-time and duty factor with percentage contribution of 1.53%, 0.14% and 0.09% respectively. Material removal is comparatively high while machining with graphite tool followed by copper and brass. Due to high value of spark energy between electrodes, graphite and copper electrodes exhibit high MRR in comparison to brass electrode. EWR is comparatively less with the use of graphite electrode followed by copper electrode because low TWR and high MRR is observed.Brass electrode exhibits the poorest performance with regard to EWR due to high TWR. Brass tool at small values of discharge current produces fine surface quality followed by copper and graphite tools due to small spark energy between electrodes causing erosion of smaller size particle from machined surface. On comparison of experiment numbers 18 (brass tool) and 22 (graphite tool) shown in Table 3.5, it is observed that MRR can be increased up to 449.21% whereas EWR can be reduced up to 92.08% while machining with graphite electrode. It is also observed that surface roughness, radial overcut and white layer thickness can reduced up to 52.77%, 77.65% and 63.85% respectively while machining with brass electrode. Graphite electrode exhibits the poor performance in regard to the radial overcut followed by copper due to high MRR. Brass electrode at small values of discharge current produces precise and accurate EDMed components owing to small MRR suited for finishing operation. Owing to higher MRR, graphite electrode produces thicker white layer thickness on the machined surface. Brass electrode at small values of spark energy produces small value of white layer on the machined surface. Copper electrode produces white layer value those between graphite and brass.Hence, it can be concluded that graphite tool is more favorable than the copper and brass electrodes for machining of Inconel 718 work material if high material removal and low tool wear is desired, particularly in roughing operation.

From the study of cryogenic treatment of tool (Chapter 4), it is observed that the thermal conductivity and micro-hardness of brass electrode improves as soaking duration increases (Table 4.3). The treated tools help in effective heat transfer away from the electrode increasing the wearing resistance of the tool. From ANOVA table (Table 4.5), it is observed that discharge current is found to be the most influential parameter for MRR with a percentage contribution of 58.48% followed by pulse-on-time, open circuit voltage and duty factor with percentage contribution of 5.85%, 5.62% and 4% respectively. From Table 4.6, it is observed that soaking duration is found to be the most influential parameter for EWR with

percentage contribution of 78.35% followed by discharge current, pulse-on-time, duty factor and open circuit voltage with percentage contribution of 10.66%, 2.13%,1.04% and 0.64% respectively.From Table 4.7, it is observed that soaking duration is found to be the most influential parameter for surface roughness with percentage contribution of 58.99% followed by discharge current, pulse-on-time and duty factor with percentage contribution of 18.60%, 9.62% and 0.39% respectively.From Table 4.8, it is observed that soaking duration is found to be the most influential parameter for radial overcut with percentage contribution of 79.01% followed by discharge current, pulse-on-time and duty factor with percentage contribution of 8.88%, 2.83% and1.18% respectively.From Table 4.9, it is observed that soaking duration is found to be the most influential parameter for white layer thickness with percentage contribution of 95.55% followed by discharge current, pulse-on-time and duty factor with percentage contribution of 2.87%, 0.22% and 0.04% respectively. The study confirms that significant reduction in EWR, surface roughness, radial overcut and white layer thickness can be achieved if the tools are subjected to longer soaking duration (treated up to 36 hrs.). Comparison of experiment numbers 35 (untreated brass tool) and 39 (cryo-treated brass tool for soaking duration of 36 hrs.) (Table 4.4), it is observed that EWR, surface roughness, radial overcut and white layer thickness can be reduced up to 48.29%, 31.72%, 88.33% and 58.45% respectively due to longer treatment soaking duration. This shows that soaking duration is an important parameter to improve performance measures in EDM. Scanning electron microscope (SEM) micrograph (Figures 4.6 a-b-c) show that electrodes treated with longer soaking duration can maintain good surface integrity of the machined surface and retain initial shape of the tool. The improvement in thermal properties of brass electrode allows easy dissipation of heat from tool material. As a result, better retention in tool shape, uniform sparking and superior quality of the machined surface is achieved. The flushing efficiency of the machined surface improves owing to improved machined surface quality which in turn reduces the deposition of molten material on the machined surface and decreases the white layer thickness. Soaking duration, discharge current, pulse-on-time and duty factor exhibit significant influence on the performance measures. Cryogenic treatment soaking duration hardly influence MRR. It was expected that deep cryogenic treatment of the brass electrode will result in higher MRR. But, the high micro-hardness and low thermal conductivity of Inconel 718 work material does not allow higher volume of material to be eroded from the work surface. With improved thermal conductivity and micro-hardness, brass can be used as potential electrode material to produce precise and accurate EDMed components, particularly in finishing operation.

From the hybrid experimental investigation of powder-mixed dielectric and cryogenically electrodes (Chapter 5), it is observed that the thermal conductivity and micro-hardness of brass electrode improves due to deep cryogenic treatment. As a result, the wearing resistance of the tool increases due to easy dissipation of heat. Due to deep cryogenic treatment, the heat dissipation capacity of Inconel 718 work material improves and helps in decreasing local temperature rise on the work piece surface owing to improvement in thermal conductivity. Consequently, the ability of the work piece to absorb and dissipate heat increases which eventually increases the MRR. The study confirms that significant improvement on material removal rate and reduction in EWR, surface roughness, radial overcut and white layer thickness can be achieved if both the electrodes are cryogenically treated. Comparisonof experiment numbers 20 (untreated work piece and treated tool)and 24 (both tool and work piece treated) (Table 5.4), it is observed that MRR can be increased upto71.92% and EWR, surface roughness, radial overcut and white layer thickness can be reduced upto 33.99%, 35.57%, 72.82% and 35.87% respectively when both the electrodes are cryogenically treated and worked in a powder mixed dielectric condition. This shows that treatment to both the electrodes results in better EDM performance measures in comparison to either treatment of the tool or treatment of the work piece. The study also reveals that the presence of suspended powder particles can enhance the machining efficiency of the process. Comparison of experiment numbers 12 (no suspended particles in dielectric, treated work piece and untreated tool) and 16 (highest concentration of suspended particles in dielectric, treated work piece and untreated tool) (Table 5.4) indicates that MRR can be increased up to 44.31% and EWR, surface roughness, radial overcut and white layer thickness can be reduced up to 24.10%, 14.97%, 19.04% and 5.17% respectively when machining is done in the presence of suspended powder particles.From ANOVA table (Table 5.5), it is observed that discharge current is found to be the most influential parameter for MRR with a percentage contribution of 70.98% followed by open circuit voltage, work-tool pair, powder concentration and pulse-on-time with percentage contribution of 8.68%, 3.03%, 2.11% and 1.17% respectively. From Table 5.6, it is observed that work-tool pair is found to be the most influential parameter for EWR with a percentage contribution of 47.84% followed by discharge current, powder concentration open circuit voltage and pulse-on-time with percentage contribution of 19.17%, 11.78%, 1.73%, 1.06% respectively. From Table 5.7, it is observed that work-tool pair is found to be the most influential parameter for surface roughness with a percentage contribution of 37.97% followed by discharge current, powder concentration and pulse-on-time with percentage

contribution of 28.58%, 12.99% and 6.07% respectively. From Table 5.8, it is observed that work-tool pair is found to be the most influential parameter for radial overcut with a percentage contribution of 58.70% followed by discharge current, powder concentration and pulse-on-time with percentage contribution of 23.91%, 3.91% and 1.52% respectively. From Table 5.9, it is observed that work-tool pair is found to be the most influential parameter for white layer thickness with a percentage contribution of 88.02% followed by discharge current, powder concentration and pulse-on-time with percentage contribution of 4.62%, 0.72% and 0.21% respectively. From above comparisons, it can be concluded that when machining is done in the presence of suspended powder particles with cryogenically treated electrodes, the influence of cryogenic treatment work-tool pair is relatively higher on performance measures than the suspended powder particles.Discharge current, pulse-on-time, powder concentration and work-tool pair exhibits significant effect on performance measures. SEM micrographs (Figures 5.6, 5.7, 5.8 (a and b)) show that machined surface quality and surface integrity is superior when machining is done in the presence of suspended powder particles and both the electrodes are cryogenically treated.

Finally, parametric study carried on thermo-structural model (Chapter 6) indicates that discharge current, open circuit voltage, and pulse-on-time exhibit significant effect on performance measures. It is observed that, craters produced with graphite and copper electrodes are wider and deeper in comparison to crater produced with brass electrode leading to higher MRR for copper and graphite electrode. Owing to higher thermal conductivity tool wear is minimal while machining with graphite and copper electrode in comparison to brass electrodes. The thermo-structural model proposed in the study, shows that compressive stresses developed beneath the crater and moving away from crater both radially and axially the stress becomes tensile. On comparison of experiment numbers 18 (brass tool) and 22 (graphite tool) shown in Table 6.2, it is observed that residual stress can be reduced up to 8.97% if machined with brass tool. .

7.3 Contribution of this research work

This work provides optimum parametric setting for achieving enhanced machining efficiency considering the current research trends and developments arising in EDM. The study reflects the complex and higher order effects of the various important process parameters on performance measures through experimental analysis and justification. Inconel 718 is used as work piece material owing to its extensive application in aerospace engineering viz. manufacturing of components for liquid fueled rockets, rings and casings,

sheet metal parts for aircraft, land-based gas turbine engines, cryogenic tank fasteners and instrumentation parts.This work shows that deep cryogenic treatment helps in achieving enhanced machining efficiency even for low conductive materials like Inconel 718 and brass as work-tool pair. The thermo-structural model proposed in this study provides an inexpensive time saving alternative to study performance of machining before going for actual cutting operation.Therefore, accurate prediction of crater dimension and induced residual stresses will help the tool engineers to set the best parameters for machining operation instead of depending on human judgments. The study offers useful information for controlling the machining parameters to improve the machining efficiency of the EDMed components.

PSO has an inherent drawback of getting trapped at local optimum due to large reduction in velocity values as iteration proceeds and poses difficulty in reaching ideal solution. The mutation operator predominantly used in genetic algorithm is embedded with PSO to avoid such drawbacks of PSO and improve solution quality. A novel multi-objective particle swarm optimization algorithm (MOPSO) has been proposed to get the pareto-optimal solution. Maximum Deviation Theory (MDT) is usedto select the best solutionfrom a large number of non-dominated solutions to avoid subjectiveness and impreciseness in the decision making for the engineers.

7.4 Limitation of the study

In spite of several advantages obtained through proposed study, the followings may be treated as limitations since they have not been addressed in this study.

Surface crack density and heat affected zone of the machined surface has not been considered as process outputs. The effect of process parameter on these performance measures has not been studied.The present study mainly develops empirical, numerical and artificial intelligence models but theoretical or mathematical approach needs to be developed to study the effect of process parameters on various performance measures.Numerical modeling has not been extended for cryogenic treatment and powder-mixed cryogenic treatment experimental investigation.

7. 5 Future scope

The present work provides a wide scope for future investigators to explore many aspects of EDM process. Followings are some recommendations for future research:

The effect of process parameters on surface crack density, heat affected zone and circularity of the machined surface can be studied. Mathematical approach can be developed to study the effect of process parameters on various performance measures.Other improved and hybrid non-traditional optimization techniques viz. cuckoo search, ant colony optimization, artificial bee colony and fire fly algorithms can be used for achieving optimal parametric setting for simultaneously optimize various important performance measures. Finite element models can be extended for cryogenic treatment and powder-mixed cryogenic treatment experimental investigation.

Bibliography

Abdulkareem, S., Khan, A. A., and Konneh, M. (2009).Reducing electrode wear ratio using cryogenic cooling during electrical discharge machining. The International Journal of Advanced Manufacturing Technology, 45(11-12), 1146-1151

Allen, P., and Chen, X. (2007).Process simulation of micro electro-discharge machining on molybdenum. Journal of materials processing technology, 186(1), 346-355

Alvarez-Benitez, J. E., Everson, R. M., and Fieldsend, J. E. (2005, January). A MOPSO algorithm based exclusively on pareto dominance concepts. In Evolutionary Multi-Criterion Optimization (pp. 459-473). Springer Berlin Heidelberg

Bachlaus, M., Pandey, M. K., Mahajan, C., Shankar, R., and Tiwari, M. K. (2008).Designing an integrated multi-echelon agile supply chain network: A hybrid taguchi-particle swarm optimization approach. Journal of Intelligent Manufacturing, 19(6), 747-761

Bai, C. Y., and Koo, C. H. (2006).Effects of kerosene or distilled water as dielectric on electrical discharge alloying of superalloy Haynes 230 with Al–Mo composite electrode. Surface and Coatings Technology, 200(12), 4127-4135

Basu, M. (2008). Dynamic economic emission dispatch using nondominated sorting genetic algorithm-II. International Journal of Electrical Power and Energy Systems, 30(2), 140-149

Batish, A., Bhattacharya, A., Singla, V. K., and Singh, G. (2012). Study of material transfer mechanism in die steels using powder mixed electric discharge machining. Materials and Manufacturing Processes, 27(4), 449-456

Belmecheri, F., Prins, C., Yalaoui, F., and Amodeo, L. (2013). Particle swarm optimization algorithm for a vehicle routing problem with heterogeneous fleet, mixed backhauls, and time windows. Journal of intelligent manufacturing, 24(4), 775-789

Beri, N., Kumar, A., Maheshwari, S., and Sharma, C. (2011).Optimisation of electrical discharge machining process with CuW powder metallurgy electrode using grey relation theory. International Journal of Machining and Machinability of Materials, 9(1), 103-115

Bharti, P. S., Maheshwari, S., and Sharma, C. (2012). Multi-objective optimization of electric-discharge machining process using controlled elitist NSGA-II. Journal of mechanical science and technology, 26(6), 1875-1883

Boothroyd, G., and Winston, A. K. (1989).Non-Conventional Machining Processes.Fundamentals of Machining and Machine Tools. Marcel Dekker, New York, p 491

Brandstatter, B., and Baumgartner, U. (2002). Particle swarm optimization-mass-spring system analogon. Magnetics, IEEE Transactions on, 38(2), 997-1000

Chattopadhyay, K. D., Verma, S., Satsangi, P. S., and Sharma, P. C. (2009). Development of empirical model for different process parameters during rotary electrical discharge machining of copper–steel (EN-8) system. Journal of materials processing technology, 209(3), 1454-1465

Chen, Y., and Mahdivian, S. M. (2000).Analysis of electro-discharge machining process and its comparison with experiments. Journal of Materials Processing Technology, 104(1), 150-157

Chow, H. M., Yan, B. H., Huang, F. Y., and Hung, J. C. (2000).Study of added powder in kerosene for the micro-slit machining of titanium alloy using electro-discharge machining. Journal of Materials Processing Technology, 101(1), 95-103

Chow, H. M., Yang, L. D., Lin, C. T., and Chen, Y. F. (2008).The use of SiC powder in water as dielectric for micro-slit EDM machining. Journal of materials processing technology, 195(1), 160-170

Coello, C. A. C., Pulido, G. T., and Lechuga, M. S. (2004). Handling multiple objectives with particle swarm optimization. Evolutionary Computation, IEEE Transactions on, 8(3), 256-279

Cogun, C., Özerkan, B., and Karacay, T. (2006). An experimental investigation on the effect of powder mixed dielectric on machining performance in electric discharge machining. Proceedings of the Institution of Mechanical Engineers, Part B: Journal of Engineering Manufacture, 220(7), 1035-1050

Collins D. N, and Dormer, J. (1997).Deep cryogenic treatment of a D2 cold-worked tool steel. Heat Treat Met, 371–74

Das, S., Klotz, M., and Klocke, F. (2003). EDM simulation: finite element-based calculation of deformation, microstructure and residual stresses. Journal of Materials Processing Technology, 142(2), 434-451

Deb, K., Pratap, A., Agarwal, S., and Meyarivan, T. A. M. T. (2002). A fast and elitist multiobjective genetic algorithm: NSGA-II. Evolutionary Computation, IEEE Transactions on, 6(2), 182-197

Dewangan, S., and Biswas, C. K. (2013).Optimisation of machining parameters using grey relation analysis for EDM with impulse flushing. International Journal of Mechatronics and Manufacturing Systems, 6(2), 144-158

Dhar, S., Purohit, R., Saini, N., Sharma, A., and Kumar, G. H. (2007). Mathematical modeling of electric discharge machining of cast Al–4Cu–6Si alloy–10wt.%SiC P composites. Journal of Materials Processing Technology, 194(1), 24-29

Dong, Y., Tang, J., Xu, B., and Wang, D. (2005).An application of swarm optimization to nonlinear programming. Computers and Mathematics with Applications, 49(11), 1655-1668

Ebrahimipour, V., Haeri, A., Sheikhalishahi, M., and Asadzadeh, S. M. (2012). Application of multi-objective particle swarm optimization to solve a fuzzy multi-objective reliability redundancy allocation problem .Journal of Safety Engineering, 1(2), 26–38

Erden, A. (1983). Effect of materials on the mechanism of electric discharge machining (EDM). Journal of Engineering Materials and Technology, 105(2), 132-138

Erden, A., and Kaftanoglu, B. (1980).Heat transfer modeling of electric discharge machining. In Proceedings of the 21st International Machine Tool Design and Research Conference, 351-358

Fieldsend, J. E., and Singh, S. (2002). A multi-objective algorithm based upon particle swarm optimisation, an efficient data structure and turbulence

Gao, Q., Zhang, Q. H., Su, S. P., and Zhang, J. H. (2008). Parameter optimization model in electrical discharge machining process. Journal of Zhejiang University Science A, 9(1), 104-108

Ghiasi, H., Pasini, D. andLessard, L. (2011). A non-dominated sorting hybrid algorithm for multi-objective optimization of engineering problems. Engineering Optimization, 43(1), 39-59

Gill, S. S., and Singh, J. (2010).Effect of deep cryogenic treatment on machinability of titanium alloy (Ti-6246) in electric discharge drilling. Materials and Manufacturing Processes, 25(6), 378-385

Gill, S. S., Singh, H., Singh, R., and Singh, J. (2010).Cryoprocessing of cutting tool materials—a review. The International Journal of Advanced Manufacturing Technology, 48(1-4), 175-192

Golshan, A., Gohari, S., and Ayob, A. (2012).Multi-objective optimisation of electrical discharge machining of metal matrix composite Al/SiC using non-dominated sorting genetic algorithm. International Journal of Mechatronics and Manufacturing Systems, 5(5), 385-398

Habib, S. S. (2009). Study of the parameters in electrical discharge machining through response surface methodology approach. Applied Mathematical Modelling, 33(12), 4397-4407

Hargrove, S. K., and Ding, D. (2007). Determining cutting parameters in wire EDM based on workpiece surface temperature distribution. The International Journal of Advanced Manufacturing Technology, 34(3-4), 295-299

Her, M.G and Weng, F.T. (2002). A study of electrical discharge machining of semiconductor Batio3.Journal of material processing Technology,122, 1-5

Ho, K. H., and Newman, S. T. (2003). State of the art electrical discharge machining (EDM). International Journal of Machine Tools and Manufacture, 43(13), 1287-1300

Huang, J. T., and Liao, Y. S. (2003). Optimization of machining parameters of wire-EDM based on grey relational and statistical analyses. International Journal of Production Research, 41(8), 1707-1720

Ikai, T., and Hashigushi, K. (1995). Heat input for crater formation in EDM. In Proceedings of the International Symposium for Electro-Machining-ISEM XI, EPFL,163-170

Izquierdo, B., Sanchez, J. A., Plaza, S., Pombo, I., and Ortega, N. (2009). A numerical model of the EDM process considering the effect of multiple discharges. International Journal of Machine Tools and Manufacture, 49(3), 220-229

Jafferson, J. M., and Hariharan, P. (2013).Machining performance of cryogenically treated electrodes in microelectric discharge machining: A comparative experimental study. Materials and Manufacturing Processes,28(4), 397-402

Jaswin M. A., and Lal, D.M., (2010).Optimization of the cryogenic treatment process for En 52 valve steel using the Grey-Taguchi method. Materials and Manufacturing Processes, 25(8), 842-850

Joshi, S. N., and Pande, S. S. (2009). Development of an intelligent process model for EDM. The International Journal of Advanced Manufacturing Technology, 45(3-4), 300-317

Joshi, S. N., and Pande, S. S. (2010). Thermo-physical modeling of die-sinking EDM process. Journal of manufacturing processes, 12(1), 45-56

Joshi, S. N., and Pande, S. S. (2011). Intelligent process modeling and optimization of die-sinking electric discharge machining. Applied Soft Computing, 11(2), 2743-2755

Kansal, H. K., Singh, S., and Kumar, P. (2005). Parametric optimization of powder mixed electrical discharge machining by response surface methodology. Journal of Materials Processing Technology, 169(3), 427-436

Kansal, H. K., Singh, S., and Kumar, P. (2006). Performance parameters optimization (multi-characteristics) of powder mixed electric discharge machining (PMEDM) through Taguchi's method and utility concept. Indian Journal of Engineering and Materials Sciences, 13(3), 209

Kansal, H. K., Singh, S., and Kumar, P. (2007a). Effect of silicon powder mixed EDM on machining rate of AISI D2 die steel. Journal of Manufacturing processes, 9(1), 13-22

Kansal, H. K., Singh, S., and Kumar, P. (2007b). Technology and research developments in powder mixed electric discharge machining (PMEDM). Journal of Materials Processing Technology, 184(1), 32-41

Kansal, H. K., Singh, S., and Kumar, P. (2008). Numerical simulation of powder mixed electric discharge machining (PMEDM) using finite element method. Mathematical and Computer Modelling, 47(11), 1217-1237

Kapoor, J., Singh, S., and Khamba, J. S. (2012). Effect of cryogenic treated brass wire electrode on material removal rate in wire electrical discharge machining. Proceedings of the Institution of Mechanical Engineers, Part C: Journal of Mechanical Engineering Science, 0954406212438804

Karimi, N., Zandieh, M., and Karamooz, H. R. (2010). Bi-objective group scheduling in hybrid flexible flowshop: a multi-phase approach. Expert Systems with Applications, 37(6), 4024-4032

Kennedy, J. andEberhart, R. (1995). Particle swarm optimization. In Proceedings of IEEE International Conference on Neural Network, Washington, USA, Nov/Dec 1995, 4, 1942-1948

Keskin, Y., Halkacı, H. S., and Kizil, M. (2006).An experimental study for determination of the effects of machining parameters on surface roughness in electrical discharge machining

(EDM). The international journal of advanced manufacturing technology, 28(11-12), 1118-1121

Kim, B. I., and Son, S. J. (2012). A probability matrix based particle swarm optimization for the capacitated vehicle routing problem. Journal of Intelligent Manufacturing, 23(4), 1119-1126

Klocke, F., Lung, D., Antonoglou, G., and Thomaidis, D. (2004). The effects of powder suspended dielectrics on the thermal influenced zone by electrodischarge machining with small discharge energies. Journal of materials processing technology, 149(1), 191-197

Kumar, A., Maheshwari, S., Sharma, C., and Beri, N. (2010). A study of multiobjective parametric optimization of silicon abrasive mixed electrical discharge machining of tool steel. Materials and Manufacturing processes, 25(10), 1041-1047

Kumar, A., Maheshwari, S., Sharma, C., and Beri, N. (2012a). Machining efficiency evaluation of cryogenically treated copper electrode in additive mixed EDM. Materials and Manufacturing Processes, 27(10), 1051-1058

Kumar, N., Kumar, L., Tewatia, H., and Yadav, R. (2012b). Comparative study for MRR on die-sinking EDM using electrode of copperandgraphite.International Journal of Advanced Technology and Engineering Research, 2(2), 170–174

Kumar, S., Batish, A., Singh, R., and Singh, T. P. (2014).A hybrid Taguchi-artificial neural network approach to predict surface roughness during electric discharge machining of titanium alloys. Journal of Mechanical Science and Technology, 28(7), 2831-2844

Kumar, S., Singh, R., Singh, T. P., and Sethi, B. L. (2009). Surface modification by electrical discharge machining: A review. Journal ofMaterials Processing and Technology, 209(8), 3675–3687

Kung, K. Y., Horng, J. T., and Chiang, K. T. (2009). Material removal rate and electrode wear ratio study on the powder mixed electrical discharge machining of cobalt-bonded tungsten carbide. The International Journal of Advanced Manufacturing Technology, 40(1-2), 95-104

Kuppan, P., Narayanan, S., and Rajadurai, A. (2011).Effect of process parameters on material removal rate and surface roughness in electric discharge drilling of Inconel 718 using graphite electrode. International Journal of Manufacturing Technology and Management, 23(3), 214-233

Kuriakose, S., and Shunmugam, M. S. (2005).Multi-objective optimization of wire-electro discharge machining process by non-dominated sorting genetic algorithm. Journal of materials processing technology, 170(1), 133-141

Lal, D. M., Renganarayanan, S., and Kalanidhi, A. (2001).Cryogenic treatment to augment wear resistance of tool and die steels. Cryogenics, 41(3), 149-155

Lee, L. C., Lim, L. C., Narayanan, V., and Venkatesh, V. C. (1988). Quantification ofsurface damage of tool steels after EDM. International Journal of Machine Toolsand Manufacture, 28(44), 359–372

Lee, L., Lim, L., and Wong, Y. (1990). Towards a better understanding of the surface features of electro-discharge machined tool steels. Journal of Material Processing Technology,24, 513–523

Lee, S. H., and Li, X. P. (2001).Study of the effect of machining parameters on the machining characteristics in electrical discharge machining of tungsten carbide. Journal of Materials Processing Technology, 115(3), 344-358

Li, X. (2004, January). Better spread and convergence: Particle swarm multiobjective optimization using the maximin fitness function. In Genetic and Evolutionary Computation–GECCO 2004 (pp. 117-128). Springer Berlin Heidelberg

Lin, J. L., and Lin, C. L. (2005).The use of grey-fuzzy logic for the optimization of the manufacturing process. Journal of Materials Processing Technology,160(1), 9-14

Lin, J. L., Wang, K. S., Yan, B. H., and Tarng, Y. S. (2000). Optimization of the electrical discharge machining process based on the Taguchi method with fuzzy logics. Journal of Materials Processing Technology, 102(1), 48-55

Lin, Y. C., Chen, Y. F., Wang, D. A., and Lee, H. S. (2009). Optimization of machining parameters in magnetic force assisted EDM based on Taguchi method. Journal of materials processing technology, 209(7), 3374-3383

Lin, Y. C., Yan, B. H., and Huang, F. Y. (2001). Surface improvement using a combination of electrical discharge machining with ball burnish machining based on the Taguchi method. The International Journal of Advanced Manufacturing Technology, 18(9), 673-682

Mahapatra, S. S., and Patnaik, A. (2007).Optimization of wire electrical discharge machining (WEDM) process parameters using Taguchi method. The International Journal of Advanced Manufacturing Technology, 34(9-10), 911-925

Mahardika, M., Tsujimoto, T., and Mitsui, K. (2008). A new approach on the determination of ease of machining by EDM processes. International Journal of Machine Tools and Manufacture, 48(7), 746-760

MahdaviNejad, R. A. (2011). Modeling and optimization of electrical discharge machining of SiCparameters, using neural network and non-dominating sorting genetic algorithm (NSGA II). Materials Sciences and Applications, 2(06), 669

Mandal, D., Pal, S. K., and Saha, P. (2007).Modeling of electrical discharge machining process using back propagation neural network and multi-objective optimization using non-dominating sorting genetic algorithm-II. Journal of Materials Processing Technology, 186(1), 154-162

Marafona, J., and Chousal, J. A. G. (2006).A finite element model of EDM based on the Joule effect. International Journal of Machine Tools and Manufacture,46(6), 595-602

Marafona, J., and Wykes, C. (2000).A new method of optimising material removal rate using EDM with copper–tungsten electrodes. International Journal of Machine Tools and Manufacture, 40(2), 153-164

Markopoulos, A. P., Manolakos, D. E., and Vaxevanidis, N. M. (2008). Artificial neural network models for the prediction of surface roughness in electrical discharge machining. Journal of Intelligent Manufacturing, 19(3), 283-292

Meena, V. K., Azad, M. S., and Mitra, S. (2012). Effect of flushing condition on deep hole micro-EDM drilling. International Journal of Machining and Machinability of Materials, 12(4), 308-320

Ming, Q. Y., and He, L. Y. (1995). Powder-suspension dielectric fluid for EDM.Journal of materials processing technology, 52(1), 44-54

Modares, H., Alfi, A., and Sistani, M. B. N. (2010).Parameter estimation of bilinear systems based on an adaptive particle swarm optimization. Engineering Applications of Artificial Intelligence, 23(7), 1105-1111

Mohan, B., Rajadurai, A., and Satyanarayana, K. G. (2002).Effect of SiC and rotation of electrode on electric discharge machining of Al–SiC composite. Journal of Materials Processing Technology, 124(3), 297-304

Mohanty, C. P., Mahapatra, S. S., and Singh, M. R. (2014). A particle swarm approach for multi-objective optimization of electrical discharge machining process. Journal of Intelligent Manufacturing, 1-20

Mohanty, C. P., Sahu J., and Mahapatra, S. S., (2013). Thermal-structural Analysis of Electrical Discharge Machining Process. Procedia Engineering, 51, 508-513

Montgomery, D. C. (2008).Design and analysis of experiments.John Wiley & Sons.

Mostaghim, S., and Teich, J. (2003, April). Strategies for finding good local guides in multi-objective particle swarm optimization (MOPSO). In Swarm Intelligence Symposium, 2003.SIS'03. Proceedings of the 2003 IEEE (pp. 26-33). IEEE

Mukherjee, R., and Chakraborty, S. (2012). Selection of EDM process parameters using biogeography-based optimization algorithm. Materials and Manufacturing Processes, 27(9), 954-962

Murugesan, S., Balamurugan, K., Narayanan, C. S., and Venkatakrishnan, P. G. (2012). Study on EDM of Al-15% SiC MMC using Solid and Multihole electrodes-A Taguchi approach. European Journal of Scientific Research, 68(2), 161-171

Natsu, W., Shimoyamada, M., andKunieda, M. (2006). Study on expansion process of EDM arc plasma.JSME International Journal SeriesC,49(2), 600–605

Padhee, S., Nayak, N., Panda, S. K., Dhal, P. R., and Mahapatra, S. S. (2012). Multi-objective parametric optimization of powder mixed electro-discharge machining using response surface methodology and non-dominated sorting genetic algorithm. Sadhana, 37(2), 223-240

Panda, D. K. (2008). Study of thermal stresses induced surface damage under growing plasma channel in electro-discharge machining. Journal of Materials Processing Technology, 202(1), 86-95

Panda, D. K., and Bhoi, R. K. (2005). Artificial neural network prediction of material removal rate in electro discharge machining. Materials and Manufacturing Processes, 20(4), 645-672

Panda, M. C., and Yadava, V. (2012). Intelligent modeling and multi-objective optimization of die sinking electrochemical spark machining process. Materials and Manufacturing Processes, 27(1), 10-25

Pandey, P. C., and Jilani, S. T. (1986). Plasma channel growth and the resolidified layer in EDM. Precision Engineering, 8(2), 104-110

Pant, M., Radha, T., and Singh, V. P. (2007, September). A simple diversity guided particle swarm optimization. In Evolutionary Computation, 2007.CEC 2007. IEEE Congress on (pp. 3294-3299). IEEE

Patel, K. M., Pandey, P. M., and Rao, P. V. (2009). Surface integrity and material removal mechanisms associated with the EDM of Al 2 O 3 ceramic composite. International Journal of Refractory metals and hard materials, 27(5), 892-899

Peças, P., and Henriques, E. (2008).Effect of the powder concentration and dielectric flow in the surface morphology in electrical discharge machining with powder-mixed dielectric (PMD-EDM). The International Journal of Advanced Manufacturing Technology, 37(11-12), 1120-1132

Pellicer, N., Ciurana, J., and Delgado, J. (2011). Tool electrode geometry and process parameters influence on different feature geometry and surface quality in electrical discharge machining of AISI H13 steel. Journal of Intelligent Manufacturing, 22(4), 575-584

Prabhu, S., and Vinayagam, B. K. (2011). Analysis of surface characteristics of AISI D2 tool steel material using electric discharge machining process with single-wall carbon nanotubes. International Journal of Machining and Machinability of Materials, 10(1), 99-119

Prabhu, S., and Vinayagam, B. K. (2013).Multi objective optimisation of SWCNT-based electrical discharge machining process using grey relational and fuzzy logic analysis. International Journal of Machining and Machinability of Materials, 13(4), 439-463

Pradhan, M. K. (2013a). Estimating the effect of process parameters on surface integrity of EDMed AISI D2 tool steel by response surface methodology coupled with grey relational analysis. The International Journal of Advanced Manufacturing Technology, 67(9-12), 2051-2062

Pradhan, M. K. (2013b). Estimating the effect of process parameters on MRR, TWR and radial overcut of EDMed AISI D2 tool steel by RSM and GRA coupled with PCA. The International Journal of Advanced Manufacturing Technology, 68(1-4), 591-605

Pradhan, M. K., and Biswas, C. K. (2009). Modeling and Analysis of process parameters on Surface Roughness in EDM of AISI D2 tool Steel by RSM Approach. International Journal of Mathematical, Physical and Engineering Sciences, 3(1)

Pradhan, M. K., and Biswas, C. K. (2010).Neuro-fuzzy and neural network-based prediction of various responses in electrical discharge machining of AISI D2 steel. The International Journal of Advanced Manufacturing Technology, 50(5-8), 591-610

Pradhan, M. K. (2010). Experimental investigation and modelling of surface integrity, accuracy and productivity aspects in EDM of AISI D2 steel (Doctoral dissertation)

Pradhan, M. K., and Das, R. (2011). Recurrent neural network estimation of material removal rate in electrical discharge machining of AISI D2 tool steel.Proceedings of the Institution of Mechanical Engineers, Part B: Journal of Engineering Manufacture, 225(3), 414-421

Pradhan, M. K., Das, R., and Biswas, C. K. (2009). Comparisons of neural network models on surface roughness in electrical discharge machining.Proceedings of the Institution of Mechanical Engineers, Part B: Journal of Engineering Manufacture, 223(7), 801-808

Prajapati, S. B., Patel, N. S., and Asal, V. D. (2013). Prediction of process parameters of wire EDM for AISI A2 using ANN. Indian Journal of Applied Research, 3:217– 218

Puertas, I., Luis, C. J., and Alvarez, L. (2004). Analysis of the influence of EDM parameters on surface quality, MRR and EW of WC–Co. Journal of Materials Processing Technology, 153, 1026-1032

Puhan, D., Mahapatra, S. S., Sahu, J., and Das, L. (2013).A hybrid approach for multi-response optimization of non-conventional machining on AlSiC p MMC. Measurement, 46(9), 3581-3592

Rajurkar, K. P., and Yu, Z. Y. (2000).3d micro-edm using cad/cam. CIRP Annals-Manufacturing Technology, 49(1), 127-130

Ramakrishnan, R., and Karunamoorthy, L. (2008).Modeling and multi-response optimization of Inconel 718 on machining of CNC WEDM process. Journal of materials processing technology, 207(1), 343-349

Rangajanardhaa, G., and Rao, S. (2009). Development of hybrid model and optimization of surface roughness in electric discharge machining using artificial neural networks and genetic algorithm. Journal of Materials Processing Technology, 209(3), 1512-1520

Rao, P. S., Ramji, K., and Satyanarayana, B. (2011). Effect of WEDM conditions on surface roughness: A parametric optimization using Taguchi method. International journal of advanced engineering sciences and technologies, 6(1), 41-48

Raquel, C. R., and Naval Jr, P. C. (2005, June). An effective use of crowding distance in multiobjective particle swarm optimization.In Proceedings of the 7th Annual conference on Genetic and Evolutionary Computation (pp. 257-264). ACM

Salah, N. B., Ghanem, F., and Atig, K. B. (2006).Numerical study of thermal aspects of electric discharge machining process. International Journal of Machine Tools and Manufacture, 46(7), 908-911

Salonitis, K., Stournaras, A., Stavropoulos, P., and Chryssolouris, G. (2009).Thermal modeling of the material removal rate and surface roughness for die-sinking EDM. The International Journal of Advanced Manufacturing Technology, 40(3-4), 316-323

Schulze, H. P., Herms, R., Juhr, H., Schaetzing, W., and Wollenberg, G. (2004).Comparison of measured and simulated crater morphology for EDM. Journal of Materials Processing Technology, 149(1), 316-322

Sen, M., and Shan, H. S. (2007).Electro jet drilling using hybrid NNGA approach. Robotics and Computer-Integrated Manufacturing, 23(1), 17-24

Senthilkumar, V., and Chandrasekar Reddy, M. (2012).Performance analysis of Cu-B 4 C metal matrix composite as an EDM electrode. International Journal of Machining and machinability of materials, 11(1), 36-50

Shankar, P., Jain, V. K., and Sundararajan, T. (1997). Analysis of spark profiles during EDM process. Machining science and technology, 1(2), 195-217.

Singh, A., and Ghosh, A. (1999).A thermo-electric model of material removal during electric discharge machining. International Journal of Machine Tools and Manufacture, 39(4), 669-682

Singh, M. R., and Mahapatra, S. S. (2012). A swarm optimization approach for flexible flow shop scheduling with multiprocessor tasks. The International Journal of Advanced Manufacturing Technology, 62(1-4), 267-277

Singh, P. N., Raghukandan, K., Rathinasabapathi, M., and Pai, B. C. (2004).Electric discharge machining of Al–10% SiC p as-cast metal matrix composites. Journal of Materials Processing Technology, 155, 1653-1657

Somashekhar, K. P., Ramachandran, N., and Mathew, J. (2010).Optimization of material removal rate in micro-EDM using artificial neural network and genetic algorithms. Materials and Manufacturing processes, 25(6), 467-475

Srivastava, V., and Pandey, P. M. (2011).Study of the cryogenically cooled electrode shape in electric discharge machining process. In Proceedings of the 60th World Academy of Science, Engineering and Technology (pp. 1017-1021)

Srivastava, V., and Pandey, P. M. (2012). Performance evaluation of electrical discharge machining (EDM) process using cryogenically cooled electrode.Materials and Manufacturing Processes, 27(6), 683-688

Su, J. C., Kao, J. Y., and Tarng, Y. S. (2004).Optimisation of the electrical discharge machining process using a GA-based neural network. The International Journal of Advanced Manufacturing Technology, 24(1-2), 81-90

Tomadi, S. H., Hassan, M. A., Hamedon, Z., Daud, R., and Khalid, A. G. (2009, March). Analysis of the influence of EDM parameters on surface quality, material removal rate and electrode wear of tungsten carbide. In Proceedings of the International Multi-Conference of Engineers and Computer Scientists (IMECS) (Vol. 2, pp. 18-20)

Tripathi, P. K., Bandyopadhyay, S., and Pal, S. K. (2007). Multi-objective particle swarm optimization with time variant inertia and acceleration coefficients. Information Sciences, 177(22), 5033-5049

Tzeng, Y. F., and Chen, F. C. (2007).Multi-objective optimisation of high-speed electrical discharge machining process using a Taguchi fuzzy-based approach. Materials and design, 28(4), 1159-1168

Vishwakarma, U. K., Dvivedi, A., and Kumar, P. (2012).FEA modeling of material removal rate in electrical discharge machining of Al6063/SiC composites. International Journal of Mechanical and Aerospace Engineering, 6(1), 398-403

Wang, K., Gelgele, H. L., Wang, Y., Yuan, Q., and Fang, M. (2003).A hybrid intelligent method for modelling the EDM process. International Journal of Machine Tools and Manufacture, 43(10), 995-999

Wang, L., and Singh, C. (2007). Environmental/economic power dispatch using a fuzzified multi-objective particle swarm optimization algorithm. Electric Power Systems Research, 77(12), 1654-1664

Wang, Y. M. (1998). Using the method of maximizing deviations to make decision for multi-indices.System Engineering Electronic, 20(7), 24–26

Wei, C., Xu, K., Ni, J., Brzezinski, A. J., and Hu, D. (2011). A finite element based model for electrochemical discharge machining in discharge regime. The International Journal of Advanced Manufacturing Technology, 54(9-12), 987-995

Wong, Y. S., Lim, L. C., Rahuman, I., and Tee, W. M. (1998).Near-mirror-finish phenomenon in EDM using powder-mixed dielectric. Journal of Materials Processing Technology, 79(1), 30-40

Wu, C. H., Wang, D. Z., Ip, A., Wang, D. W., Chan, C. Y., and Wang, H. F. (2009). A particle swarm optimization approach for components placement inspection on printed circuit boards. Journal of Intelligent Manufacturing, 20(5), 535-549

Xu, J., Liu, Y., Wang, J., Kui, X., Gao, Y., andXu, Z. (2007). A study on double glow plasma surface metallurgy Mo–Cr high speed steel of carbon steel. Surface and Coatings Technology, 201(9), 5093-5096

Yadav, V., Jain, V. K., and Dixit, P. M. (2002). Thermal stresses due to electrical discharge machining. International Journal of Machine Tools and Manufacture,42(8), 877-888

Yang, S. H., Srinivas, J., Mohan, S., Lee, D. M., and Balaji, S. (2009). Optimization of electric discharge machining using simulated annealing. Journal of Materials Processing Technology, 209(9), 4471-4475

Yih-Fong, T., and Fu-Chen, C. (2005). Investigation into some surface characteristics of electrical discharge machined SKD-11 using powder-suspension dielectric oil. Journal of Materials Processing Technology, 170(1), 385-391

Yoshida, H., Kawata, K., Fukuyama, Y., Takayama, S., and Nakanishi, Y. (2000). A particle swarm optimization for reactive power and voltage control considering voltage security assessment. Power Systems, IEEE Transactions on, 15(4), 1232-1239

Zhao, W. S., Meng, Q. G., and Wang, Z. L. (2002). The application of research on powder mixed EDM in rough machining. Journal of materials processing technology, 129(1), 30-33

List of Publications

International Journals

1. **Chinmaya P. Mohanty** ,Siba Sankar Mahapatra and Manas Ranjan Singh, "A particle swarm approach for multi-objective optimization of electrical discharge machining process", Journal of Intelligent Manufacturing, 2014, DOI: 10.1007/s10845-014-0942-3
2. **Chinmaya P. Mohanty**, Jambeswar Sahu and Siba Sankar Mahapatra, "Parametric optimization of electrical discharge machining process using numerical analysis", International Journal of Industrial and System Engineering, (Article in press).
3. **Chinmaya P. Mohanty**, Jambeswar Sahu and Siba Sankar Mahapatra, "A thermal structural model for process performance analysis", International Journal of Productivity and Quality Management (Article in press).
4. Jambeswar Sahu, Siba Sankar Mahapatra and **Chinmaya P. Mohanty**, "Multi response optimization of EDM parameters using data envelopment analysis", International Journal of Productivity and Quality Management (Article in press)
5. **Chinmaya P. Mohanty**,Siba Sankar Mahapatra and Manas Ranjan Singh, "Effect of deep cryogenic treatment on electrical discharge machining", Measurement (Communicated).
6. **Chinmaya P. Mohanty**, Siba Sankar Mahapatra and Manas Ranjan Singh, "A combined approach of utility function and QPSO for multi-response optimization in electrical discharge machining", Journal of the Brazilian Society of Mechanical Sciences and Engineering (Communicated).
7. **Chinmaya P Mohanty,** Siba Sankar Mahapatra and Manas Ranjan Singh, "Performance estimation of EDM process using hybrid approach of cryogenic treatment and powder-mixed dielectric", Journal of Intelligent Manufacturing (Communicated).

International Conferences

1. **Chinmaya P. Mohanty**, JambeswarSahu, Siba Sankar Mahapatra (2013). Thermal-structural analysis of electrical discharge machining process. Proceedings of the 3rdNirma University International Conference on Engineering (NUiCONE2012),06th-08th December, 2012, Ahmedabad, (Procedia Engineering), 51, 508-513.
2. **Chinmaya P. Mohanty**, Jambeswar Sahu, Siba Sankar Mahapatra (2014). An Experimental Investigation of Machinability of Inconel 718 in Electrical Discharge Machining. Proceedings of the 3rd International Conference on Materials Processing and Characterization (ICMPC 2014)8th–9th March, Hyderabad, 2014, (Procedia Materials Science), 6, 605-611.
3. **Chinmaya P. Mohanty**, , Siba Sankar Mahapatra, Manas Ranjan Singh, 'Multi Response Optimization of Electrical Discharge Machining Process Using Particle Swarm Approach'

The 2nd Asia Symposium on Engineering and Information, 9th -11th April, 2014, Bangkok, Thailand.

4. **Chinmaya P. Mohanty**, Biswesh R. Acharya, Siba Sankar Mahapatra, 'A numerical approach of modelling and Simulation of Electrical-discharge machining on AISI D2steel', Proceedings of the 3rd International conference on Advancements in Polymeric Materials , APM-2013,CIPET,Locknow.
5. **Chinmaya P Mohanty,** Jambeswar Sahu, Siba Sankar Mahapatra, 'Performance estimation of EDM process using numerical analysis and neural network', Proceedings of the 2nd International conference on Advanced Manufacturing and Automation(INCAMA-2013) 28th-30th March 2013.
6. **Chinmaya P. Mohanty**, ManasRanjan Singh, Siba Sankar Mahapatra, Suman Chatterjee, A Particle Swarm Approach Embedded with Numerical analysis for Multi-response Optimization in Electrical Discharge Machining.5th International Conference on Swarm, Evolutionary and Memetic Computing (SEMCCO-2014)8th-20th December, 2014, Bhubaneswar, Odisha
7. Jambeswar Sahu, **Chinmaya P. Mohanty**, Siba Sankar Mahapatra. (2013). A DEA approach for optimization of multiple responses in electrical discharge machining of AISI D2 steel. 3rdNirma University International Conference on Engineering (NUiCONE2012), 06th-08th December, 2012, Ahmedabad, (Procedia Engineering), 51, 585-591.
8. Biswesh Ranjan Acharya. **Chinmaya P. Mohanty**, Siba Sankar Mahapatra, (2013). Multi-objective Optimization of Electrochemical Machining of Hardened Steel Using NSGAII. 3rdNirma University International Conference on Engineering (NUiCONE2012),06th-08th December, 2012, Ahmedabad, (Procedia Engineering), 51, 554-560.